N O T I C E

THIS DOCUMENT HAS BEEN REPRODUCED FROM MICROFICHE. ALTHOUGH IT IS RECOGNIZED THAT CERTAIN PORTIONS ARE ILLEGIBLE, IT IS BEING RELEASED IN THE INTEREST OF MAKING AVAILABLE AS MUCH INFORMATION AS POSSIBLE

JPL PUBLICATION 79-91

A Controlled Rate Freeze/Thaw System for Cryopreservation of Biological Materials

V. J. Anselmo
R. G. Harrison

(NASA-CR-162531) A CONTROLLED RATE FREEZE/THAW SYSTEM FOR CRYOPRESERVATION OF BIOLOGICAL MATERIALS (Jet Propulsion Lab.) 182 p HC A09/MF A01 CSCL 06B

N80-14675

Unclas
G3/51 46431

June 1, 1979

Prepared for
Union Carbide Company
by
Jet Propulsion Laboratory
California Institute of Technology
Pasadena, California

JPL PUBLICATION 79-91

A Controlled Rate Freeze/Thaw System for Cryopreservation of Biological Materials

V. J. Anselmo, Principal Investigator
R. G. Harrison, Technical Manager

June 1, 1979

Prepared for
Union Carbide Company
by
Jet Propulsion Laboratory
California Institute of Technology
Pasadena, California

FOREWORD

Under contract to Union Carbide, the Jet Propulsion Laboratory has undertaken the design and construction of a temperature controlled device for the freezing and thawing of red blood cells. Stringent temperature control is obtained from electrical circuitry used on the Viking Mars Mission for thermal control of spacecraft instruments. This control methodology allows precision freezing and thawing in a reproducible manner and at rates which may be optimal for maximum recovery of the red blood cells.

This is the final report for the project.

The development phase of the project is described in the Red Blood Cell Freezer Task Interim Report, JPL internal document number 5030-134, dated October 1, 1977.

ABSTRACT

A system has been constructed which allows programmable temperature-time control for a 5cc sample volume of an arbitrary biological material. It also measures the parameters necessary for the determination of the sample volume specific heat and thermal conductivity as a function of temperature, and provides a detailed measurement of the temperature during phase change and a means of calculating the heat of the phase change.

Steady-state and dynamic temperature control is obtained by supplying heat to the sample volume through resistive elements constructed as an integral part of the sample container. For cooling purposes, this container is totally immersed into a cold heat sink. Sample volume thermodynamic property data are obtained by measurements of heater power and heat flux through the container walls. Using a mixture of dry ice and alcohol at -79°C, the sample volume can be controlled from +40°C to -60°C at rates from steady state to ± 65°C/min. Steady-state temperature precision is better than 0.2°C while the dynamic capability depends on the temperature rate of change as well as the thermal mass of both the sample and the container.

Preliminary tests, conducted with distilled water, saline, and red blood cells, showed the feasibility for using the device for extremely accurate temperature control. The performance capabilities of the system allow the application of an increased dimension of thermal control to the study of freeze storage of biological materials. The system's ability to determine the temperature dependent thermodynamic properties allows a greater understanding of the thermodynamics of freeze damage to biological cells. The unique capability in determining phase change and measuring its heat, may lead to a new consideration of the roles of the electrolytes through a more thorough understanding of the solution eutectics and their resulting osmotic pressure histories.

ACKNOWLEDGEMENT

The authors wish to express their appreciation of the support of Dr. Arthur Rinfret, formerly of Union Carbide Corporation, for his contribution to the Bioscience aspects of the project, and the following JPL personnel for their technical support:

Mr. Thomas Andrews, Mechanical Design and Fabrication
Mr. Ed Bailey, System Operation and Lab Support
Mr. C. Martin Berdahl, Sensor Design and Flux Measurements
Mr. Earl Collins, Design Integration
Mr. Harold Conway, Sensor Fabrication
Mr. Alex Engel, Computer Programs
Mr. Richard Heyser, Electronic Consultant
Dr. Wiktor Jaworski, Thermal Analysis
Mr. Robert Lester, Engineering Consultant
Mr. Kenton MacDavid, Sensor Layout
Mr. Jess Martinez, Electronic Fabrication
Mr. Richard Rice, Materials and Mechanical Design
Mr. James Stephens, Cryogenics Consultant
Mr. Gordon Wiker, Electronic Design

CONTENTS

APPENDIXES

Figures

SECTION I

INTRODUCTION AND BACKGROUND

Numerous attempts have been made to freeze biological materials and show that viability is maintained upon thawing. In some cases, satisfactory freeze preservation has been possible when cryophylactic agents, such as dimethyl sulfoxide (DMSO) or glycerol, have been added to materials before freezing. The exact manner by which these materials afford protection is not known, but by understanding the various temperature related factors which cause cryogenic destruction, some understanding of the effects of freeze/thaw protocols may be possible.

The problems arising during the freezing process include: (1) intracellular and extracellular ice formation, (2) high solute concentration, (3) pH changes, (4) dehydration, and (5) others. It is known however, that the freeze/thaw rates and storage temperature affect both the character of ice formation and other variables which indirectly influence the survivability of frozen materials. Temperature rates which are either too slow or too fast are known to cause increased cellular destruction.

The use of frozen thawed human erythrocytes for transfusion is becoming increasingly important for many reasons, including, for one, the convenience of having rare blood types available when needed. The fact that frozen blood is not even more widespread in its use can be attributed to its relatively high cost in relation to the unfrozen product. The high cost is largely because large quantities of glycerol must be added as a cryoprotectant and then later removed. The removal of glycerol is a complex, time consuming, and costly procedure.

This work describes a device which allows the study of a new approach to the freeze preservation of human erythrocytes and which, if successful, will have a significant impact on the frozen blood industry. The approach utilizes technology developed at the Jet Propulsion Laboratory (JPL) to allow precise control of instrument temperature aboard spacecraft. With this precise control, it may be possible to understand the role of temperature for minimizing freeze damage, thereby minimizing the costs for low-temperature preservation. Application of the JPL-designed temperature control system to the problem of red cell freezing may provide solutions to these and other problems of freeze preservation.

SECTION II

TECHNICAL DISCUSSION

A. OVERALL SYSTEM DESCRIPTION

1. Concept

In the initial phase of this work, a basic design concept was adopted which allowed the red blood cell container to also serve as the primary means for heating the cell mass while immersed within a cold environment. Such an approach maximized utilization of the temperature control available from the bridge circuit proposed for use and discussed in Appendix A of this report. This design concept is summarized in Figure 1. The desired freezing and/or thawing protocol is established in the computer. The computer measures the heat dissipation in the heater and adjusts it by sensing the temperature of the cell mass or other control point and referencing this against the desired temperature for a particular protocol. The heat of phase change as well as the thermal conductivity and specific heat of the cell mass are also determined from temperatures and heat dissipated in the container. These parameters are necessary for thermal dimensional scaling to larger volumes of cells which may be of commercial interest in the future as well as for the normalization of the thermodynamic behavior of the red blood cell samples obtained from various donors.

2. Approach

The final system block diagram is given as Figure 2. The function of the various blocks of this configuration are discussed in this section.

a. Temperature Controller. The controller sets the temperature levels for the system. It is discussed in Section II-C-1.

b. IDAC. The IDAC provides automatic operation of the controller, transmits digital data to the tape deck, and produces a video display in engineering units for any selected input. The IDAC is described in Section II-D of this report.

c. Freeze/Thaw container - Model III. The configuration of the container used for the final experiments in this report is described in detail in Section II-B-2 of this report. Samples of water, saline solutions, red cells, or other liquids can be placed in the container for experimental purposes. The sample volume is 5 cc. A thermocouple is located in the center of the sample. The container walls are hard anodized aluminum separated by a Vespel rectangular annulus. The walls contain the temperature sensors and heaters which provide the total thermodynamic information for the system.

d. Digital Voltmeter. Any digital voltmeter (DVM) with an input impedance greater than 100 kΩ and a resolution of at least 1 μV can be used with this system. The DVM is used to monitor the various temperature sensors during operation or calibration, and to monitor the sensor excitations and controller sensitivity during system set up.

e. Heater Power Supply. Any dc power supply that can provide 150 Vdc at 10 A can be used with this system. Typical operation is 100 Vac and 7.5 A at full power in the alcohol-frozen CO_2 heatsink. The dc supply provides dc power to the temperature controller which in turn provides the pulse width modulated power to the heaters in the container walls.

f. X-Y plotters. The 2 pen plotters are used to graph any combination of sensor and heater signals desired. The plotters provide real-time demonstrations of the performance of the system.

g. Tape Deck and Video display. The tape deck stores the complete thermal history of each test. The video display is used for monitoring up to four channels of real-time test data. These are discussed in detail in the IDAC section of the report.

B. FREEZER DESCRIPTION

1. Early Development

Two concepts were considered in the initial design phase. The first, based on a rotating cylindrical tube container, is discussed in Appendix B. This approach was determined to be inappropriate for the basic studies initially required. In the second concept, a container having parallel flat plates separated by a guard material would be used. The entire heat transfer between the cell mass and the heat sink would occur across the flat plates. These plates would also contain the necessary heaters and sensors. This approach was chosen for the study because of its simplicity and ease of analysis.

A schematic of an early model of this configuration, Model I shown in Figure 3, was built for the primary purpose of exercising the temperature control circuit. Model I consisted of a pair of plane parallel 3 x 6-in. walls held apart by an 0.08 in. aluminum spacer and enclosed in a plexiglass rim. Each wall contained a pair of 0.040-in. beryllium copper plates which sandwiched an 0.080 in. Electrofilm patch heater. The heater and plates were bonded together by RTV 60 cement.

The temperatures for Model I were monitored by a pair of 0.5-in. square nickel sensors placed at the center of the wall between the inner plate and the patch heater. The interior volume of 31 cc was used to contain distilled water for the initial experiments.

The actual thermal performance of Model I, although inadequate for blood freezing studies, provided data which suggested design modifications for the control electronics and the subsequent container configurations.

These changes led to the design of Model II, shown in Figure 4. The primary purpose of this model was to test the thermal control capability of specially designed heater and sensor elements.

In Model II, the cell mass is contained between a pair of 4 x 6 in. plane parallel walls, separated and insulated from each other by a styrofoam rim and an 0.080-in. Vespel SP21 Spacer which served as a guard volume for the cell mass. Vespel has thermodynamic properties similar to packed red cells. It introduced no noticeable phase change during the freeze/thaw protocols being considered. The wall itself is composed of four elements, bonded to each other with Micro-measurements M-Bond 610. This bond was successfully tested under extreme thermal stresses by immersion of various combinations of bonded surfaces into liquid nitrogen from room temperature. No separations were experienced even though the bonded materials had considerably different thermal coefficients of expansion.

The interior element of the wall was a 0.032 in. anodized aluminum plate whose primary function was to provide a high thermal conductivity path between the cell mass and the control sensor, the adjacent element of the wall. The control sensor was a 0.0005 in. nickel grid deposited on a 0.001 in. Kapton sheet. This sensor provided an integrated measure of the cell mass surface temperature on each interior wall of the container. The next element of the wall is physically the same.

The outer element of the wall was a 0.090 in. anodized aluminum plate whose primary function was strength with a high thermal conductance path to the heat sink. Because of the reduced thermal mass of Model II over Model I, Model II was used to indicate the true order of magnitude of the temperature control available from the pulse width modulated heater control system. Experiments with Model II were conducted to optimize the heat transfer performance of the container.

Model IIIA, shown in Figure 5, was also considered in concept but never constructed. It had the potential of exhibiting a maximum thermal coupling between the cell mass, its surface sensor and the heater. This would have been accomplished by depositing both the nichrome heater and the nickel sensor on a single sheet of 0.001 in. Kapton. Electrical insulation between the heater and sensor and between the sensor and the cell mass would be obtained by a thin deposited layer of silicon monoxide. The remainder of the wall elements would be the same as described for Model III.

Although Model IIIA would have required some additional development work, it would have had other important advantages. Its basic construction would simulate the presence of a plastic bag by the inner Kapton sheet. This simulation could be important in a developmental sense in that the use of a plastic blood bag for freezing and storage is commercially attractive.

2. Final Freezer Configuration

a. Model III Description. Model III was designed and constructed as a container for red blood cells having sensors to accurately measure temperatures, temperature gradients, heat flow and state changes during the freeze/thaw process. It is operable in the temperature range from room temperature to -60°C when used with a heat sink of -79°C. The rate of cooling/heating can be controlled either from the data sensed by a thermocouple in the cell mass or from sensors in contact with the cell mass surface. The latter method was chosen for these experiments. The directional heat flow is measured by sensing elements within each wall. This heat flow measurement provides data to determine the thermodynamic properties of the cell mass and to measure the heats of phase change.

b. Description and Explanation. Figure 6 is a schematic representation of the Model III container. The Model III contained a total of 5 ml of cell volume with 11% expansion allowable for volume change during freezing. The Model III design was developed from the results of earlier tests.

Each wall of the container is composed of 9 individual elements as shown in Figure 6. Each element is attached to the adjacent element with Micromeasurements AE-15 bond. The two walls sandwich the Vespel rectangular annulus (V) allowing a 2mm spacing of the walls and the formation of the 6.5cc sample volume. Material is transferred to and from the sample volume by syringe which can be inserted into ports drilled through the Vespel frame. A hydrophobic grease is placed between the Vespel and the walls to eliminate leaks and a spring provides the necessary tension to hold both walls and Vespel in place.

All the plates shown in each wall are hard anodized aluminum. The anodized coating provides electrical insulation between the plates and the sensors or heaters, and provides an acceptable surface for contact with the sample mass. The positioning of the aluminum plates between the heaters and sensors provides the necessary electrostatic shielding to prevent the pulsed heater power from coupling into the sensors.

The dimensions of the wall elements are 2.625 x 3.35 in. The sensors shown in Figure 7 are 0.0005 in. nickel deposited on 0.001 in. Kapton. Both heaters and sensors are bifilar wound to reduce electrostatic coupling. The total heater resistance is 25 ohms and the total sensor resistance is 94 ohms. The internal aluminum plates are all 0.020 in. thick and the two outer plates, R_{5A} and R_{5B}, are 0.080 in. thick.

Sensors S_{1A} and S_{1B} measure the surface temperature of the sample mass. The temperature differential across a portion of the wall is made from the S_{2A} - S_{3A} and the S_{2B} - S_{3B} sensors. These later temperature differentials are important in calculating the heat flux through each wall. This heat flux is required for determination of the thermodynamic properties of the sample mass.

Figure 8 shows another view of the container walls and associates each sensor and heater with its appropriate temperature or heater symbol used in this text. For example, the temperature measured by sensor S_{1A} is T_{A1} and the power generated by heater H_A is P_A.

Figure 9 is a photograph illustrating a side view of the parallel plate construction of one half of the container and showing the Vespel frame on top. It also shows the heater and sensor leads coming from the wall.

Figure 10 is a photograph of one half of the sample container. The Vespel frame is seen as the dark rectangular annulus. The heater and sensor element wiring from the wall uses plastic covered shielded twisted pair conductors.

Figure 11 shows the outer plate of one side, together with the styrofoam edge insulators mounted in the lower half of the instrumentation frame.

Figure 12 shows the instrumentation fixture and illustrates the expandex spring material which exerts increasing pressure on the two halves of the container stack as the temperature is lowered. This photograph also shows the screw means for joining the two halves of the instrumentation fixture and illustrates the coolant flow apertures.

c. Typical Model III Test Data. Figure 13 shows a typical temperature-time history for freezing and thawing of distilled water. Two cooldown rates were used: Rate 1, 10 °C/min, and Rate 2, 5 °C/min. Curves AA and BB are the corresponding power curves for heater P_A. As the sample (distilled water) is cooled, it initiates a phase change at a temperature below its normal freezing point (supercooling). The exothermic freezing process causes the temperature to increase in the direction of the theoretical freezing point, 0°C. After the exothermic freeze process has been completed, continued heat removal from the sample causes the temperature to drop rapidly to the ramp level (End of Phase Change). Further cooling continues at the ramp rate to either the next phase change point or to the termination of the cooling ramp.

It should be noted that the curves A and E are sensed by the thermocouple, T_0, at the center of the sample mass. Had the control sensor S_1 been plotted, it would show a straight line through the phase change indicating precise temperature control of the actual control point. This characteristic is demonstrated in the test data to be discussed.

C. CONTROL SYSTEM DESCRIPTION

1. Temperature Controller

The data system temperature control block diagram is shown in Figure 14. The temperature controller provides sensor excitation and pulsed heater power to the container, and digital information of controller set point temperature reference and the analog signals of the various nickel temperature sensors to the Integrated Data Acquisition and Control System (IDAC). Other analog outputs are provided for the X-Y plotters. Any of the freezer temperatures and heater powers can be plotted in real time. The controller provides the freeze/thaw control ramps and the rates at which these ramps are accomplished. The controller starts, stops and holds at manually selected control points or the programmed control points provided by the IDAC. All functions of the controller can be set manually or can be programmed in the IDAC. The IDAC then conducts a complete freeze/thaw experiment. The temperature controller circuitry is described in the following Sections.

Figures 15 and 16 are front views of the controller chassis with and without the front chassis plate. Figure 17 is the back view of the chassis. A schematic showing the interconnection of the controller card circuit is shown in Figure 18. These card circuits will be discussed in the following paragraph. The temperature controller provides for both manual or programmed operation.

a. Programmed Operation. For programmed operation the front panel run switch is in the hold position. Initially, it is desirable to have the freeze/thaw container at room temperature. The set point counter is then adjusted by the switches on the front panel until a proper setting is indicated by the output lights. The enable switch that provides a dc voltage to the power drivers, can then be turned on with appropriate change in the sample container temperature. The sample container is then placed in the coolant. The heater power immediately increases to the proper level to maintain the set temperature. The IDAC program then sets the proper temperature rate and start temperature. The experiment program begins and the system accomplishes all of the programmed temperature rates, starts, stops, and holds.

The control system utilizes sets of composite subprograms as building blocks to develop a total protocol. Each composite subprogram consists of (1) start temperature, (2) hold time at the start temperature, (3) temperature ramp rate, (4) final temperature, and (5) hold time at the final temperature. An example of this composite subprogram is shown in Figure 18a.

The control system is capable of storing and managing up to 15 of these composite subprograms per test protocol. Should more than this be required, the system can be placed into a manual hold mode while a new protocol is set in the computer.

Should the start temperature for a given test not be equal to the current initial temperature of the system, the controller will take the system to that start temperature under the maximum rate possible. After holding the system at its final temperature for the appropriate time, the controller will automatically retain this same temperature for an additional indefinite time period or until it receives a manual or programmed command to do otherwise.

b. Manual Operation. For manual operation the run switch is in the hold position and the set point counter is adjusted in the same manner as for the programmed operation. The sample container is placed in the coolant. The rate counter is set to the desired rate. The enable switch is positioned to on. To begin a cooling ramp, the run switch is placed in the down position. To stop and hold, the run switch is placed in hold position. The rate can be changed as desired. For thawing, the run switch is placed in the up position. Care should be exercised in manual thawing to prevent overheating the sample container. For manual operation, the sample temperature must be monitored continuously to achieve the desired start and stop points.

c. Front Panel Controls. The operating controls (Fig. 19) are front panel push button switches and toggle switches, or external voltage signals from the data acquisition system, that can set the ramp rate divider register and control the initial and final values of a temperature-time history ramp. The data acquisition system monitors the temperature bridge outputs and has an operating control program that provides the control logic for sequencing a series of ramps and holds.

d. Up/Down Counter and Ramp Rate Clock. An up/down counter provides the 16-bit binary signals to control the D/A converter (see Figs. 19, 20 and 25). It counts up, down, or stop under control of external voltage or switch contact inputs. The count rate is controlled by a clock. The ramp clock rate is set by another digital binary counter that divides the source clock by numbers from 1 to 63 in unit steps. The division ratio is controlled by an externally set register. This register is monitored and set by the external data acquisition system prior to the start of any voltage ramp out of the D/A converter.

e. Comparator. This circuit (Fig. 21) is a high-gain, low-drift operational amplifier, LM108A, operating as a voltage comparator. One input is connected to the filtered output of the temperature bridge; the other input is connected to the output voltage of the controlled reference digital to analog converter plus the proportional band triangle wave signal (Fig. 24). The comparator output is on or off and provides drive to the switch mode power driver.

f. Power Driver. The power driver (Figs. 18 and 21) is a switching mode power transistor circuit that operates on the ground end of the heaters and completes the circuit through the heaters from the dc power supply. On-off switching times are in the microsecond range. The switching frequency is generated by the proportional band oscillator (400 Hz), and the duty cycle is controlled by the comparator output over the range of 0 to 100%. The power driver circuits also include

attenuators that provide conditioning of duty cycle signals and heater dc power for monitor by the exernal data acquisition system. The dc power for the heaters is provided by an adjustable, regulated dc power supply. The power supply must be capable of 150 Vdc at 10 A.

g. Bridge Supply. The bridge voltage supply (Fig. 22 and Fig. 23) consists of a buffered set of stable inverting operational amplifiers that provides plus and minus 6.4 V dc for the temperature sensors. The reference source for the supply is the voltage reference output of the D/A converter. Since this reference is also used as the reference for the variable voltage output of the D/A converter, the temperature bridge operates in a full bridge compensated mode.

h. Digital to Analog Converter. The D/A converter (Fig. 22) is a stable monotonic, 16-bit binary, voltage output D/A module. (Analog Devices. DAC HR16B). It provides the voltage reference for the bridge supply, and the variable output voltage controlled by the 16-bit binary signals from the up-down counter to the comparator reference. The comparator reference is generated by adding a chopper stabilized operational inverter (the D/A output voltage) and an adjustable triangle voltage (Fig. 24) for proportional band set. The comparator reference voltage ranges from 3.2 volts to 6.4 volts for a binary input ranging from 000000_8 to 177777_8. This allows a potential control range from +40°C to -80°C.

i. Container Heaters. The heater elements are thin film nichrome, in a bifilar configuration on a Kapton substrate. The heaters are located in the walls on each side of the freezing container. The heater resistance is 25 ohms. A photograph of the heater is shown in Figure 7.

j. Container Temperature Sensors. The temperature sensors are thin film nickel in a bifilar configuration on a Kapton substrate. The sensors are located in the walls on each side of the freezing container. The nominal resistance of the sensor, at 22°C, is 94 ohms. A photograph of the sensor is shown in Figure 7.

The power supplies for the controller circuits are shown in Figure 26.

D. INTEGRATED DATA ACQUISITION AND CONTROL (IDAC) SYSTEM DESCRIPTION

The Integrated Data Acquisition and Control (IDAC) data system was designed in 1966 as a general purpose digital data system for JPL's propulsion test programs. The IDAC includes real time data output and control capabilities. The analog input subsystem is typical of many digital systems in that it has 500 channels, 14-bit ADC, scan rates to 10 kHz, addressable gain, and channel selection. The system includes an 8K, 18-bit memory and 78 in/sec digital magnetic tape recorder. Real-time engineering data is provided by a printed paper tape, two video displays, and 16 digital

to analog converters. An engineering units capability includes ranging and scale factors for all standard transducers, thermocouple linearization, and data output unit definition. The system is able to limit check 64 data channels in real time. The IDAC also has a sophisticated digital data input capability. The digital input capability was used to provide the automatic control of the freezer. The operator supplies the freeze/thaw control parameters to the control system of the IDAC. The system temperature controller supplies a reference input to the digital system.

This digital reference input is compared with the freezer wall temperatures and the freeze/thaw control parameters. The result of the comparison is transmitted to the temperature controller which in turn sets the heater power of the freezer. The IDAC sets the rates of freezing and thawing, the start and stop temperatures and the hold times at the predetermined set points. The signal flow of the IDAC is shown in Figure 27.

E. SYSTEM CALIBRATION

The nickel sensors were calibrated by the JPL Standards Laboratory for resistance vs temperature. The temperature range of the calibration was from 22°C to -60°C and produced the following equation:

$$R = 83.699105 + 0.4065255\ T + 0.000373\ T^2$$

Calibration in the freezing system was accomplished by submerging the container in a distilled water-ice bath. When the system reached equilibrium, the bridge excitation voltages were adjusted to produce a 0°C output from the data system. The system was also checked by submerging the container in room temperature water. The T_o thermocouple was used as a reference standard for these measurements. This is a type E thermocouple and was calibrated by the JPL Standards Laboratory and found to be within .01% of the laboratory standard from 22°C to -60°C.

The heater resistances have a nominal value of 24.3 ohms at 0°C. This value was adjusted by a computer program, using the nichrome temperature vs resistance table, to produce an accurate measurement of each heater power. This is necessary since the heater temperatures were essentially the same as those of the control sensors, and changed with the cooling and warming protocols.

1. Data Printout

The typical output data presented in the following figures are obtained through an acquisition process conducted by the IDAC and which results in the data being stored on magnetic tape. A special program, modified from existing software, was prepared to accept this data, provide the necessary calibration and produce three listings of

the data in appropriate units. Typical examples of these listings are shown in the following figures. The first column of each listing is the time during the test in hours, minutes, and seconds, (HH:MM:SS).

Figure 28 presents the basic temperature and power data taken at one second intervals during a portion of a test. The temperatures T_{A3}, T_{A2}, and T_{A1} are on the outside wall of the container adjacent to the cooling bath, within the package wall and at the interior face adjacent to the sample mass respectively. The temperatures T_{B3}, T_{B2}, and T_{B1} are in similar positions on the opposite wall of the container. The temperature at the center of the sample mass is T_o. The temperature set as a voltage within the controller to define the required temperature for a given protocol is T_{REF}. The power dissipated in the container wall heaters is given as P_A and P_B.

Figure 29 presents data characteristic of the system performance. The term (T_o-T_{REF}) indicates the difference between the actual temperature as measured at the center of the sample mass and that set by the controller. This is a measure of the overall ability of the controller to influence the temperature of the least responsive area of the sample mass. The term indicates the effects of thermal inertia, and phase change, as well as sensor and thermocouple calibrations. The value of (T_o-T_{A1}), is the gradient from the center of the sample mass to the surface of the sample mass on the (A) side. The term (T_o-T_{B1}) is similar except on the (B) side. These terms also reflect the sensor calibrations and are useful for indicating the velocity of the wave front during phase change as well as the thermal conductivity of the sample mass.

The terms $(T_{A2}-T_{A3})$ and $(T_{B2}-T_{B3})$ are the differences in the temperature between a plane within the container wall and one at the exterior surface where the container wall comes into contact with the coolant. These terms provide a measure of the heat transfer through the container walls and establish the thermal conductance of the walls used to evaluate the thermodynamic properties of the sample mass. Approximate values of these thermal conductances are calculated and presented in the columns under the title K_A and K_B of Figure 29. They are "effective" values which are true measurements of the exterior wall conductance only under conditions of steady state. Under transient conditions, their perturbations from the true value may reflect conditions of non-equilibrium due to thermal inertia or phase change. The final column, average power, is that calculated by taking one-half of the sum of the power from the (A) and (B) side heaters. This term is used for plotting the thermodynamic cycle presented by each protocol in the test data section of this report.

Figure 30 presents data of general engineering interest. The term $(T_{A1}-T_{REF})$ indicates the control system's ability to produce changes in an area of maximum sensitivity to the control heater, i.e., at the sample mass/container wall interface. Typical data for steady state conditions are shown as curve (a) of Figure 32.

Because of the importance of making accurate measurements of the outer wall conductance, a second indication of the temperature gradient across the outer wall of the container is available by a differential measurement. These values are presented as "Measured" (T_{A2}-T_{A3}) and "Measured" (T_{B2}-T_{B3}). They can be used for a more detailed analysis of the data.

The term "Heater Source" (E3) is used in the calculation of the power dissipation in heaters (A) and (B) and is the square of the power source voltage. The adjacent column is the calculated resistance used for heaters (A) and (B) and which is obtained from the appropriate calibration curve as a function of temperature. The column labeled "Shorted Channel" is the effective temperature produced by an unused channel, shorted near the experimental freezer. It therefore is an indication of the noise from the cable, the multiplexer scanner, the multiplexer amplifier, and the A/D converter. These data are used to indicate the failure of any major part of the control and acquisition system which processes data in parallel. Noise levels indicated here can be directly added to the performance curves of Figure 31a but are negligible.

2. Steady-State Operation

Curve (a) of Figure 31a presents the difference between the steady-state thermocouple temperature as measured in the center of the sample mass (T_o), and that established by the controller (T_{REF}). The data was obtained for water but should be typical for any sample mass. Examination indicated that this error was consistent and could be removed from the measurements. An approximate correction can be made to curve (a) of Figure 31a with the following equation

$$(T_o - T_{REF})_{corrected} = -9.8271 \times 10^{-4}\, T_{SET}^2 + 1.0654 \times 10^{-2}\, T_{SET} - 1.344 \times 10^{-1} + (T_o - T_{REF}).$$

With this correction, the maximum error is 0.2°C as shown in Figure 31b. This correction is not applied to the test data presented in this report and consequently it will appear that a hold at a low temperature will be in error a few degrees.

Curve (b) in Figure 31a shows the difference between the temperature measured at the B sensor (T_{B1}) and that set by the controller (T_{REF}). This is an indication of the control capability of the system and does not involve the sensor calibration. The curve is repeated on a magnified scale as curve (a) of Figure 32 which shows that there is less than 0.15°C error in steady state temperature control and this error is greatest at the higher temperatures. In the range below 0°C, a more important area for thermal control, this error is less than 0.10°C.

Curve (b) of Figure 32 shows the difference between the temperature requested of the control system (T_{SET}) and that interpreted by the control system as the desired set point (T_{REF}). The difference

is an indication of the inability of the control system to read and establish the proper set point. Since the error has an approximate dc level around +0.05°C, it may be possible to remove some of that error through a bias of the temperature submitted to the controller. If the error of curve (b) is due only to the dead band of the controller, then adjustment may not be possible.

Curve (c) of Figure 31a is the net error between the desired steady-state temperature (T_{SET}) and that measured at surfaces of the sample mass (T_{A1}) and (T_{B1}). The (A) face temperatures are indicated by the open triangles and the (B) face by the solid ones. Curve (c) is the maximum expected error of the control system in producing a repeatable steady state temperature. If a bias of the (T_{SET}) can be made to correct for the error shown in Curve (b), then the error indicated in Curve (c) may also be reduced by an equivalent amount. In addition, the characteristic system noise level of the IDAC system is monitored in each test by calculation of the equivalent temperature of an unused and shorted channel as shown in Figure 30. This level is always less than +0.005°C.

3. Dynamic Operation

In the transient thermal condition, control effectiveness must be defined by considering the influence of the container and sample mass thermal inertia. In the design of the present container, a trade-off was made which sacrificed the low thermal inertia of the container for the ability to determine the heats of phase change, the thermal conductivity and the specific heats of the sample mass. This was done by adding sensors in each wall of the container. The ability to obtain these properties makes the system unique and extremely attractive as a research tool for the development of protocols for freezing and thawing biological tissues.

Typical real-time recorded plots of temperature and power versus time for distilled water are shown in Figures 33 and 34. These are the first-order calibrated data. The plots were made on an X-Y plotter with Y as temperature or power and X as time. The curve identified as ($T_{o(1)}$) presents part one of the sample mass temperature-time history. At the end of this plot the recorder was reset so that the final time history could be plotted. This is labeled as ($T_{o(2)}$). The curve ($T_{o(1)}$) presents the cooling history from +20°C to -40°C at 11°C/min and the curve ($T_{o(2)}$) presents the subsequent warming history, returning to the initial temperature at the same rate. In a similar manner the curves ($P_{A(1)}$) and ($P_{A(2)}$) present the initial and final histories of the power dissipation of the (A) face heater P_A. The curves are qualitative and meant to present the overall view of the test.

Curve ($T_{o(1)}$) shows an initial hold at a constant temperature of 20°C followed by a cooling ramp of 20°C/min. During the cooling ramp there is a sudden increase in temperature associated with a reduction in power. This is caused by the freezing of water, an exothermic process. Note from the position of the beginning and ending points of the ramp that the power curves ($P_{A(1)}$) and ($P_{A(2)}$) are shifted one unit to the right of the temperature

curves. Consequently the deviations of temperature and power occur simultaneously. This is an indication of the excellent response between the heaters and the sensor within the sample mass even though direct control of the heaters is by the sample mass surface temperature T_{A1} as indicated on the $T_{A(1)}$ curve. Upon resetting the time axis of the recorder after the temperature of -40°C is attained and held for 120 seconds, the warming history of the sample mass center is presented as curve ($T_{O(2)}$). Once again the change of phase is noted for both the temperature and power curves. This occurs during the melting process which is endothermic, therefore requiring additional heat to maintain a steady temperature rise. Finally the temperature is held at the starting value of +20°C.

Figure 34 presents the temperatures on either side of the sample mass for the same experiment presented in Figure 33. These are the temperatures under the direct control of the heaters. The temperature and power curves are shifted one horizontal unit from each other on the graph. Note the excellent linearity of the temperature ramp during cooling, and the elimination of the phase change temperature deviation from this ramp during the warming process. In the freezing process a small control loss becomes apparent because of the suddenness of the phase change from the supercooled state. In some tests where supercooling is minimal the freezing perturbation as seen here is not evident from the curve. Some investigators have claimed that the temperature of a finite mass can be controlled during the phase change. As is shown in Figures 33 and 34, this may be apparent for a portion of the mass, e.g., the surface in this case, but because of the finite thermal conductivity of the mass, it can not be true in general.

Figure 35 presents a thermodynamic cycle of the same test given in Figures 33 and 34. The temperature at the center of the sample mass (T_O) is plotted versus the average power of the heaters. Point one is the starting point of the cycle; the temperature is held at +20°C. As power is decreased the temperature is reduced in a non-linear manner until the thermal inertia of the system and mass is overcome. When this has occurred, there is a linear reduction of temperature with power until freezing of the sample mass begins. The actual freezing point of distilled water is 0°C, however supercooling can delay freezing until about -10°C. At this point there is a rapid decrease in power with an associated increase in temperature. As the phase change reaches completion, there is an increase in power to drive the sample mass temperature back to the controlled ramp followed by a second nearly linear ramp. Point two is the second hold point in the test and is obtained by an increase in power with little change in temperature again associated with the system thermal inertia. After holding for two minutes at point 2 the warming cycle was started. There is a nearly linear increase in temperature with power until about -5°C where thawing becomes evident and an increased power is required to provide the additional heat for melting. Finally, the system returns to the starting point and the test is concluded.

The area within the primary envelope of the cycle presented in Figure 35 is the hysteresis loss due to thermal inertia of the sample mass and its container. This area is a function of the starting and ending temperatures and, for a given sample mass, the rates of cooling and warming. This loss is described by measuring the lag between the control system's reference temperature and the response of the point in the sample mass of least sensitivity to temperature control, i.e., the sample mass center. To describe this dimension of the envelope the thermal inertia power (TIP) is defined as the average power measured at constant temperature for a given cooling or warming protocol. This measurement disregards deviations of the envelope due to phase changes. Figure 36 presents the relationship of TIP as a function of cooling or warming rate for distilled water. At present, the only significance for the TIP is that of a performance characteristic of the entire system. For detailed analysis, however, it may be a significant parameter in dealing with the sample mass performance during phase change. The relationship of the TIP to the temperature rate appears, within the accuracy of existing data, to be the same for all sample masses considered thus far. This includes distilled water, 0.9% saline solutions, and packed red blood cells.

Figure 37 shows a method for describing the performance of the control cycle for the same test discussed in Figures 33 to 36. It describes a "worst case" condition, since it presents the difference between the reference temperature of the controller and the temperature of the center of the sample mass. Deviations from the primary envelope are due to phenomena resulting in maximum loss of control, i.e., phase changes. The general shape of the primary envelope is an indicator of the thermal inertia of the system. Because the data in the figure are not corrected as shown in Figure 31b, the value of the function does not remain at zero but varies to positive and negative values. This plot is interesting because it tends to amplify the phase change as an event in the cycle and may be useful for the determination of other events during the detailed analysis of red blood cells or other biological media.

F. WATER TEST RESULTS

1. Freezing Water

The freezing of water is an exothermic (heat release) process that theoretically occurs slightly below the ice/water equilibrium temperature of 0°C. Pure bulk water, in the absence of ice crystals however has to be supercooled to -10°C before freezing occurs. Ordinary water containing foreign bodies freezes from about -6°C to -25°C.

Once ice begins to form, the latent heat must be removed from the sample to insure continued phase change. This is the cause of the temperature excursions seen in Figures 33, 34, 35, and 37. This heat removal may occur from heat transfer a) through the supercooled liquid phase under a temperature gradient directed toward the freezing

interface or b) through the solid phase under a temperature gradient in the ice. Any motion of the ice/water front is conditioned by thermal conduction of the system to a heat sink. Cooling rate and rate of ice formation is determined by the temperature gradient in the water or the ice. Both cases mentioned above are seen to occur in the experiments presented in the following figures.

2. Test Data For Distilled Water

Freezing and thawing tests were conducted with pure distilled water to arrive at a better understanding of the behavior of the system during temperature control and the sample mass during phase change. Figures 38a to 38d show data recorded during an experiment in which the temperature of the water was reduced in steps from +20°C to -60°C as noted on Figures 38a and 38b, and subsequently increased back to +20°C at a constant rate of +2°C/min. as shown in Figures 38c and 38d. Each step was held for a period of 2 minutes and cooling occurred between steps at a rate of 1°C/minute. Two curves are plotted on Figure 38a. T_o is the temperature at the center of the sample mass (water) and T_o (1), T_o (2) and T_o (3) present a sequential temperature history for this point. P_A is the power dissipated in the (A) side heater and is also presented sequentially. Each point on $P_A(1)$ corresponds in time to each point on $T_A(1)$ with the P_A curves shifted one unit to the right. Since these curves are for qualitative study, the vertical axis is not calibrated, although temperature can be inferred from the hold points. In all cases, each major unit on the horizontal axis is 50 seconds as indicated in Figure 38a.

Freezing occurred during the cooling between the steps at 0°C and -5°C. This is shown in Figure 38a by noting the increased temperature in the $T_o(1)$ curve and the decreased power in the $P_A(1)$ curve. Because of the tight temperature control of the T_{A1} and T_{B1} sensors, this phase change is not apparent in Figure 38b. This was not the case for the experiment described in Figure 34 where both T_{A1} and T_{B1} indicated phase change at the same cooling rate for the curve of Figure 38a. This difference is attributed to the fact that the Figure 34 test allowed the water to supercool to -10°C before freezing. The associated change in the sample mass temperature was too sudden to allow control. This is seen by the sudden drop in heater power as shown in Figure 33. In contrast, the apparent temperature control of T_{A1} and T_{B1} as indicated in Figure 38b and the small deviation in the value of $T_o(1)$ in Figure 38a resulted from less of a demand on the heater as indicated by the more gradual changes in the heater power $P_A(1)$ as shown during the phase change in Figure 38a. Consequently the intuitively predictable result is that the lesser the degree of supercooling prior to phase change, the greater is the apparent temperature control of the sample mass. The term "apparent temperature control" is used because a temperature gradient must always exist in the sample mass in order to exchange the heat of phase change. Nevertheless, allowing this change of phase to occur over a longer period of time as was the case shown in Figure 38a, appears to reduce the temperature gradients within the sample

mass and consequently allows the appearance of being under better thermal control. Because of published evidence that indicates reduced freezing damage to cells undergoing phase change under minimal supercooling, the control and measurement of the supercooling/phase change phenomena as just discussed is of considerable importance in the study of cellular freezing.

Figure 38e presents a plot of the center temperature, T_o, versus the average heater power. Points 2-11 indicate points where a constant temperature/power setting was held for a period of 120 sec as indicated in Figure 38a. Point 1 is the start of the test and point 12 is the end. The hold points do not fall on the cooling curve due to the thermal mass of the container and the sample (water). The freezing process occurs between points 3 and 4. Thawing occurs in nearly the same temperature range on the warming curve.

It has already been mentioned that the test of Figures 38a-38d showed freezing under a reduced supercooling condition compared to that of Figure 33. This is shown more clearly by considering the same two tests as indicated by the comparison of Figure 35 with 38c and Figure 37 with 38f. It is readily apparent from the temperature excursions during freezing indicated in Figures 38e and 38f, that this case experienced a reduced gradient within the sample mass. This condition is easier to note by comparison of the temperature/power cycles than by the temperature or power time histories, and presents a valid agrument for consideration of the cyclic process plots.

The remaining water test experimental data are presented in Appendix D. There is no discussion of this data but they are included for the purpose of completeness of this report. They add no new concepts to those already presented but they do support the conclusions obtained on the performance of the system.

G. SALINE TEST RESULTS

1. Freezing Saline

When ice forms in a salt solution, the crystals are pure water. As the temperature is lowered below this, the dissolved saits become concentrated until all the water that can be crystallized as ice freezes leaving only the solutes and their water of hydration. Further reduction in temperature results on the solidification of the remaining solution. The lowest temperature at which the solution remains liquid is called the eutectic temperature. For NaCl solutions, this is -21.8°C. The concentration of solute necessary to achieve this minimum temperature is the eutectic concentration.

2. Test Data For Saline

Figures 39a through 39f present data typical of the freeze/thaw tests conducted with 0.9% NaCl solution (physiological saline). As in

the discussion of the distilled water experiments, the data are presented in plots of actual test data and thermodynamic cycle of temperature versus power.

Figures 39a to 39d present the time histories of T_o, P_A, T_{A1} and T_{B1} for the cooling and heating phases of the test. The test is similar to that accomplished for distilled water with the exception that the -60°C hold point is not included in the plots. The hold points were for a duration of 120 sec. and the cooling rate between hold points was 11°C/min. As in the water experiments, the warming rate was at 2°C/min.

In Figure 39a the exothermic freezing process is seen to occur during the -10°C hold point. The sample mass center temperature (T_o) rise during $T_o(2)$, occurs simultaneously with the sudden power decrease shown during $P_A(2)$. After this occurrence, there is no further indication of sudden phase change activity.

Figure 39b shows the T_{A1} and T_{B1} temperatures during the cooling phase of the experiment. The phase change was not apparent on this plot. It is obvious from Figure 39a however that the sample mass temperature was not held at a constant -10°C as may be erroneously concluded from Figure 39d but varied considerably as indicated by the gradient between T_o of Figure 39a and T_{A1} or T_{B1} of Figure 39b.

Figure 39c presents the T_o and P_A time histories for the warming phase of the experiment. The endothermic phase change occurs slowly over a period of about 200 sec. During this time the temperature is seen to drop below the desired control ramp indicated by the dashed line, and the power is seen to slightly increase above its nominal ramp for the given warming rate. The temperature decrease below the desired ramp is a measure of the gradient across the sample mass since no apparent temperature deviation appears at the control sensors T_{A1} and T_{B1} as seen in Figure 39d.

Figure 39e presents the sample center temperature T_o as a function of the average heater power in a fashion similar to Figure 38c. The freeze phase change occurs at the -10°C hold point and the thaw appears as a subtle bend in the warming curve near 0°C.

Figure 39f is analogous to Figure 38f, representing the temperature differential between the sample mass center temperature (T_o) and the reference temperature which the system is attempting to reach. The large difference in this value during the non phase change process is because the data calibration is approximate and the corrective equation (Figure 31b) was not applied. The important point of the plot is the large excursions which occur during the freeze and thaw phase changes, once again indicating that this correlation may be an excellent method to analyze the phase changes of a complex biological media.

The remainder of the saline test data are presented in Appendix E.

H. RED BLOOD CELL TEST RESULTS

1. Freezing Red Blood Cells

The quality of freeze-preserved blood products has improved significantly over the past 10 years. The increasing use of these products in medicine has been encouraging but still falls short of their full potential. The high cost of processing red blood cells through the freeze preservation protocol and with the use of cryoprotectants is most likely the reason for the lack of use of this method. In an attempt to reduce this cost, a system has been built for the conduct of research on red blood cells without the use of cryoprotectives.

The literature on the freezing of red blood cells is quite complex and, in some cases, contradictory. Consequently, no attempt is made in this study to describe the biochemical and mechanical changes associated with the cells but to show that an effective device has been produced to accurately control the temperature-time history of the cells and to yield certain thermodynamic properties of the cells as a function of temperature.

2. Test Data For Red Blood Cells

Fresh blood was drawn in 10 cc vaccutainers containing 1 cc of acid citrate dextrose (ACD). The blood was centrifuged in the vaccutainers at 3000 rpm for 3 minutes to separate the red cells. Cells to be used in each test were aspirated from the center 5 cc of each vaccutainer. The cells were transferred to the test apparatus by syringe. The container and transfer apparatus were flushed with 0.9% saline solution and finally with ACD prior to cell transfer.

Potential cell damage due to the transfer of packed cells with this method was studied by aspirating the cells from the freezer/container after allowing the cells to rest in the container for 30 minutes at room temperature. After aspiration, the cells were placed in a vaccutainer rinsed with ACD and containing 5 cc of 0.9% saline. After mild agitation, the sample was centrifuged at 3000 rpm for 3 minutes. No noticeable hemolysis was indicated, thereby assuring minimal cell mechanical damage due to the transfer protocol.

Figure 40a presents the center temperature (T_o) and the A surface power (P_A) histories of a typical test with packed red blood cells. The initial temperature hold point was set at 15°C. A cooling ramp at 10°C/min. was conducted until a temperature of -5° was met. The temperature of -5°C was held for nearly 350 sec. during which the phase change occurred. A second cooling ramp at 10°C/min. was then conducted to a temperature of -40°C. This

temperature was held for 120 sec. after which a warming ramp of 10°C/min. was conducted to a temperature of -1°C. Prior to reaching this point the ice began to melt. This is seen by the slow change in the T_o (3) curve as it approached -1°C and by the slow return of the power curve P_A (3) to a steady state condition. During the 400 sec. hold at -1°C, the phase change continued. Finally, a second warming ramp at 10°C/min. was established. This stimulated the final melting as indicated by the nonlinear temperature curve and the increased heater power. The test concluded at the temperature of +15°C.

The response of the sample volume center temperature to control and the obvious occurrences of phase change during freeze and thaw are excellent examples of the application of the control system to the thermodynamic study of freeze preservation of biological media.

Figure 40b presents the sample volume center temperature versus the heater average power in a thermodynamic cycle for the entire test presented in Figure 40a. Note that the phase change occurs at the hold point (2). Cooling then continued to the second hold point at (3). The thawing of ice begins to appear during the warming phase prior to reaching the hold point (4) as shown by the nonlinear behavior of the curve. After leaving hold point (4), the non-linear behavior continues to show a phase change. The test ends at the starting point, (1).

Figure 40c is a thermodynamic cycle for the same test but presenting the difference between the sample center temperature (T_o) and the controller reference temperature (T_{REF}) as a function of the average heater power. This differential temperature is an indication of the dynamic temperature control of the system and is exaggerated during any phase change. Again note the excursions which occur during the hold at (2), and immediately before and after the hold at (4). In this case the excursion prior to the hold at (4) is even more obvious than the preceding graphs. This cycle analysis approach as applied to the identification and location of phase changes, may prove to be quite useful for future research in freeze preservation techniques.

Similar plots for the remainder of the red blood cell tests are presented in Appendix F.

Approximate tests for the presence of hemolysis were conducted on some of the experiments. These were accomplished by mixing the aspirate from the test apparatus with an equal volume of 0.9% saline, centrifugation at 3000 rpm for 3 min., and visually checking the supernatant for discoloration. The results were categorized into 3 qualitative descriptions of severe, moderate and slight as indicated in Figure 41. The intent of these tests was not to prove or disprove the efficacy of a particular protocol but to show differentiation for the tests where freezing damage was obviously present. Note from Figure 41, cases 7, 13, 14 and 15, that the mere occurrance of a phase change was not sufficient to result in severe hemolysis. In cases where no phase change occurred, however, as in 1-6, 8, and 11, slight or no hemolysis was always indicated.

SECTION III

CONCLUSIONS

Considerable effort has been made to understand the performance of the system. This has been done in order to produce a precise method for the study of freeze/thaw protocols of biological tissues. These tissues exhibit complex and in many cases, unknown changes with temperature. The ability to make accurate and precise measurements of the heats of phase changes as well as of the thermal conductivities and specific heats will relate directly to the understanding of these changes. The system that presently exists is not just a blood freezer. It is an instrument to study the cryogenic behavior of complex substances of organic or biological nature.

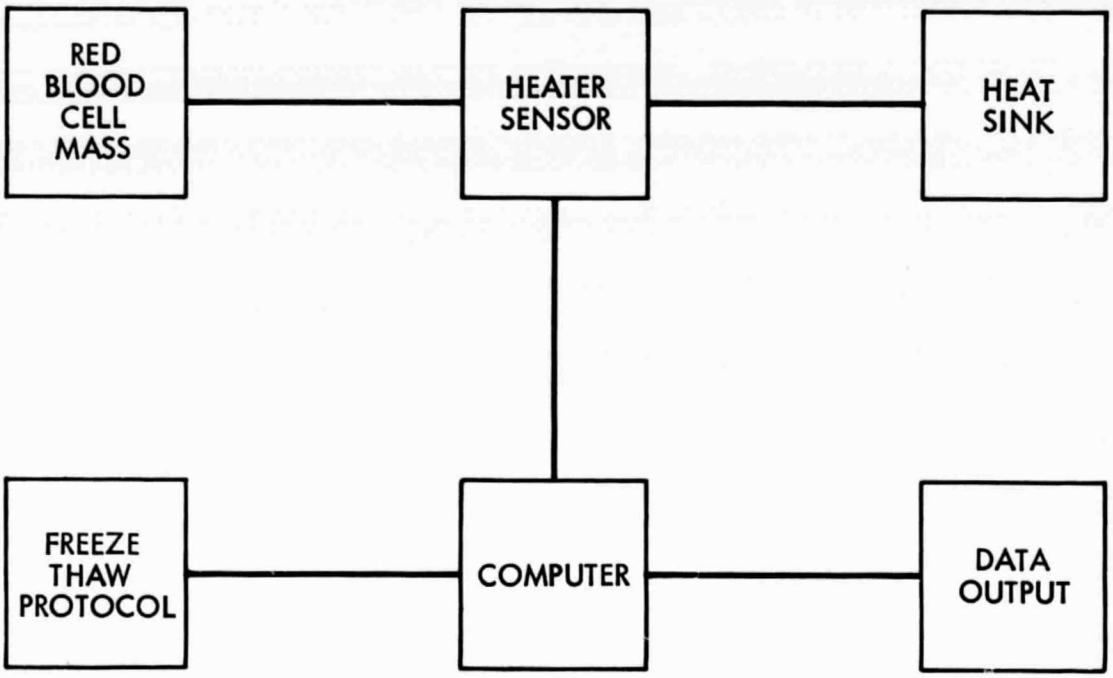

Figure 1. Basic Design Concept

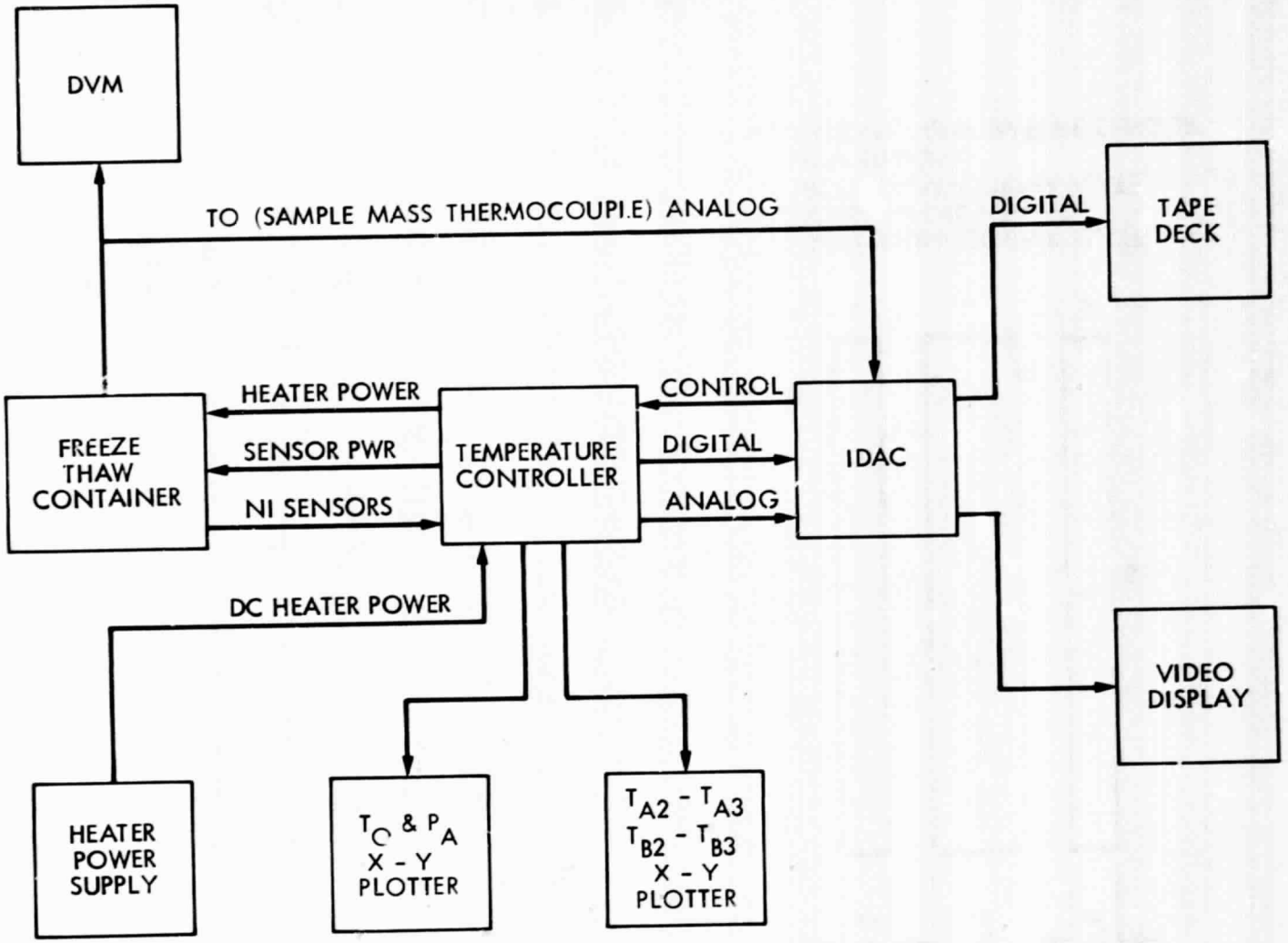

Figure 2. System Block Diagram

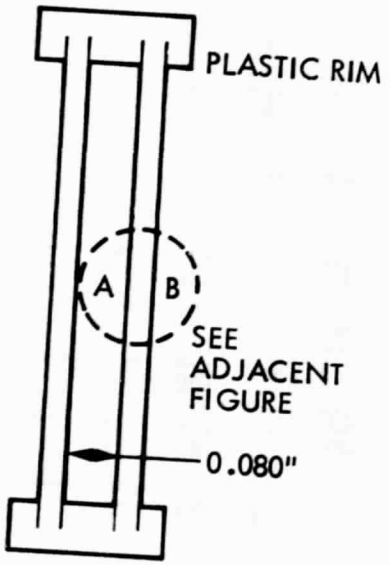

PLATE DIMENSIONS: 4" x 6"
INTERNAL VOLUME: 31 cc

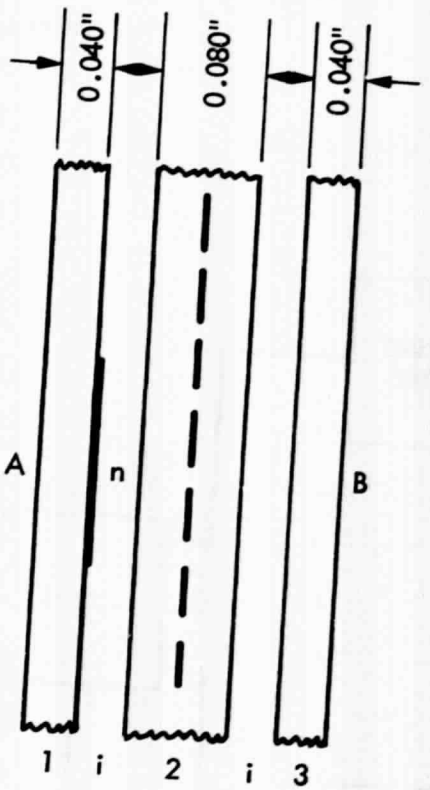

1. BERYLLIUM-COPPER PLATE
2. RUBBER-FOIL HEATER
3. BERYLLIUM-COPPER PLATE
i. RTV 60 BOND
n. NICKEL TEMPERATURE SENSOR

Figure 3. Model I Configuration

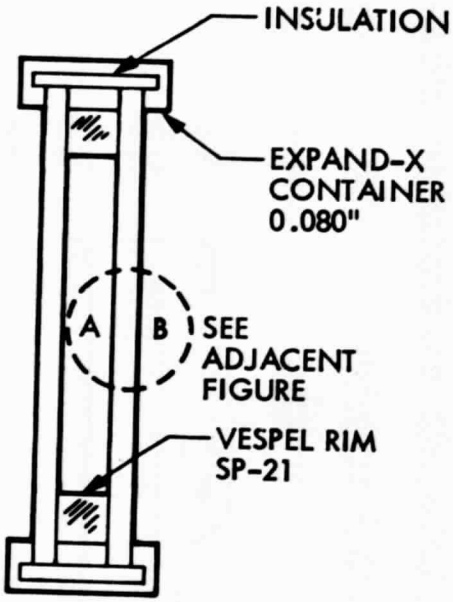

PLATE DIMENSIONS: 4" x 6"
INTERNAL VOLUME: 31 cc
VESPEL VOLUME: 9.0 cc

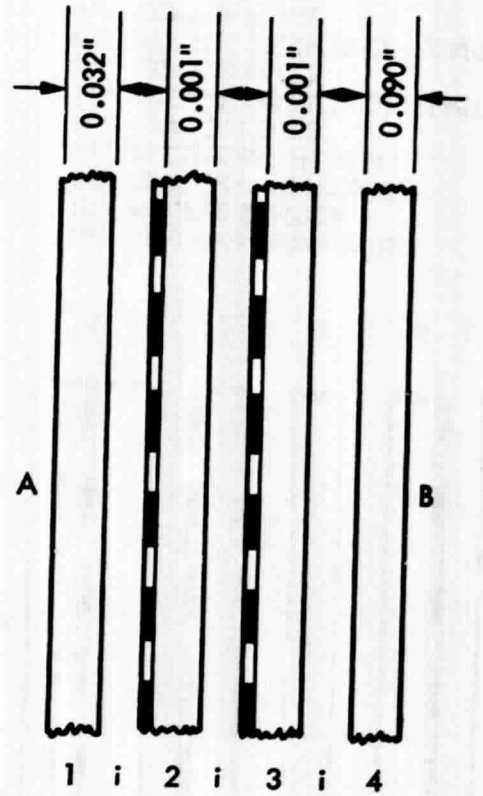

1. ANODIZED ALUMINUM PLATE
2. NICKEL FOIL SENSOR ON KAPTON
3. NICKEL FOIL HEATER ON KAPTON
4. ANODIZED ALUMINUM PLATE
i. M-BOND 610

Figure 4. Model II Configuration

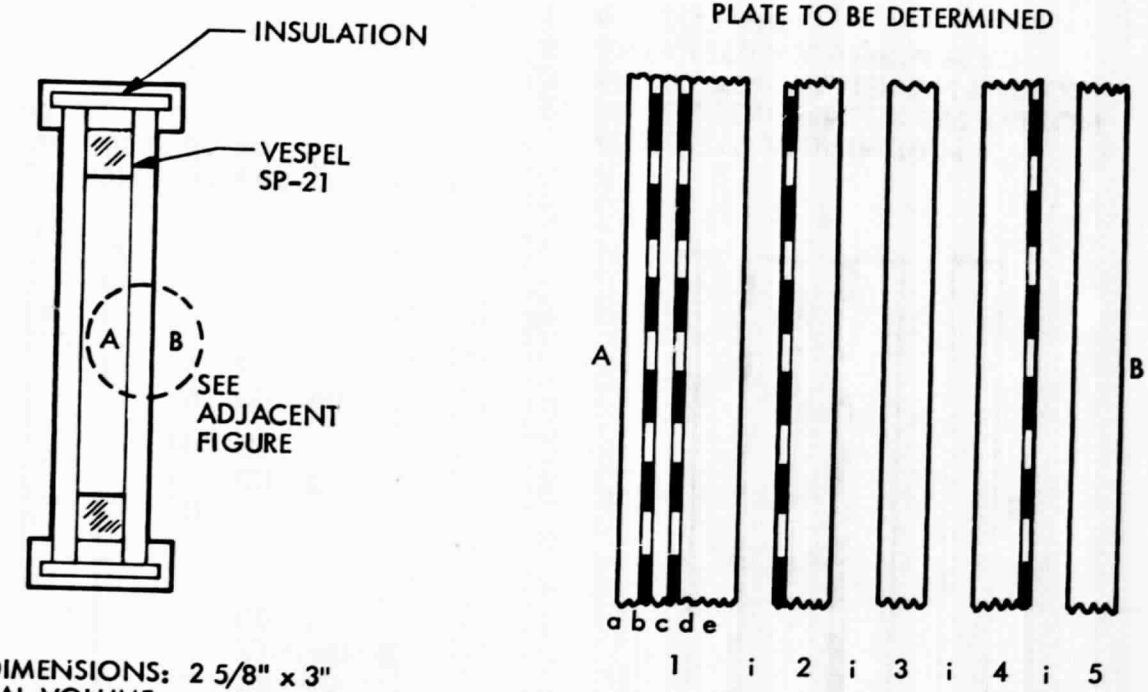

Figure 5. Model IIIA Configuration

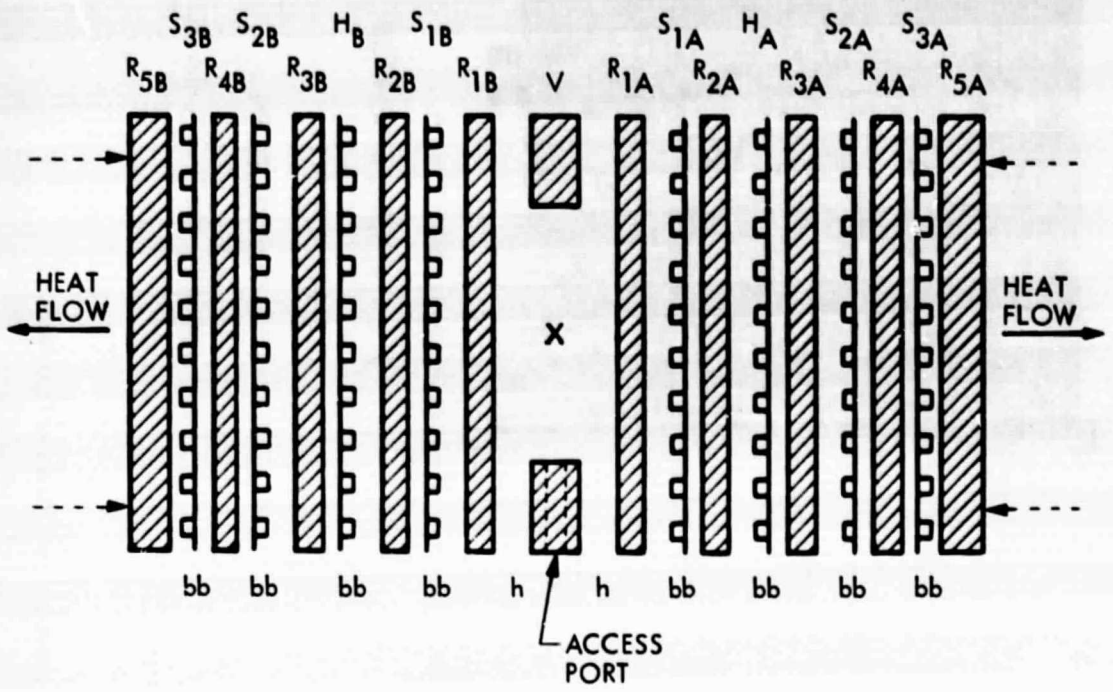

V = VESPEL SP21

R_{1-5} = ALUMINUM PLATES, HARD ANODIZED

S_{1-3} = NICKEL TEMPERATURE SENSORS WITH KAPTON BACKING

H = NICHROME HEATER WITH KAPTON BACKING

X = LOCATION OF THERMOCOUPLE AT CENTER OF MASS TO BE FROZEN

S_1 = CONTROL SENSORS

S_{2-3} = HEAT FLUX SENSORS

Figure 6. Model III Configuration

7 cm x 8.5 cm HEATER ELEMENT

1.0 MIL NICH ROME

25 Ω PER SECTION

1.0 MIL KAPTON BACK

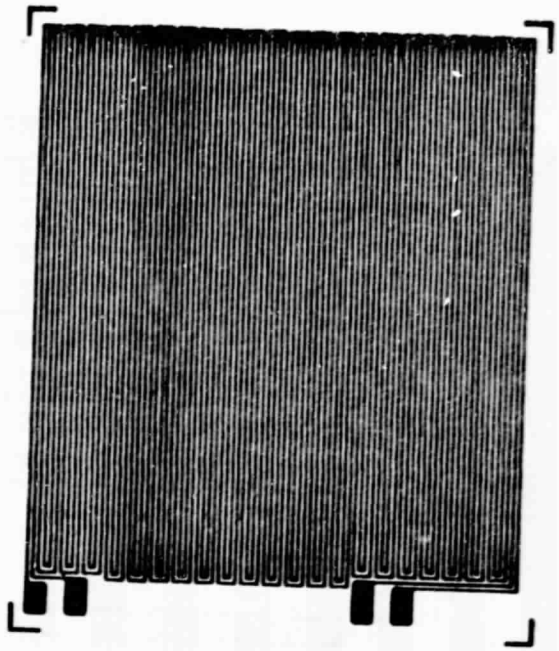

7 cm x 8.5 cm SENSOR

0.5 MIL NICKEL

47 Ω PER SECTION

1.0 MIL KAPTON BACK

Figure 7. Model III Heater and Sensor Elements

ORIGINAL PAGE IS
OF POOR QUALITY

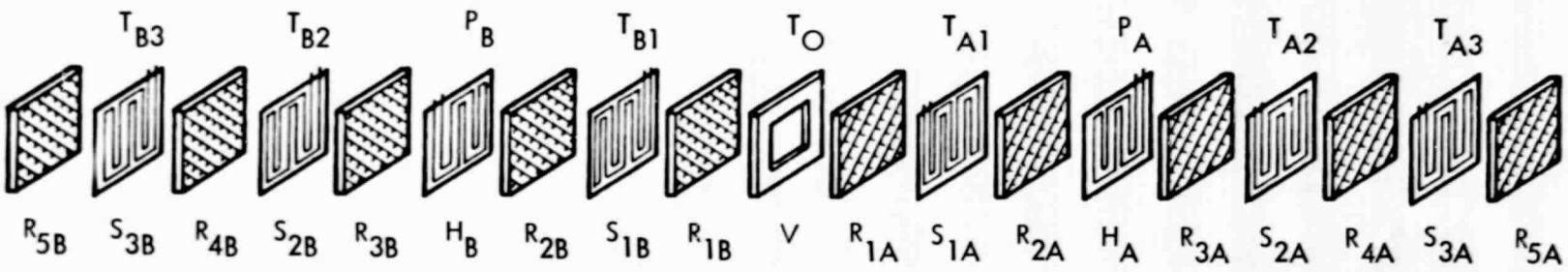

Figure 8. Detailed Model III Wall Element Identification

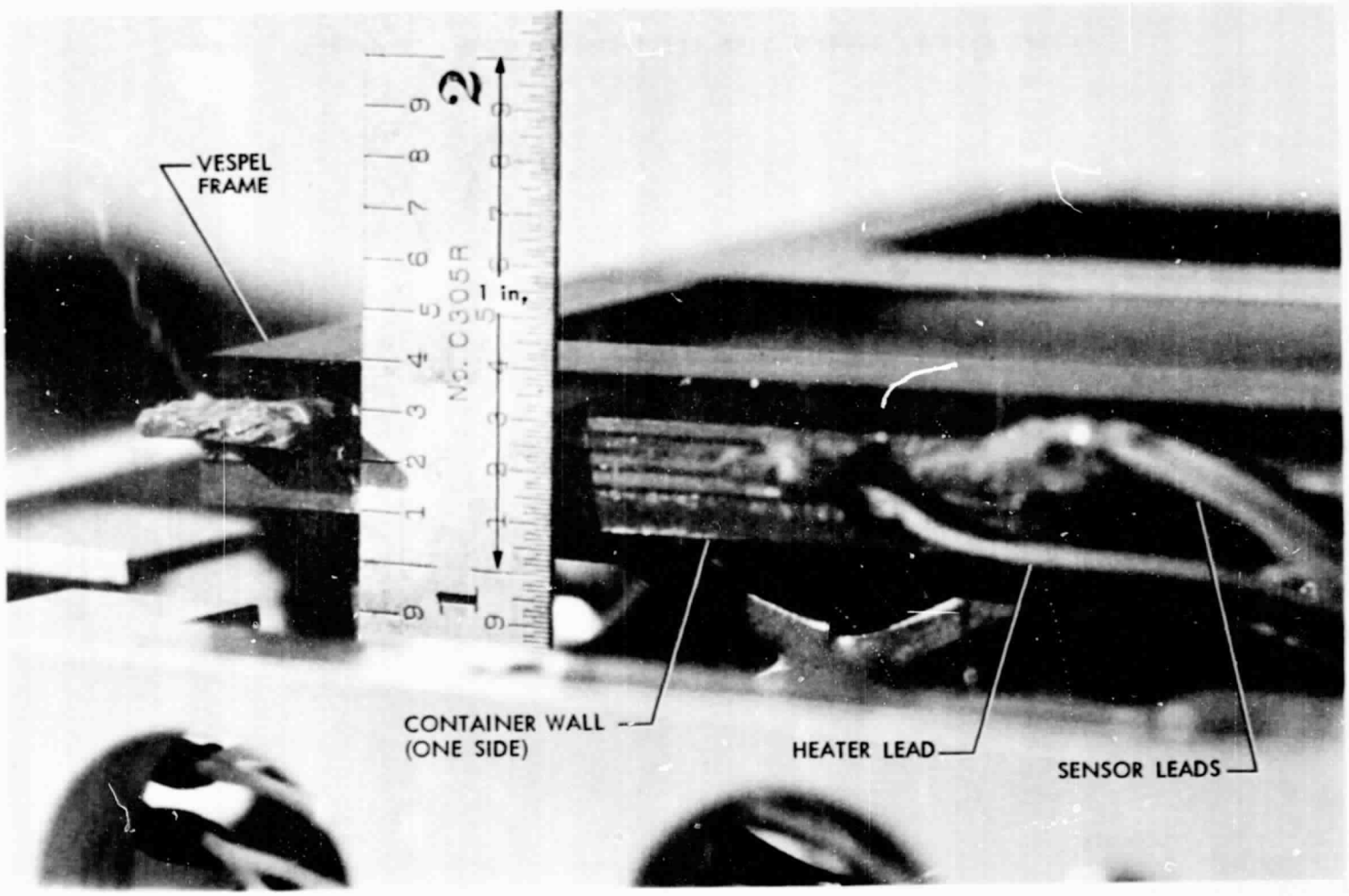

Figure 9. Programmable Freeze/Thaw Container for Biological Cells: Wall Side View

ORIGINAL PAGE IS
OF POOR QUALITY

ORIGINAL PAGE IS
OF POOR QUALITY

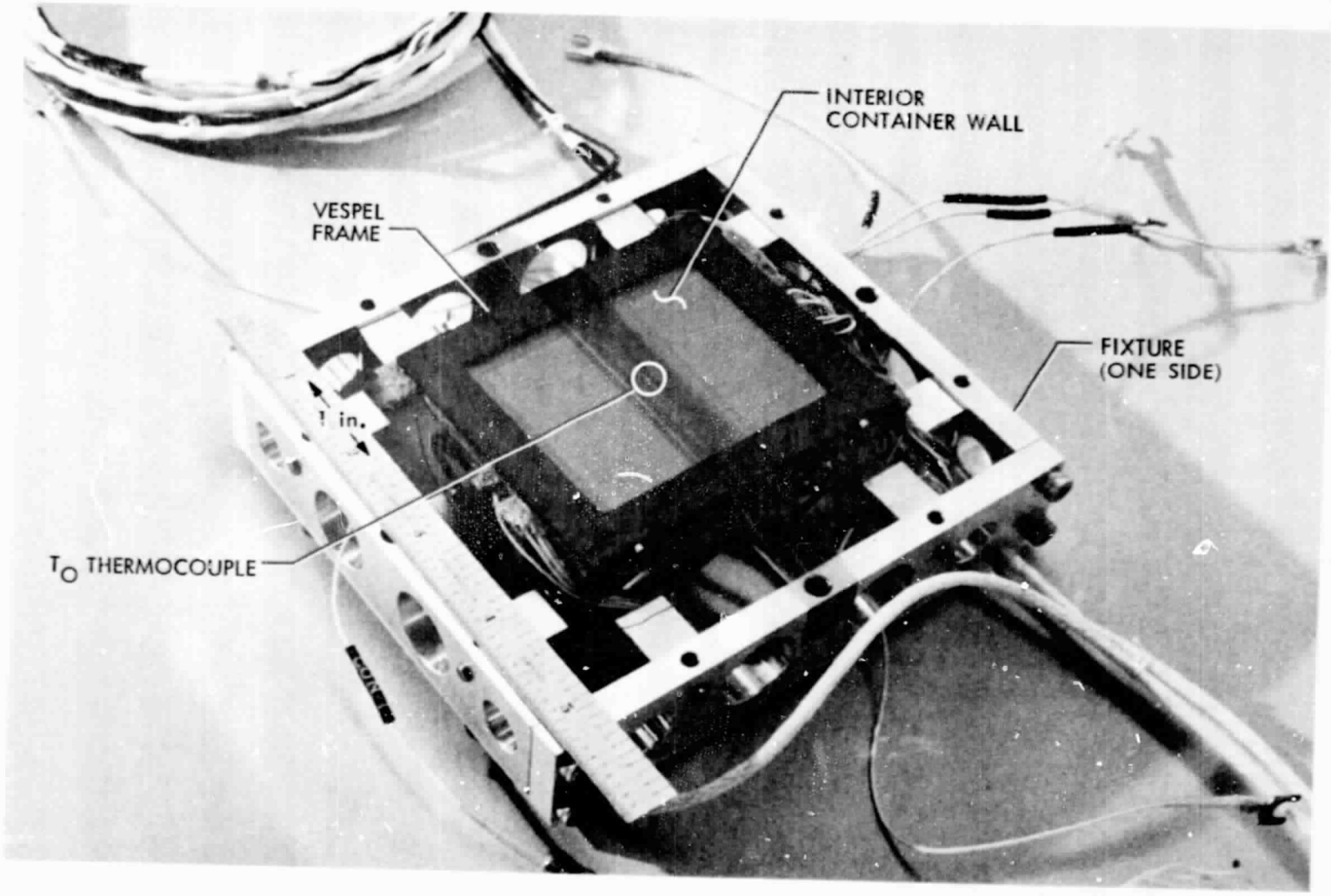

Figure 10. Programmable Freeze/Thaw Container for Biological Cells: View of Interior Wall

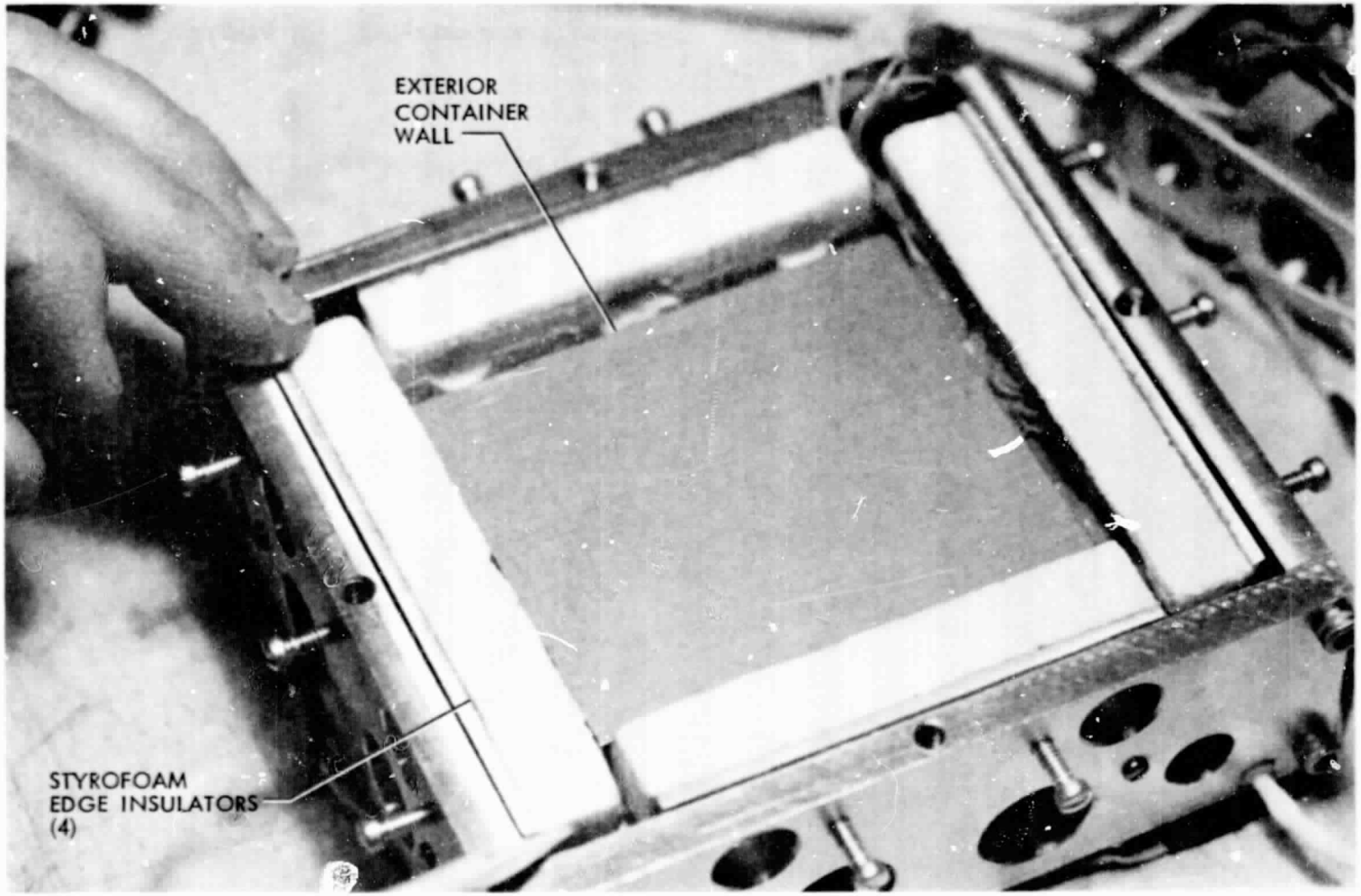

Figure 11. Programmable Freeze/Thaw Container for Biological Cells: View of Exterior Wall

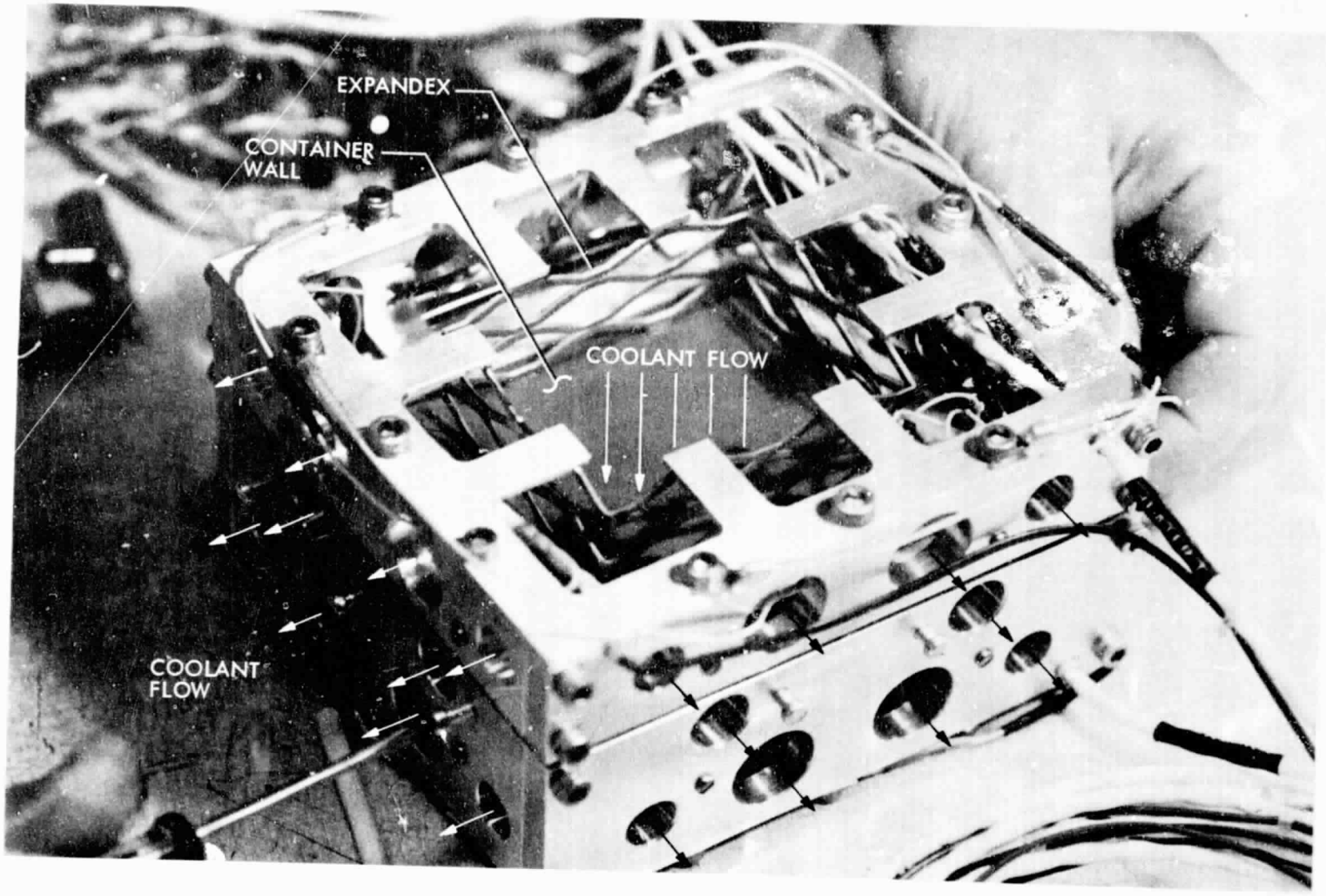

Figure 12. Programmable Freeze/Thaw Container for Biological Cells: View of Fixture

ORIGINAL PAGE IS OF POOR QUALITY

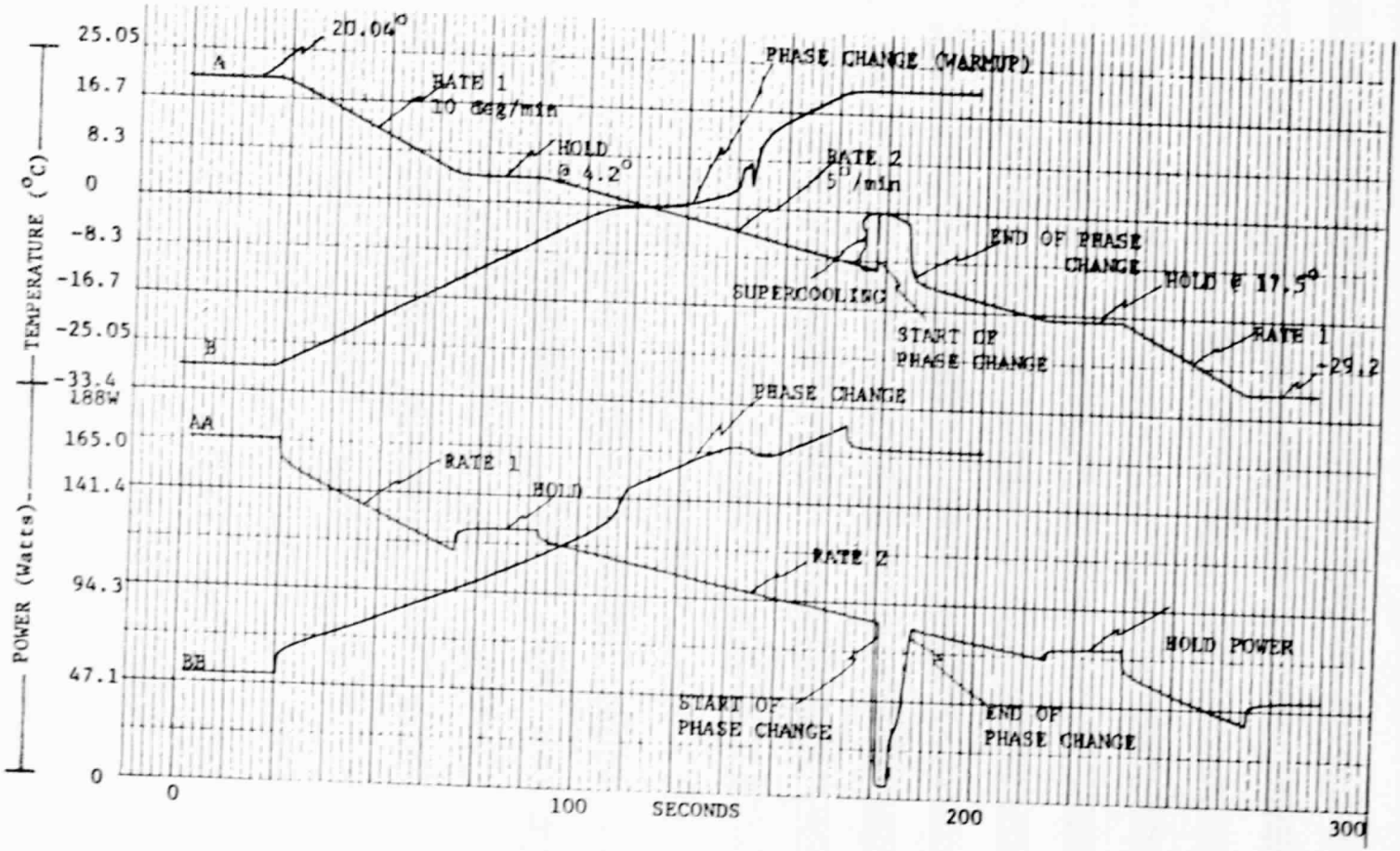

CURVE A Shows the COOLDOWN instantaneous temperature at T_0 thermocouple at center of mass.
AA Shows the instantaneous power in the heater corresponding in time to curve A.
CURVE B Shows the WARMUP instantaneous temperature at T_0 thermocouple at center of mass.
BB Shows the instantaneous power in the heater corresponding in time to curve B.

Figure 13. Cooldown and Warmup Characteristics with Distilled Water

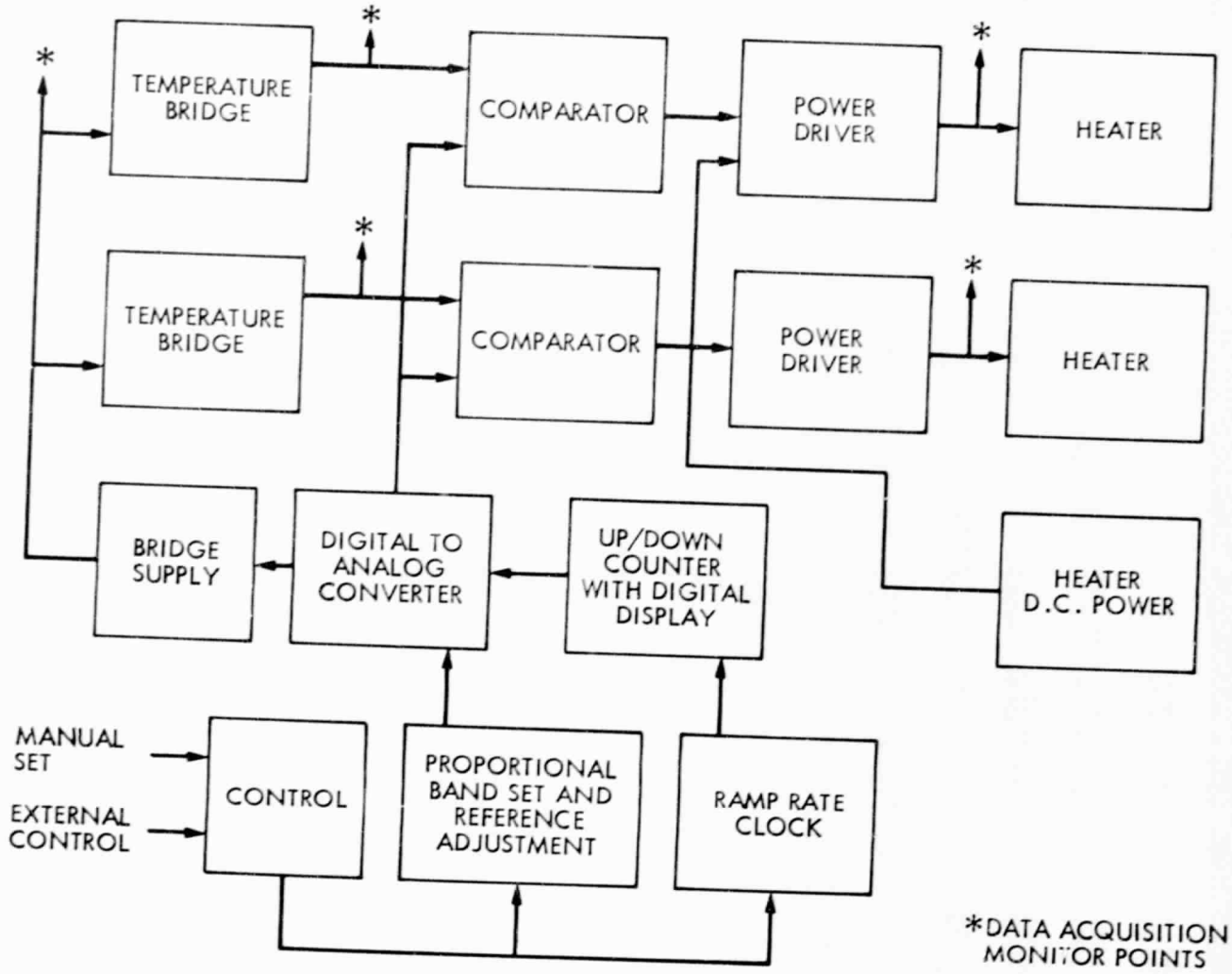

Figure 14. Data System Temperature Control Block Diagram

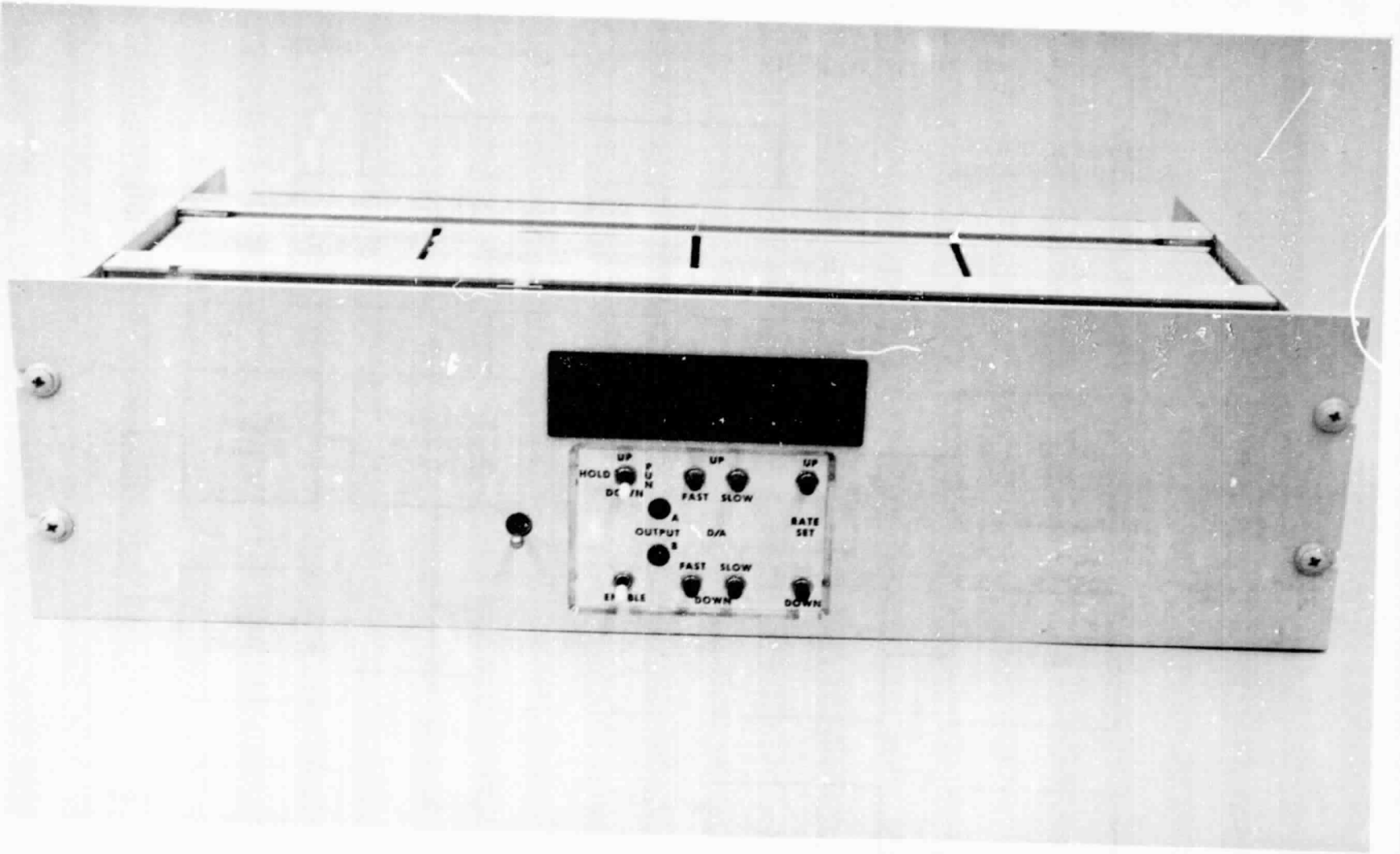

Figure 15. Temperature Controller, View 1

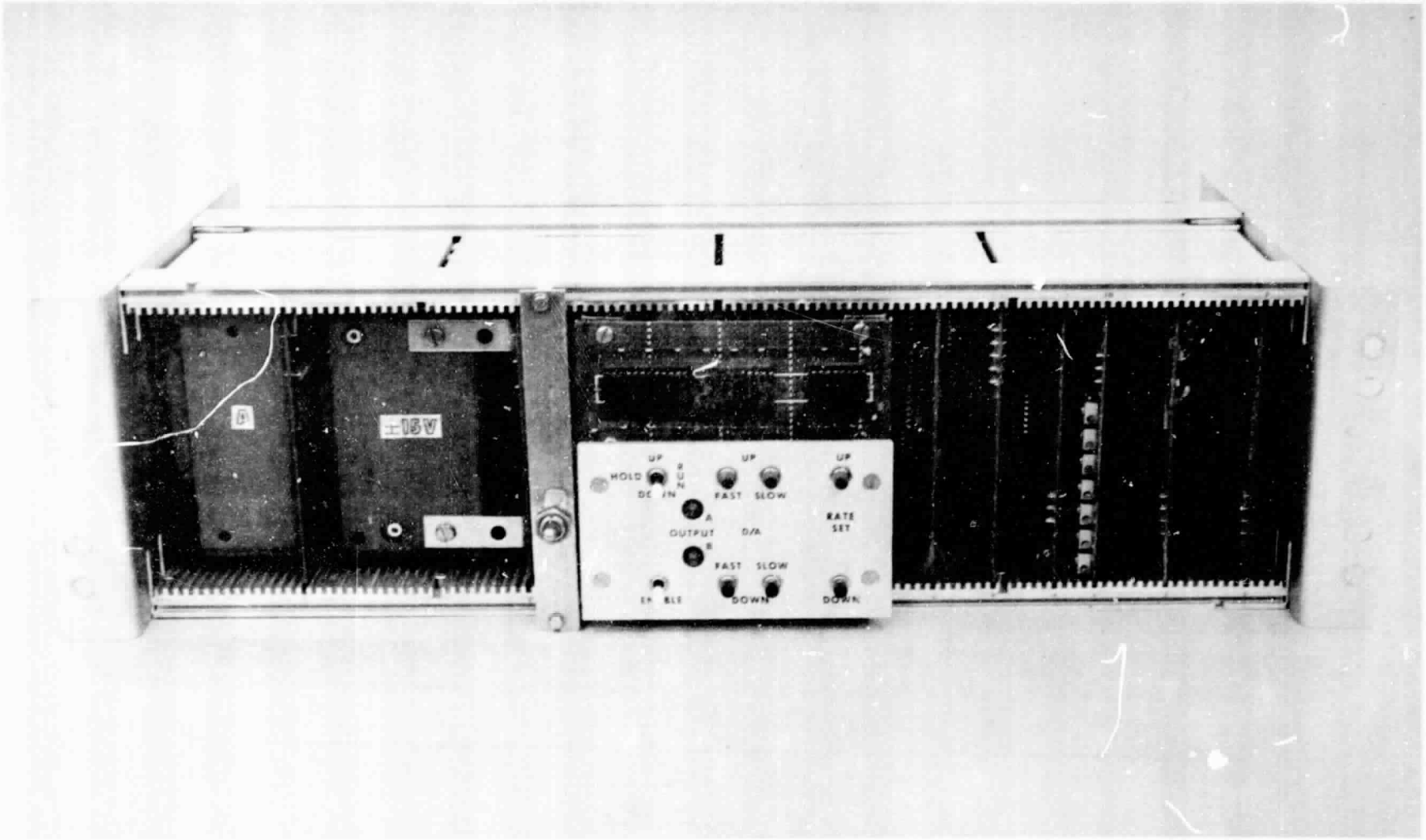

Figure 16. Temperature Controller, View 2

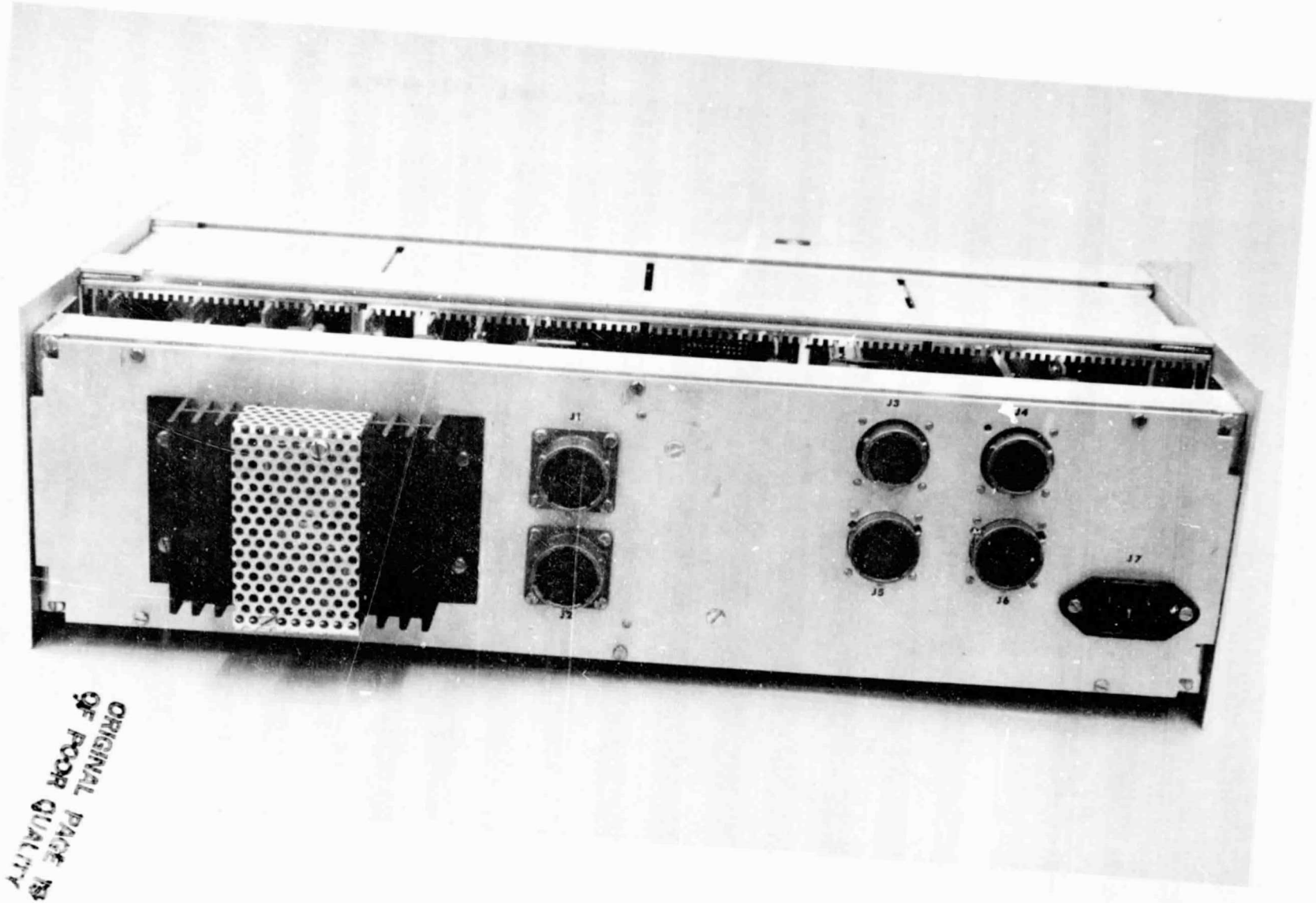

ORIGINAL PAGE IS
OF POOR QUALITY

Figure 17. Temperature Controller, Back View

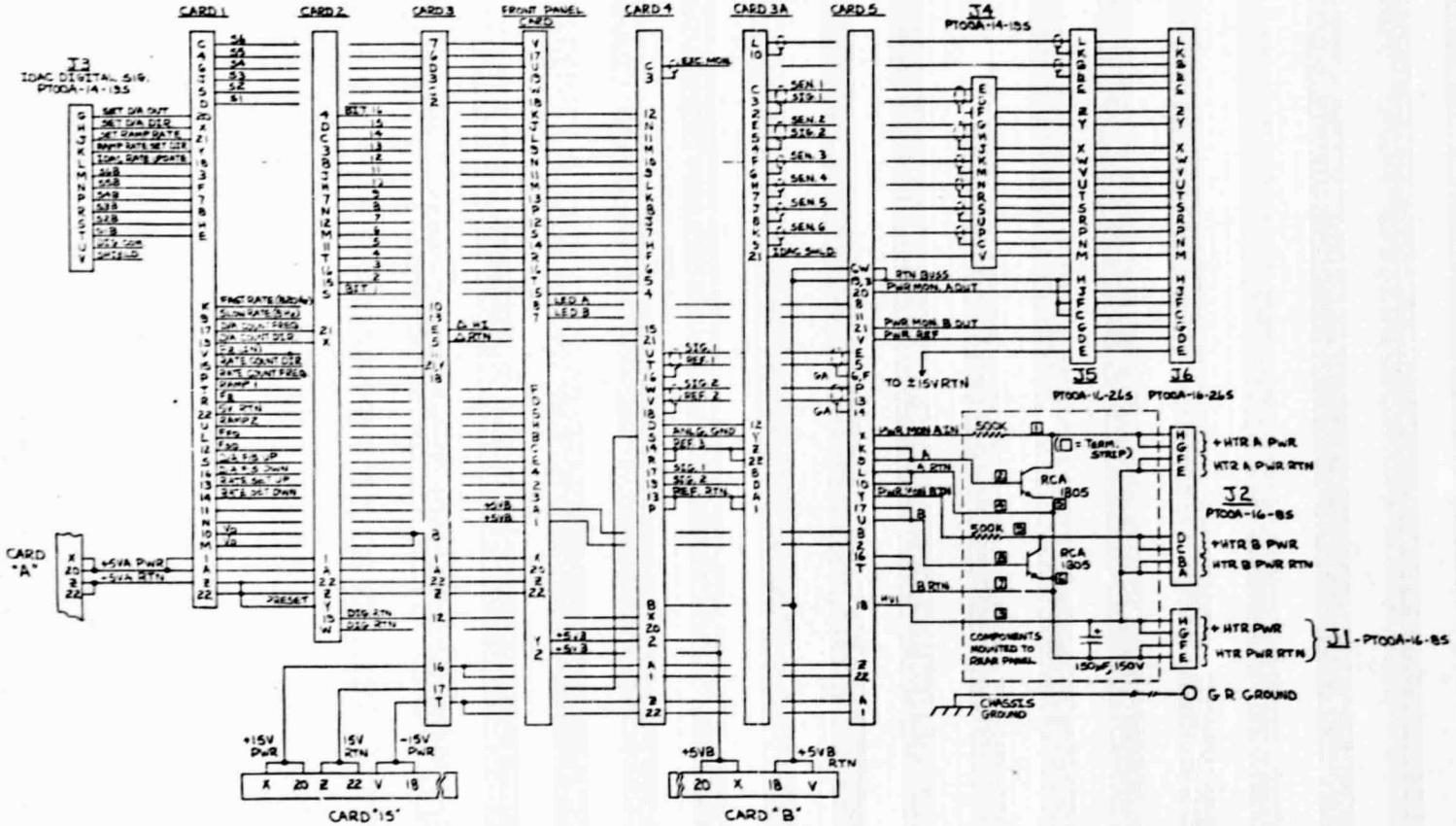

Figure 18. Inter-Card & Connector Schematic: Power Drivers

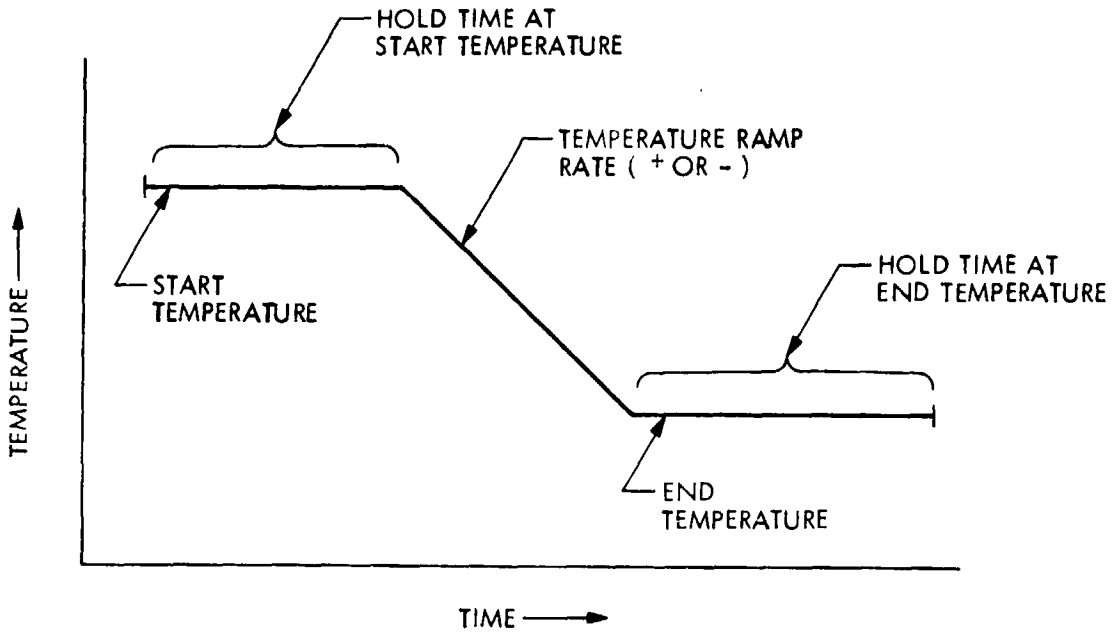

Figure 18a. Composite Subprogram Element for Temperature Control Protocol

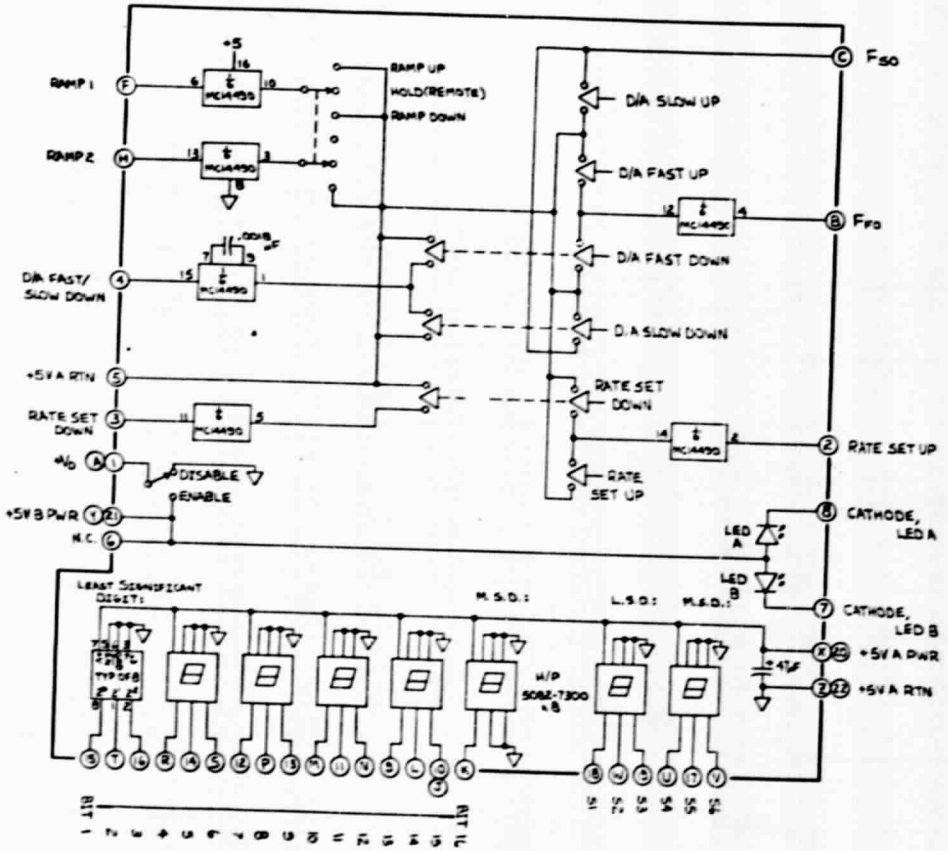

Figure 19. Front Panel Card

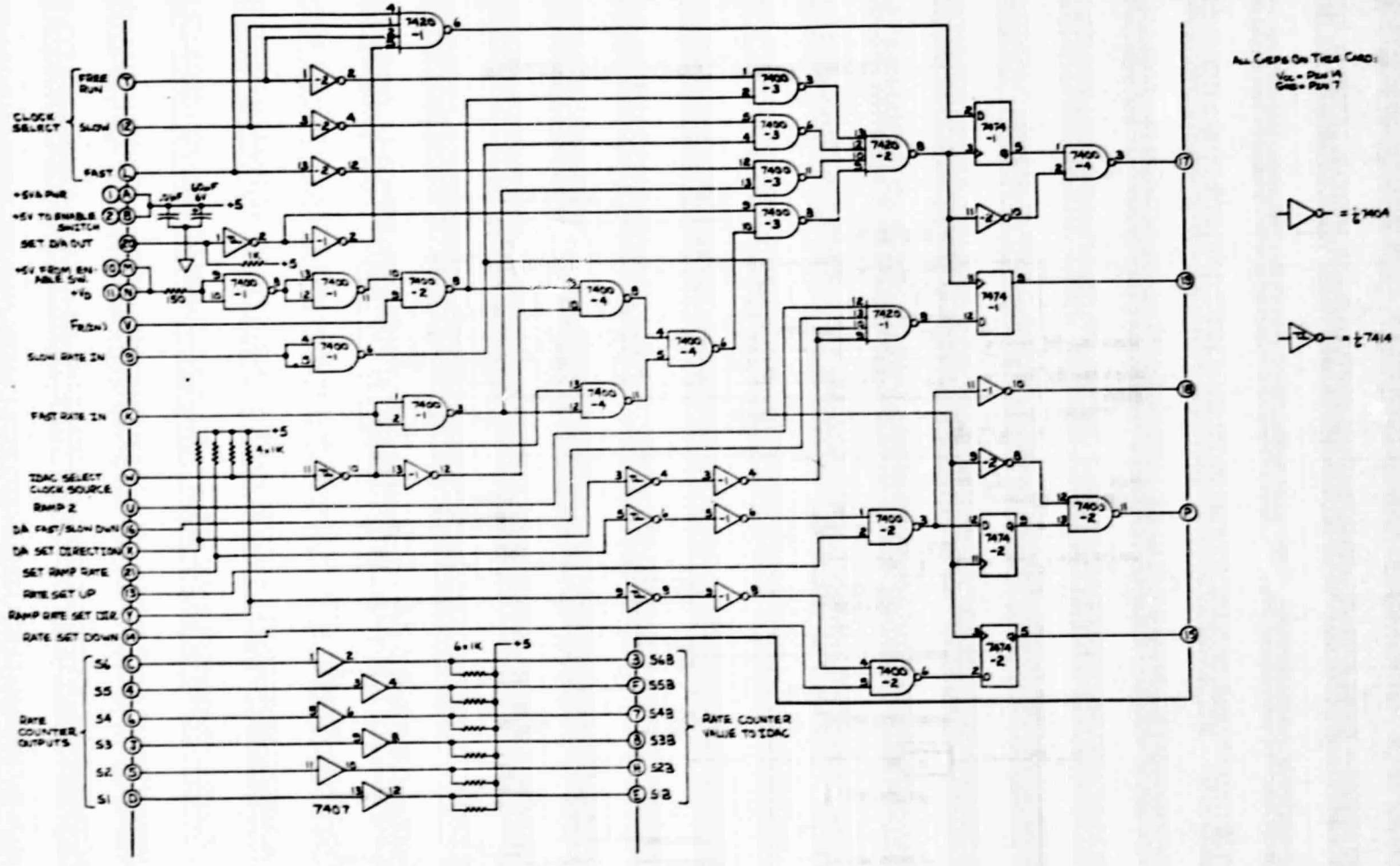

Figure 20. Card #1: Rate Counter

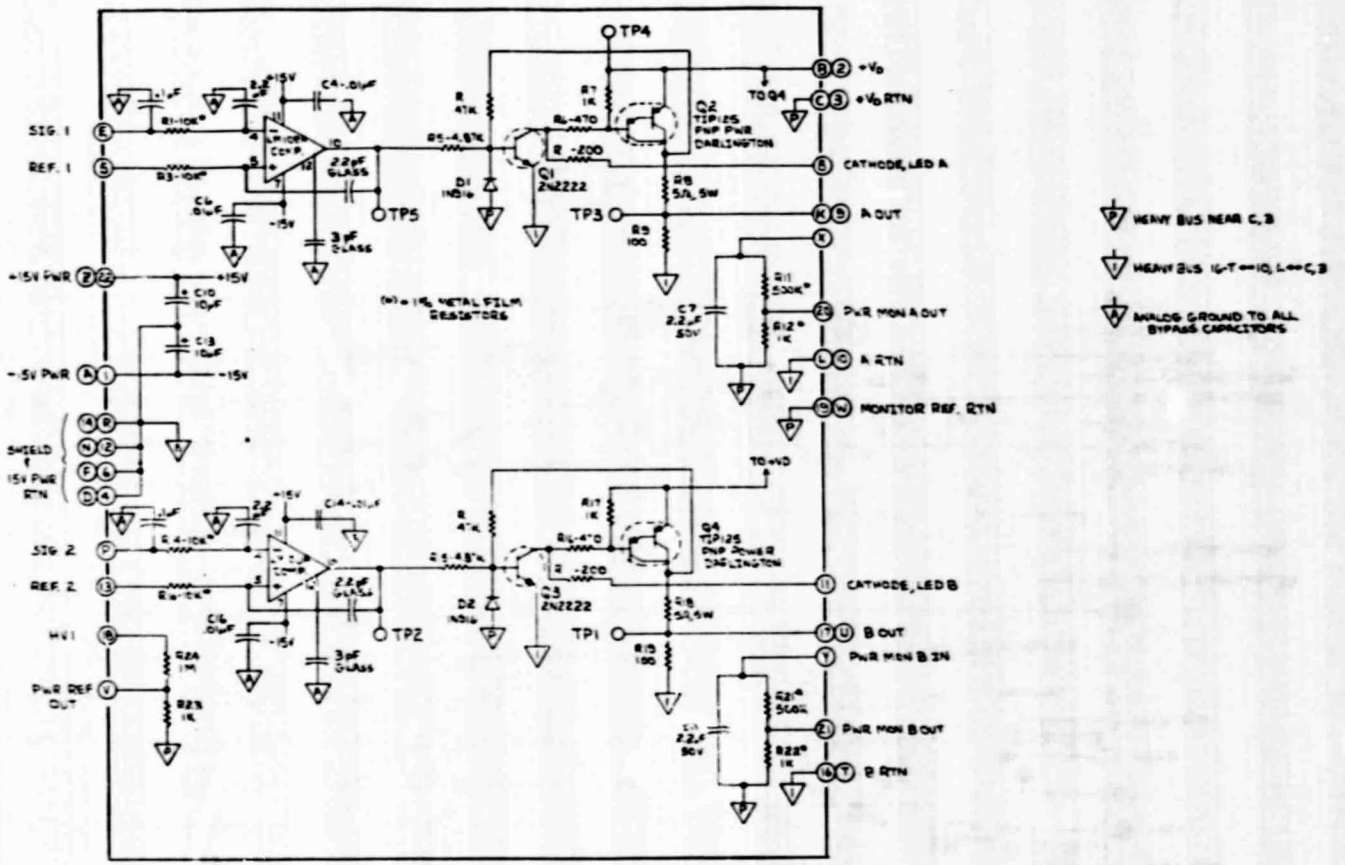

Figure 21. Comparators and Power Driver Switches

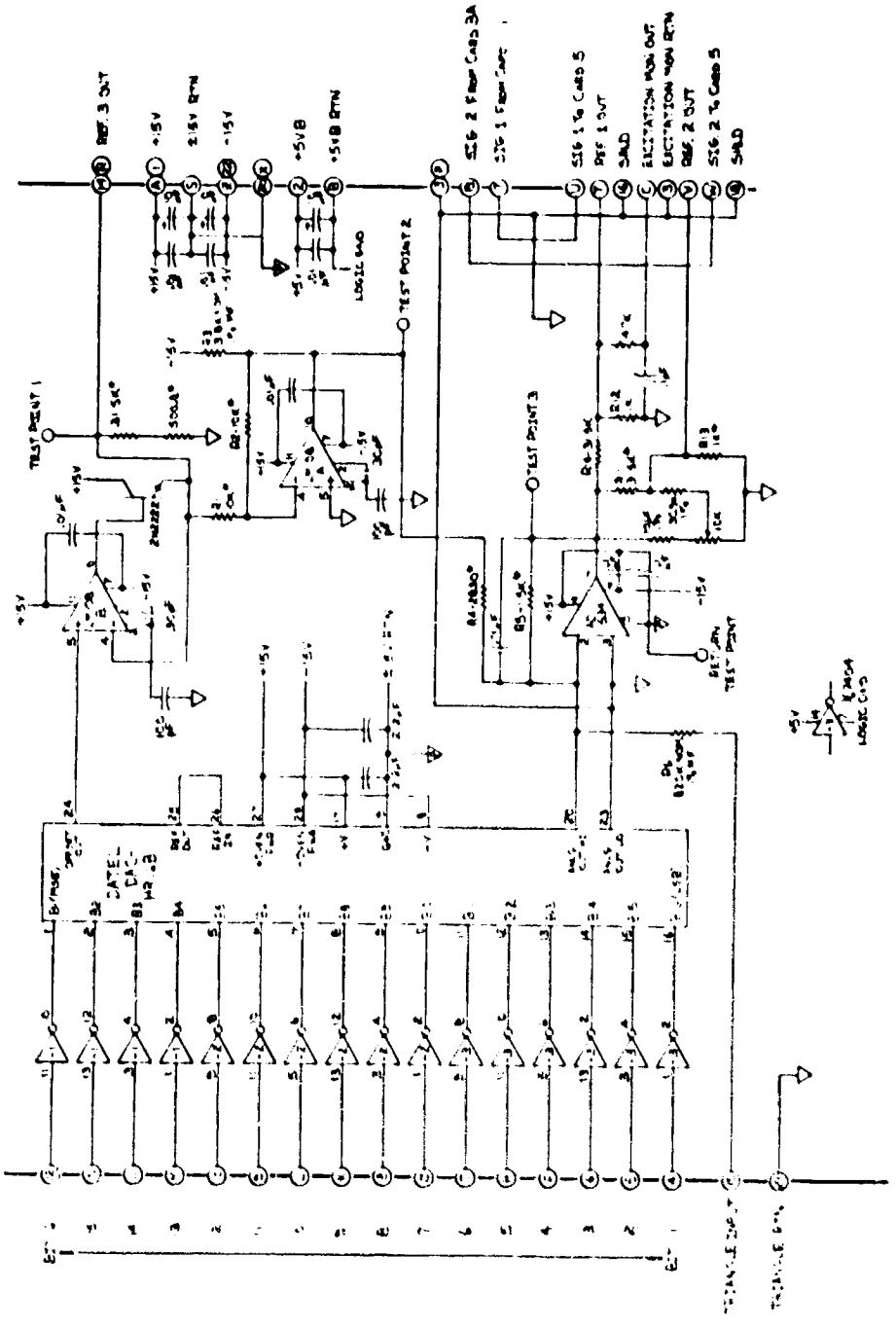

Figure 22. Card #4 D/A Converter and Sensor Excitation Supply

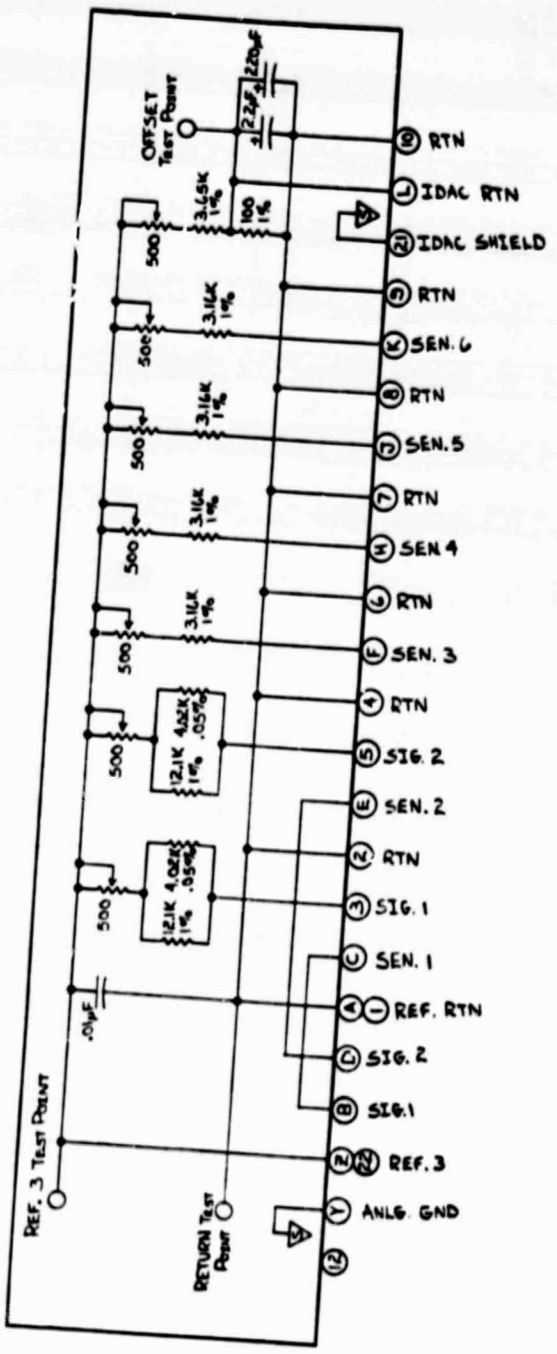

Figure 23. Card #3A Sensor Excitation Distribution

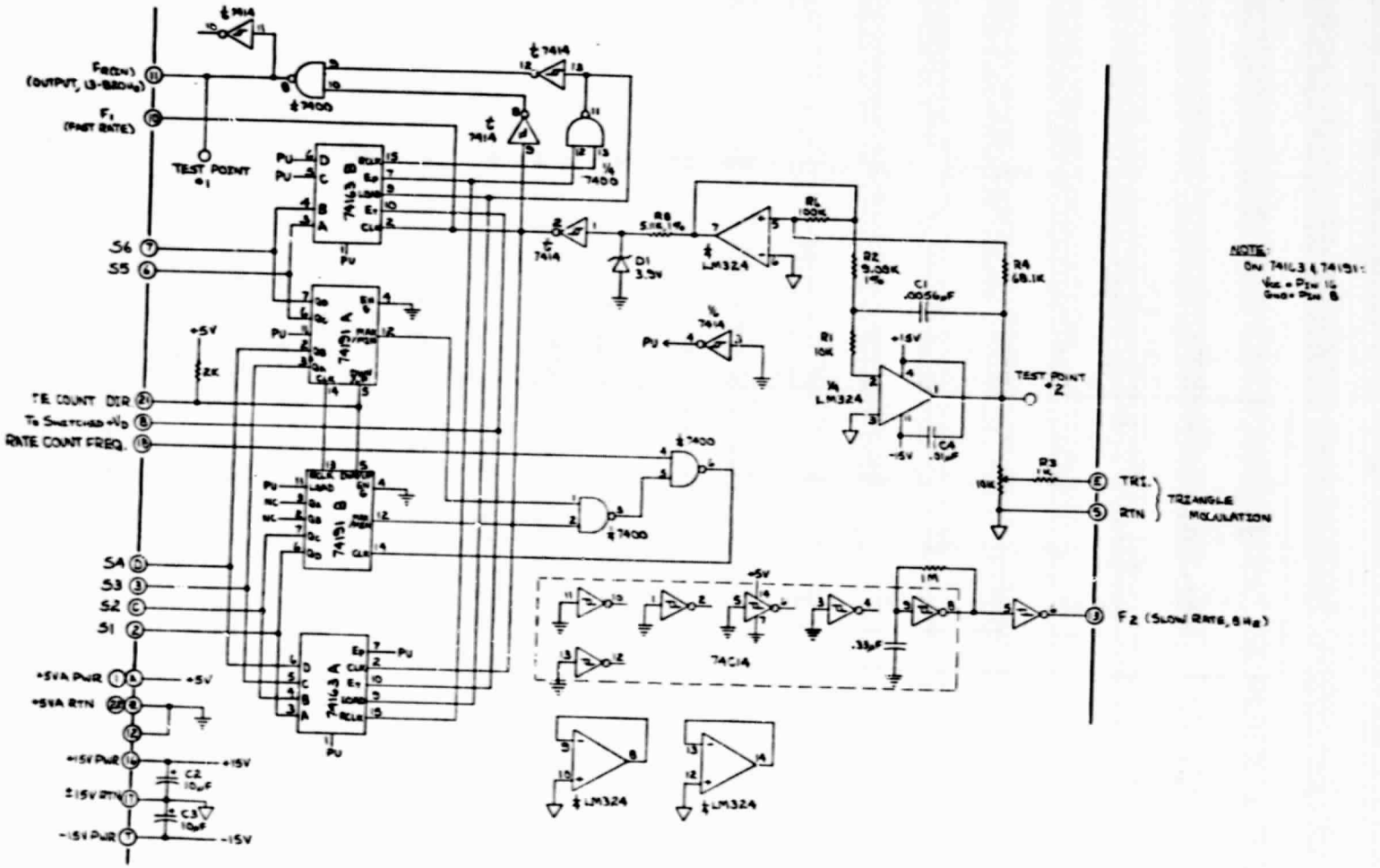

Figure 24. Adjustable Triangle

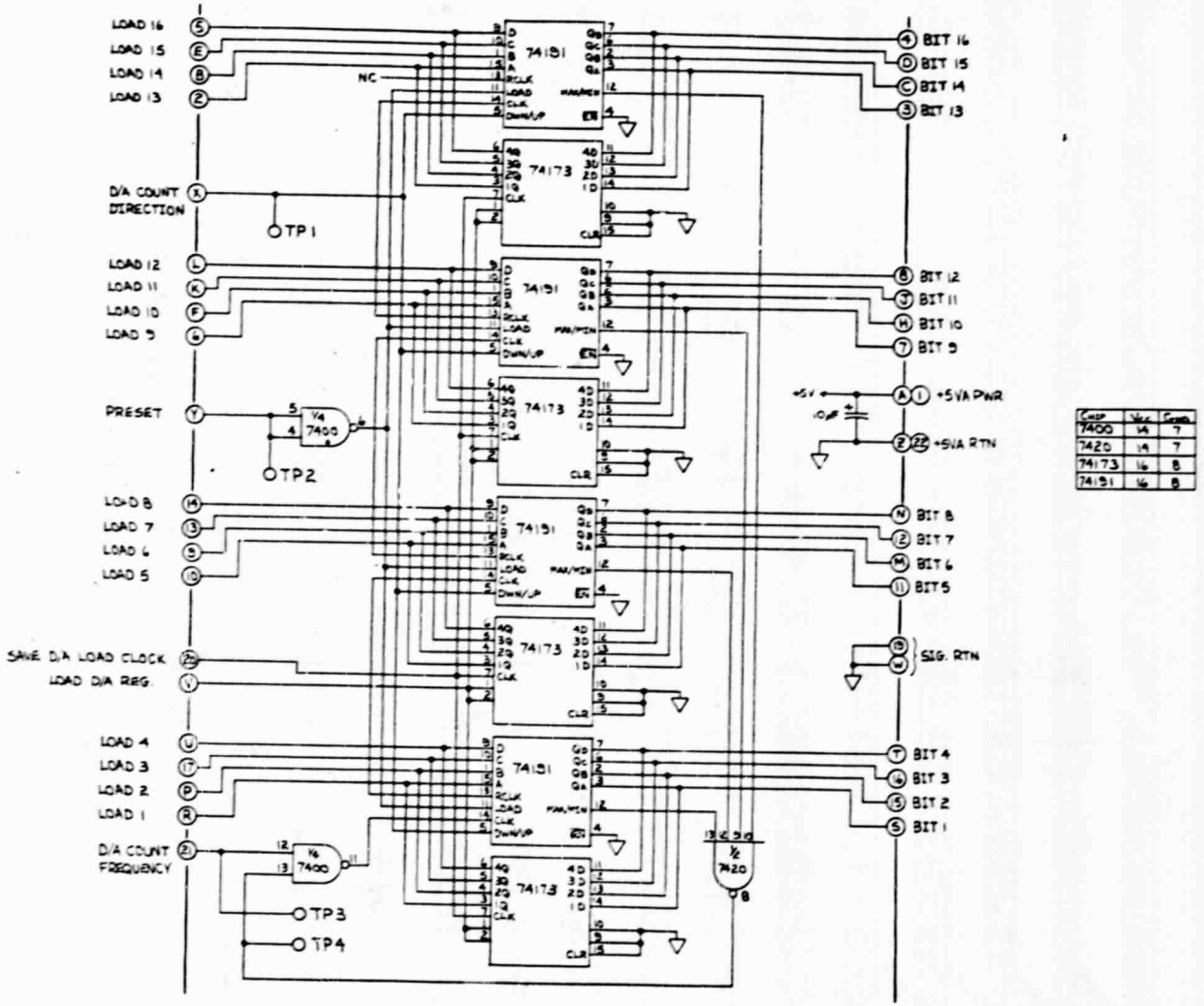

CHIP	Vcc	Gnd
7400	14	7
7420	14	7
74173	16	8
74151	16	8

Figure 25. Card #2: Counter

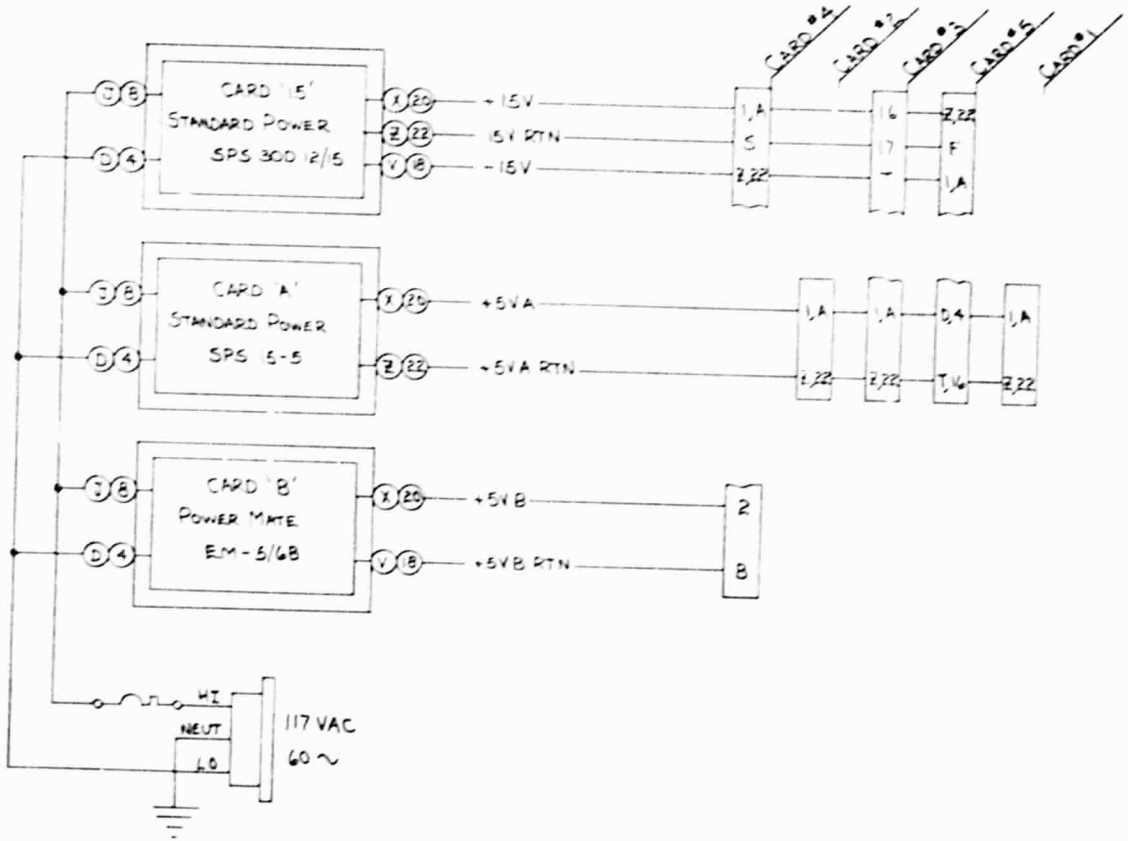

Figure 26. Cards A, B, and 15 Power Supply Wiring

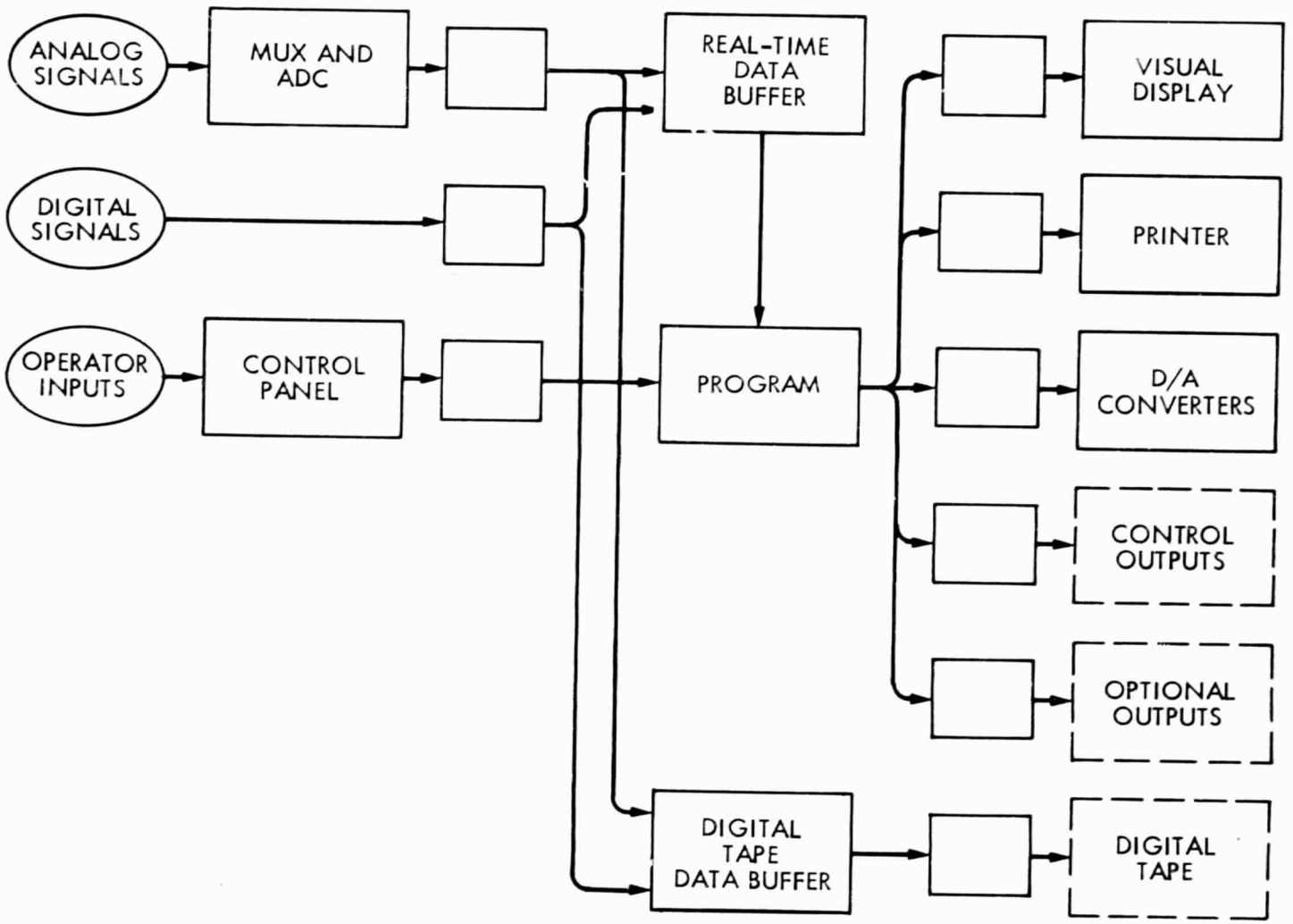

Figure 27. IDAC Functional Block Diagram

IDAC: HRC CELL: 103 TEST: 3 TAPE: YY61M DATE: 296 TIME: 15136 ABBY: 051878 DATE 102978 PAGE 6

TIME OF DAY	TA3	TA2	TA1	T0	T01	T02	T03	TREF	HEATER A POWER	HEATER B POWER
HH:MM:SS	DEG C	DEG.C	DEG C	DEG C	DEG C	DEG C	DEG C	DEG C	WATTS	WATTS
15:41:09	+22.540	+10.386	+2.081	+1.497	+2.068	+9.851	+20.462	+2.111	91.657	78.699
15:41:10		+10.530	+2.204	+1.669	+2.251	+9.991	+20.560	+2.298	91.346	78.260
15:41:11	+22.718	+10.671	+2.451	+1.905	+2.459	+10.140	+20.670	+2.472	90.887	77.826
15:41:12	+22.833	+10.832	+2.633	+2.012	+2.616	+10.288	+20.789	+2.667	90.350	77.498
15:41:13		+10.972	+2.812	+2.248	+2.799	+10.441	+20.904	+2.856	89.916	77.088
15:41:14	+23.032	+11.125	+2.994	+2.420	+2.977	+10.594	+21.010	+3.033	89.553	76.917
15:41:15	+23.134	+11.270	+3.181	+2.591	+3.173	+10.747	+21.134	+3.220	89.202	76.319
15:41:16	+23.215	+11.414	+3.360	+2.765	+3.355	+10.900	+21.235	+3.402	88.773	76.010
15:41:17	+23.318	+11.558	+3.551	+2.978	+3.538	+11.044	+21.342	+3.585	88.442	75.661
15:41:18	+23.410	+11.711	+3.734	+3.128	+3.721	+11.202	+21.435	+3.755	87.982	75.350
15:41:19	+23.491	+11.852	+3.912	+3.365	+3.899	+11.350	+21.537	+3.942	87.677	75.048
15:41:20	+23.568	+12.006	+4.099	+3.494	+4.090	+11.482	+21.626	+4.137	87.217	74.665
15:41:21	+23.651	+12.128	+4.273	+3.709	+4.273	+11.614	+21.733	+4.328	86.700	74.226
15:41:22	+23.738	+12.268	+4.460	+3.902	+4.451	+11.779	+21.856	+4.498	86.271	73.873
15:41:23	+23.823	+12.412	+4.643	+4.053	+4.634	+11.932	+21.970	+4.685	85.734	73.515
15:41:24	+23.912	+12.561	+4.830	+4.311	+4.808	+12.068	+22.085	+4.864	85.299	73.158
15:41:25	+24.005	+12.693	+5.012	+4.441	+4.999	+12.230	+22.187	+5.046	84.896	72.856
15:41:26	+24.103	+12.841	+5.195	+4.656	+5.186	+12.378	+22.289	+5.225	84.276	72.468
15:41:27	+24.201	+12.990	+5.378	+4.828	+5.365	+12.531	+22.391	+5.424		
15:41:28	+24.286	+13.134	+5.556	+5.022	+5.547	+12.676	+22.497	+5.603	83.510	71.701
15:41:29	+24.366	+13.275	+5.743	+5.217	+5.734	+12.824	+22.591	+5.781	83.189	71.455
15:41:30	+24.460	+13.423	+5.926	+5.475	+5.917	+12.973	+22.701	+5.977	82.780	71.046
15:41:31	+24.549	+13.564	+6.108	+5.648	+6.087	+13.113	+22.782	+6.151	82.351	70.693
15:41:32	+24.644	+13.712	+6.291	+5.778	+6.287	+13.262	+22.896	+6.329	81.843	70.223
15:41:33	+24.766	+13.865	+6.482	+5.950	+6.469	+13.415	+23.003	+6.520	81.445	69.865
15:41:34	+24.846	+14.005	+6.660	+6.123	+6.665	+13.559	+23.105	+6.699	81.041	69.486
15:41:35	+24.940	+14.141	+6.839	+6.296	+6.835	+13.708	+23.202	+6.881	80.632	69.102
15:41:36	+25.054	+14.298	+7.026	+6.512	+7.022	+13.852	+23.287	+7.077	80.193	68.637
15:41:37	+25.156	+14.447	+7.213	+6.707	+7.200	+13.997	+23.385	+7.242	79.892	68.335
15:41:38	+25.241	+14.596	+7.395	+6.967	+7.391	+14.145	+23.487	+7.446	79.565	67.938
15:41:39	+25.324	+14.740	+7.578	+7.075	+7.570	+14.290	+23.597	+7.568	78.975	67.520
15:41:40	+25.420	+14.880	+7.752	+7.270	+7.748	+14.438	+23.716	+7.790	78.618	67.136
15:41:41	+25.518	+15.029	+7.908	+7.486	+7.935	+14.600	+23.839	+7.998	78.269	66.860
15:41:42	+25.611	+15.178	+8.135	+7.681	+8.126	+14.749	+23.937	+8.177	77.774	66.497
15:41:43	+25.704	+15.322	+8.309	+7.898	+8.313	+14.893	+24.039	+8.360	77.390	66.165
15:41:44	+25.769	+15.471	+8.496	+8.050	+8.487	+15.038	+24.133	+8.533	77.011	65.837
15:41:45	+25.879	+15.611	+8.683	+8.245	+8.674	+15.191	+24.260	+8.725	76.483	65.397
15:41:46	+25.959	+15.756	+8.865	+8.397	+8.857	+15.343	+24.371	+8.891	76.111	65.116
15:41:47	+26.061	+15.896	+9.044	+8.592	+9.039	+15.496	+24.468	+9.099	75.757	64.788
15:41:48	+26.150	+16.044	+9.231	+8.765	+9.226	+15.645	+24.583	+9.277	75.297	64.455
15:41:49	+26.252	+16.189	+9.417	+9.004	+9.405	+15.789	+24.685	+9.466	74.887	64.123
15:41:50	+26.354	+16.337	+9.596	+9.178	+9.587	+15.938	+24.795	+9.643	74.487	63.735
15:41:51	+26.461	+16.486	+9.787	+9.345	+9.774	+16.091	+24.880	+9.825	73.986	63.351
15:41:52	+26.554	+16.635	+9.965	+9.548	+9.957	+16.227	+24.987	+10.008	73.402	62.992
15:41:53	+26.643	+16.779	+10.152	+9.787	+10.100	+16.380	+25.088	+10.199	73.245	62.502
15:41:54	+26.737	+16.928	+10.331	+9.961	+10.327	+16.524	+25.182	+10.377	72.865	62.279
15:41:55	+26.839	+17.107	+10.488	+10.113	+10.462	+16.745	+25.284	+10.552	64.156	50.870
15:41:56	+27.047	+18.151	+10.195	+5.217	+10.038	+17.540	+25.471	+10.739	26.618	37.177
15:41:57	+27.357	+18.967	+9.927	+1.905	+9.723	+18.228	+25.764	+10.913	12.135	21.926
15:41:58	+27.671	+19.498	+10.072	+1.412	+9.846	+18.665	+26.066	+11.100	7.962	13.168

Figure 28. Basic Temperature and Power Data (Typical)

IDACI R&C CELLI 183 TEBII 3 TAPEI V961M DATI 296 TIMEI 15136 ABBYI 051878 DATE 102978 PAGE 6

TIME OF DAY	T0-THEP	T0-TAI	TA2-TA3	T1-TB1	TB2-TB3	PA/ (TA2-TA3)	PB/ (TB2-TB3)	T0	AVERAGE POWER
HH:MM:SS	DEG.C	DEG.C	DEG C	DEG.C.	DEG C.	MA	MB	DEG C	MATTS.
15:01:09	0.613	0.583	12.153	0.570	10.611	7.541	7.416	+1.497	85.170
15:01:10	0.628	0.594		0.582	10.569	7.547	7.404	+1.669	84.803
15:01:11	0.567	0.545	12.087	0.554	10.536	7.548	7.390	+1.905	84.356
15:01:12	0.655	0.621	12.060	0.608	10.501	7.528	7.379	+2.012	83.922
15:01:13	0.606	0.563		0.551	10.462	7.516	7.360	+2.248	83.462
15:01:14	0.615	0.574	11.907	0.557	10.416	7.520	7.346	+2.428	83.035
15:01:15	0.628	0.590	11.864	0.581	10.384	7.518	7.347	+2.591	82.760
15:01:16	0.617	0.575	11.801	0.570	10.335	7.522	7.355	+2.785	82.396
15:01:17	0.607	0.573	11.754	0.560	10.297	7.524	7.347	+2.978	82.051
15:01:18	0.626	0.605	11.699	0.592	10.233	7.520	7.363	+3.128	81.668
15:01:19	0.577	0.547	11.639	0.534	10.186	7.532	7.367	+3.365	81.362
15:01:20	0.643	0.605	11.563	0.596	10.144	7.502	7.368	+3.494	80.981
15:01:21	0.619	0.584	11.524	0.568	10.118	7.522	7.335	+3.709	80.463
15:01:22	0.595	0.557	11.469	0.549	10.076	7.521	7.351	+3.902	80.072
15:01:23	0.632	0.589	11.410	0.581	10.038	7.513	7.323	+4.053	79.624
15:01:24	0.552	0.518	11.350	0.496	10.016	7.514	7.303	+4.311	79.229
15:01:25	0.605	0.571	11.312	0.558	9.957	7.504	7.316	+4.441	78.876
15:01:26	0.568	0.534	11.261	0.530	9.910	7.483	7.312	+4.656	78.372
15:01:27	0.595	0.549	11.210	0.536	9.859			+4.828	
15:01:28	0.580	0.533	11.151	0.524	9.821	7.488	7.300	+5.022	77.606
15:01:29	0.564	0.526	11.091	0.517	9.766	7.500	7.316	+5.217	77.322
15:01:30	0.501	0.450	11.036	0.441	9.728	7.500	7.303	+5.475	76.913
15:01:31	0.542	0.460	10.985	0.438	9.668	7.496	7.311	+5.648	76.522
15:01:32	0.551	0.513	10.951	0.508	9.634	7.469	7.288	+5.778	76.013
15:01:33	0.569	0.531	10.900	0.518	9.587	7.471	7.286	+5.950	75.655
15:01:34	0.575	0.537	10.841	0.541	9.545	7.475	7.279	+6.123	75.266
15:01:35	0.585	0.542	10.798	0.538	9.494	7.467	7.278	+6.296	74.867
15:01:36	0.564	0.513	10.756	0.509	9.434	7.455	7.274	+6.512	74.415
15:01:37	0.535	0.505	10.709	0.491	9.388	7.460	7.278	+6.707	74.113
15:01:38	0.479	0.428	10.645	0.424	9.341	7.473	7.271	+6.967	73.767
15:01:39	0.473	0.503	10.586	0.494	9.307	7.460	7.254	+7.075	73.248
15:01:40	0.520	0.482	10.539	0.478	9.281	7.459	7.233	+7.270	72.877
15:01:41	0.508	0.461	10.488	0.448	9.235	7.462	7.219	+7.486	72.562
15:01:42	0.495	0.453	10.431	0.444	9.188	7.454	7.237	+7.681	72.136
15:01:43	0.461	0.410	10.382	0.415	9.146	7.454	7.234	+7.898	71.777
15:01:44	0.488	0.446	10.318	0.437	9.095	7.463	7.238	+8.050	71.424
15:01:45	0.480	0.437	10.267	0.429	9.069	7.445	7.210	+8.245	70.928
15:01:46	0.498	0.468	10.203	0.460	9.027	7.459	7.213	+8.397	70.613
15:01:47	0.506	0.451	10.165	0.447	8.971	7.452	7.221	+8.592	70.273
15:01:48	0.511	0.465	10.106	0.460	8.937	7.450	7.211	+8.765	69.876
15:01:49	0.459	0.413	10.063	0.400	8.895	7.441	7.208	+9.004	69.505
15:01:50	0.484	0.417	10.016	0.409	8.857	7.432	7.195	+9.178	69.091
15:01:51	0.429	0.391	9.974	0.378	8.789	7.417	7.207	+9.395	68.668
15:01:52	0.460	0.417	9.919	0.409	8.759	7.420	7.191	+9.548	68.297
15:01:53	0.412	0.365	9.863	0.352	8.708	7.405	7.186	+9.787	67.913
15:01:54	0.416	0.369	9.808	0.365	8.657	7.408	7.193	+9.961	67.572
15:01:55	0.438	0.370	9.651	0.349	8.538	6.687	6.895	+10.113	61.515
15:01:56	5.521	4.978	4.895	4.821	7.931	2.991	8.687	+5.217	31.895
15:01:57	9.008	8.022	8.389	7.818	7.536	1.446	2.989	+1.905	17.831
15:01:58	9.687	8.659	8.173	8.434	7.488	0.974	1.779	+1.412	10.565

Figure 29. Characteristic System Performance Data (Typical)

|DAC: HNC | CELL: 183 | TEST: 3 | TAPE: V9B1M | DAY: 296 | TIME: 15136 | ABBY: 051878 | DATE 102978 | PAGE 3

TIME OF DAY	TA1-TMEP	MEASURED (TA2-TA3)	MEASURED (TH2-183)	HEATER BOUNCE	HEATER A RESISTANC	BMONTED CHANNEL	TB	AVERAGE POWER
HH:MM:SS	DEG. C	DEG C	DEG C	E3	OHMS	DEG C	DEG C	#ATTS.
15:41:09	0.024	12.180	10.420	9953.803	24.252	0.000	+1.897	85.178
15:41:10		12.077	10.594	9952.556	24.252	0.000	+1.669	84.803
15:41:11	0.021	12.004	10.530	9952.556	24.251	0.000	+1.905	84.356
15:41:12	0.033	12.004	10.526	9952.556	24.250	0.000	+2.012	83.922
15:41:13		11.869	10.467	9952.556	24.249	0.004	+2.248	83.462
15:41:14	0.038	11.898	10.369	9951.309	24.248	0.000	+2.420	83.035
15:41:15	0.038	11.856	10.403	9952.556	24.247	0.000	+2.591	82.760
15:41:16	0.042	11.720	10.305	9953.803	24.247	0.000	+2.785	82.396
15:41:17	0.033	11.756	10.310	9953.803	24.246	0.000	+2.978	82.051
15:41:18	0.021	11.673	10.259	9953.803	24.245	0.000	+3.128	81.660
15:41:19	0.029	11.669	10.127	9953.803	24.244	0.004	+3.365	81.362
15:41:20	0.038	11.563	10.157	9953.803	24.243	0.000	+3.494	80.941
15:41:21	0.055	11.482	10.089	9952.556	24.242	0.000	+3.709	80.463
15:41:22	0.038	11.469	10.067	9953.803	24.242	0.000	+3.902	80.072
15:41:23	0.042	11.401	10.063	9953.803	24.241	0.004	+4.053	79.624
15:41:24	0.033	11.227	9.982	9953.803	24.240	0.000	+4.311	79.229
15:41:25	0.033	11.304	9.965	9955.050	24.239	0.000	+4.481	78.876
15:41:26	0.029	11.244	9.919	9953.803	24.238	0.000	+4.656	78.372
15:41:27	0.046	11.112	9.863		0.000	0.000	+4.828	
15:41:28	0.046	11.182	9.829	9953.803	24.237	0.000	+5.022	77.606
15:41:29	0.038	11.074	9.779	9956.297	24.236	0.000	+5.217	77.322
15:41:30	0.050	10.989	9.711	9956.297	24.235	0.000	+5.475	76.913
15:41:31	0.042	10.989	9.665	9957.544	24.234	0.000	+5.648	76.522
15:41:32	0.038	10.942	9.651	9955.050	24.233	0.000	+5.778	76.013
15:41:33	0.038	10.853	9.600	9955.050	24.232	0.000	+5.950	75.655
15:41:34	0.038	10.832	9.549	9956.297	24.232	0.000	+6.123	75.264
15:41:35	0.042	10.794	9.502	9956.297	24.231	0.000	+6.296	74.867
15:41:36	0.050	10.705	9.417	9955.050	24.230	0.000	+6.512	74.415
15:41:37	0.029	10.700	9.409	9956.297	24.229	0.000	+6.707	74.113
15:41:38	0.050	10.624	9.337	9957.544	24.228	0.000	+6.967	73.787
15:41:39	+0.029	10.581	9.341	9957.544	24.227	0.000	+7.075	73.288
15:41:40	0.038	10.501	9.298	9957.544	24.227	0.004	+7.270	72.877
15:41:41	0.046	10.479	9.247	9958.792	24.226	0.000	+7.486	72.562
15:41:42	0.042	10.407	9.184	9957.544	24.225	0.000	+7.681	72.136
15:41:43	0.050	10.377	9.086	9957.544	24.224	0.000	+7.898	71.777
15:41:44	0.042	10.284	9.107	9958.792	24.223	0.000	+8.050	71.424
15:41:45	0.042	10.250	9.035	9957.544	24.222	0.000	+8.245	70.920
15:41:46	0.025	10.174	9.048	9957.544	24.222	+0.012	+8.397	70.613
15:41:47	0.055	10.161	8.959	9958.792	24.221	0.000	+8.592	70.273
15:41:48	0.046	10.097	8.925	9958.792	24.220	0.000	+8.765	69.876
15:41:49	0.046	10.063	8.903	9958.792	24.219	0.000	+9.004	69.505
15:41:50	0.046	9.995	8.852	9957.544	24.218	0.012	+9.170	69.091
15:41:51	0.038	9.876	8.699	9957.544	24.217	0.000	+9.395	68.668
15:41:52	0.042	9.889	8.776	9957.544	24.217	0.000	+9.548	68.297
15:41:53	0.046	9.795	8.704	9957.544	24.216	0.000	+9.787	67.913
15:41:54	0.046	9.753	8.661	9958.792	24.215	0.000	+9.961	67.572
15:41:55	0.067	9.371	8.347	9965.030	24.214	0.000	+10.113	61.515
15:41:56	0.543	8.504	7.608	9965.030	24.216	0.000	+5.217	31.895
15:41:57	0.985	8.211	7.425	9967.526	24.217	0.000	+1.905	17.031
15:41:58	1.028	8.109	7.370	9970.022	24.216	0.000	+1.812	16.565

Figure 30. General Engineering Data (Typical)

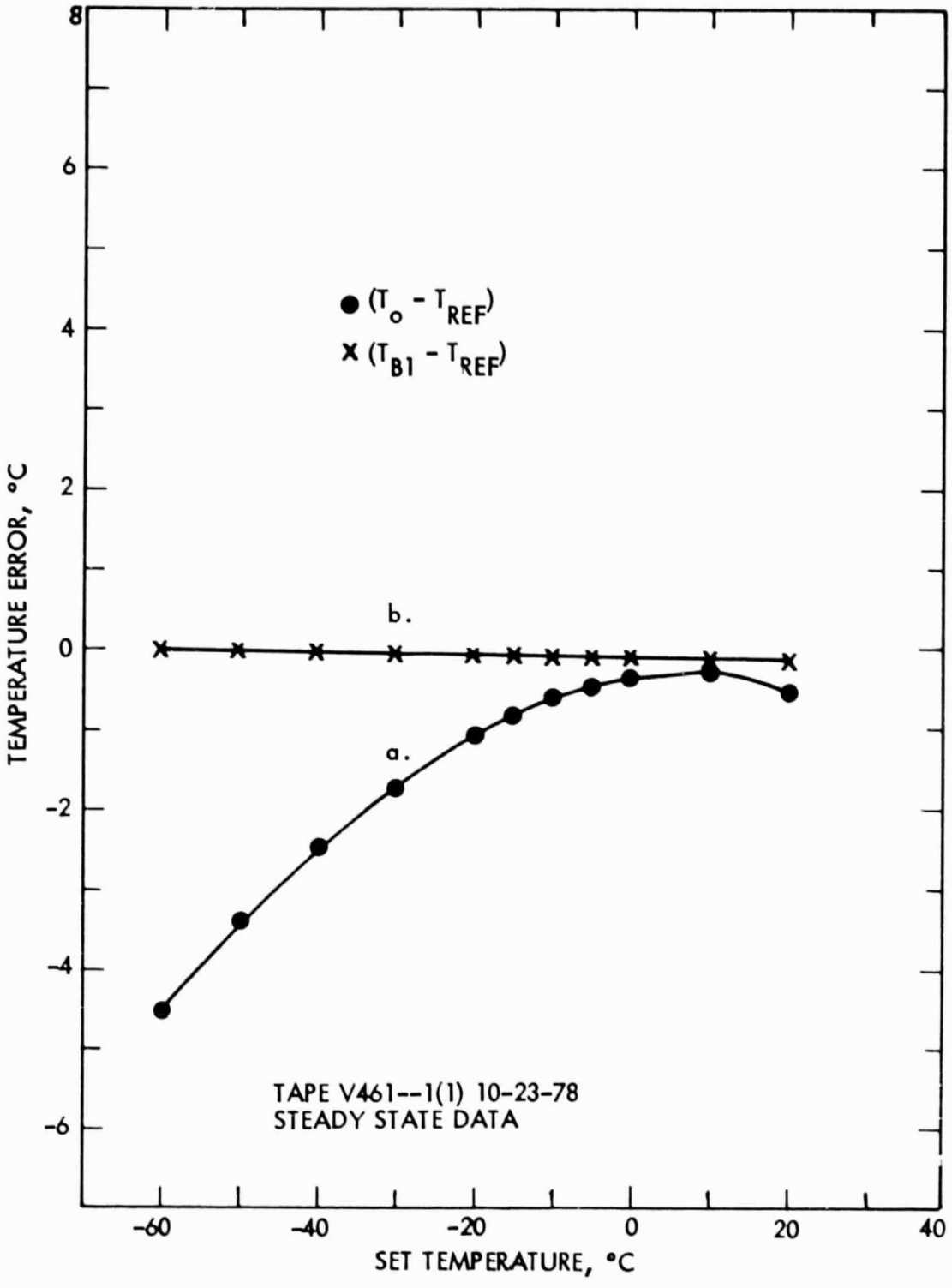

Figure 31a. Temperature Error Versus Set Temperature (Uncorrected)

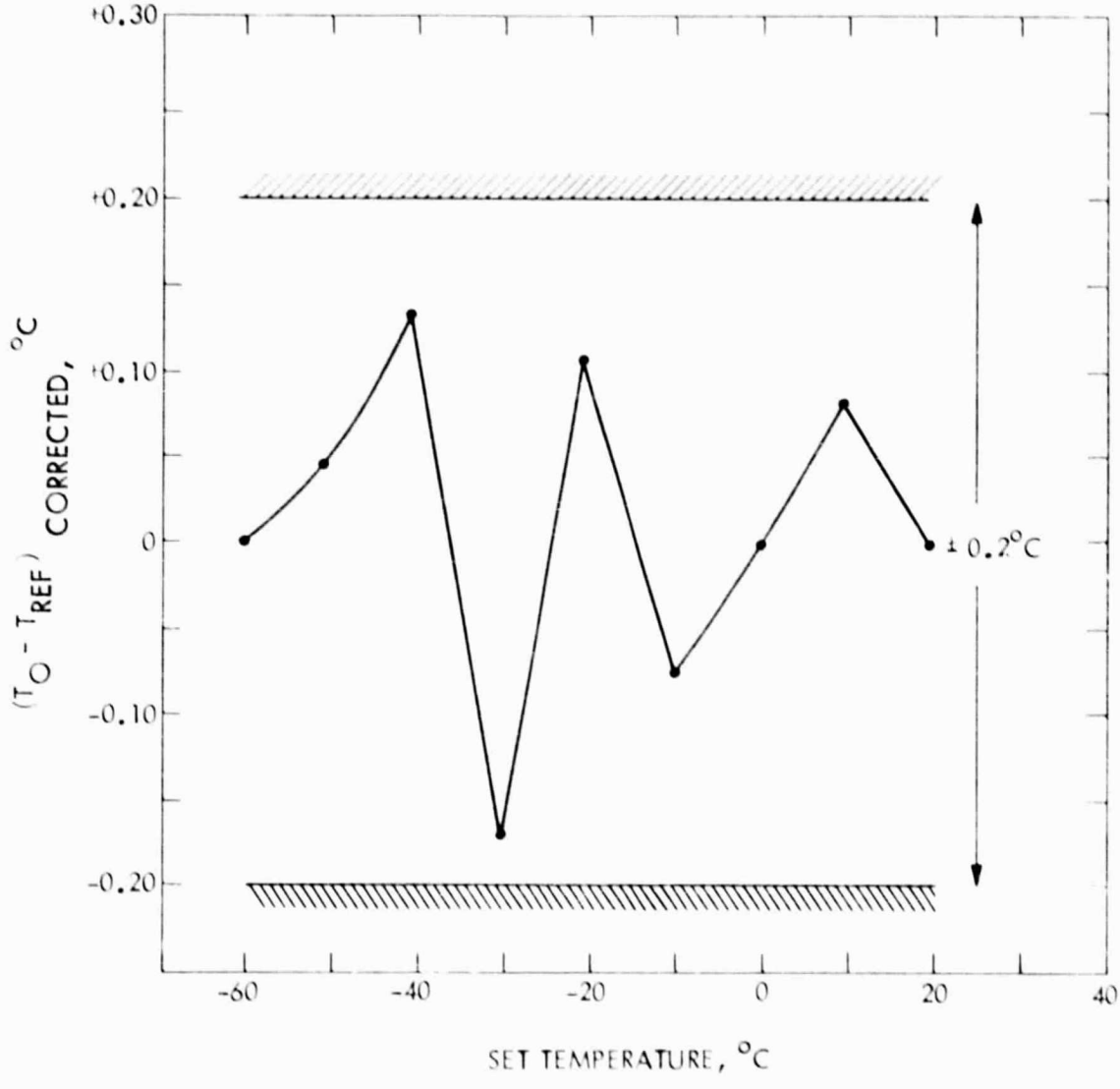

Figure 31b. Temperature Error Versus Set Temperature (Corrected)

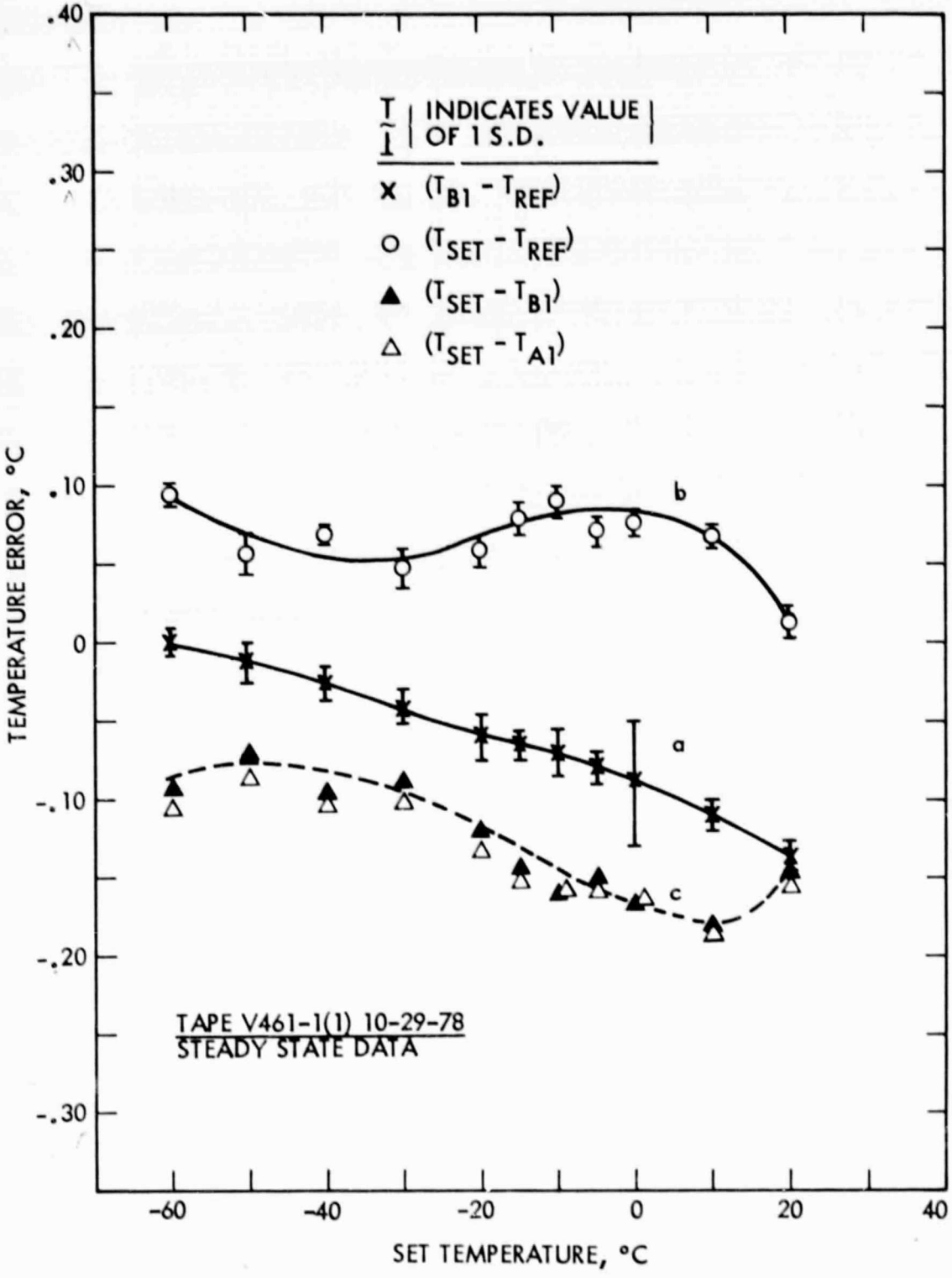

Figure 32. System Relative Temperature Error

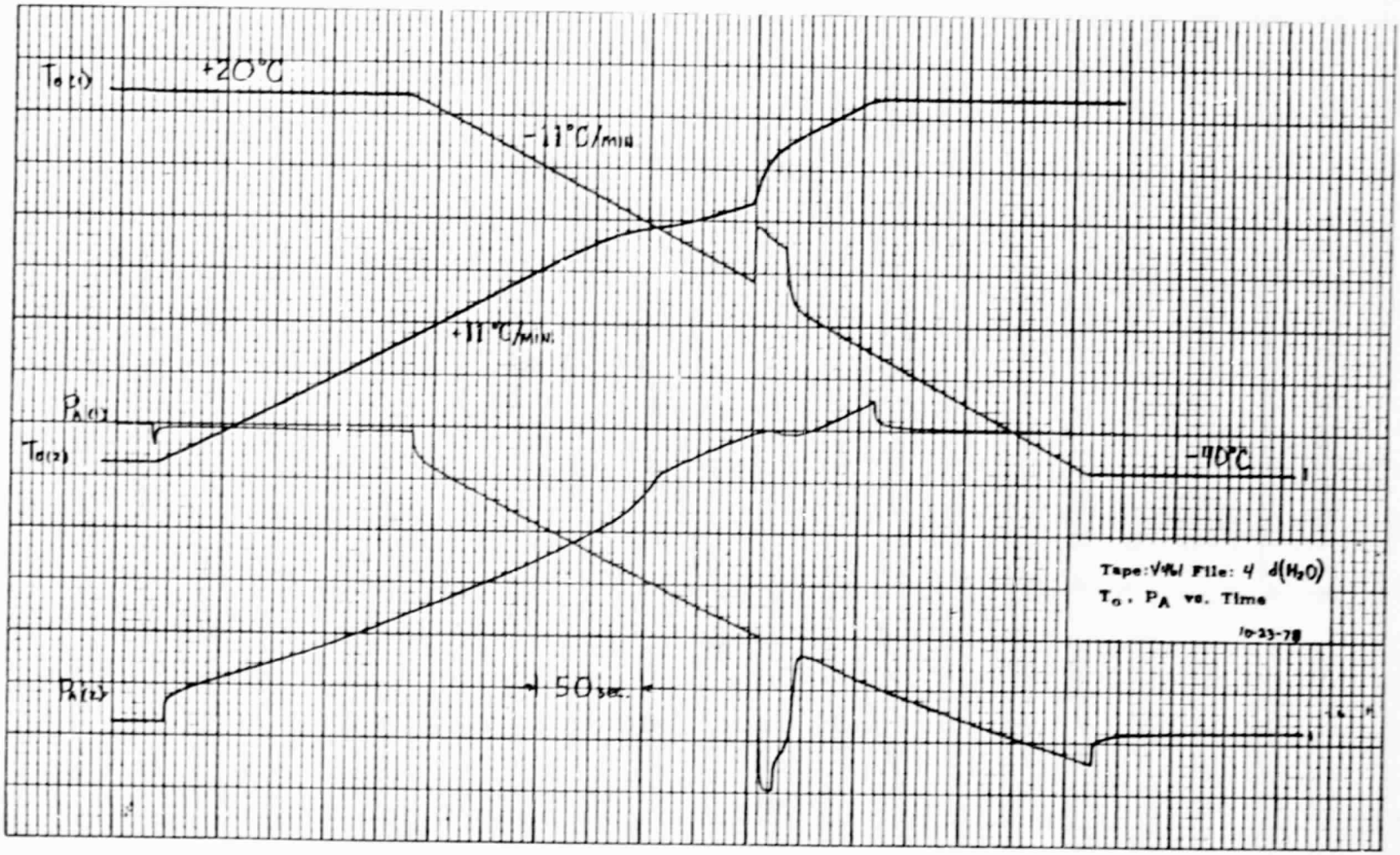

Figure 33. T_o and P_A Versus Time for Distilled Water (Typical)

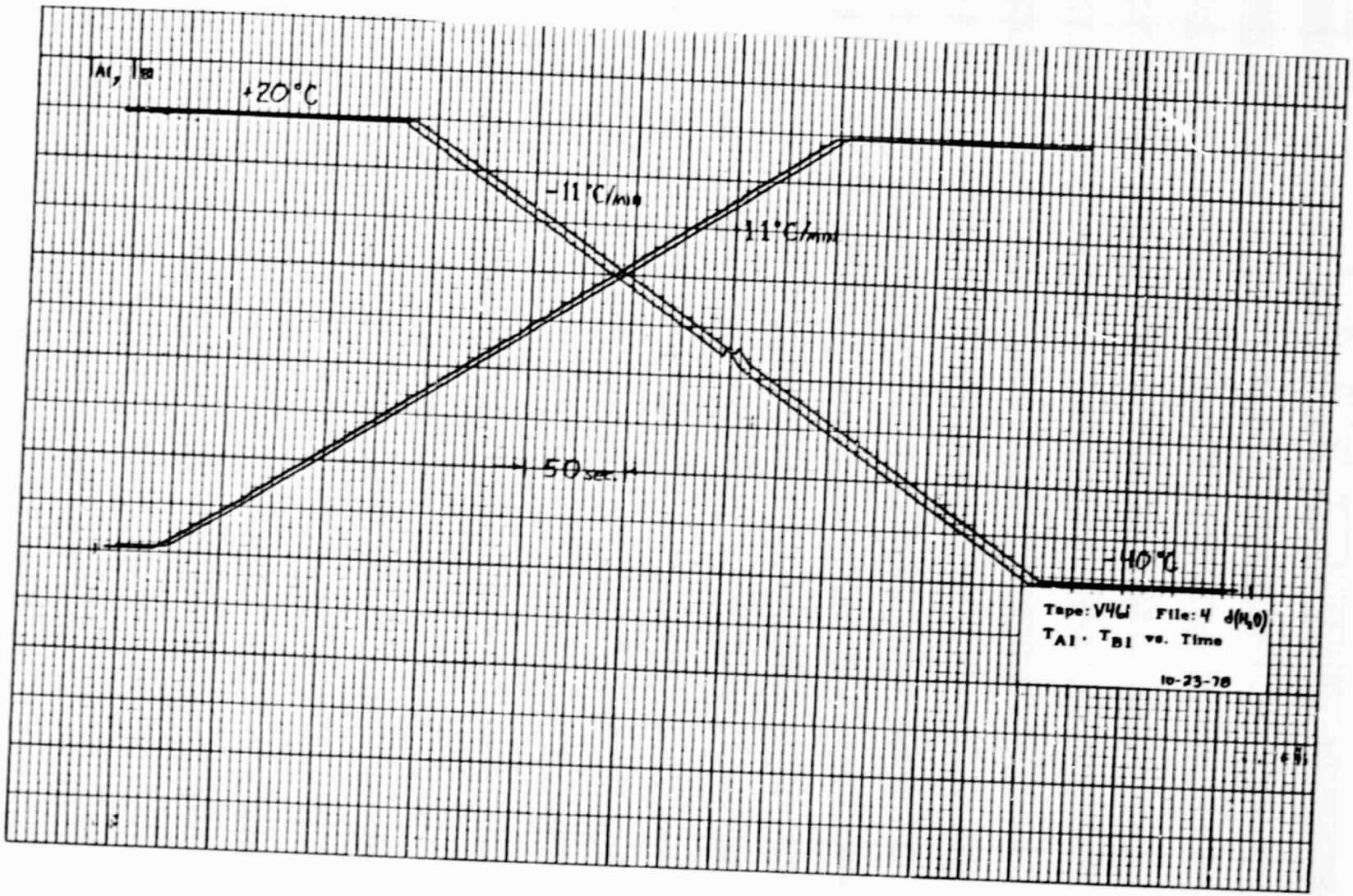

Figure 34. Interior Wall Temperature Versus Time (Typical)

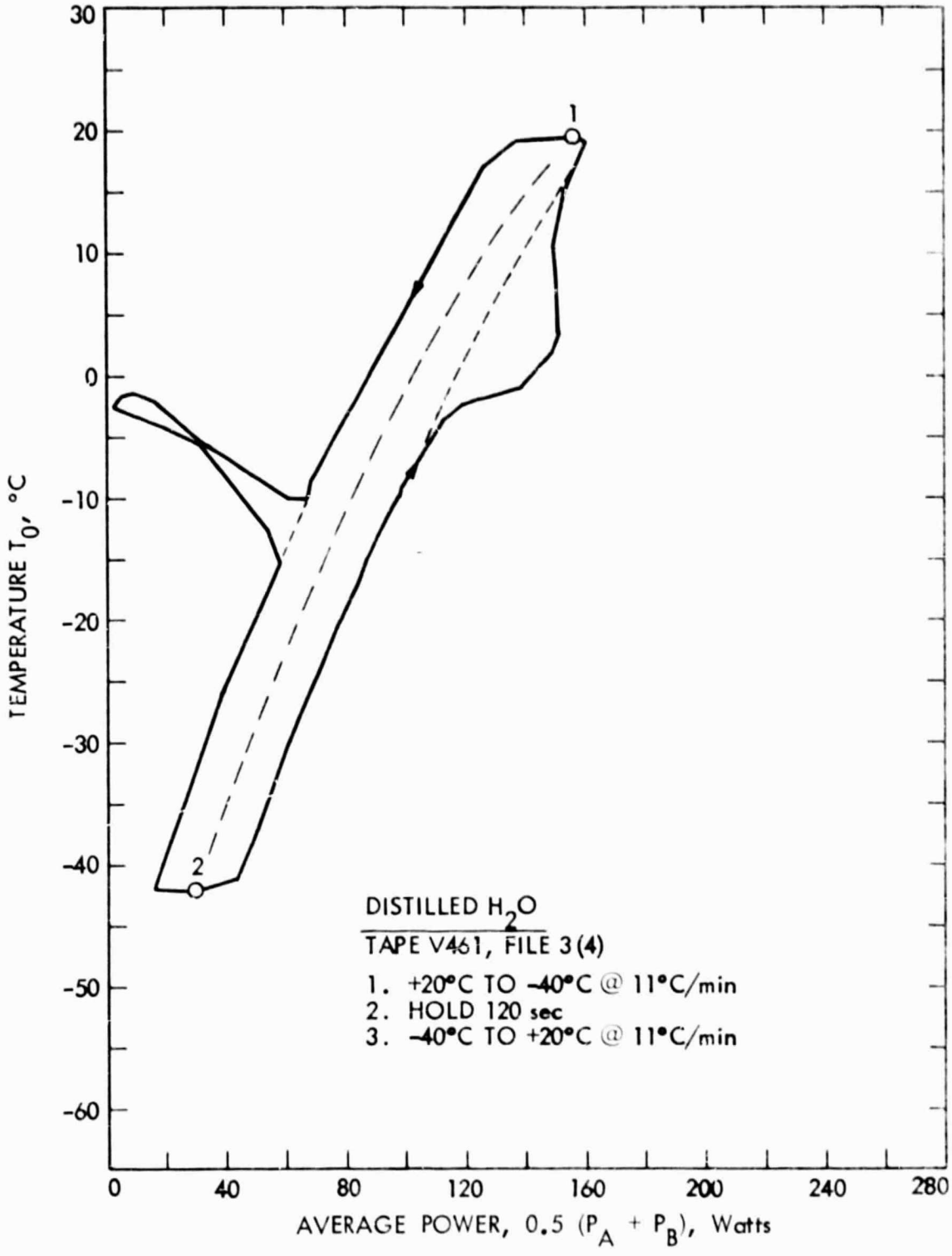

Figure 35. T_o Versus Average Power for Distilled Water (Typical)

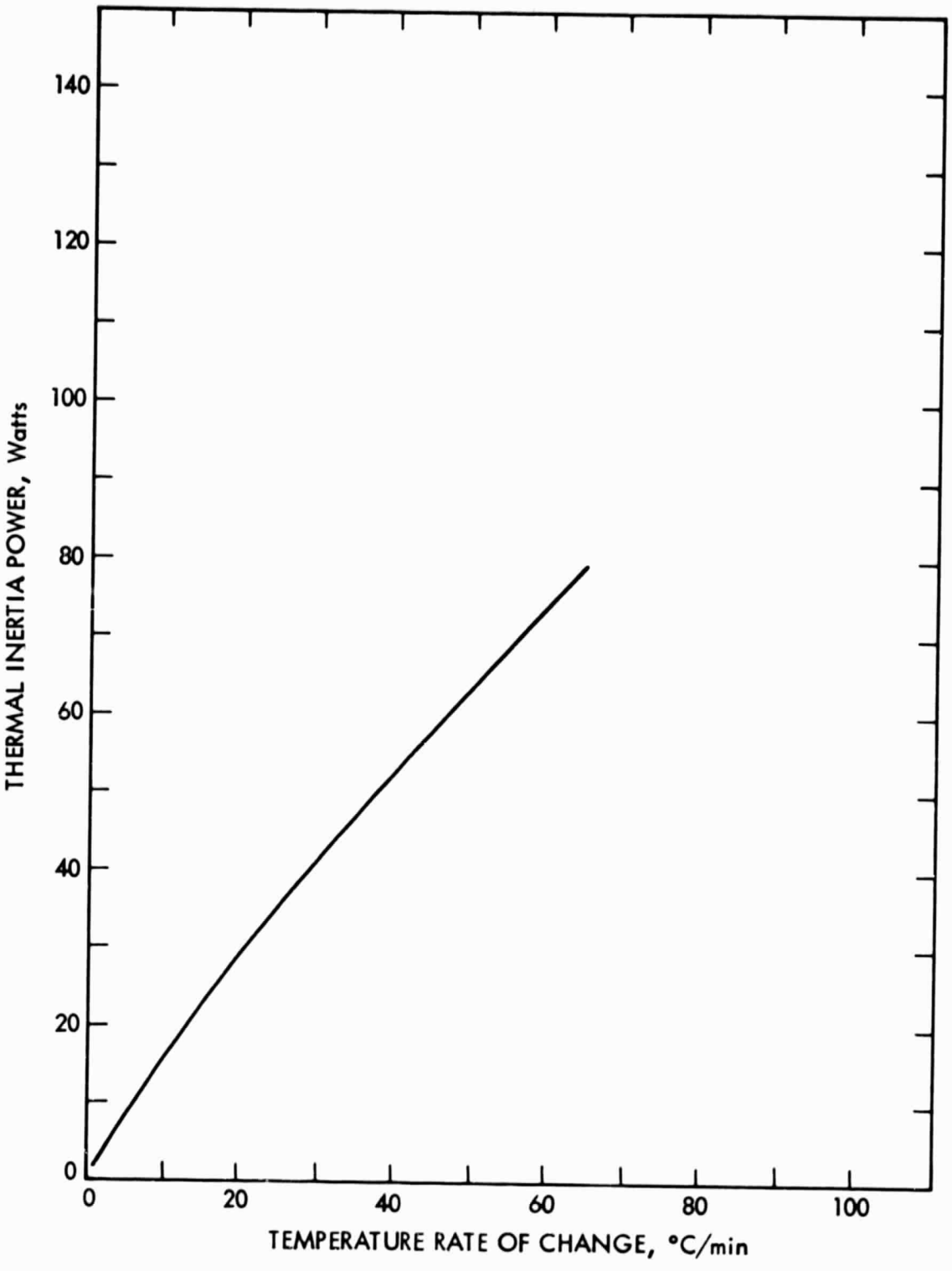

Figure 36. Thermal Interia Power Versus Temperature Rate of Change

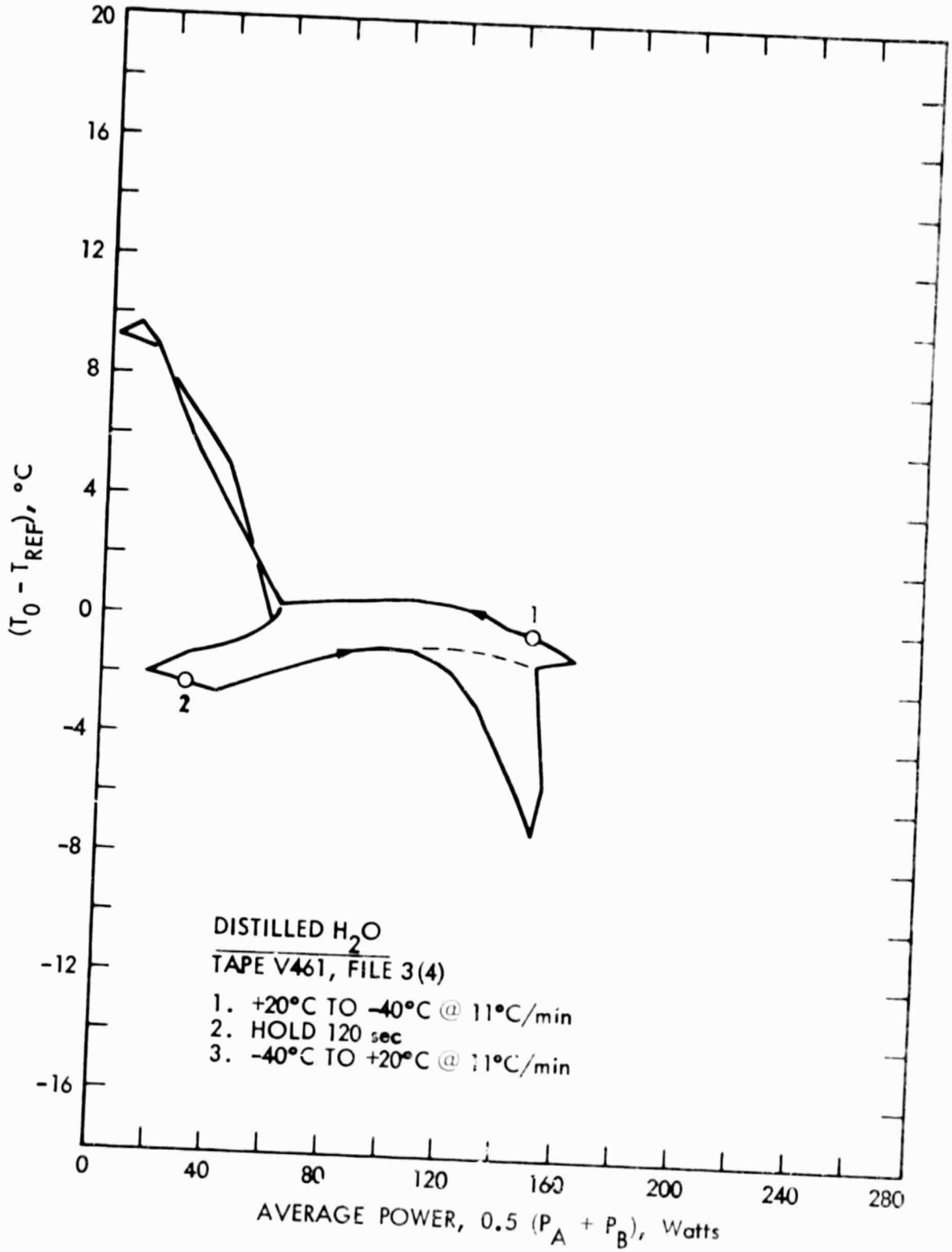

Figure 37. Mass Center to Reference Temperature Differential Versus Average Power (Typical)

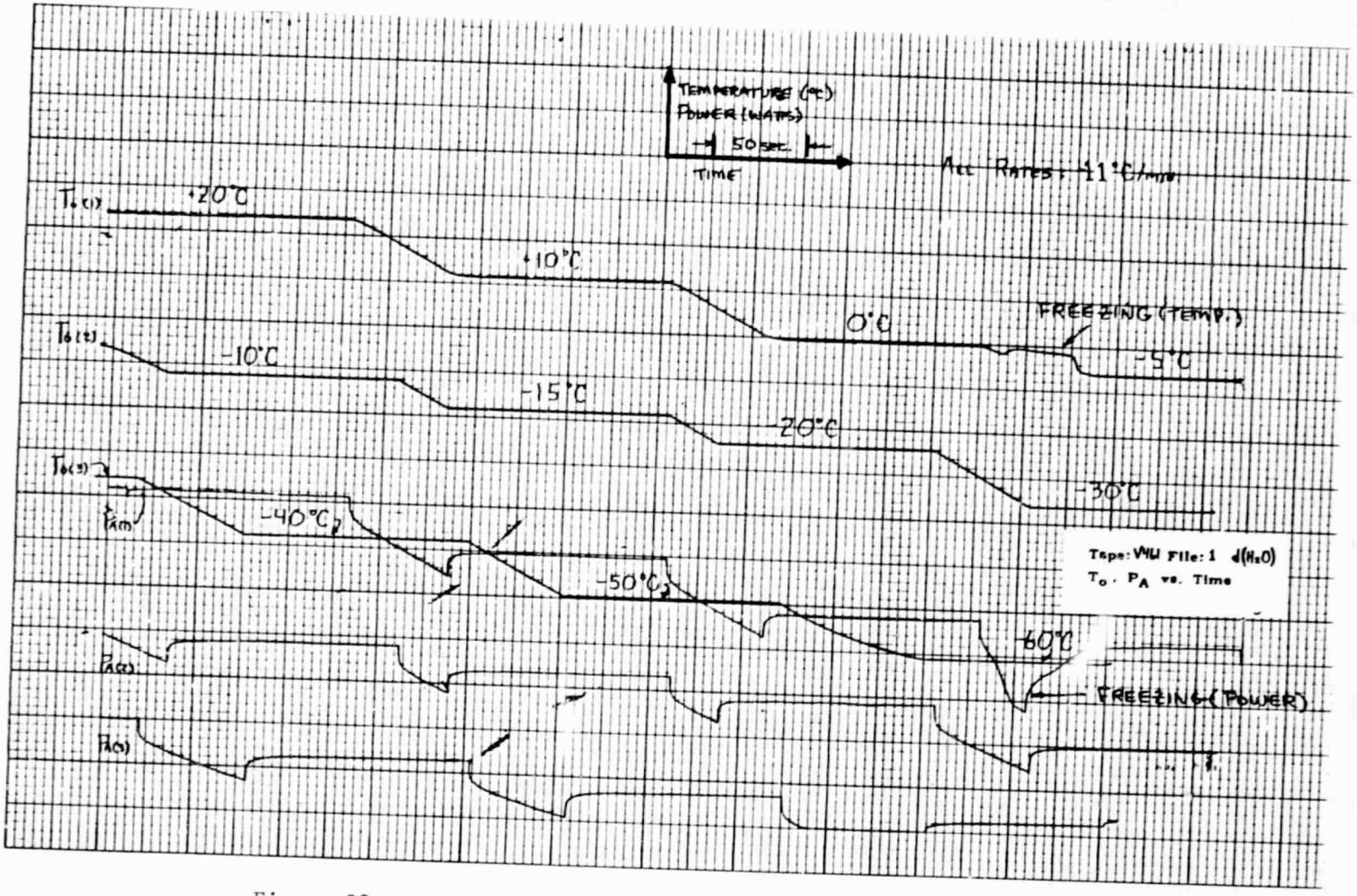

Figure 38a. T_o and P_A Versus Time for Distilled Water During Cooling (Typical)

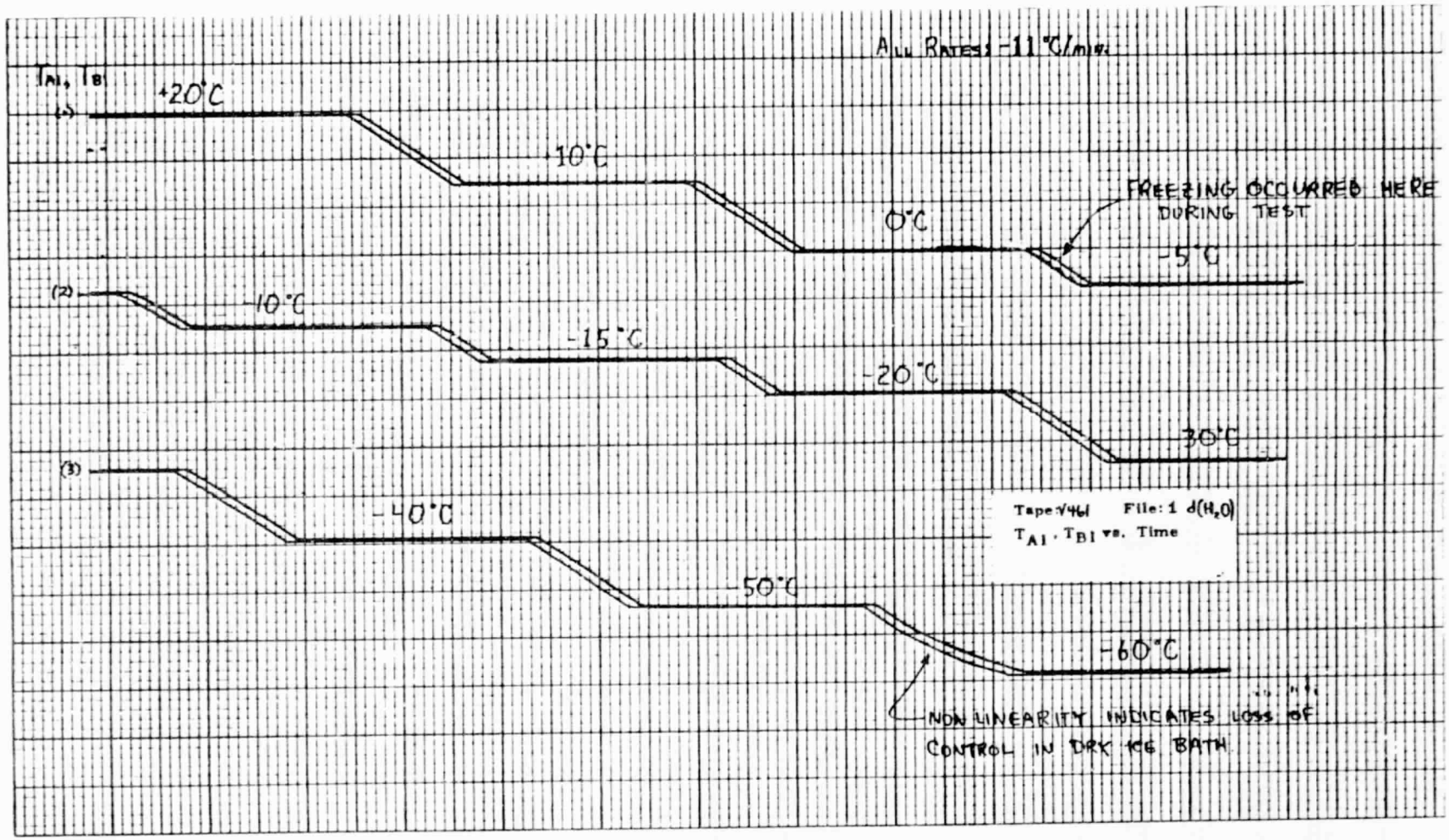

Figure 38b. T_{A1} and T_{B1} Versus Time for Distilled Water During Cooling (Typical)

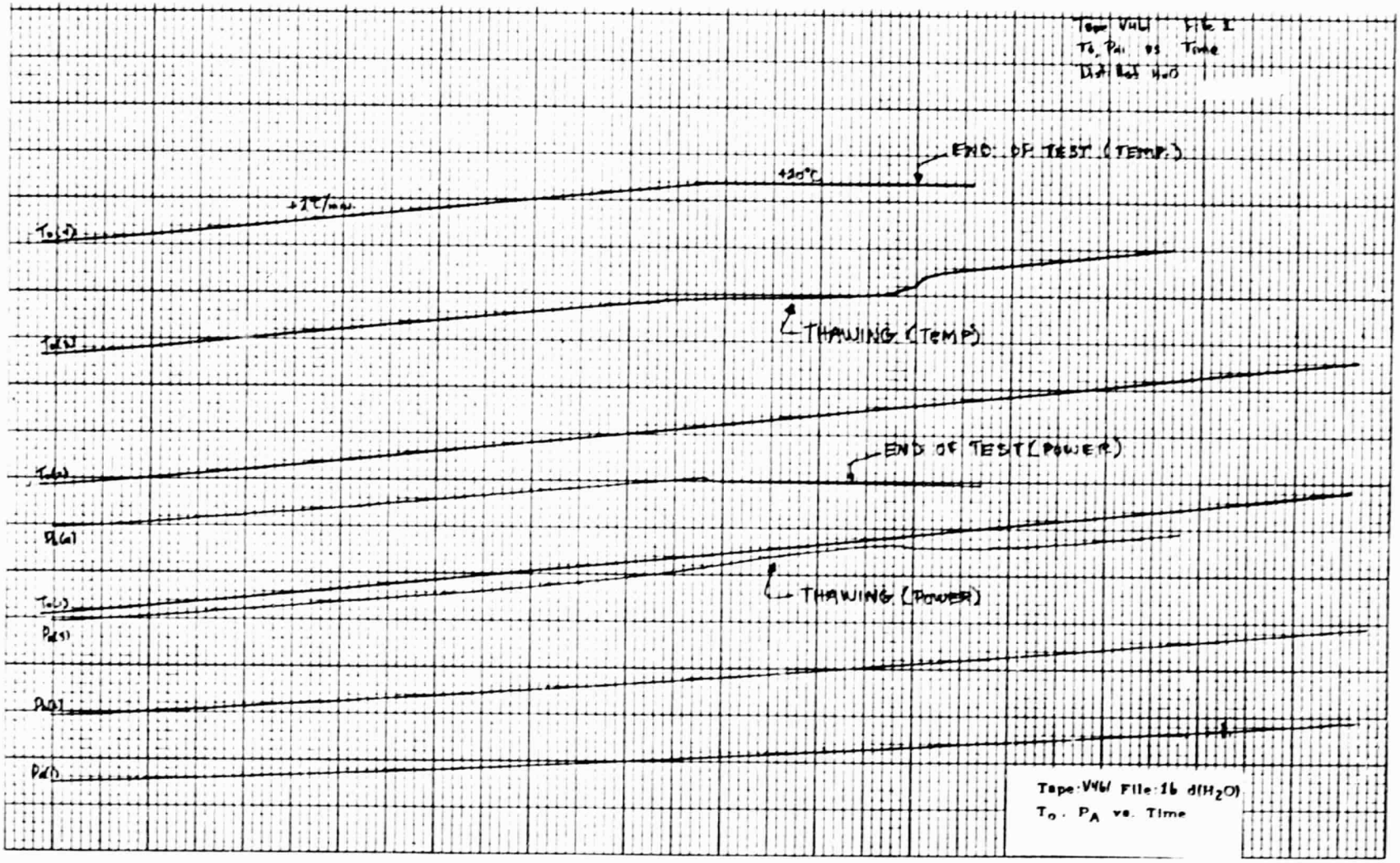

Figure 38c. T_o and P_A Versus Time for Distilled Water During Warming (Typical)

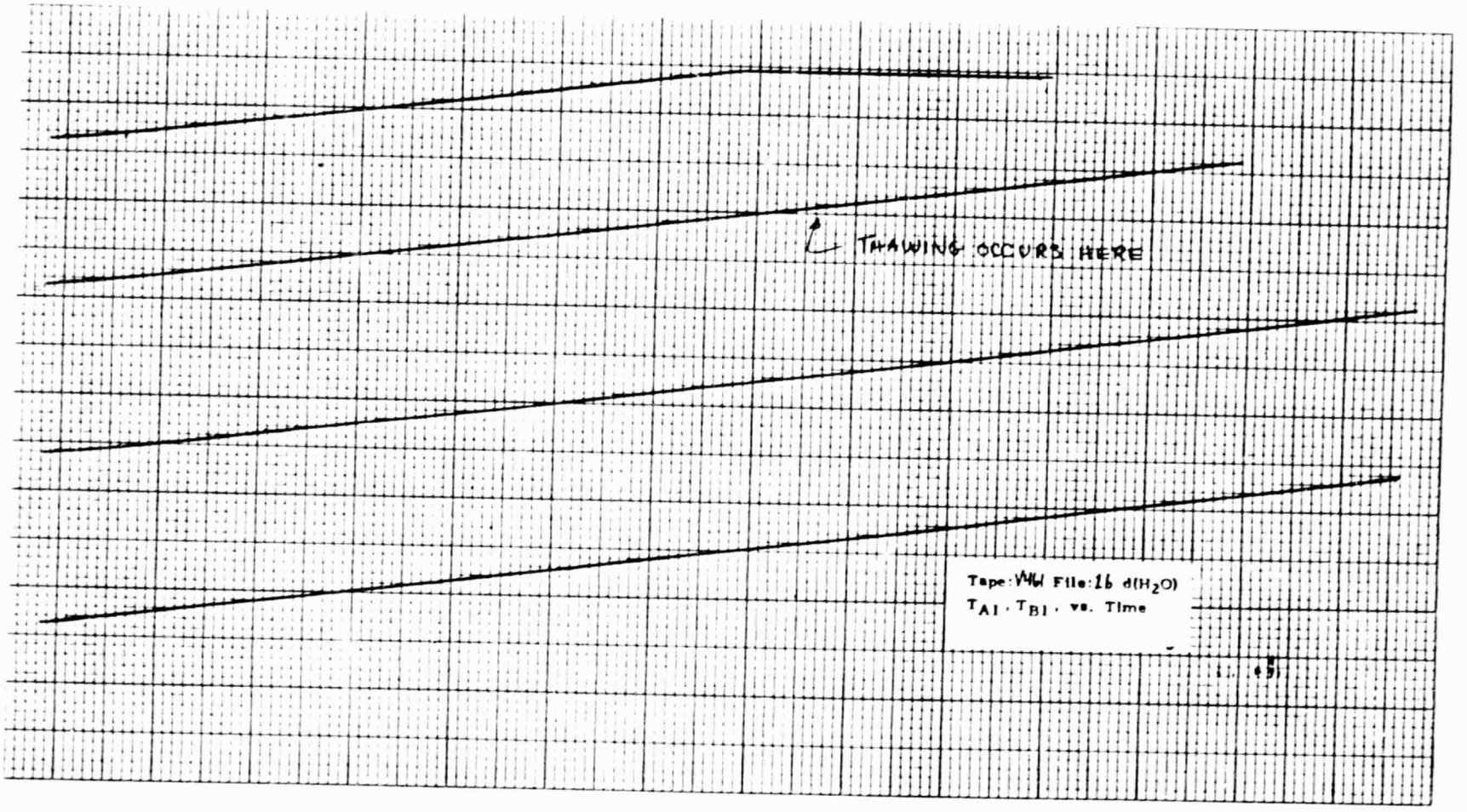

Figure 38d. T_{A1} and T_{B1} Versus Time for Distilled Water During Warming (Typical)

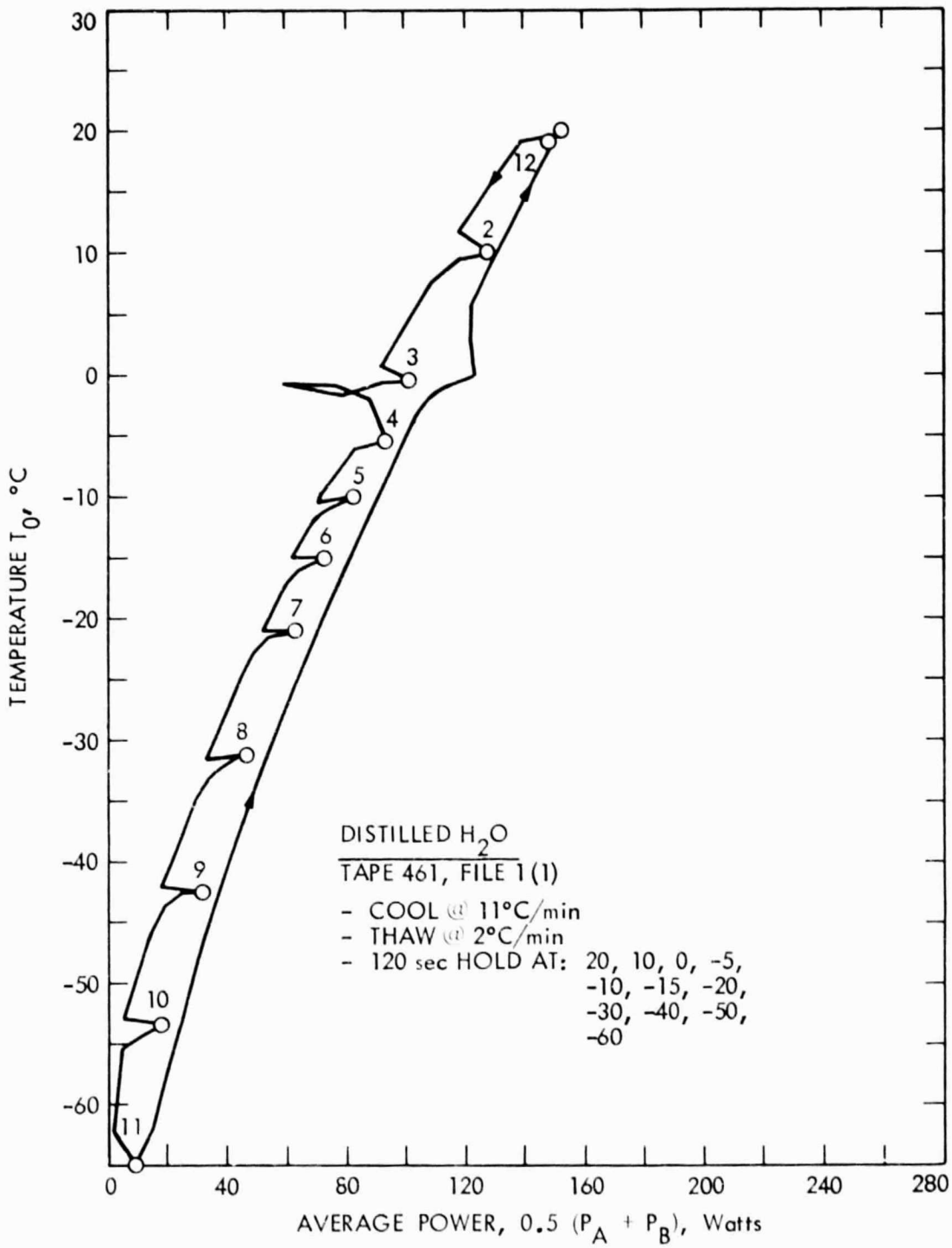

Figure 38e. T_o Versus Average Power for Distilled Water (Typical)

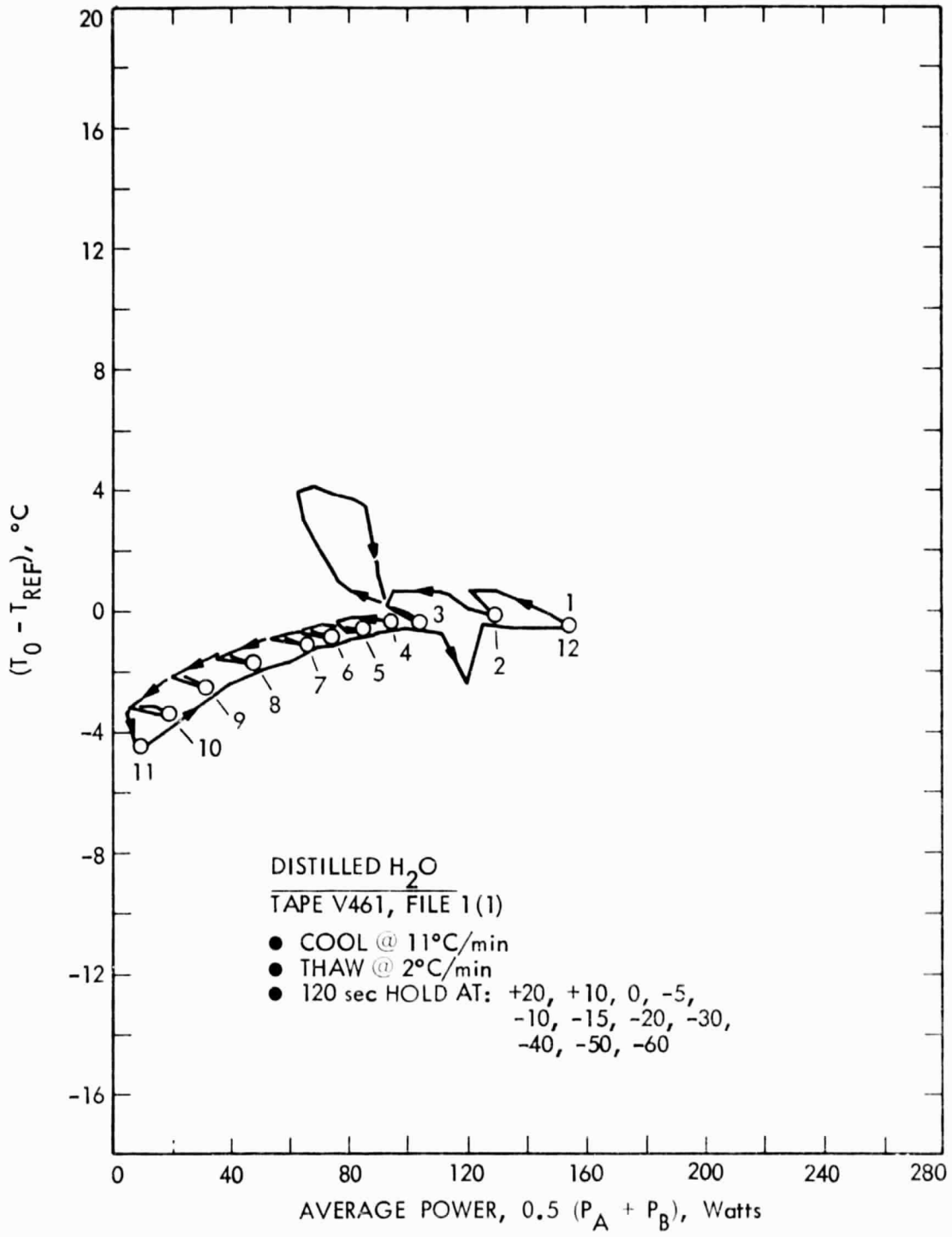

Figure 38f. T_o to Reference Temperature Differential Versus Average Power for Distilled Water (Typical)

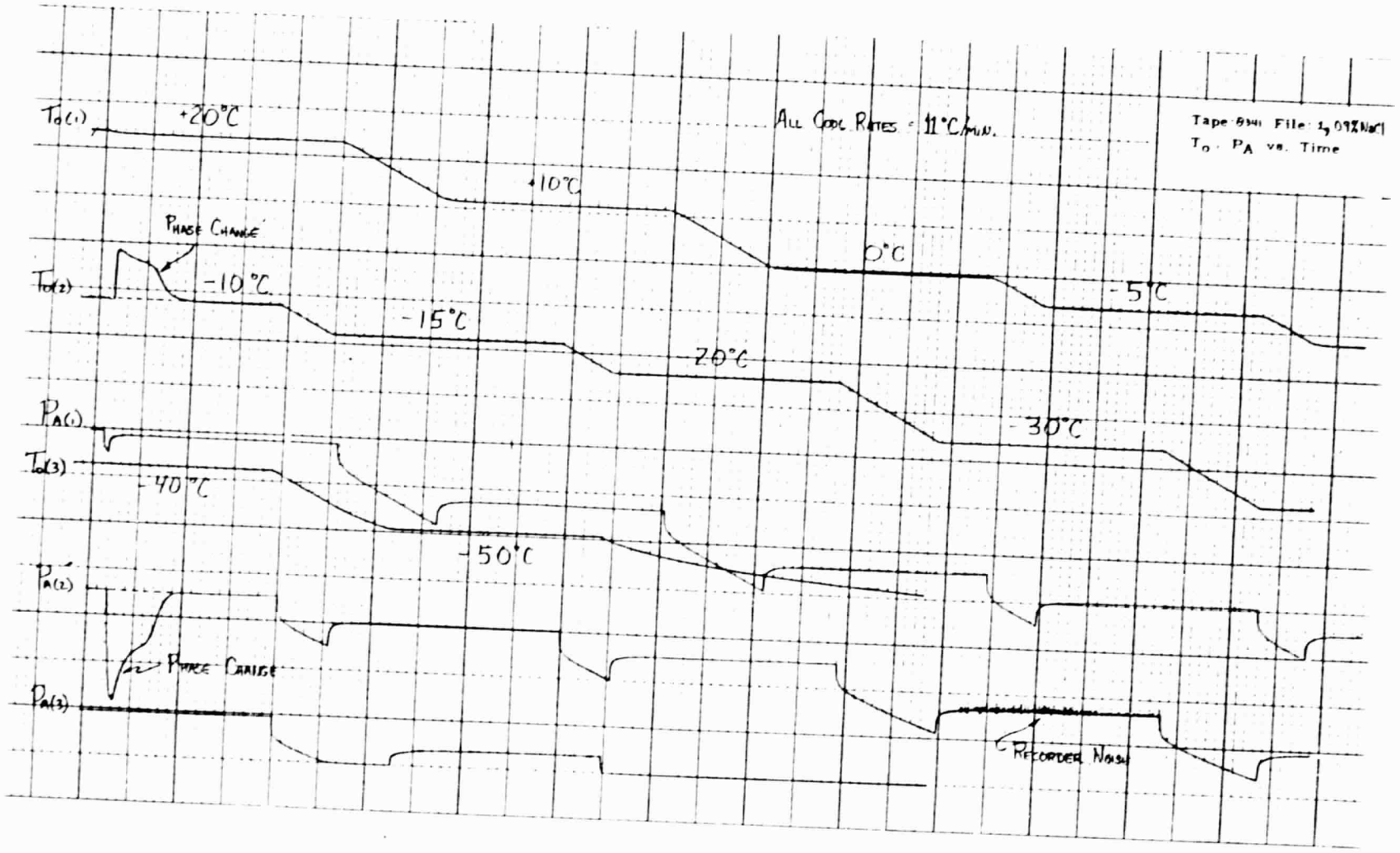

Figure 39a. T_o and P_A for Saline During Cooling (Typical)

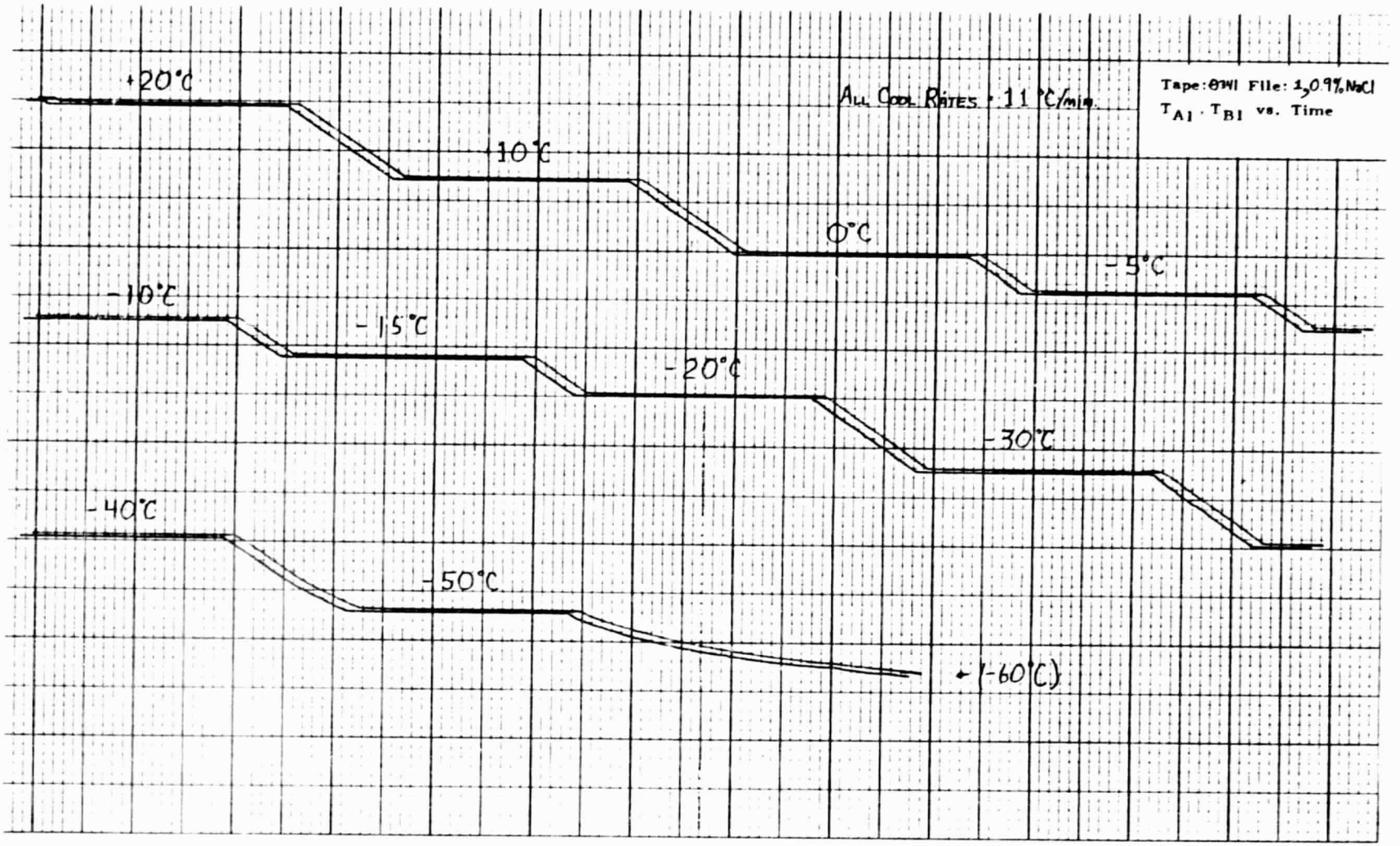

Figure 39b. T_{A1} and T_{B1} Versus Time for Saline During Cooling (Typical)

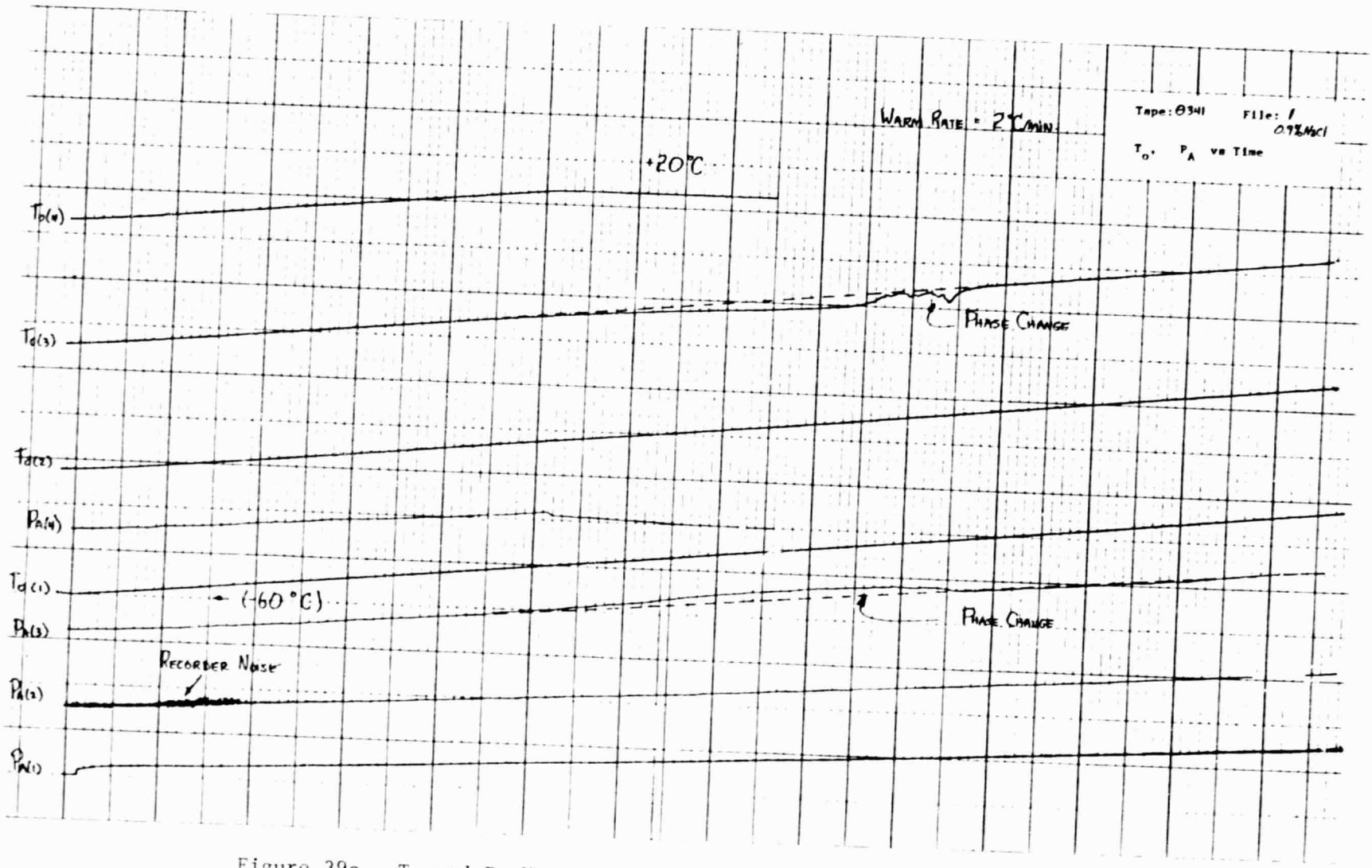

Figure 39c. T_o and P_A Versus Time for Saline During Warming (Typical)

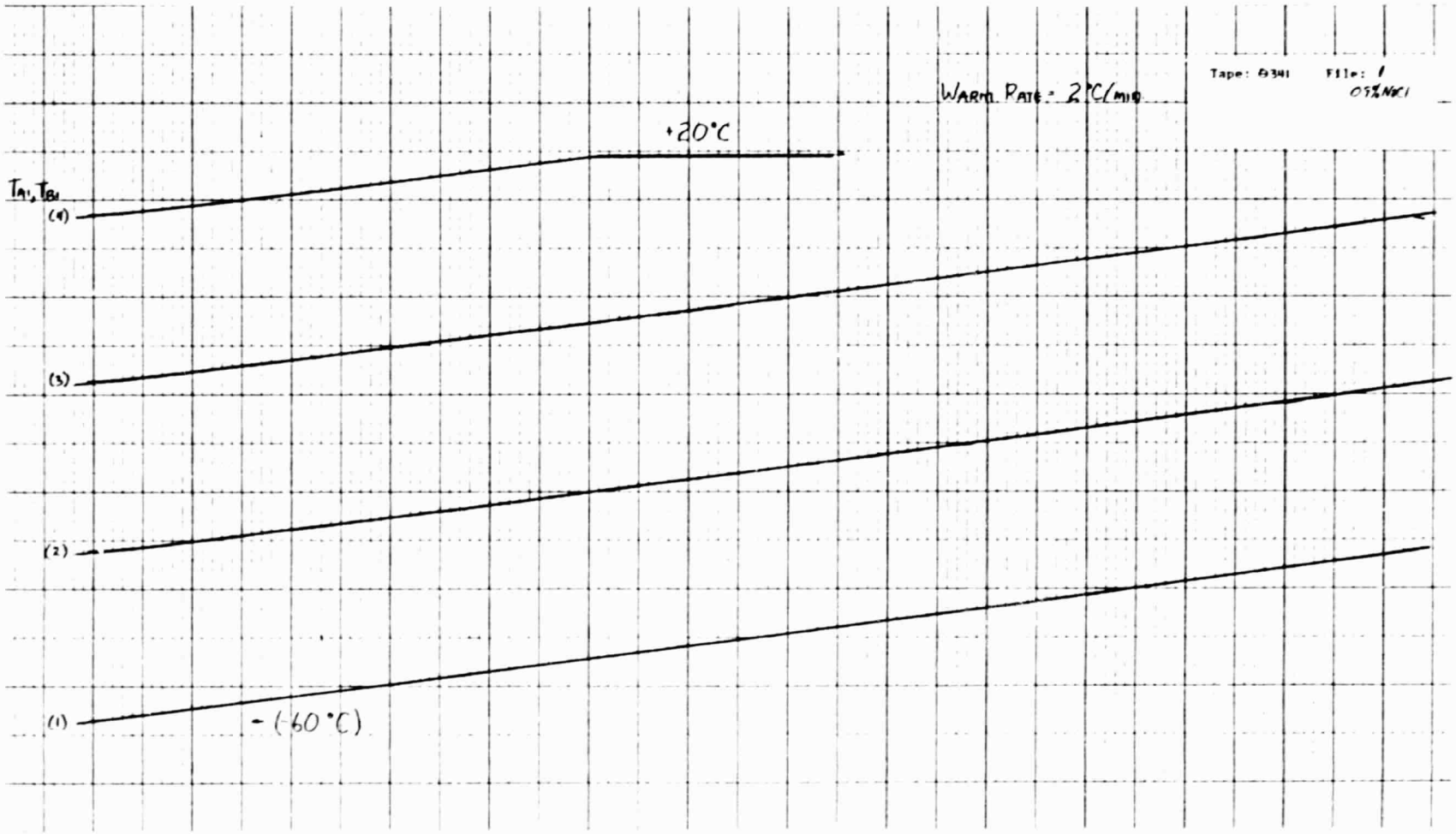

Figure 39d. T_{A1} and T_{B1} Versus Time for Saline During Warming (Typical)

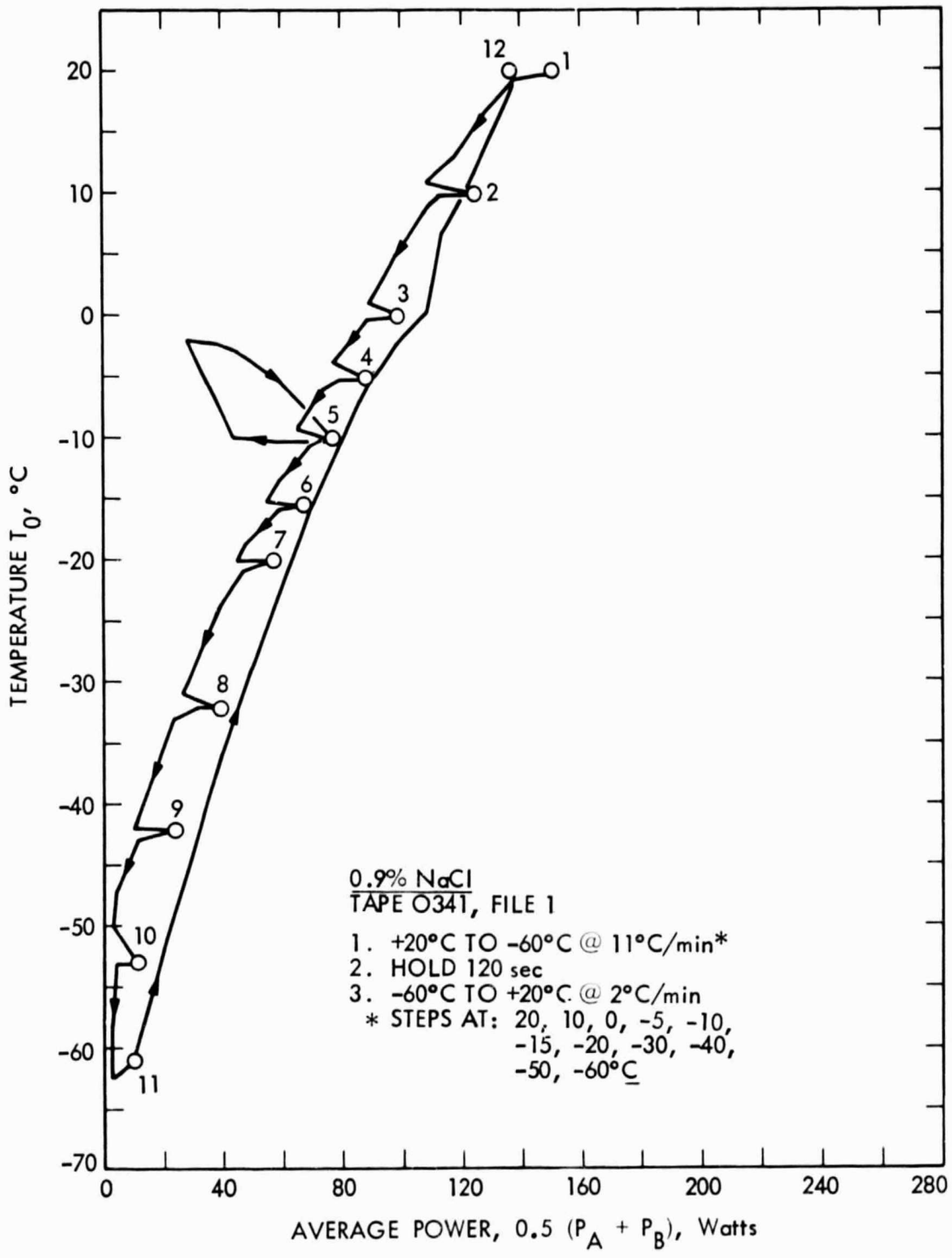

Figure 39e. T_o Versus Average Power for Saline (Typical)

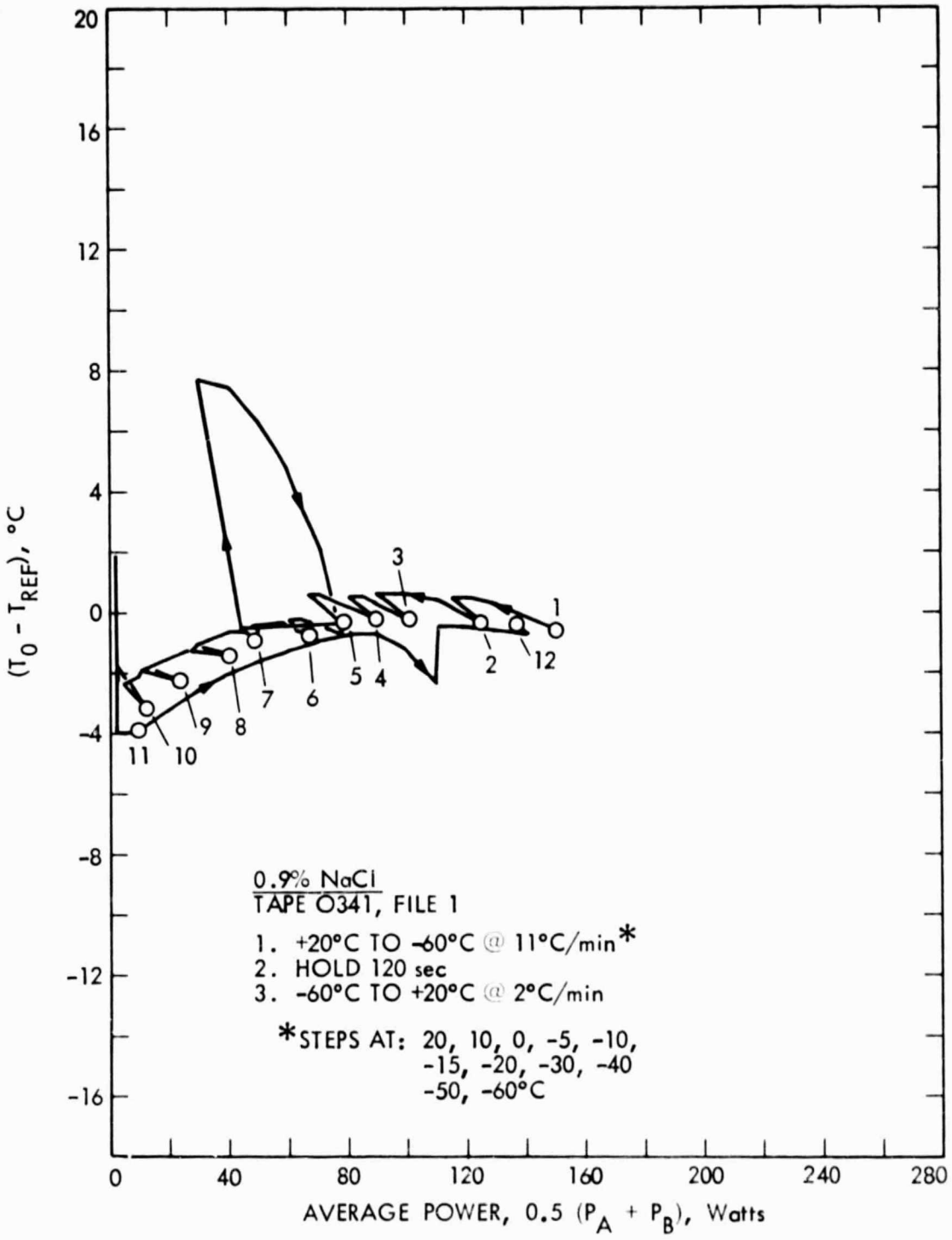

Figure 39f. T_o to Reference Temperature Differential Versus Average Power Saline (Typical)

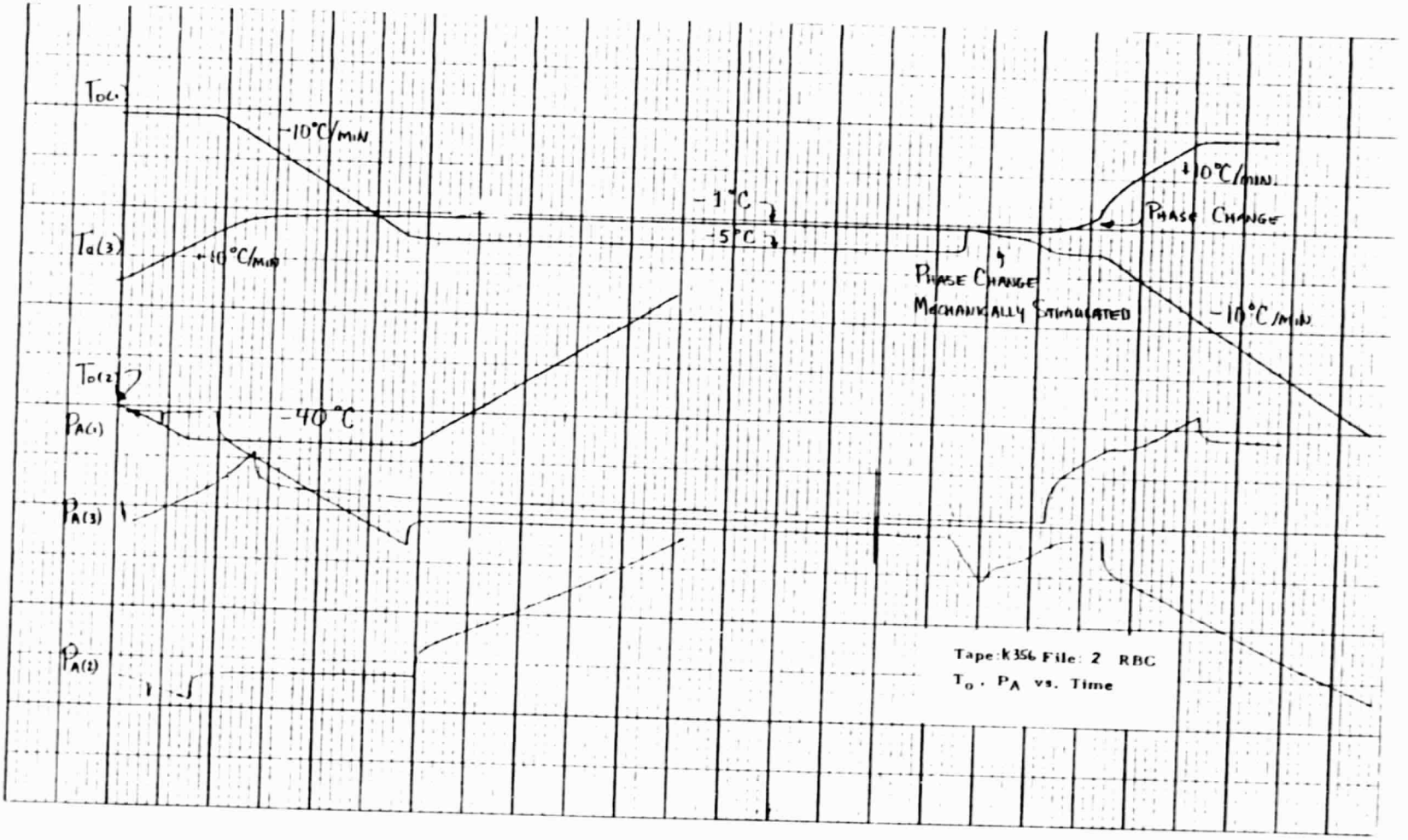

Figure 40a. T_o and P_A Versus Time for Red Blood Cell Cooling and Warming (Typical)

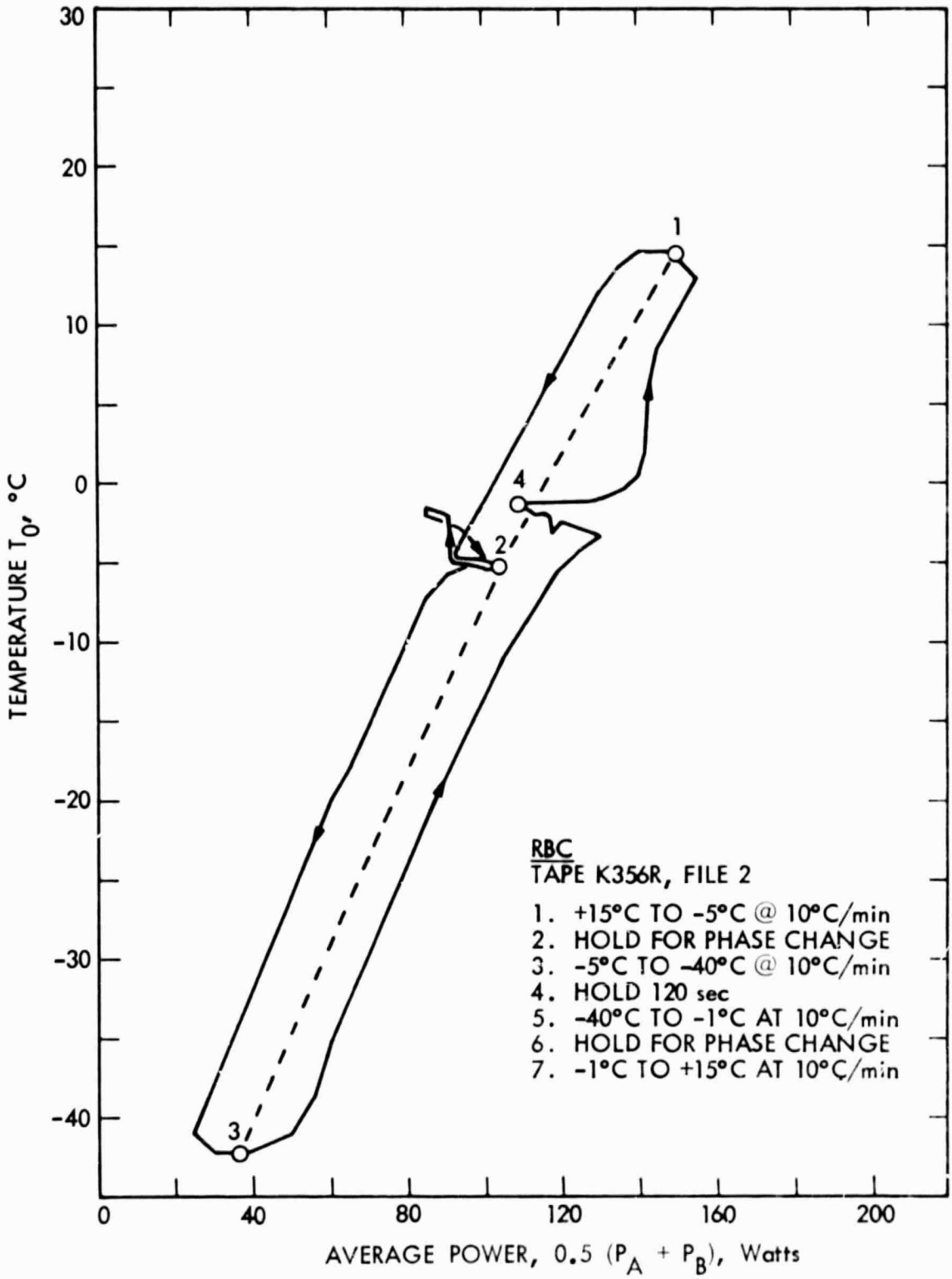

Figure 40b. T_o Versus Average Power for Red Blood Cells (Typical)

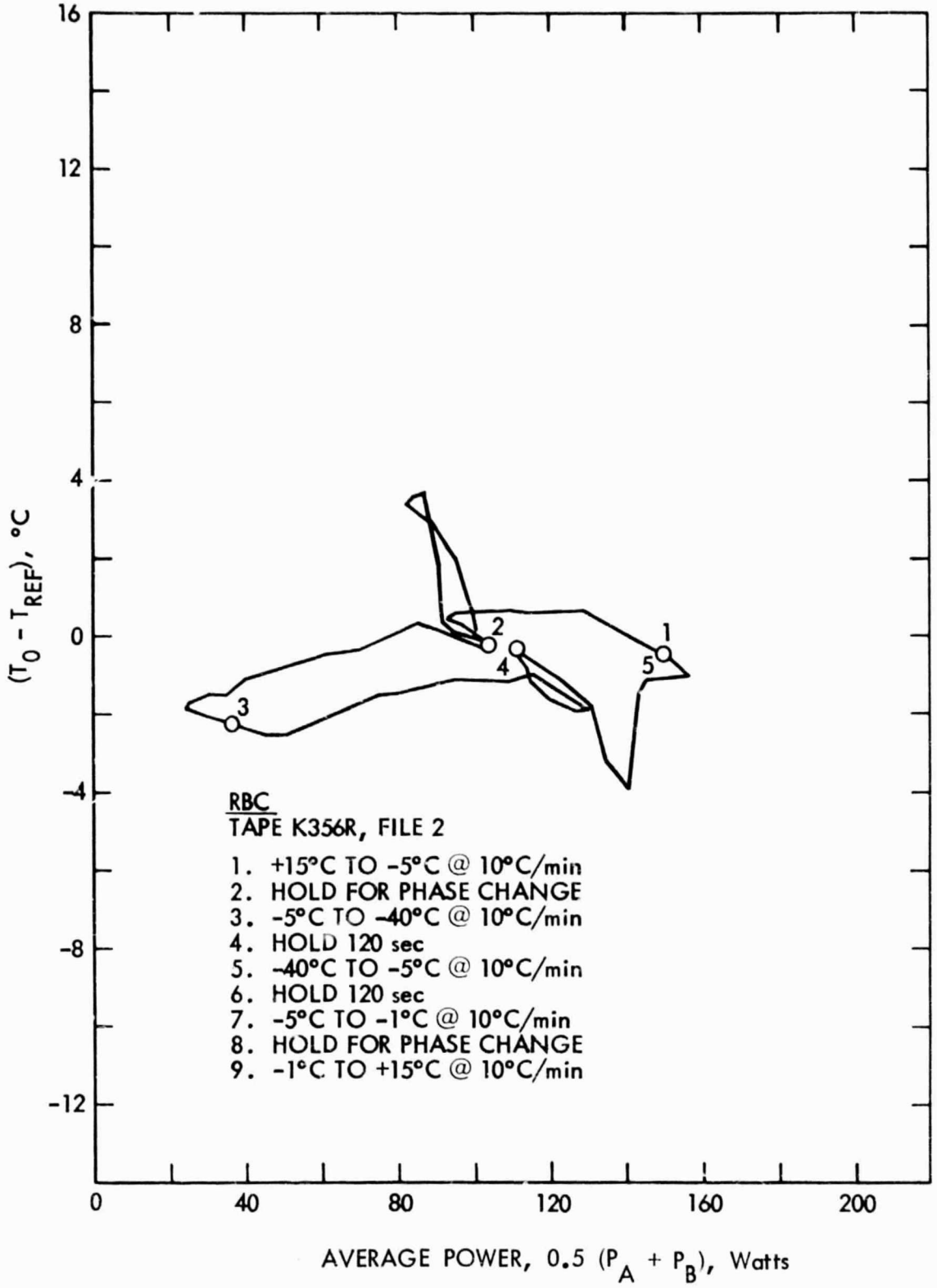

Figure 40c. T_o to Reference Temperature Differential Versus Average Power for Red Blood Cells (Typical)

			Cooling			Warming			H_2O Phase Change		Hemolysis			
Case	Tube ID	File No.	Start °C	End °C	Rate °C/Min.	Start °C	End °C	Rate °C/Min.	Yes	No	Severe	Moderate	Slight or None	No Test
1	V467	1	+15	+1	2	+1	+15	2		X			X	
2	V467	2	+15	+1	2	+1	+15	11		X			X	
3	V467	3	+15	+1	2	+1	+15	65		X			X	
4	J851	3	+15	+1	65	+1	+15	65		X			X	
5	M011	3	+15	-1	2	-1	+15	2		X			X	
6	M011	1	+15	-1	2	-1	+15	65		X			X	
7	M011	2	+15	-5	2	-5	+15	2	X			X		
8	N506	1	+15	-5	2	-5	+15	11		X			X	
9	K346	3	+15	-5	2	-5	+15	65	X					X
10	K356	1	+15	-5	2	-5	+15	65	X					X
11	N506	5	+15	-5	10	-5	+15	10		X			X	
12	0448	1	+20	-5	65	-5	+20	65	X		X			
13	N506	4	+15	-5	65	-5	+15	2	X			X		
14	N506		+15	-5	65	-5	+15	10	X				X	
15	K346	1	+15	-10	2	-10	+15	2	X				X	
16	K356	2	+15	-40	10	-40	+15	10	X		X			

Figure 41. Summary of Red Blood Cell Test Results

APPENDIX A

PATENT DESCRIPTION

Property of
U. S. Government

United States Patent [19]

Low et al.

[11] **3,733,463**

[45] **May 15, 1973**

[54] **TEMPERATURE CONTROL SYSTEM WITH A PULSE WIDTH MODULATED BRIDGE**

[76] Inventors: **George M. Low**, Acting Administrator of the National Aeronautics and Space Administration with respect to an invention of, **Richard C. Heyser**, Tujunga, Calif.

[22] Filed: **Dec. 24, 1970**

[21] Appl. No.: **101,214**

[52] **U.S. Cl.** **219/499**, 219/50

[51] **Int. Cl.** **H05b 1/02**

[58] **Field of Search** ..... 219/494, 497, 499, 219/501; 317/42; 323/75 H, 75 K

[56] **References Cited**

UNITED STATES PATENTS

2,819,372	1/1958	Booker et al.	219/499
3,526,272	9/1970	Watts et al.	219/497 X
2,681,431	6/1954	Wannamaker, Jr.	323/75 K
3,159,796	12/1964	Van Sandwyk	323/75 K
3,546,434	12/1970	Apel	219/499 UX

Primary Examiner—Bernard A. Gilheany
Assistant Examiner—F. E. Bell
Attorney—Monte F. Mott, Paul F. McCaul, John R. Manning

[57] **ABSTRACT**

A temperature control system is disclosed which includes a modified wheatstone bridge with a resistive-capacitive (RC) circuit in one leg of the bridge. The RC circuit includes a resistor which provides an effective resistance as a function of its absolute resistance and the on-time to off-time ratio of pulses supplied to a switch connected thereacross. A sawtooth voltage is produced across the RC circuit, the voltage being compared with the voltage across a temperature sensor, with heat being applied during each pulse period portion when the sawtooth voltage exceeds the voltage across the temperature sensor.

8 Claims, 2 Drawing Figures

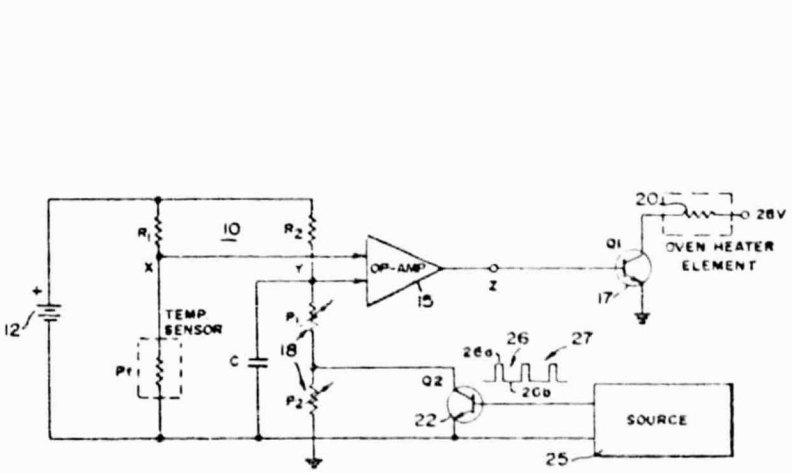

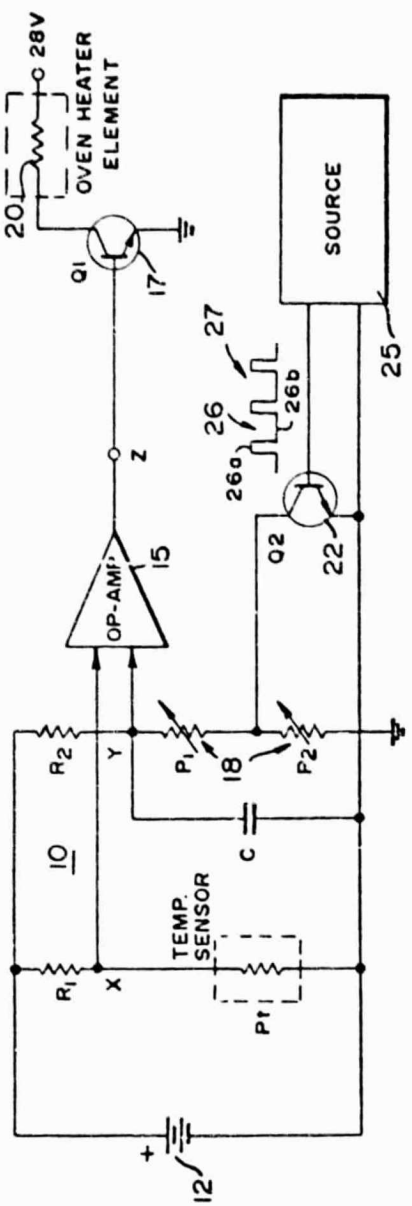

FIG. 1

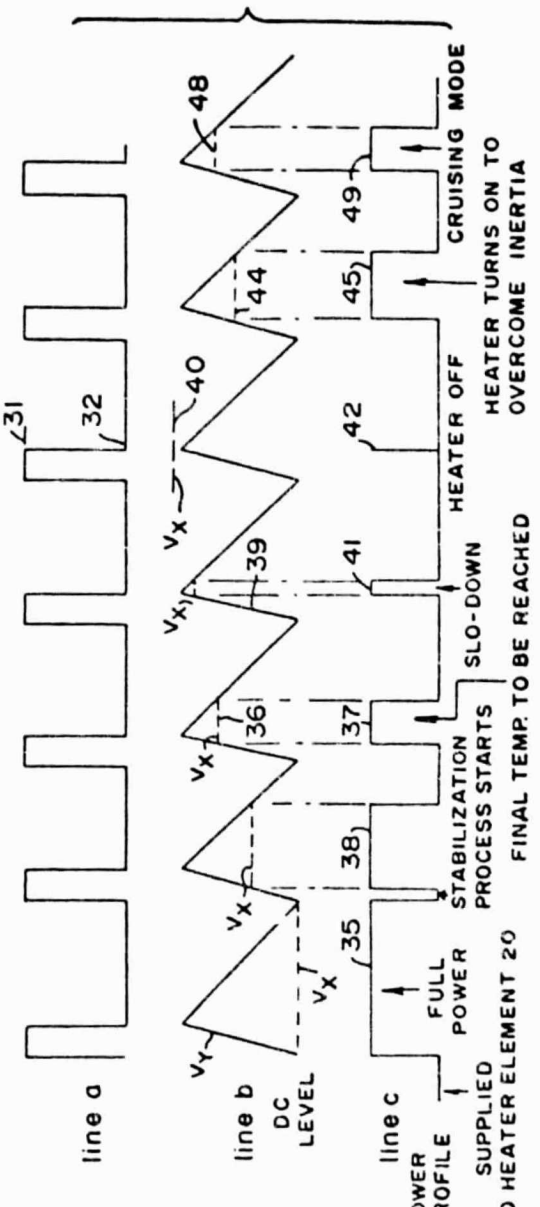

FIG. 2

RICHARD C. HEYSER
INVENTOR.

BY
ATTORNEYS

TEMPERATURE CONTROL SYSTEM WITH A PULSE WIDTH MODULATED BRIDGE

ORIGIN OF THE INVENTION

The invention described herein was made in the performance of work under a NASA contract and is subject to the provisions of Section 305 of the National Aeronautics and Space Act of 1958, Public Law 85–568 (72 Stat. 435; 42 USC 2457).

BACKGROUND OF THE INVENTION

1. Field of the Invention

The present invention generally relates to a temperature regulator and more particularly, to a system for accurately controlling the temperature of an environment within an oven or the like.

2. Description of the Prior Art

A typical temperature control system such as that described in U.S. Pat. No. 3,136,877 consists of a conventional wheatstone bridge circuit. The bridge circuit includes a temperature sensitive resistor located in the environment, whose temperature is to be controlled. When the temperature is too low, a first bridge unbalance condition arises which is detected by a sensor which closes a switch, thereby enabling power to be supplied to a heater which heats up the environment. The environment is heated up until the temperature exceeds a desired nominal temperature. As a result, a second bridge unbalance condition arises, causing the sensor to open the switch and thereby terminate the supply of power to the heater.

With such a prior art system, the environment temperature can only be controlled within a finite significant range, since power supply to the heater occurs whenever the temperature drops below the nominal temperature and is terminated whenever the temperature is above the nominal temperature. Even with sensitive instruments, the temperature range is quite significant, and is often greater than that required for very precise studies or applications, such as in space exploration studies. Thus a need exists for an improved system for accurate temperature control.

OBJECTS AND SUMMARY OF THE INVENTION

It is a primary object of the present invention to provide a new improved temperature control system.

Another object of the present invention is to provide an improved temperature control system which incorporates a novel wheatstone bridge circuit.

A further object of the present invention is to provide a new system which is programmable to control the rise in and the maintenance of an environment temperature.

These and other objects of the present invention are achieved in one embodiment by incorporating in one leg of a wheatstone bridge circuit first and second serially connected resistors, with the second resistor being connected across a switching transistor. The transistor is successively switched between on and off states, during which the second resistor is either shorted out or is in series with the first resistor. During each switching cycle the effective resistance of the second resistor which is in series with the first resistor depends on the ratio of the transistors on-time to off-time. By varying this ratio, namely by pulse width modulating the switching of the transistor, the effective resistance can be changed.

In accordance with the teachings of the present invention, a capacitor is connected across the two resistors. During each switching cycle the voltage across the capacitor which is in the form of a sawtooth is compared with the voltage across the temperature sensor in the bridge. During each cycle, power is applied to a heater only if the capacitor voltage exceeds the temperature sensor in the bridge.

The novel features of the invention are set forth with particularity in the appended claims. The invention will be best understood from the following description when read in conjunction with the accompanying drawings.

BRIEF DESCRIPTION OF THE DRAWINGS

FIG. 1 is a diagram of a basic embodiment of the present invention; and

FIG. 2 is a multiline diagram useful in explaining the embodiment shown in FIG. 1.

DESCRIPTION OF THE PREFERRED EMBODIMENTS

Attention is now called to FIG. 1 which is a combination block and schematic diagram of the present invention. Therein, numeral 10 represents a wheatstone bridge circuit, connected across a source of potential, such as a DC battery 12. The bridge 10 includes a resistor R1 which is connected in series with a temperature sensitive resistor or simply a temperature sensor Pt across the battery 12. It is sensor Pt which is located in the environment or oven whose temperature is to be controlled, and whose resistance varies as a function of temperature. The junction point X between R1 and Pt is connected to one input of an operational amplifier 15. The bridge also includes another resistor R2 which is serially connected with variable resistors P1 and P2 across battery 12. A capacitor C is connected in parallel across P1 and P2 and the junction point Y between R2 and P1 and C is connected to the other input of amplifier 15.

The latter is operated as a comparator to provide an output at point Z of a preselected level which closes a switch 17 only when the voltage at point Y is greater than that at point X. When the switch 17, which is represented in FIG. 1 by a transistor Q1, is closed it connects an oven heater element 20 across a source of potential, shown in FIG. 1 at +28V. Thus, only when switch 17 is closed is heat supplied to the oven by element 20.

As shown in FIG. 1, connected across the resistor P2 is a switch 22, in the form of a transistor Q2, which is activated by pulses such as pulses 26 and 27, from a source 25, which are supplied at a selected rate. Each pulse, such as pulse 26, has an on-time 26a during which the switch is closed so that P2 is shorted out, and an off-time 26b, during which the switch is open so that P2 is not affected. The ratio of on-time to off-time is assumed to be controlled by source 25, which may in turn be controlled by a programmed computer (not shown). The control of the on-time to off-time ratio may be thought of as controlling or modulating the pulse width of each pulse. Therefore, source 25 can be thought of as a source of pulse-width-modulated (PWM) pulses.

In effect, during the on-time of each pulse P2 is shorted out, thus its resistance is zero, neglecting the collector to emitter resistance of Q2. On the other hand, during pulse off-time the full resistance of P2 is

in series with P1. Thus, by controlling the on-time to off-time ratio the effective resistance of P2 during the full pulse duration is controlled. For example, if the on-time is only 25 percent of the pulse period, the effective resistance is one-fourth the resistance of P2. On the other hand, if the on-time is half the pulse period, the effective resistance is half the P2 resistance. In practice P1 is selected to equal the resistance of Pt at an ambient temperature, while the effective resistance of P2 is chosen to equal the change (increase) in the resistance of Pt due to a change from the ambient temperature to a chosen temperature to be controlled.

The voltage at point Y changes due to the change in the resistance which P2 provides in series with P1. In the absence of C the voltage at Y would have a square wave shape as shown in line a of FIG. 2. The upper voltage level 31 would be present when Q2 is off and the lower voltage level 32 would be present when Q2 is on and P2 is shorted out. Therein, it is assumed that the off-time to on-time ratio is about 1:3. That is, during each pulse period the transistor Q2 is on for about 75 percent of the period. However, with C in the circuit due to the time constant of the circuit formed by C, P1 and P2, the voltage at point Y during the period of each pulse from source 25 does not have the square wave shape shown in line a but rather the sawtooth shape as shown in FIG. 2, line *b* and designated V_X.

From the foregoing description it should thus be appreciated that in the present invention, during each pulse period, heat is applied to element 20 only during that portion of the pulse period when the voltage at point X designated in FIG. 2 by the dashed line V_X is less than V_Y. Assuming that V_X is less than V_Y during an entire pulse period, power is supplied to heater element 20 during the entire period, as represented by numeral 35 in line *c* which is used to diagram the power profile supplied to heater element 20, and which corresponds to the output of amplifier 15. On the other hand, if V_X is greater than the maximum value of V_Y during an entire pulse period, the heater element is completely off during the entire period. Thus, the amount or quantity of heat which is supplied by heater element 20 to the oven during each pulse period is a function of the actual oven temperature as represented by V_X and the shape of V_Y which is controllable by the time constant and the pulse width modulation.

From the foregoing it should be appreciated that, assuming a constant pulse frequency, by controlling the pulse width modulation, the rate at which the oven temperature is raised to a desired temperature may be controlled. Furthermore, once this temperature is reached it may be accurately maintained by controlling the pulse width modulation so that during each pulse period only that amount of heat which is necessary to maintain the oven at the desired temperature is provided by heater element 20. Maximum rate of temperature rise may be achieved by making the on-time per pulse period equal to zero thereby raising the level of V_Y to a maximum so that power is supplied to the heater element during the full period of each pulse. The rate at which temperature is increased from a first temperature such as *t*1 to *t*2 may be controlled by the pulse width modulation of the pulses to produce a desired rate at which power is supplied to the heater element 20. Once the desired temperature is reached, the pulse width modulation is selected to insure the supply of power per pulse period which is required to maintain the oven at the desired temperature. Experience with the novel invention has demonstrated the ability to control an oven temperature to within less than 0.01°C, e.g., 0.001°C.

Referring again to FIG. 2, let it be assumed that the final desired temperature is that represented by the line 36 for V_X and that the power or heat per pulse needed to maintain that temperature is represented by numeral 37. Let it further be assumed that the oven is below the desired temperature. Thus, more power than is required to maintain the desired temperature is supplied to the heater per pulse, as represented by lines 35 and 38. In practice, the oven temperature may briefly oscillate above and below the desired temperature until the temperature is stabilized. In FIG. 2, lines 39 and 40 represent V_X when the temperature is above the desired temperature. In response to the level represented by line 39, less than the required heat is supplied as represented by line 41. Since level 40 is above the maximum value of V_Y no power is applied to heater element 20 as represented by line 42. Line 44 represents an oven temperature below the desired temperature. Consequently, more power than necessary to maintain the desired temperature is applied as represented by line 45. Lines 48 and 49 respectively, represent V_X at the desired temperature and the power per pulse period needed to maintain the desired temperature.

Although particular embodiments of the invention have been described and illustrated herein, it is recognized that modifications and variations may readily occur to those skilled in the art and, consequently, it is intended that the claims be interpreted to cover such modifications and equivalents.

What is claimed is:

1. A temperature control system comprising:

a wheatstone-like bridge having first and second parallel legs and including a temperature sensitive element, whose resistance varies as a function of temperature, connected in series with a first bridge resistor in said first leg, and a resistor-capacitor circuit connected in series with a second bridge resistor in said second leg;

a source of power;

heating means for providing heat when connected to said source;

means for applying a voltage across said bridge, whereby the voltages across said element circuit are functions of the resistances thereacross, respectiveiy,

means coupled to said element and to said circuit for connecting said heating means to said source when the voltage across said circuit is greater than the voltage across said element; and

control means coupled to said circuit for controlling the resistance across said circuit to vary in a preselected manner during each of a succession of pulse periods with the capacitor of said circuit controlling the voltage of said circuit to vary in a preselected manner from a first level to a second level during a first portion of each pulse period and from said second level to said first level during the rest of the pulse period following said first portion.

2. The arrangement as recited in claim 1 wherein said circuit consists of first and second resistors connected in series and said capacitor is connected in parallel across at least one of said resistors and said control means is coupled to said second resistor and includes

first means for shorting out said second resistor during said first portion of each pulse period, with said first portion being selectively variable.

3. The arrangement as recited in claim 2 wherein said control means include second means for providing a succession of equal period pulses, each pulse being of a first level during said first portion of each pulse period and of a second level during the rest of the pulse period, and means for applying said pulses to said first means to short out said second resistor during the first portion of each pulse period.

4. The arrangement as recited in claim 2 wherein said capacitor is connected in parallel across both said first and second resistors, whereby when said second resistor is shorted out the voltage across said capacitor, representing the voltage across said circuit, rises gradually from said first level to said second level and falls gradually from said second level to said first level during the rest of each pulse period when said second resistor is not shorted out, with the voltage across the circuit during each pulse period having the shape of a sawtooth.

5. The arrangement as recited in claim 4 wherein said control means include second means for providing a succession of equal period pulses, each pulse being of a first level during the first portion of each pulse period and of a second level during the rest of the pulse period, and means for applying said pulses to said first means to short out said second resistor during the first portion of each pulse period.

6. In a temperature control system of the type comprising a bridge with a temperature sensitive element whose resistance varies as a function of temperature in one leg of said bridge, said system further including means for comparing the voltage across said element with the voltage across another leg of said bridge, an arrangement comprising:

a resistor having first and second terminals in said other leg;

control means for controlling the resistance across said terminals to vary from the full resistance of said resistor to substantially zero during a selected portion of each of a succession of periods, whereby the effective resistance across said terminals during each period is less than the resistance of said resistor; and

a capacitor in said other leg connected in parallel across at least said resistor whereby the voltage across said other leg increases toward a peak value when the resistance across said terminals is the full resistance of said resistor and decreases from said peak value when the resistance across said terminals is substantially zero.

7. The arrangement as recited in claim 6 wherein said control means includes a switch which is connected across said first and second terminals, said switch being switchable to an on state in which said terminals are effectively shorted out and an off state during which the resistance across said terminals is the resistance of said resistor, and source means coupled to said switch means for controlling said switch to be in the on state during a selected portion of each of said periods and in the off state during the rest of each of said periods.

8. The arrangement as recited in claim 7 wherein said source means is a source of a succession of equal period pulses, each pulse being of a first level which switches said switch to its on state during a variably selected period portion and of a second level which switches said switch to its off state during the rest of the pulse period.

* * * * *

APPENDIX B

CENTRIFUGAL RED BLOOD CELL FREEZE/THAW CONCEPT

In the initial conceptual design phase of this work a parallel design effort was established which considered both the flat plate container as discussed in the bulk of this text and the centrifugal device which is described in this appendix.

The centrifugal system can be divided into three groups of components as shown in Figures B-1, B-2 and B-3. Figure B-1 depicts the gaseous nitrogen (GN_2) temperature control system. Liquid nitrogen (LN_2) or gaseous nitrogen (GN_2) is passed through an electrical heater which establishes an environment temperature as measured by the thermocouple rakes to within about $1^{o}C$ of the desired blood mass temperature. The mixers are a set of baffles which produce an isothermal flow cross section. The flow then passes through a flow laminator to provide uniform convective heating or cooling of the cylindrical rotating tube which contains the red blood cells. The red blood cell mass is divided into a test volume, accompanied by adjacent guard volumes, so that maximum control and information of the test volume dynamics can be obtained. The tube is rotated by a stepper motor to allow uniform circumferential heat exchange with the flow. Electrical connections between the electronic control and monitoring system, and the temperature sensors and heaters on the tube itself are made through the mercury (Hg) slip rings at either edge of the tube.

The tube assembly which contains the red blood cells is depicted in Figure B-2. The test volume of cells is separated from the guard volumes by spacers which can move in the longitudinal direction to accommodate freeze expansion. The thickness of the blood annulus within the tube is less than the spacers; consequently, radial freeze expansion is also possible. The fine temperature control of the cell mass is accomplished by a pair of bifilar heater/sensor windings, separated by a thin Kapton film which acts as an electrical insulator. These are shown in detail in Figure B-3.

Figure B-4 depicts the block diagram for the system. A temperature profile memory is fed to the sequencer comparator which in turn senses the temperature of the cell mass and controls the heater power so that the input temperature profile is followed by the cell mass. The sequencer comparator also sets the heat sink (or flow) temperature by adjusting the GN_2/LN_2 mixture ratio and by setting the GN_2 heater power.

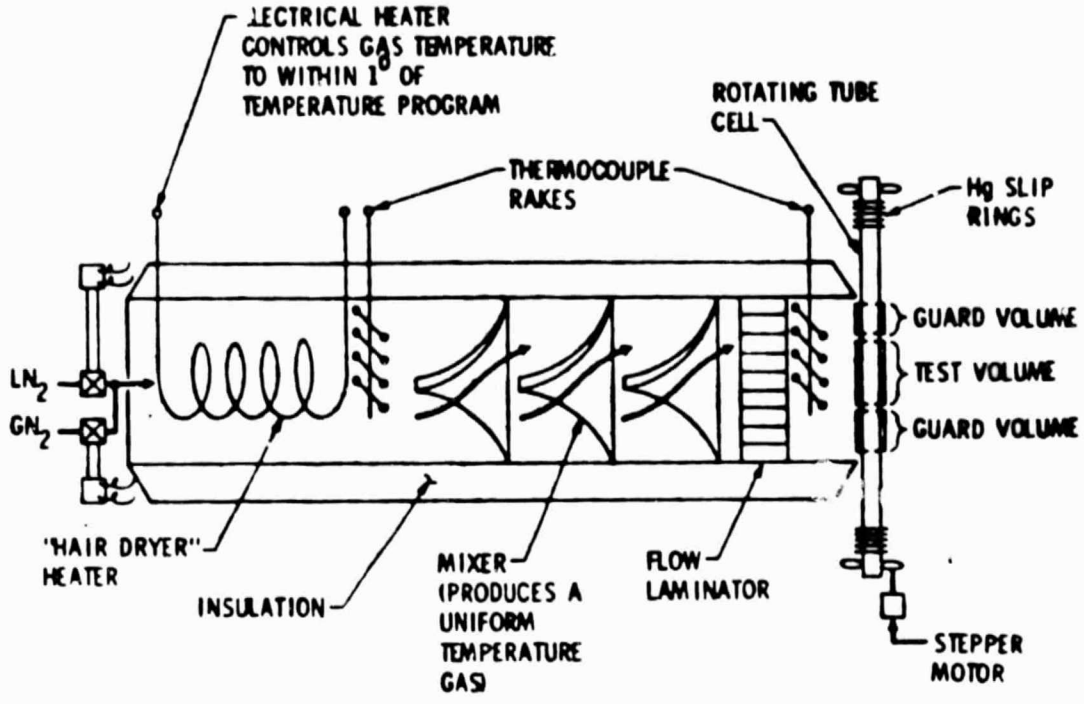

Figure B-1. GN_2 Temperature Control System

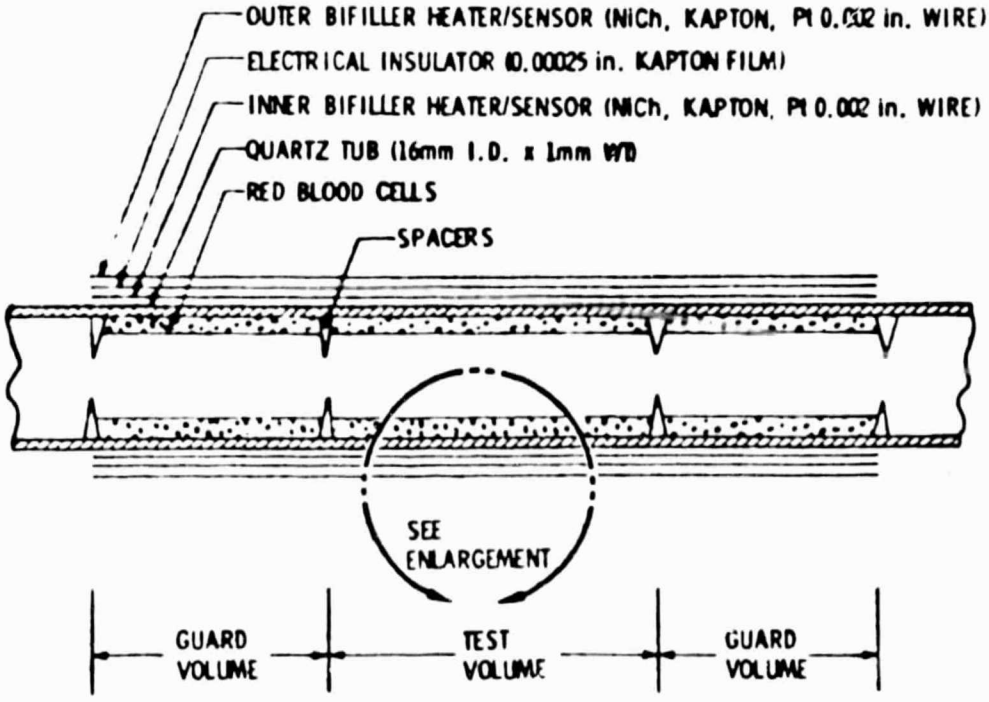

Figure B-2. Freeze/Thaw Cell Tube Assembly

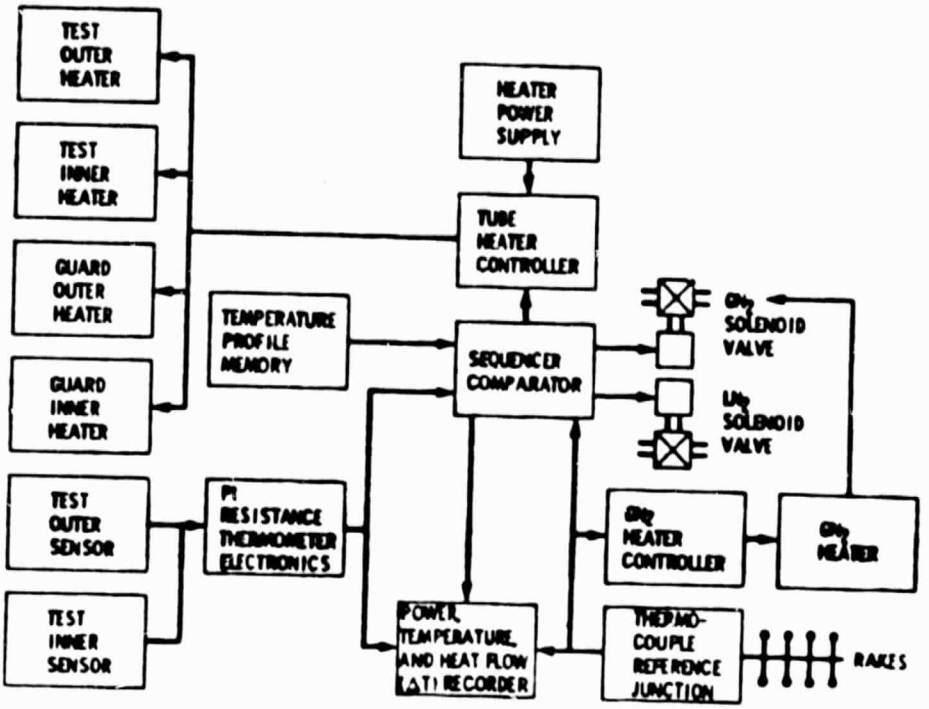

Figure B-3. System Block Diagram

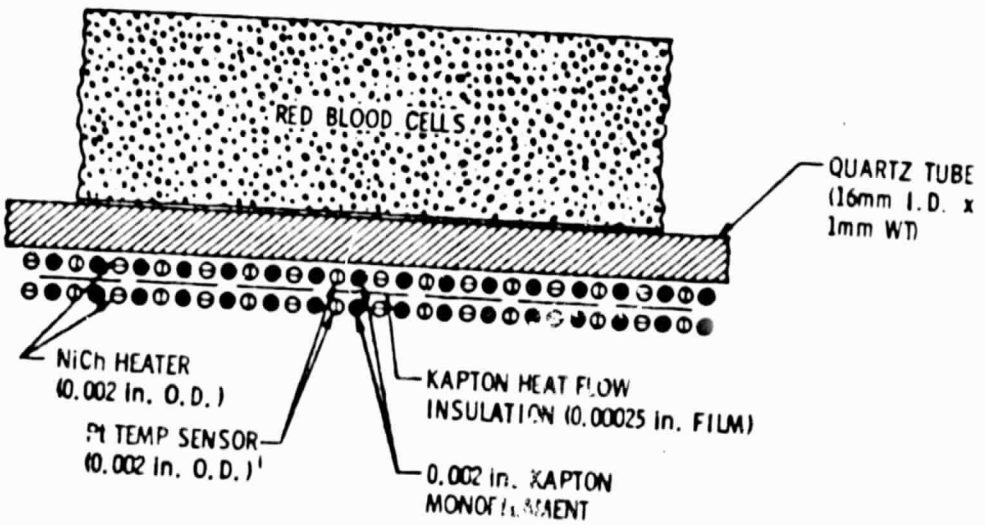

Figure B-4. Enlargement of Tube Wall

APPENDIX C

THERMAL ANALYSIS OF RED BLOOD CELL FREEZING SYSTEM

In order to provide an approximate thermal analysis of the freeze/thaw system, the component structural elements of the container were reorganized into the heat transfer analysis model shown in Figure C-1. Figure C-1 relates each element of the model with that of the actual container as described in Figure 7. For the purposes of this analysis it is not as important to identify the real thermal properties of the device as it is to demonstrate the procedures by which the thermodynamic properties and characteristics of the sample mass can be evaluated. This is accomplished assuming one dimensional heat flow through the container walls and neglecting the effects of radiation and convection.

An energy balance is derived for each element of the analytical model except for the exterior elements. The temperatures of these elements are used as boundary conditions for the analysis and the thermal coupling of these elements with the cold sink is uninformative for the purposes of this work.

When the energy balances are described for the general transient condition, the relationships for the thermal resistances between each of the model elements are derived in terms of temperatures and powers monitored by the existing system. Having these physical characteristics of the container, equations are developed for the temperature dependent thermal conductivity and specific heat of the sample mass, and for the sample mass heat of phase change

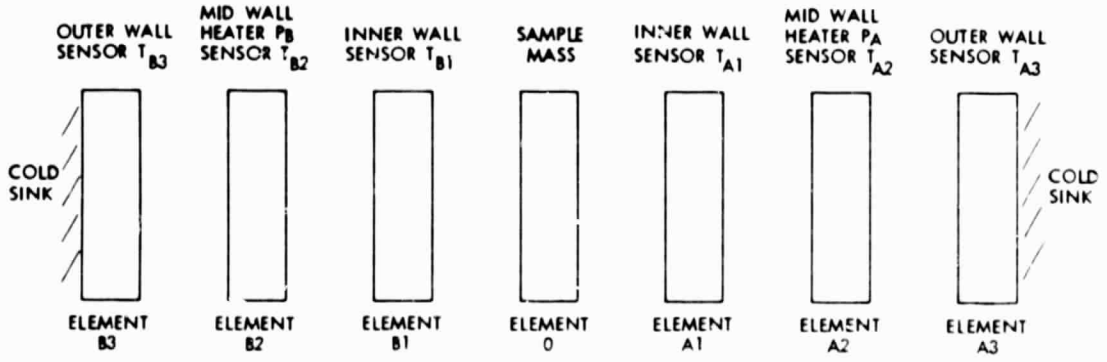

Figure C1. Heat Transfer Analysis Model

LIST OF SYMBOLS

A	-	area of element normal to heat transfer
C_x	-	specific heat of element x
$f_{(x)}$	-	correction factor (equation 41)
$g_{(x)}$	-	correction factor (equation 45)
h_o	-	instantaneous rate of heat production or absorption due to phase change
K_x	-	thermal conductivity of element x
M_x	-	mass of element x
P_x	-	power generated in element x
$R_{(X-Y)}$	-	thermal resistance between elements X and Y
t	-	thickness of element in direction of heat transfer
T_x	-	temperature of element x
T_{MN}	-	average temperature of elements M and N
θ	-	time
ψ	-	experiment function (equation 40)
ϕ	-	experiment function (equation 44)
$*$	-	at a steady state condition with uniform temperatures between heaters
$'$	-	at a steady state condition with an imposed temperature gradient between heaters

1. Basic Energy Balance

The energy balance for a model element is formed by equating the rate of change of the internal energy of that element to the power dissipated within the element less the heat conducted from the element. In general this is written as:

$$MC \frac{dT}{d\theta} = P \frac{\Delta T}{R_{(X-Y)}} \qquad (1)$$

C-2

Writing this for each of the elements of the analytical model there results

a. Central Element (o)

$$M_o C_o \frac{dT_o}{d\theta} = h_o - \left(\frac{T_o - T_{A1}}{R_{(o-A1)}}\right) - \left(\frac{T_o - T_{B1}}{R_{(o-B1)}}\right) \tag{2}$$

b. Element (A1)

$$M_{A1} C_{A1} \frac{dT_{A1}}{d\theta} = P_A - \left(\frac{T_{A1} - T_o}{R_{(A1-o)}}\right) - \left(\frac{T_{A2} - T_{A1}}{R_{(A2-A1)}}\right) \tag{3}$$

c. Element (B1)

$$M_{B1} C_{B1} \frac{dT_{B1}}{d\theta} = P_B - \left(\frac{T_{B1} - T_o}{R_{(B1-o)}}\right) - \left(\frac{T_{B2} - T_{B1}}{R_{(B2-B1)}}\right) \tag{4}$$

d. Element (A2)

$$M_{A2} C_{A2} \frac{dT_{A2}}{d\theta} = - \left(\frac{T_{A2} - T_{A1}}{R_{(A2-A1)}}\right) - \left(\frac{T_{A2} - T_{A3}}{R_{(A2-A3)}}\right) \tag{5}$$

e. Element (B2)

$$M_{B2} C_{B2} \frac{dT_{B2}}{d\theta} = - \left(\frac{T_{B2} - T_{B1}}{R_{(B2-B1)}}\right) - \left(\frac{T_{B2} - T_{B3}}{R_{(B2-B3)}}\right) \tag{6}$$

f. Element (A3)

Boundary Condition: T_{A3} Known as function of time

g. Element (B3)

Boundary Condition: T_{B3} Known as function of time

2. SOLUTION FOR THERMAL RESISTANCE VALUES

For a given steady state condition, the derivative of temperature with respect to time is zero, and the electrical power and temperature differentials are constant

$$\frac{dT}{d\theta} = o \tag{7}$$

$$P = \text{constant} = P^* \tag{8}$$

$$\Delta T = \text{constant} = \Delta T^* \tag{9}$$

Using these values in Equation (1), there results the relation for the thermal resistance as a function of temperature.

$$R_{(X-Y)} = \frac{\Delta T^*}{P^*} \tag{10}$$

If the resistance is not a strong function of temperature, it can be approximated by noting that the temperature differential is the difference of two known temperatures.

$$\Delta T = T_i - T_j \tag{11}$$

Therefore the approximate temperature level of the element is calculated by

$$T^* = 0.5(T_i + T_j) \tag{12}$$

The resistance is then expressed as a function of the approximate temperature level T^*

$$R_{(X-Y)}\ (T^*) = \frac{\Delta T^*}{P^*} \tag{13}$$

This basic approach, discussed above, is used to obtain the thermal resistances of the analysis model

a. Thermal Resistance: $R_{(A2-A1)}$

Under steady state conditions, the temperature gradient between all elements internal to the heaters, i.e., T_o, T_{A1} and T_{B1}, vanishes so that

$$T_o^* = T_{A1}^* = T_{B1}^* \tag{14}$$

Applying Equation (14) to the steady state form of Equation (3), yields

$$R_{(A2-A1)}\ (T_{AA}^*) = \frac{(T_{A2}-T_{A1})^*}{P_A^*} \tag{15}$$

where

$$T_{AA}^* = 0.5(T_{A2}^* + T_{A1}^*) \tag{16}$$

Equation (15) states that the thermal resistance between elements (A1) and (A2) is an approximate function of the average temperature of those elements, T_{AA}^*.

b. Thermal Resistance: $R_{(B2-B1)}$

Equation (14) is applied to the steady state form of Equation (4) to yield

$$R_{(B2-B1)}(T_{BA}^{*}) = \frac{(T_{B2}-T_{B1})^{*}}{P_{B}^{*}} \tag{17}$$

where

$$T_{BA}^{*} = 0.5\,(T_{B2}^{*}+T_{B1}^{*}) \tag{18}$$

The elements of equations (17) and (18) are defined in a way similar to those of equations (15) and (16). With the application in this case being to the "B" wall.

c. Thermal Resistance: $R_{(A2-A3)}$

The steady state form of Equation (5) yields

$$R_{(A2-A3)}\left(T_{AB}^{*},T_{AA}^{*}\right) = R_{(A2-A1)}\,(T_{AA}^{*})\,\frac{(T_{A2}-T_{A3})^{*}}{(T_{A1}-T_{A2})^{*}} \tag{19}$$

where

$$T_{AB}^{*} = 0.5\,(T_{A2}+T_{A3}) \tag{20}$$

Equation (19) gives the resistance between elements (A2) and (A3) in terms of that between (A1) and (A2). Consequently the dependent variable is a function of both the average temperature between (A2) and (A3), given as T_{AB}^{*}, and that for the (A1) and (A2) elements, given as T_{AA}^{*}. The presence of this unusual dependence is not a real physical

dependence but simply results from the analysis approach. Inserting Equation (15) into Equation (19) there results.

$$R_{(A2-A3)} \ (T_{AB}{}^{*}) = \frac{(T_{A3}-T_{A2})^{*}}{P_{A}{}^{*}} \tag{21}$$

d. Thermal Resistance: $R_{(B2-B3)}$

Using a method analogous to the development of Equation (21), there results

$$R_{(B2-B3)} \ (T_{BB}{}^{*}) = \frac{(T_{B3}-T_{B2})^{*}}{P_{B}{}^{*}} \tag{22}$$

where

$$T_{BB}{}^{*} = 0.5(T_{B3}+T_{B2}{}^{*}) \tag{23}$$

e. Thermal Resistance: $R_{(o-A1)}$ (thermal conductivity of sample)

The thermal resistance between the sample volume (o) and the interior wall (A1) is composed of two elements. One element corresponds to the sample volume, the other to the interior wall

$$R_{(o-A1)} = R_{o} + R_{A1} \tag{24}$$

In general an arbitrary thermal resistance is inversely proportional to the thermal conductivity and the cross sectional area of the material for which it is being applied and directly proportional to the thickness of the material in the direction of the heat flow.

$$R = \frac{t}{KA} \tag{25}$$

Then Equation (24) becomes

$$R_{(o-A1)} = \frac{t_o}{R_o A_o} + \frac{t_{A1}}{K_{A1} A_{A1}} \tag{26}$$

For the device in question

$$\left(\frac{t_o}{A_o}\right) \approx \left(\frac{t_{A1}}{A_{A1}}\right) \approx \left(\frac{t'}{A'}\right) \tag{27}$$

and the resistance becomes

$$R_{(o-A1)} = \frac{t'}{A'} \left(\frac{1}{K_o} + \frac{1}{K_{A1}}\right) \tag{28}$$

Considering that a typical sample mass will have the conductivity (K_o) of water and the inner wall is aluminum (K_{A1}), then it is true that

$$\frac{1}{K_o} \gg \frac{1}{K_{A1}} \tag{29}$$

so that Equation (28) can be rewritten totally in terms of the sample mass

$$R_{(o-A1)} \approx \frac{t_o}{K_o A_o} = R_o \tag{30}$$

Similarly for the (B) side

$$R_{(o-B1)} \approx \frac{t_o}{K_o A_o} = R_o \tag{31}$$

During periods when there is no phase change

$$h_o = 0 \tag{32}$$

Now a unique capability of the system will be involved. A steady state gradient is established such that

$$P_A' > P_B' \tag{33}$$

and

$$T_{A2}' > T_{A1}' > T_o' > T_{B1}' > T_{B2}' \tag{34}$$

If the temperature difference across the sample mass is of the order of a few degrees centigrade, then T_o' is a good representation of the sample mass temperature. Applying Equations (30), (31), and (32) to Equation (3) under the conditions of the steady state gradient.

$$R_o(T_o') = \frac{(T_{A1}-T_o)'}{\left[P_A' - \frac{(T_{A2}-T_{A1})'}{R_{(A2-A1)}*}\right]} \tag{35}$$

The thermal resistance $R_{(A2-A1)}*$ is obtained from Equation (15)

$$R_o(T_o') = \frac{(T_{A1}-T_o)'}{\left[P_A' - \frac{(T_{A2}-T_{A1})'}{(T_{A2}-T_{A1})*} P_A*\right]} \tag{36}$$

Solving for the thermal conductivity of the sample mass from Equation (30)

$$k_o = \left(\frac{t_o}{A_o}\right) \times \frac{1}{R_o} \tag{37}$$

Incorporating Equation (36) into Equation (37)

$$k_o(T_o') = \frac{t_o}{A_o}\left[\frac{P_A' - \frac{(T_{A2}-T_{A1})'}{(T_{A2}-T_{A1})^*}P_A^*}{(T_{A1}-T_o)'}\right] \tag{38}$$

A similar equation can be derived for the (B) wall. If this is done, k_o is determined as the average of the two values.

$$k_o(T_o') = \left(\frac{t_o}{2A_o}\right)\left[\frac{P_A' - \frac{(T_{A2}-T_{A1})'}{(T_{A2}-T_{A1})^*}P_A^*}{(T_{A1}-T_o)'} + \frac{P_B' - \frac{(T_{B2}-T_{B1})'}{(T_{B2}-T_{B1})^*}P_B^*}{(T_{B1}-T_o)'}\right] \tag{39}$$

Equation (39) presents a valid theoretical prediction for the thermal conductivity of the sample mass. However, it often is advisable to reference the calculation to a mass of known conductivity such as distilled water. Given the same apparatus and the same value for (T_o'), Equation (39) can be used to calculate the conductivity for water. This will involve the relationship given in Equation (39) plus a correction factor assumed to be a function of (T_o'). If Equation (39) is written as

$$k_o(T_o') = \left(\frac{t_o}{2A_o}\right)\psi_o \tag{40}$$

where ψ_o is the experiment function in the brackets of equation (39), then the corrected equation for water is

$$k_w(T_w') = \left(\frac{t_o}{2A_o}\right)\psi_w \cdot f(T_w') \tag{41}$$

where $f(T'_w)$ is the correction correlation which also accounts for the presence of Vespel in the sample volume. Applying the correction factor to the calculation of Equation (40) yields

$$k_o(T'_o)_{CORRECTED} = \left(\frac{\psi_o}{\psi_w}\right) \quad k_w(T'_w)$$

where $(T'_w) = (T'_o)$

$$k_o(T'_o)_{CORRECTED} = \left(\frac{\psi_o}{\psi_w}\right) k_w(T'_o) \tag{42}$$

Equation (42) presents the proposed algorithm to be used for the calculation of the temperature dependent thermal conductivity of the sample mass.

3. SPECIFIC HEAT

Having calculated the thermal conductivity of the sample mass, the value of R_o (equal to $R_{(o-Al)}$ and $R_{(o-Bl)}$) can be obtained from Equations (30) and (31). For experimental regions without phase change, Equation (1) can be solved for the thermal mass

$$M_o C_o(T_o) = \frac{1}{R_o\left(\frac{dT_o}{d\theta}\right)} (T_{Al} + T_{Bl} - 2T_o) \tag{43}$$

The application of Equation (43) is theoretically correct as stated. However the normalization of the relation to water allows the application of a correction factor which is assumed a function of (T_o). Rewriting Equation (43) as

$$M_o C_o(T_o) = \phi_o(T_o) \tag{44}$$

Applying Equation (44) to measure the known specific heat of water, the correction factor $g(T_o)$ is applied as with the calculation of the thermal conductivity.

$$M_w C_w(T_w) = \phi_w(T_w) \cdot g(T_w) \tag{45}$$

Solving for the correction factor and applying this to Equation (44) there results (letting $T_o = T_w$)

$$M_o C_o(T_o) = M_w C_w(T_o) \frac{\phi_o(T_o)}{\phi_w(T_o)} \tag{46}$$

Equation (46) presents the recommended formula for the calculation of the specific heat of the sample mass.

4. HEAT OF PHASE CHANGE

Having calculated the thermal conductivity and specific heat of the sample mass outside the regions of phase change, it is assumed that during phase change, these properties can be linearly interpolated. It is proposed that Equation (2) is directly used to calculate the heat of phase change. Because this heat is evolved over a finite period of time, i.e., during the phase change, h_o represents an instantaneous rate of heat dissipation. If this occurs over a time increment of $\Delta\theta$, then from Equation (2)

$$h_o = M_o C_o \left(\frac{dT_o}{d\theta}\right) + \left(\frac{T_o - T_{A1}}{R_o}\right) + \left(\frac{T_o - T_{B1}}{R_o}\right) \tag{47}$$

and the total heat of phase change is

$$\int_{\Delta\theta} h_o d\theta = \int_{\Delta\theta} \left\{ M_o C_o \left(\frac{dT_o}{d\theta}\right) + \left(\frac{1}{R_o}\right)(2T_o - T_{A1} - T_{B1}) \right\} d\theta \tag{48}$$

Equation (48) is solved numerically to determine the heat of phase change of the sample media.

5. SUMMARY

It has been shown that important thermodynamic properties of a sample mass can be determined by comparison with samples of known thermodynamic properties such as distilled water. This is possible because of the unique capabilities of the device discussed in this report. A sensitivity analysis of the proposed equations remains to be accomplished. This may show that a more optimum approach should be used. In any case, sufficient data are available for the determination of the thermodynamic properties of the sample mass. These properties may well hold an important key in the understanding of changes experienced by biological tissues during freeze, thaw or low temperature preservation. If such is the case, an understanding of these phenomena may lead to the development of optimum protocols for the frozen preservation of valuable biological tissues.

APPENDIX D

DISTILLED WATER TEST DATA

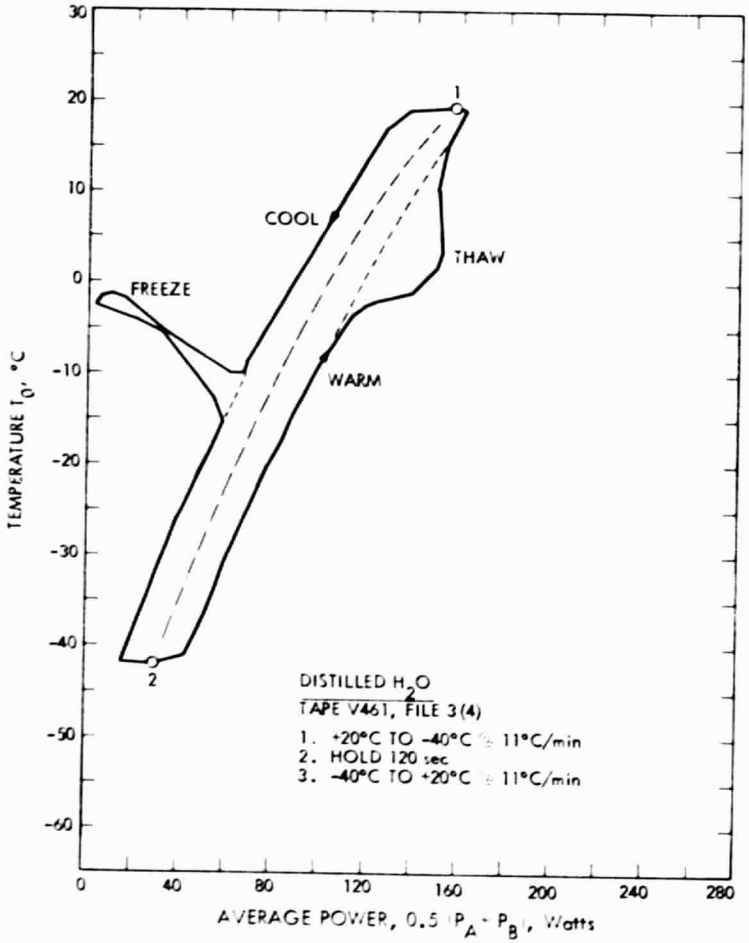

Figure D-3c

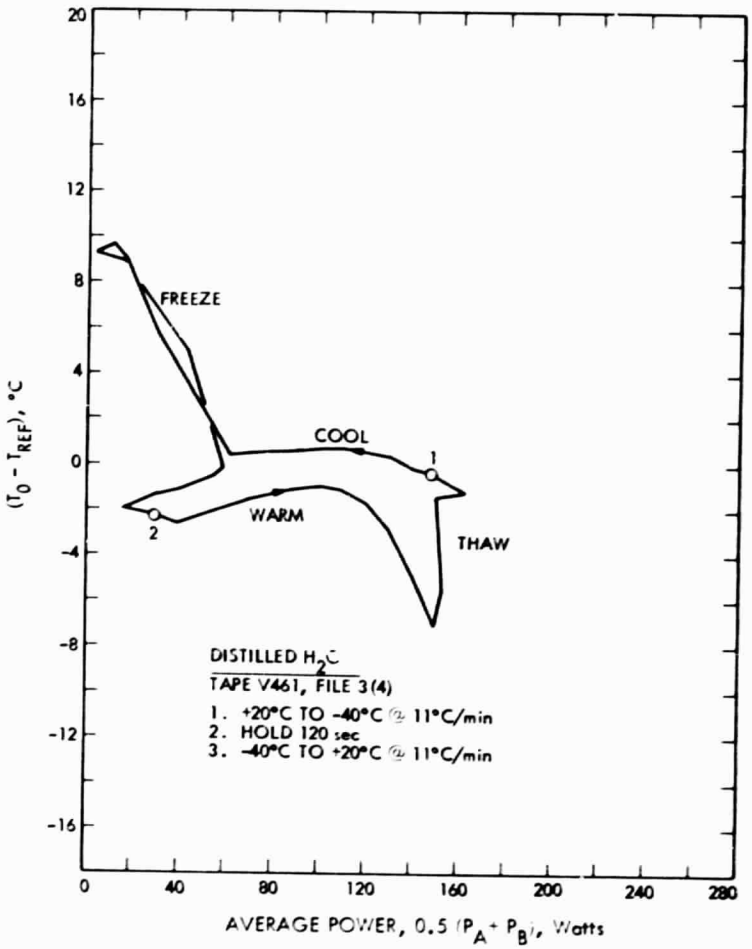

Figure D-3d

Table D-1. Distilled Water Test Data Summary

Tape ID	File No.	Cooling Start °C	Cooling End °C	Cooling Rate °C/ Min.	Warming Start °C	Warming End °C	Warming Rate °C/ Min.	H_2O Phase Change Yes	H_2O Phase Change No
V461	1	(Multiple Step)		11	-60	+20	2	X	
0280	1	+20	-40	1	-40	+2	1	X	
A909	1	+20	-40	2	-40	+20	2	X	
V461	4	+20	-40	11	-40	+20	11	X	
V461	3	+20	-40	22	-40	+20	22	X	
V461	2	+20	-40	65	-40	+20	65	X	
0336	1	+20	-60	2	(Multiple Step)		11	X	
A909	2	+20	-40	4	-40	+20	4	X	
0446	1	+20	-40	1	-40	+20	1	X	
0375	1	+20	-40	2	(Multiple)		10	X	
0375	2	+20	-40	4	-40	+20	4	X	

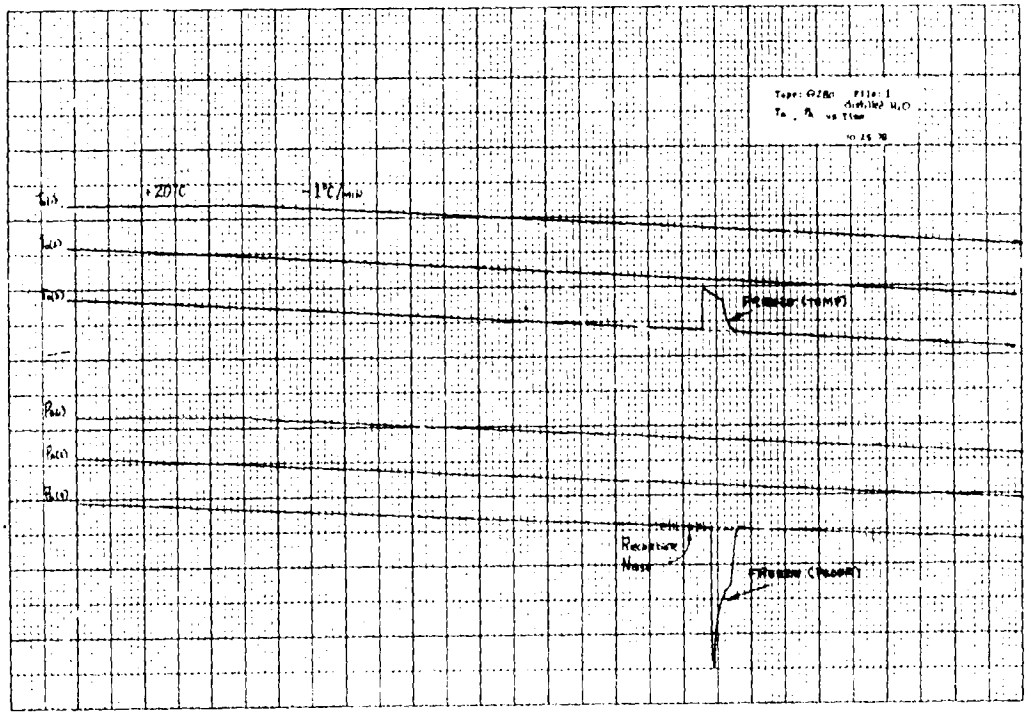

Figure D-1a

COPY FURNISHED TO DTIC
DO NOT REPRODUCE

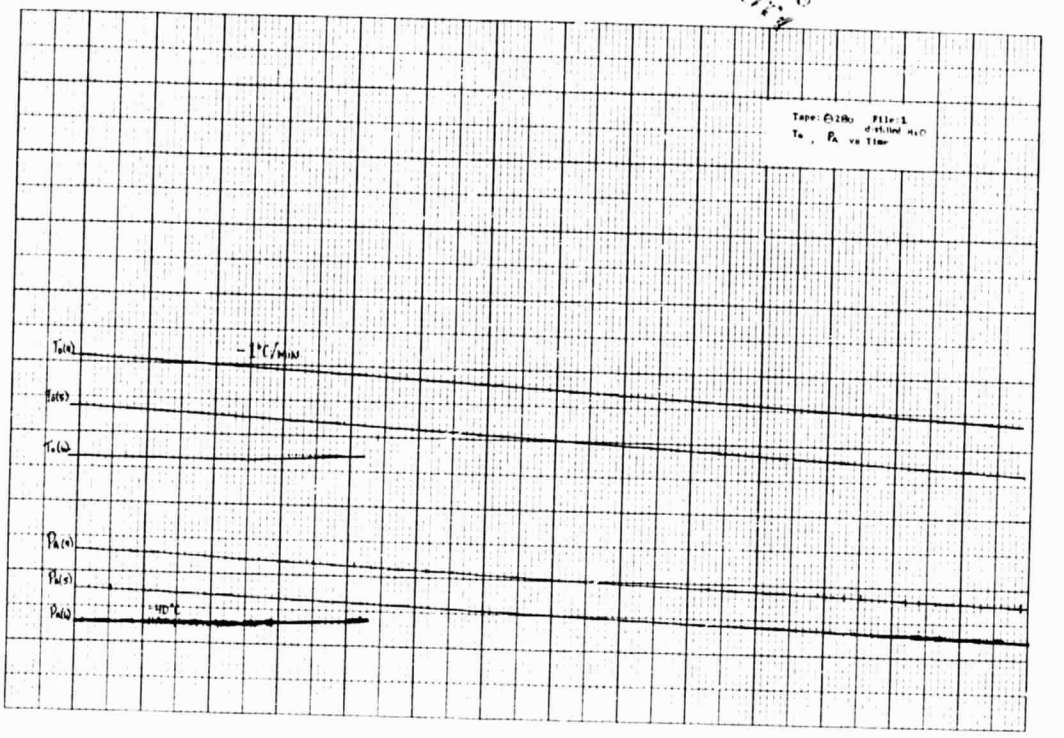

Figure D-1b

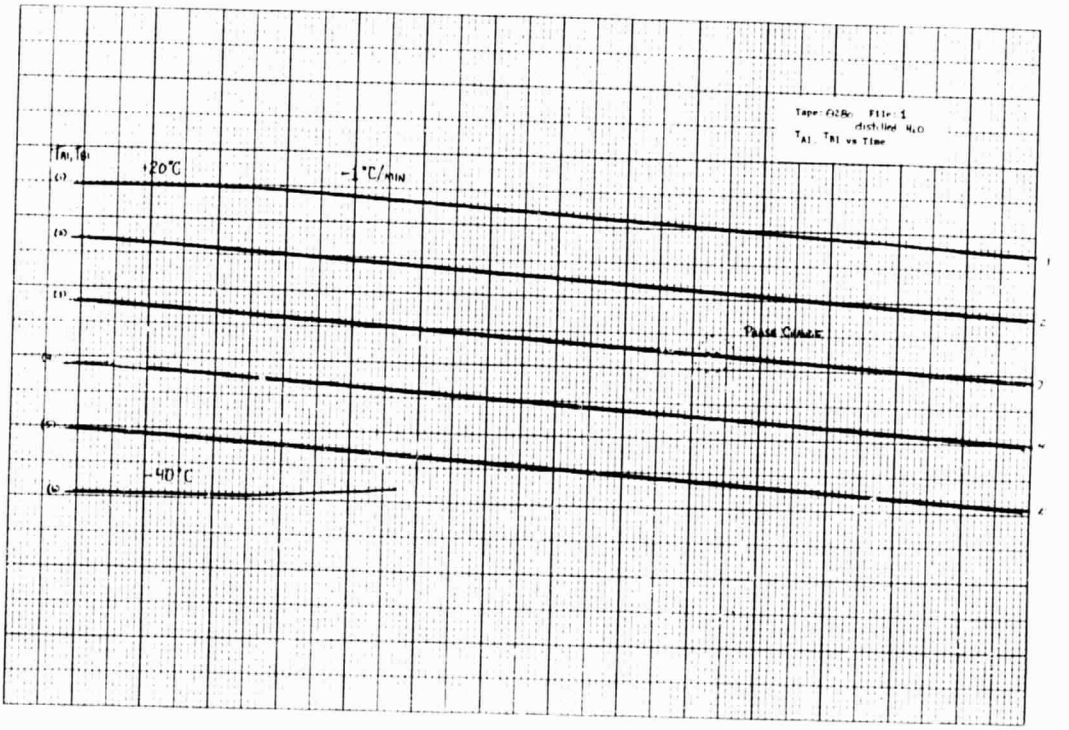

Figure D-1c

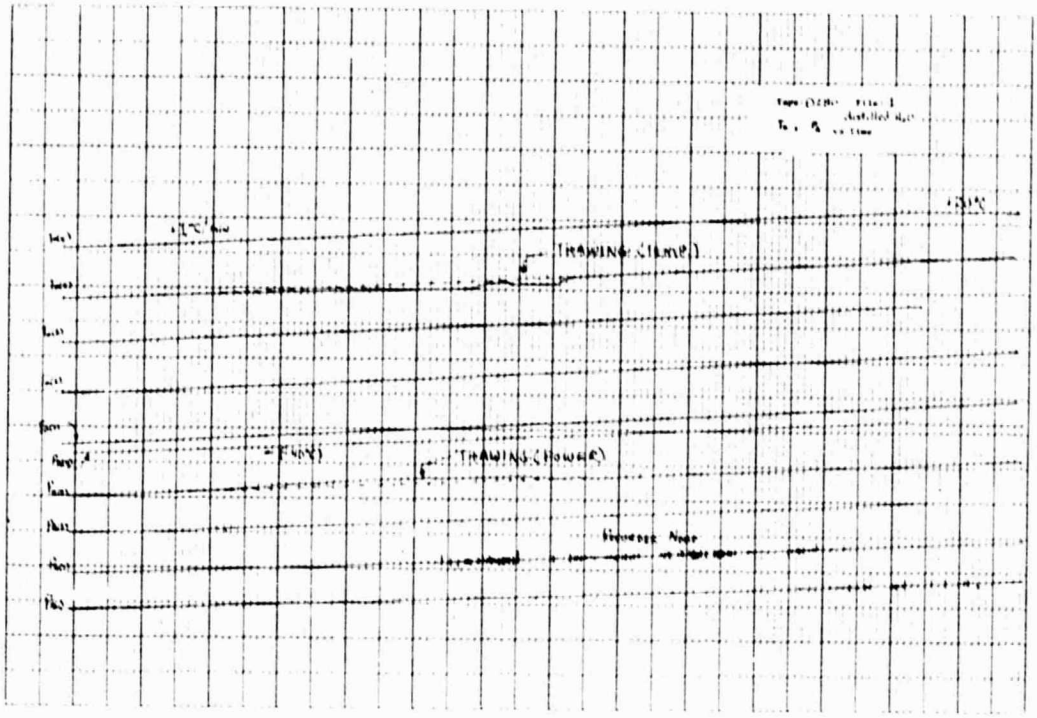

Figure D-1d

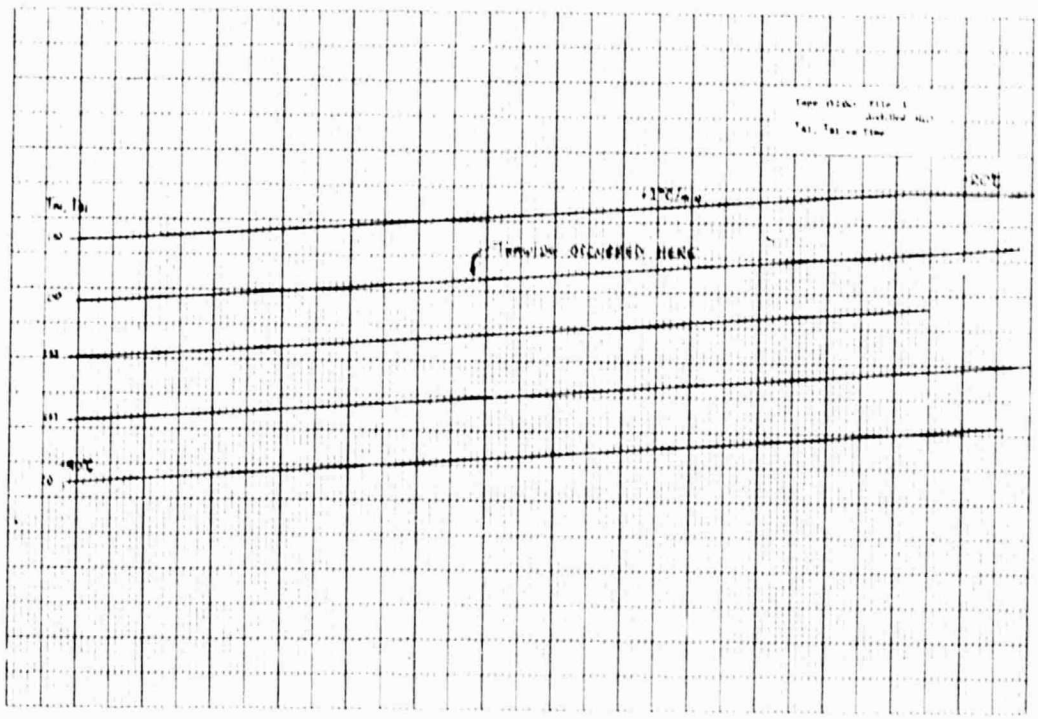

Figure D-1e

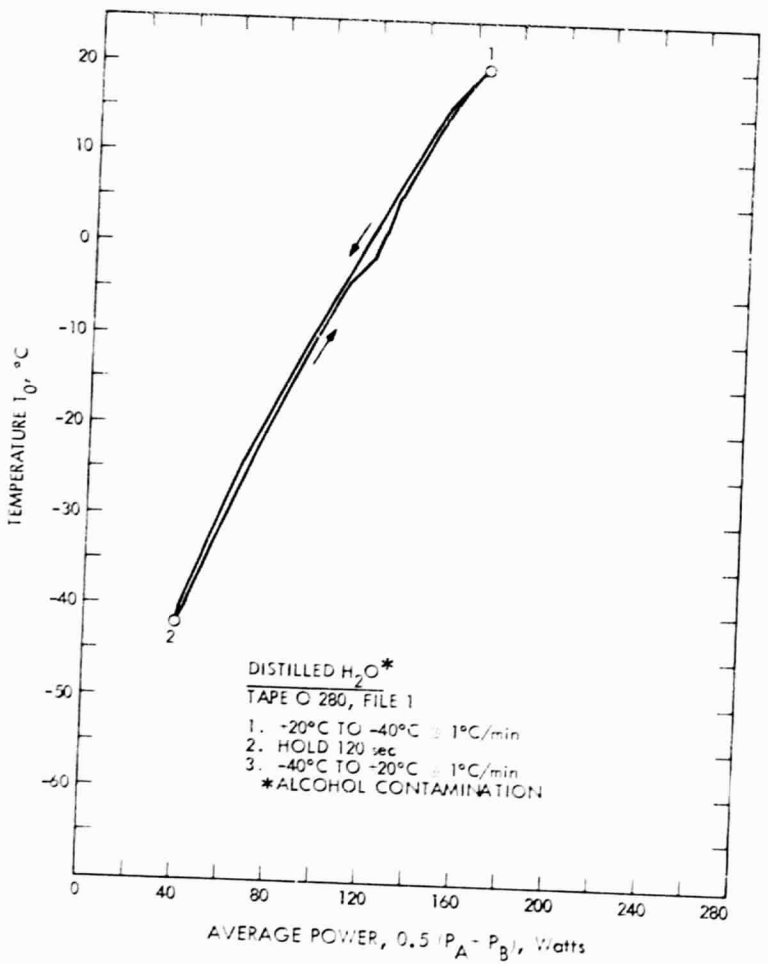

Figure D-1f

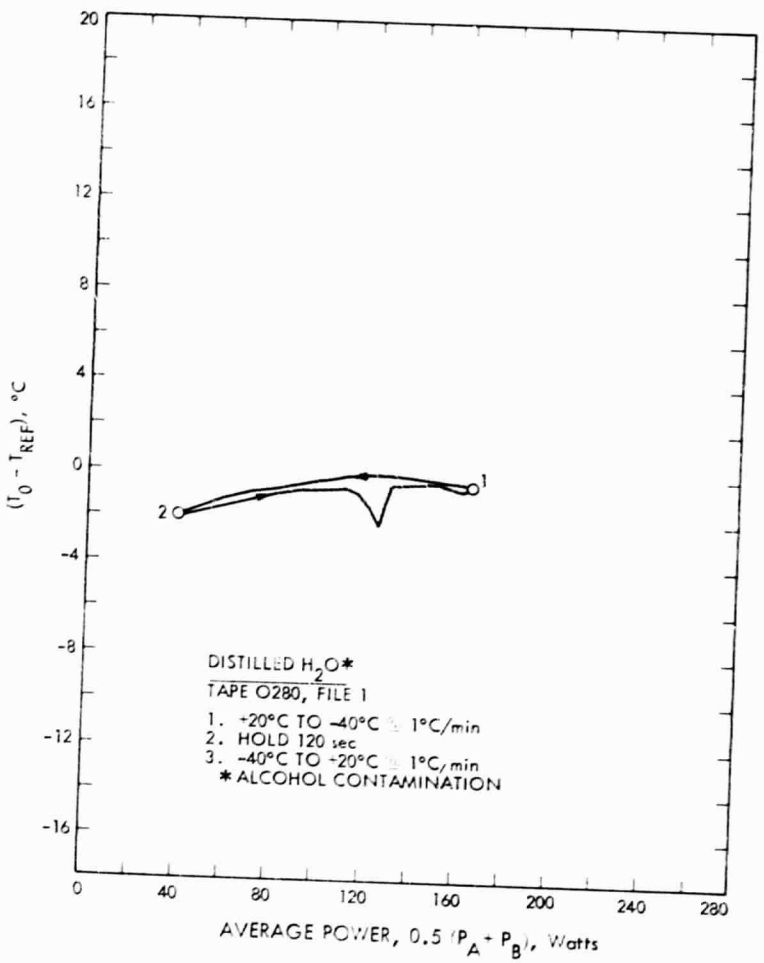

Figure D-1g

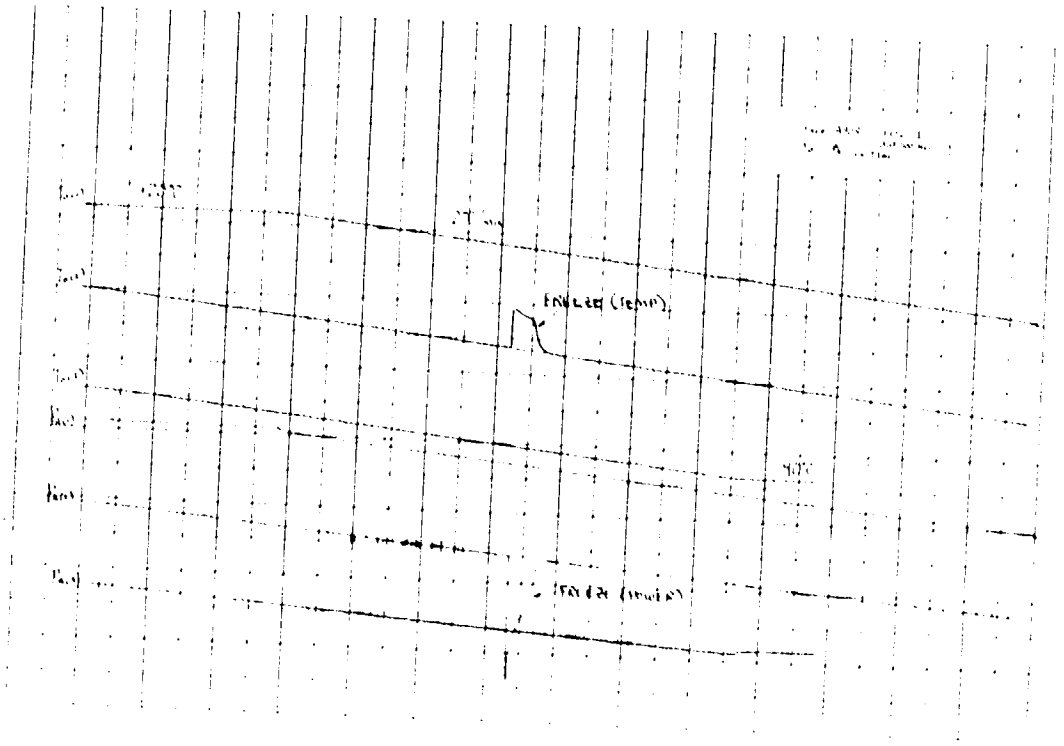

Figure D-2a

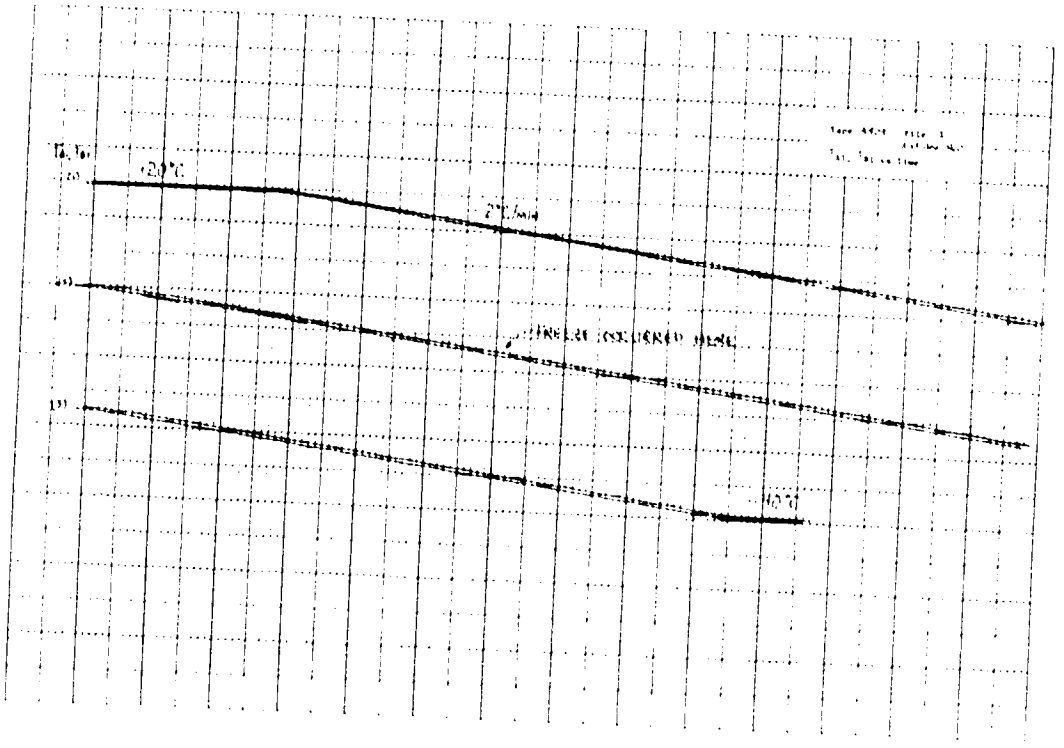

Figure D-2b

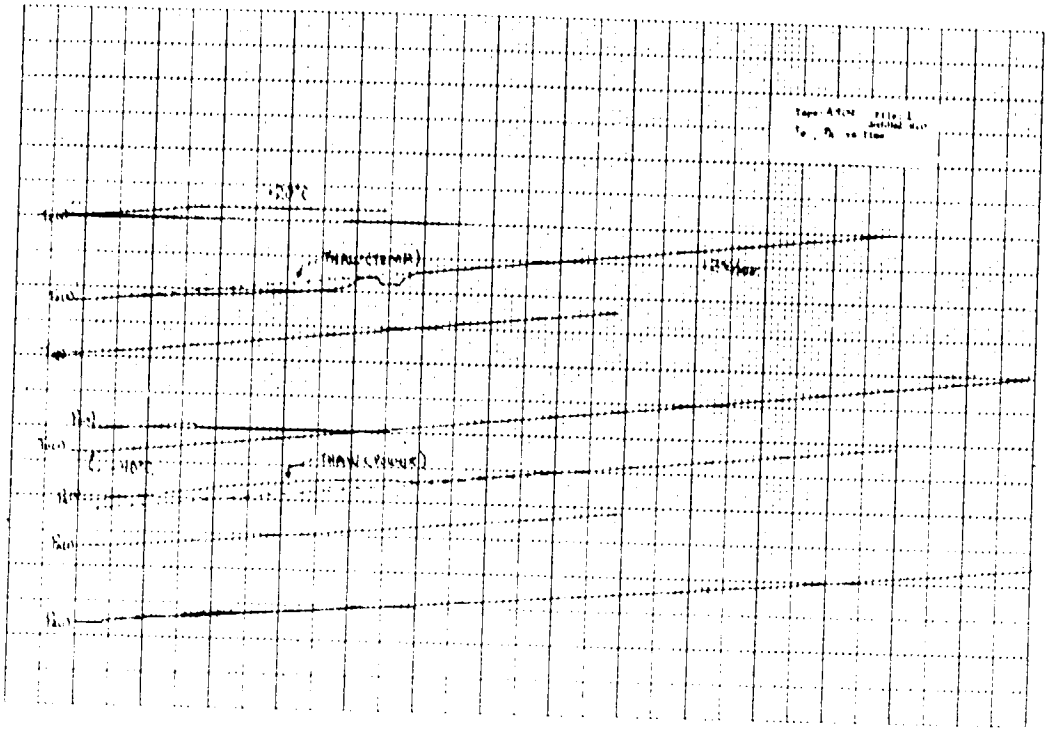

Figure D-2c

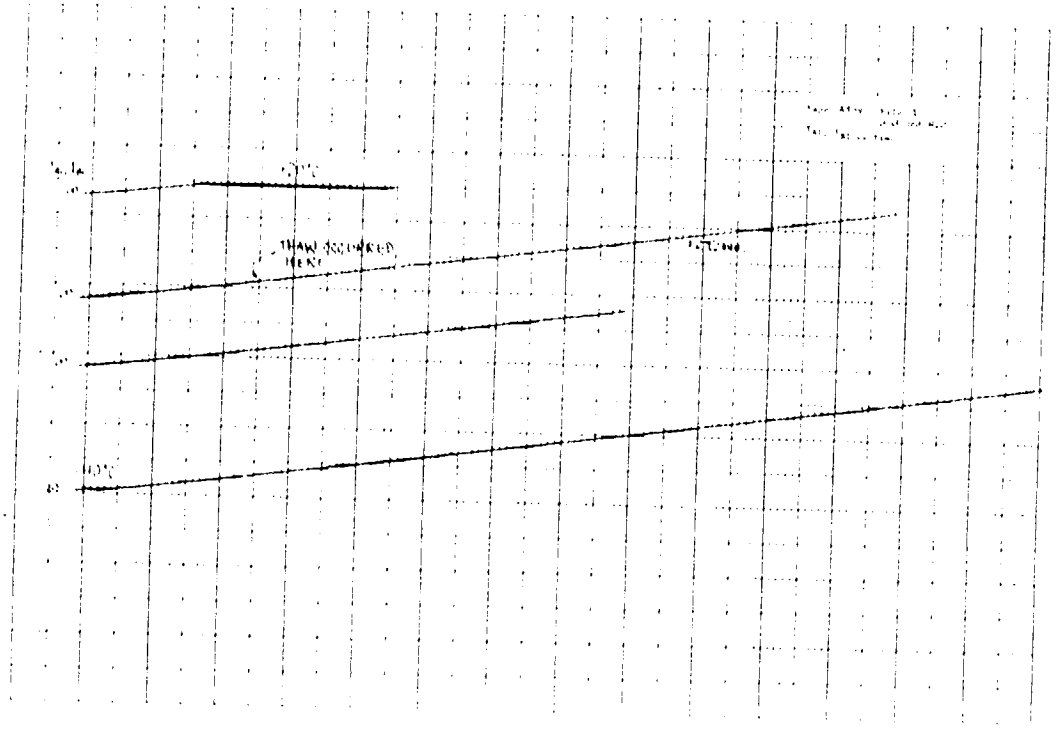

Figure D-2d

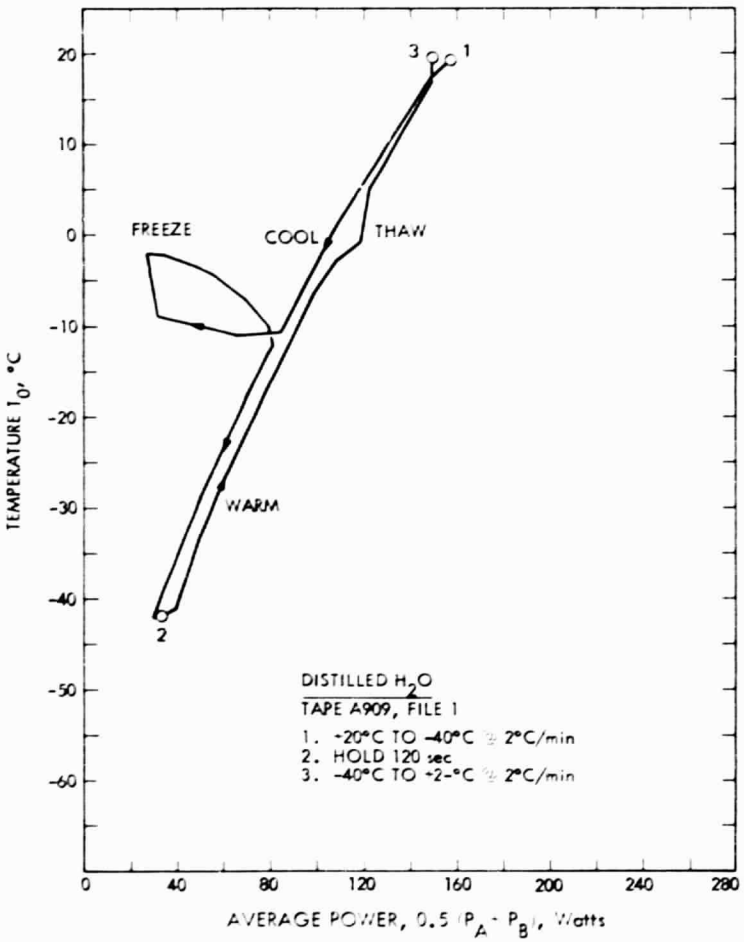

Figure D-2e

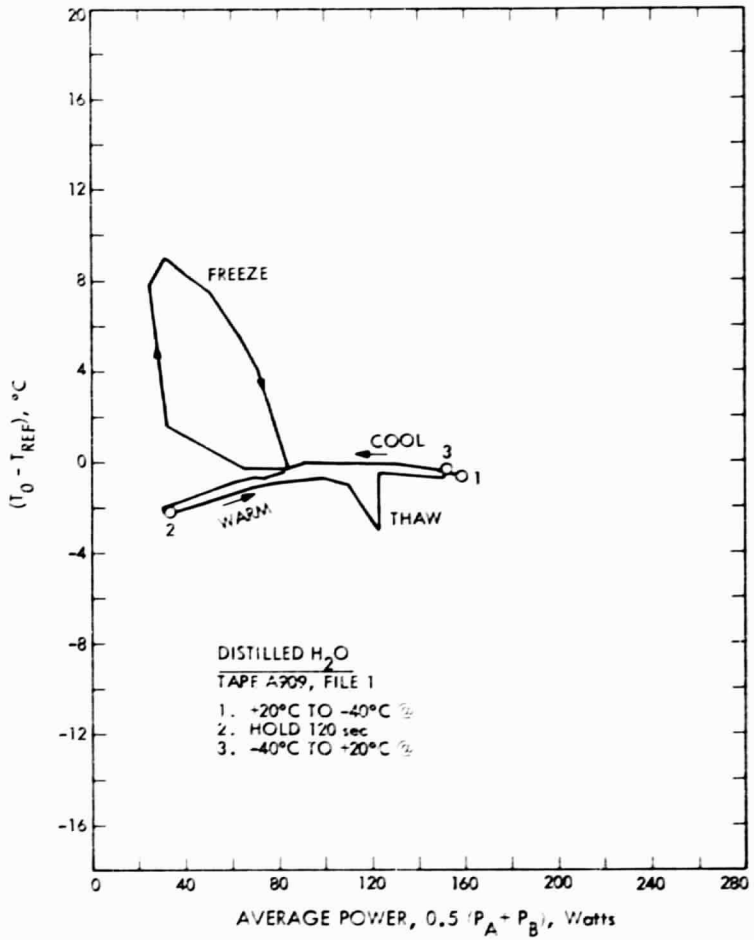

Figure D-2f

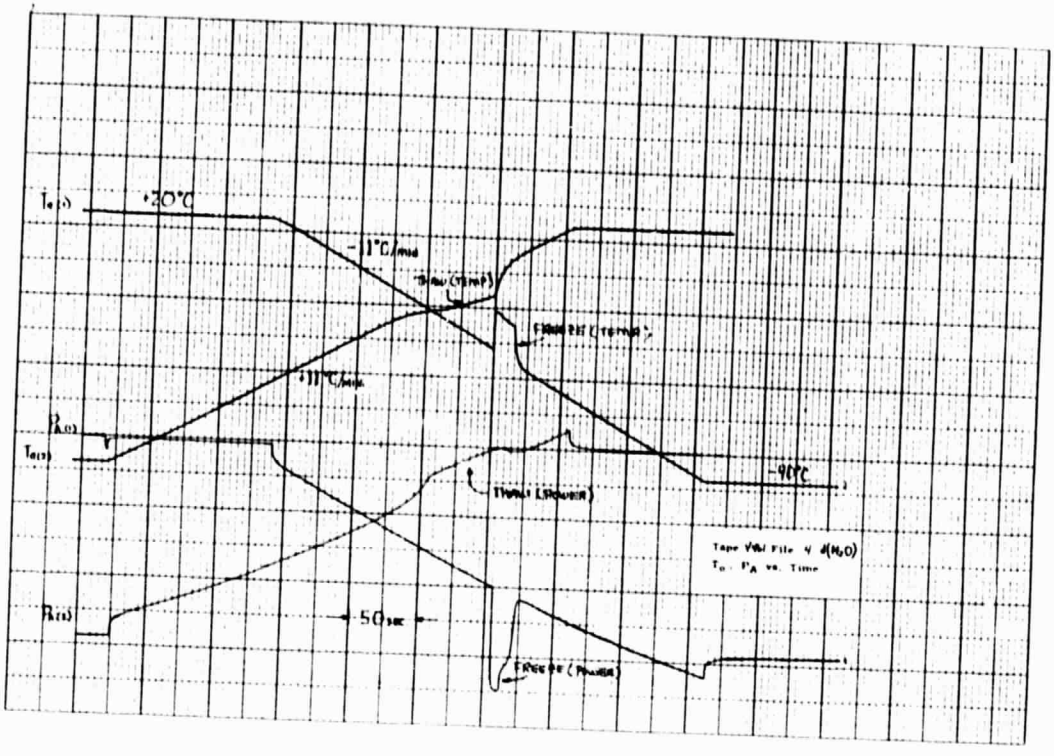

Figure D-3a

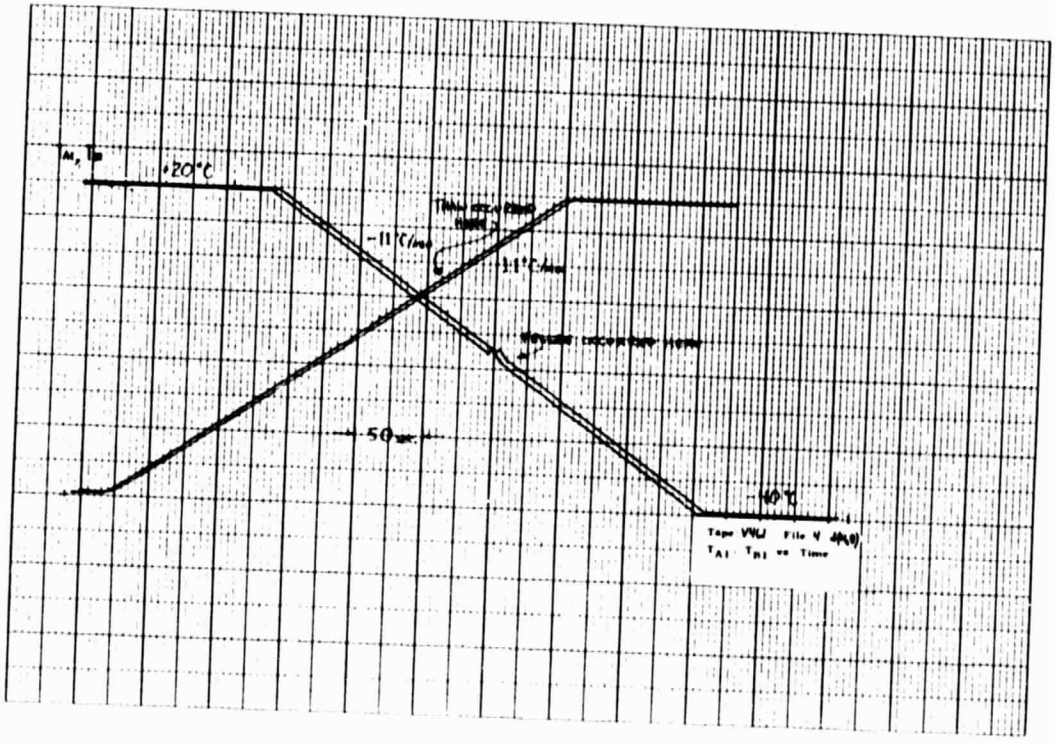

Figure D-3b

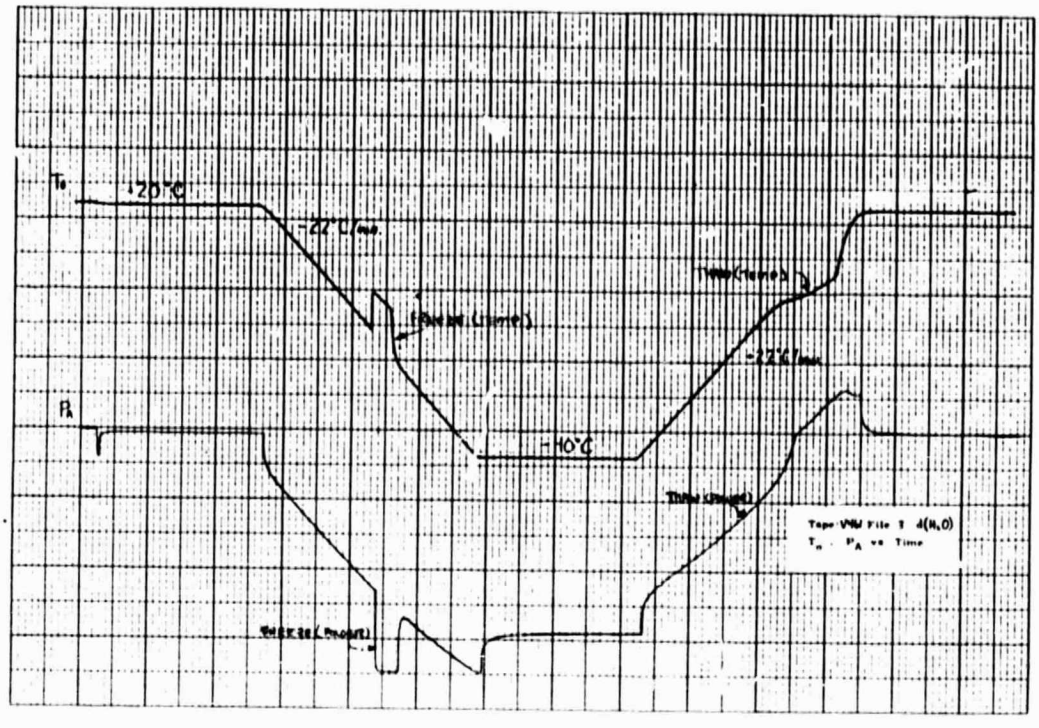

Figure D-4a

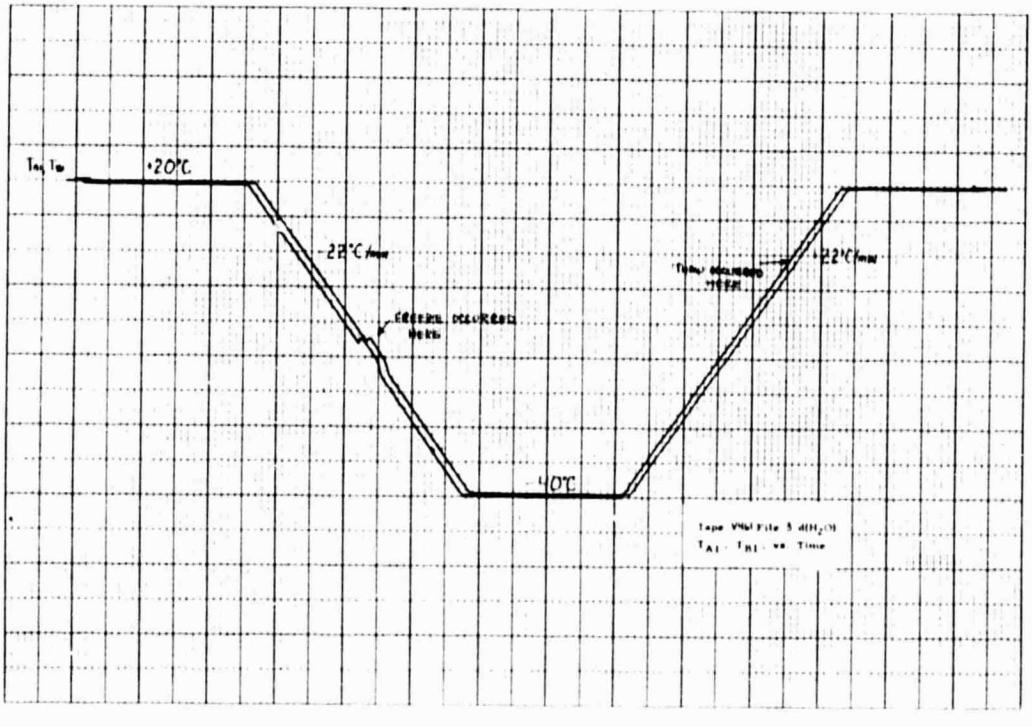

Figure D-4b

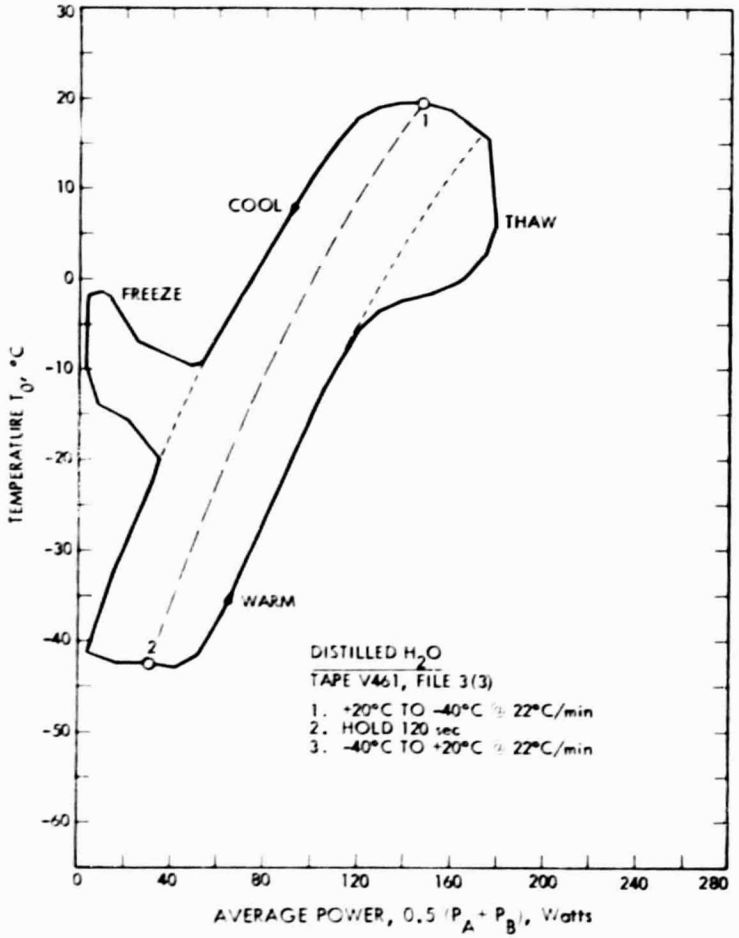

Figure D-4c

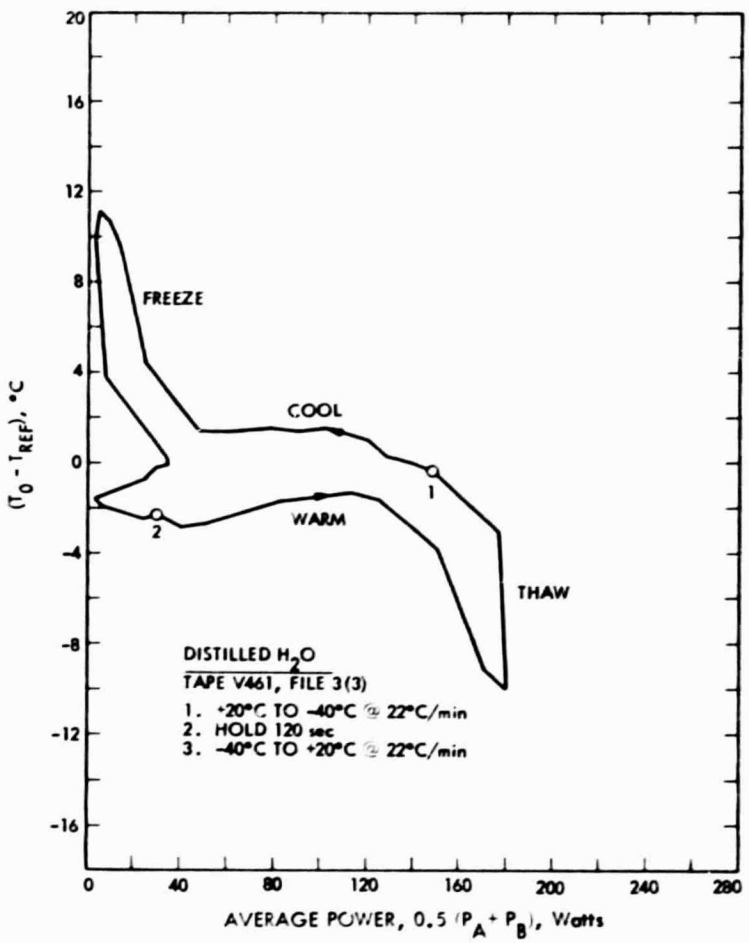

Figure D-4d

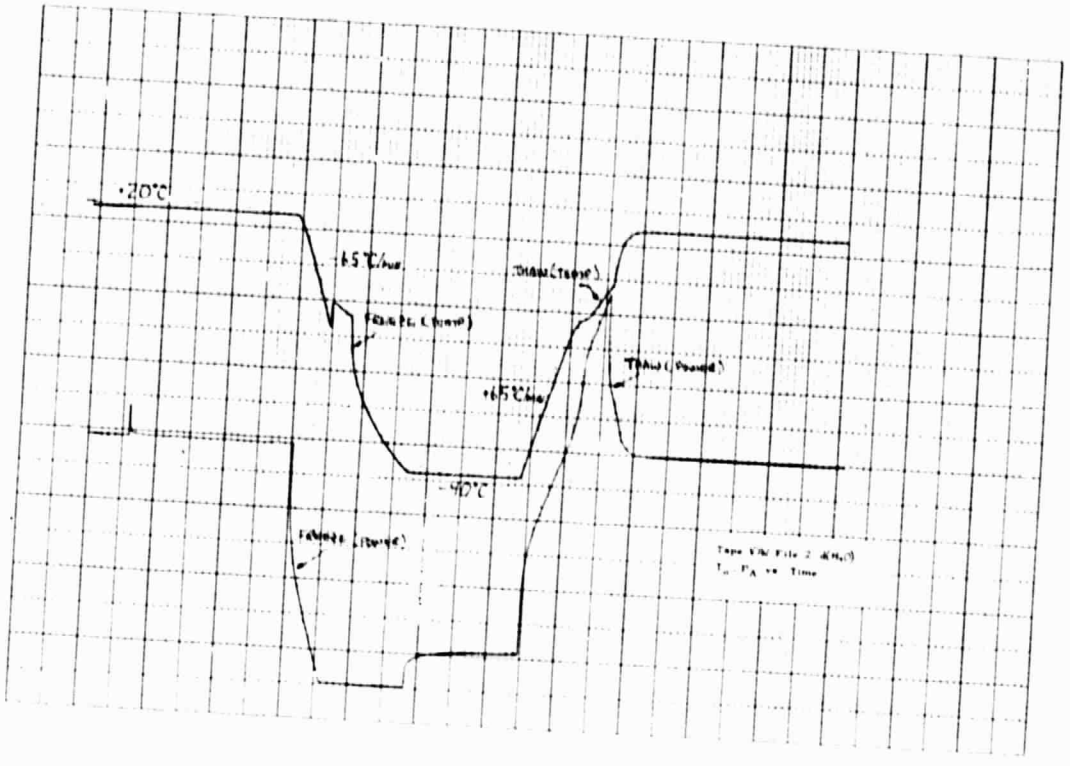

Figure D-5a

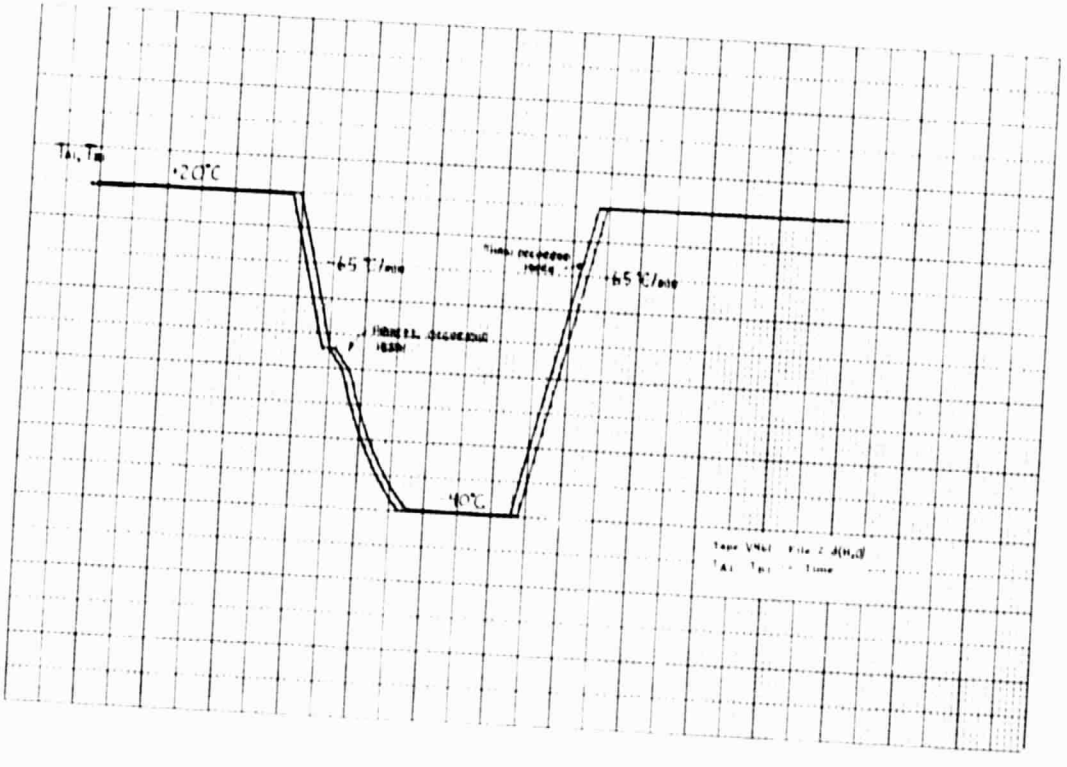

Figure D-5b

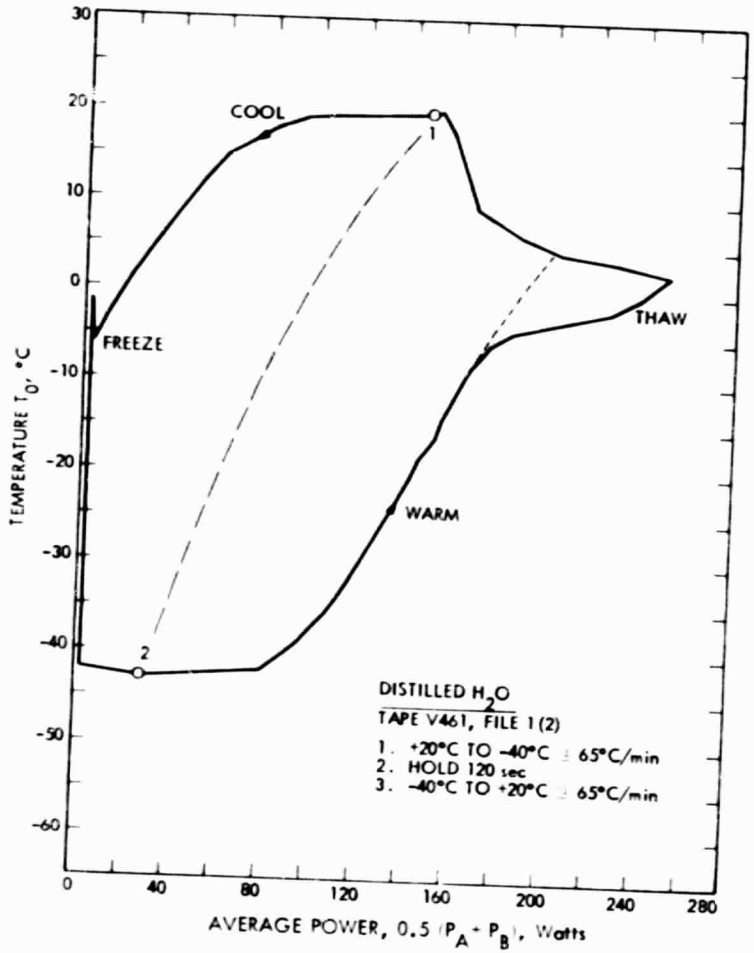

Figure D-5c

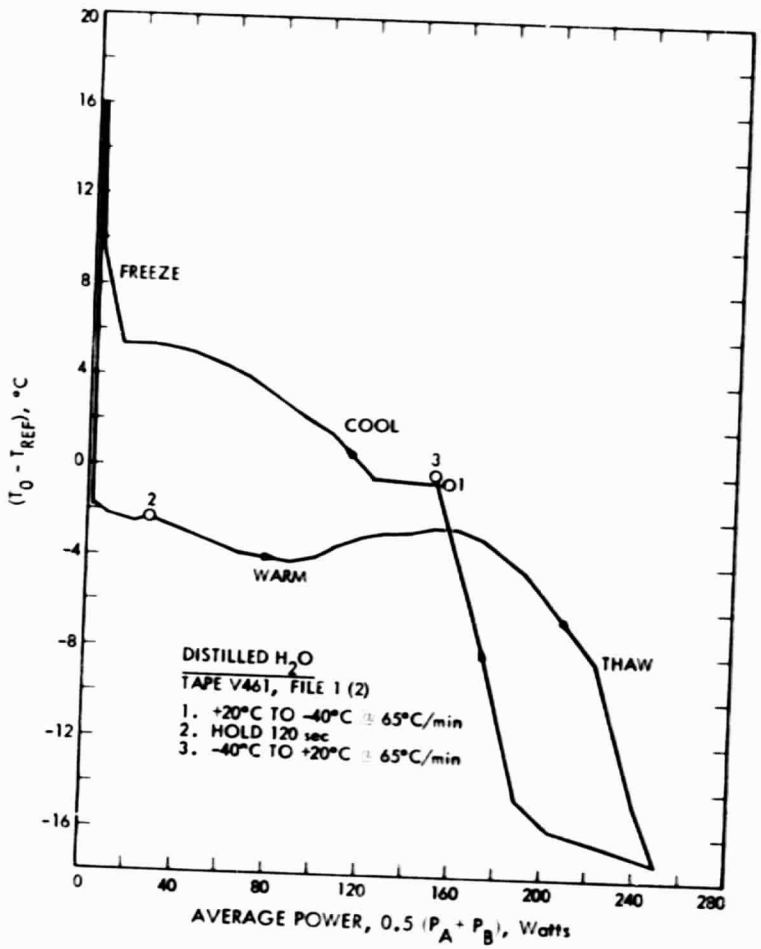

Figure D-5d

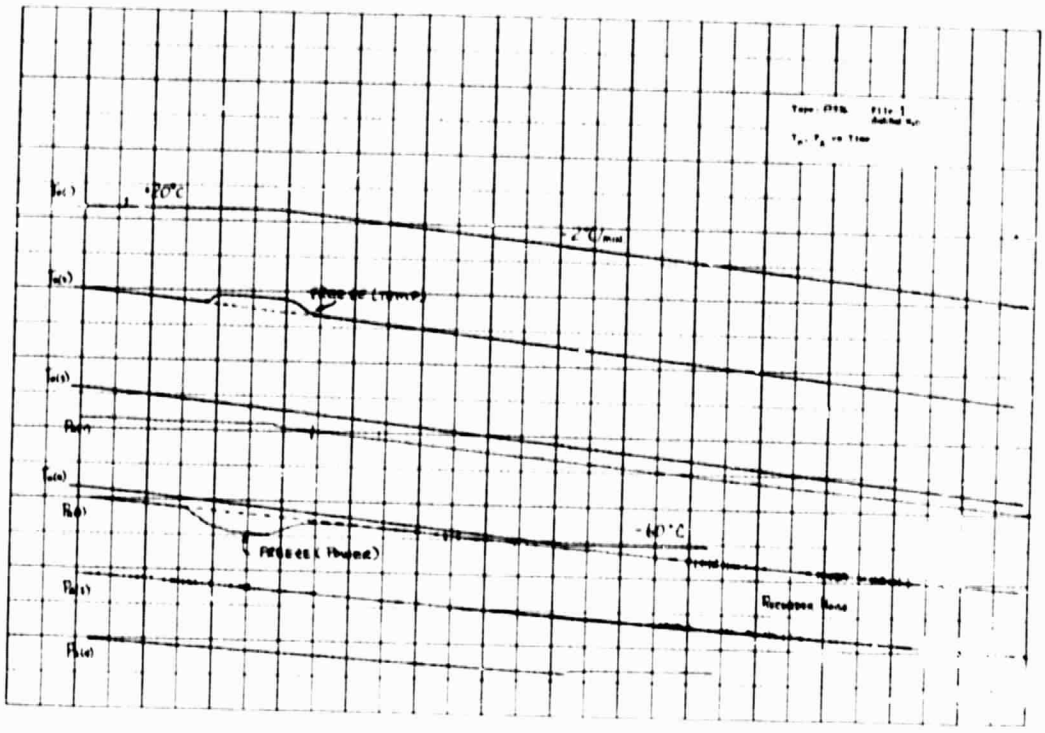

Figure D-6a

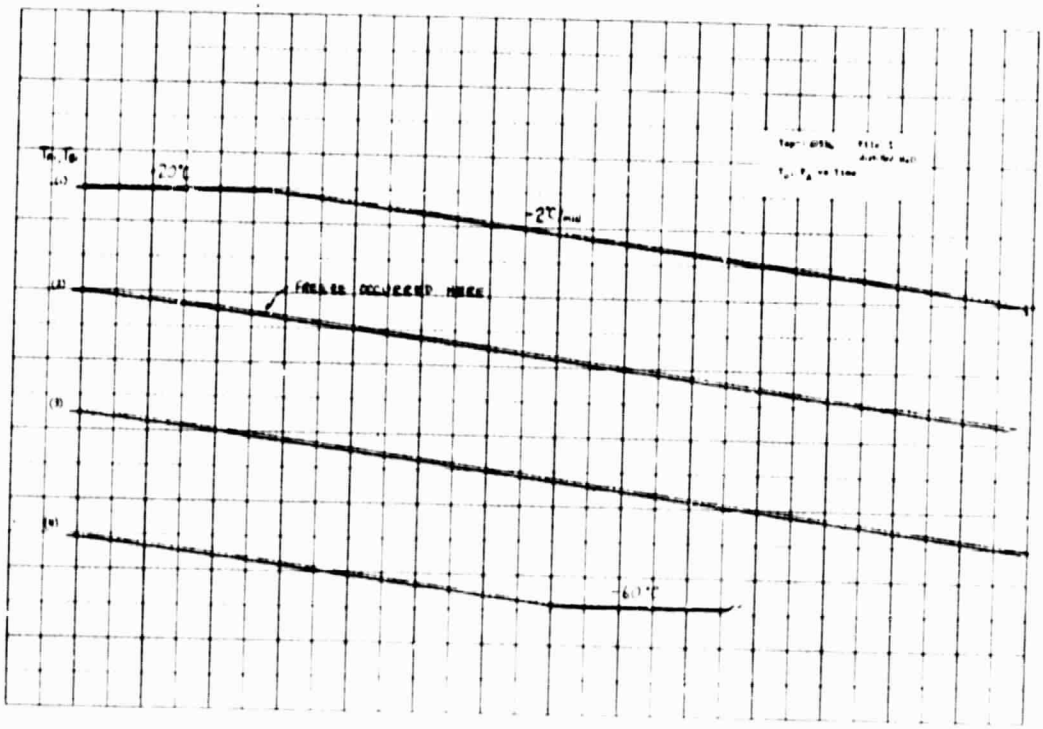

Figure D-6b

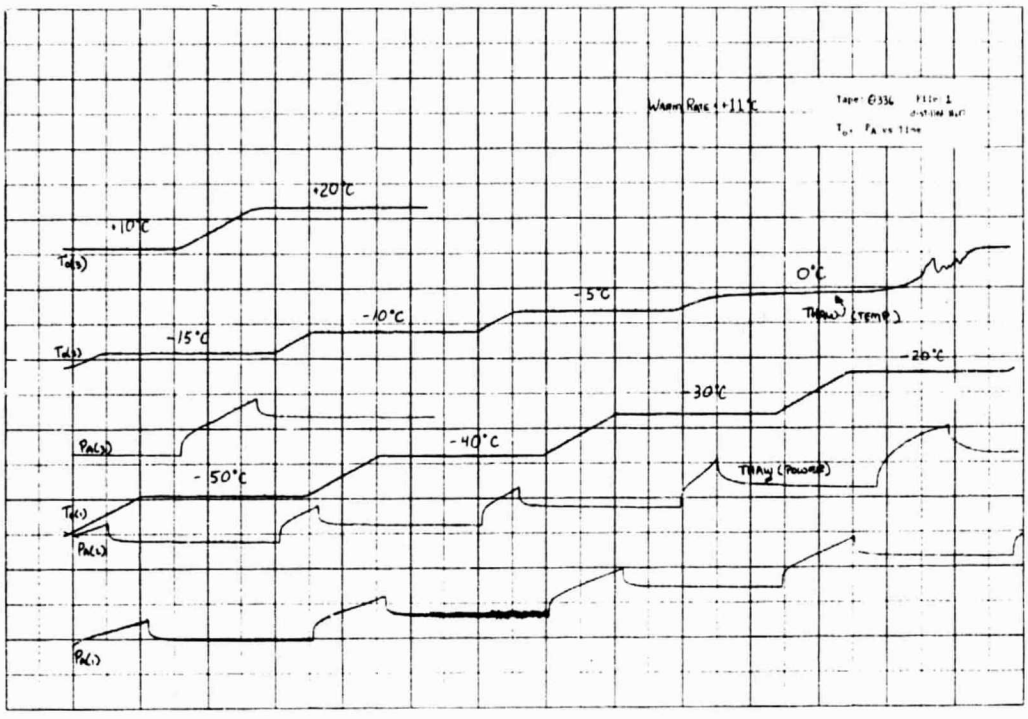

Figure D-6c

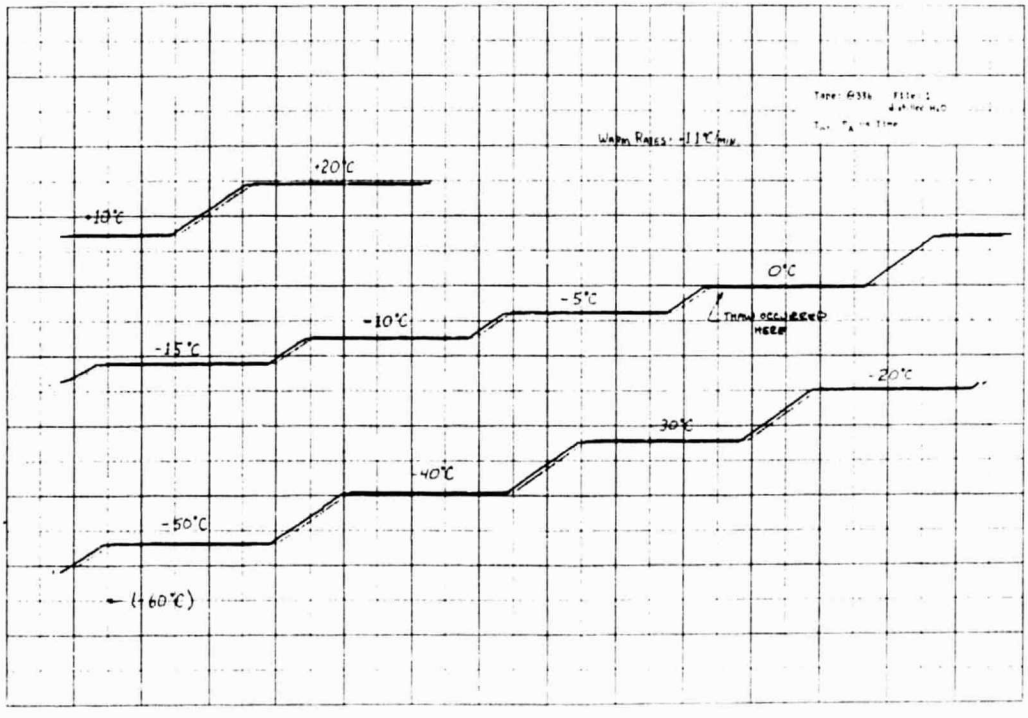

Figure D-6d

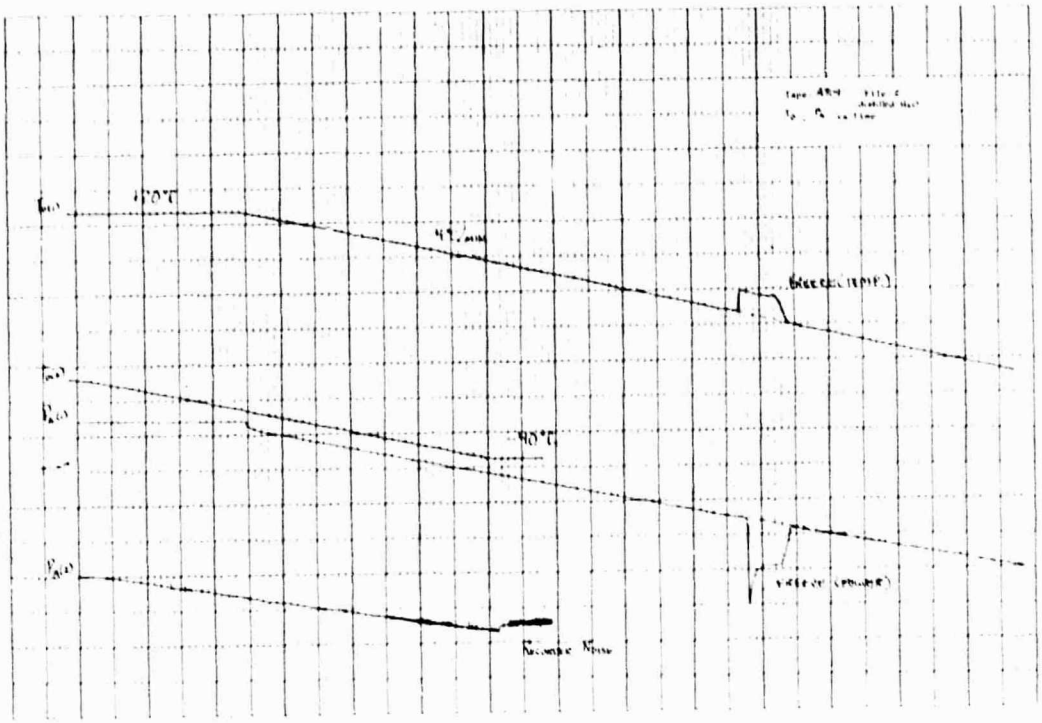

Figure D-7a

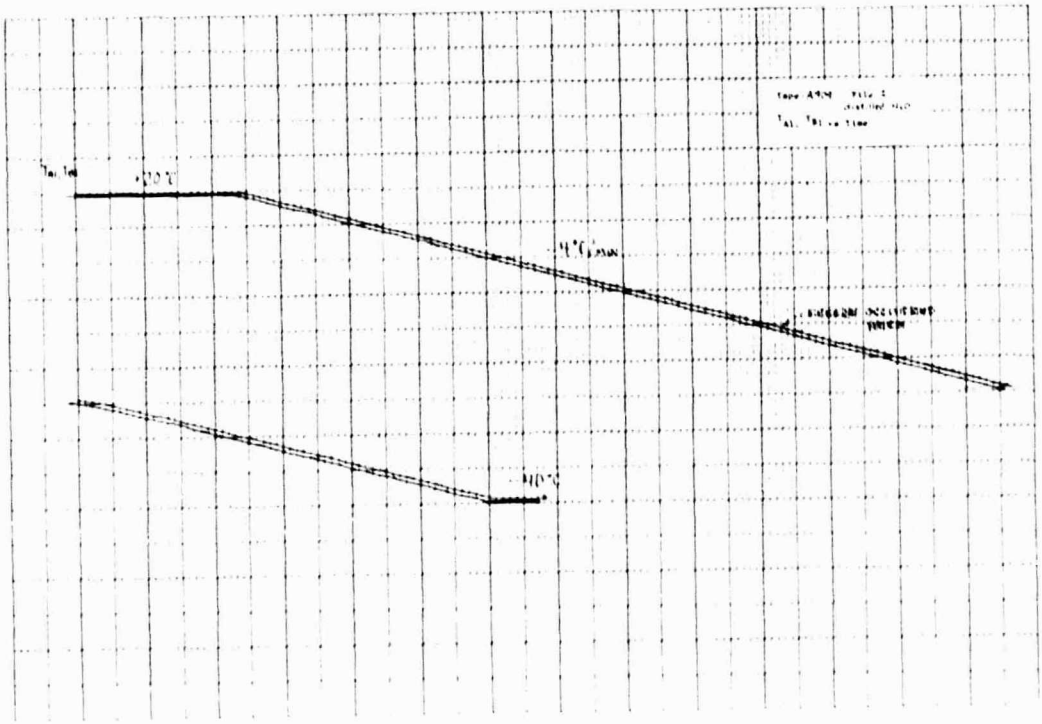

Figure D-7b

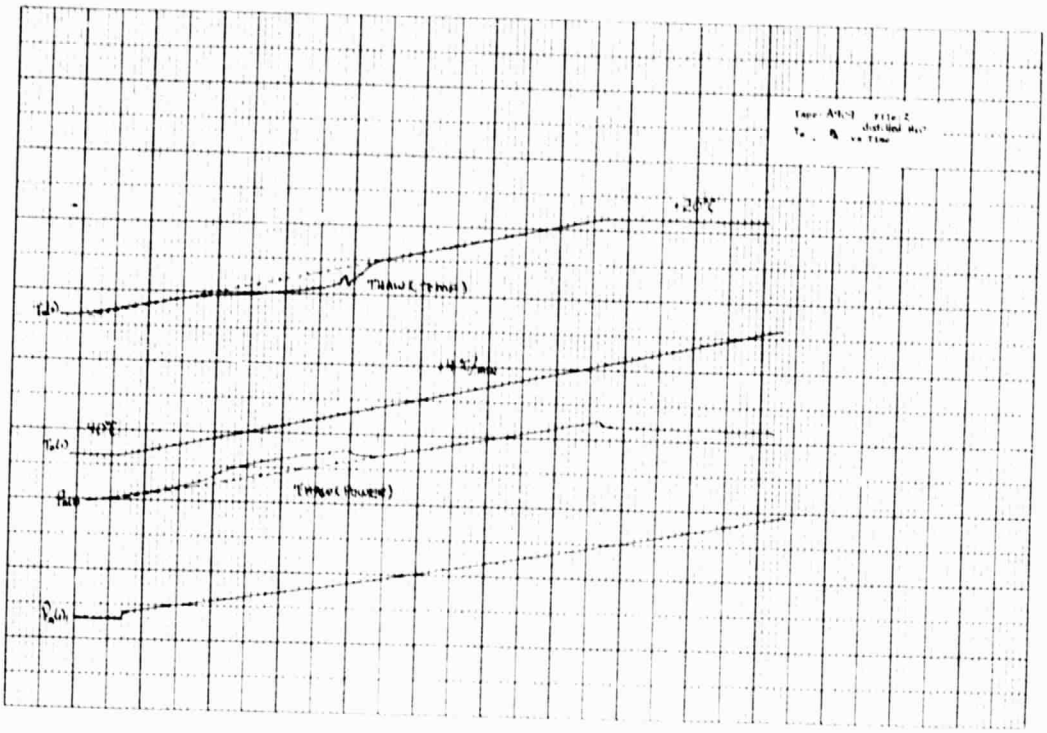

Figure D-7c

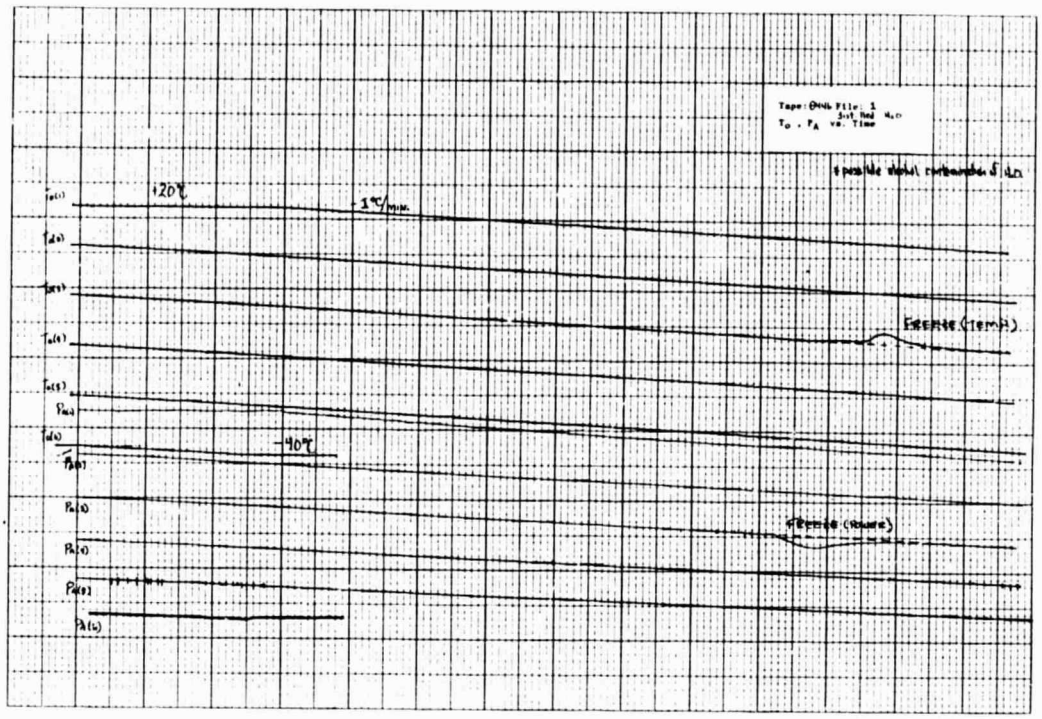

Figure D-8a

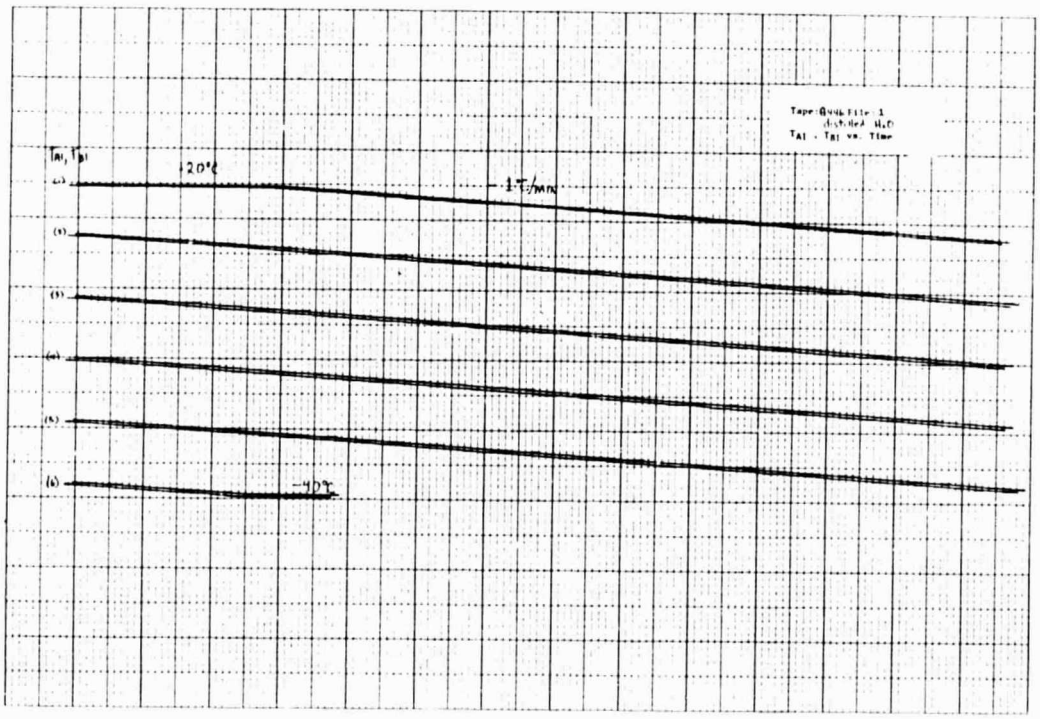

Figure D-8b

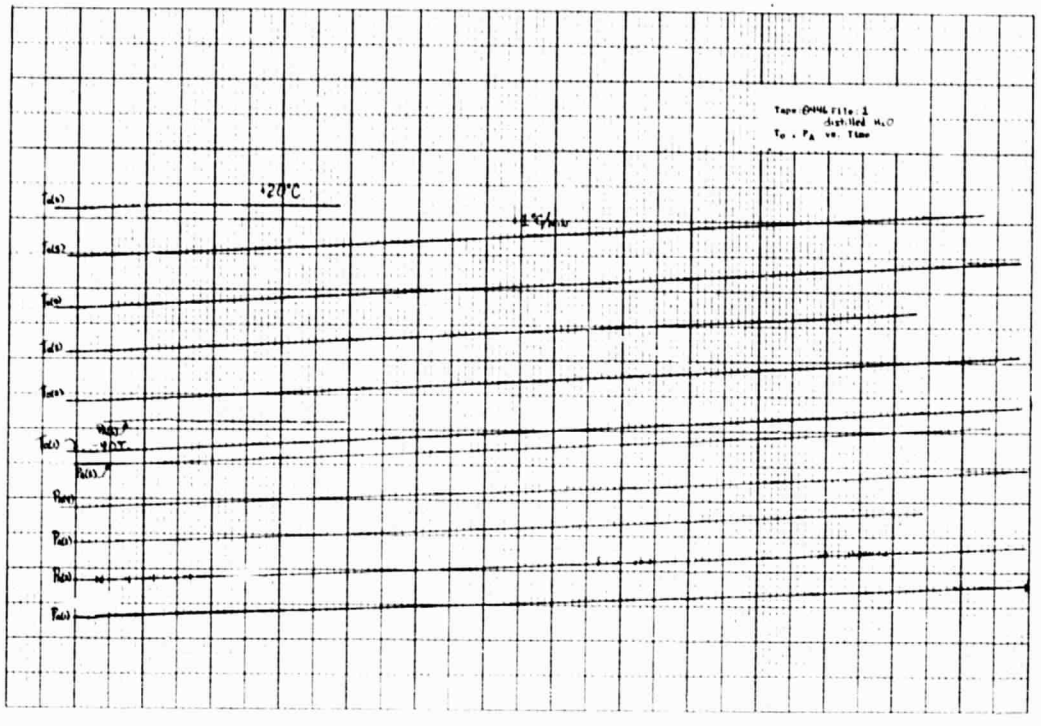

Figure D-8c

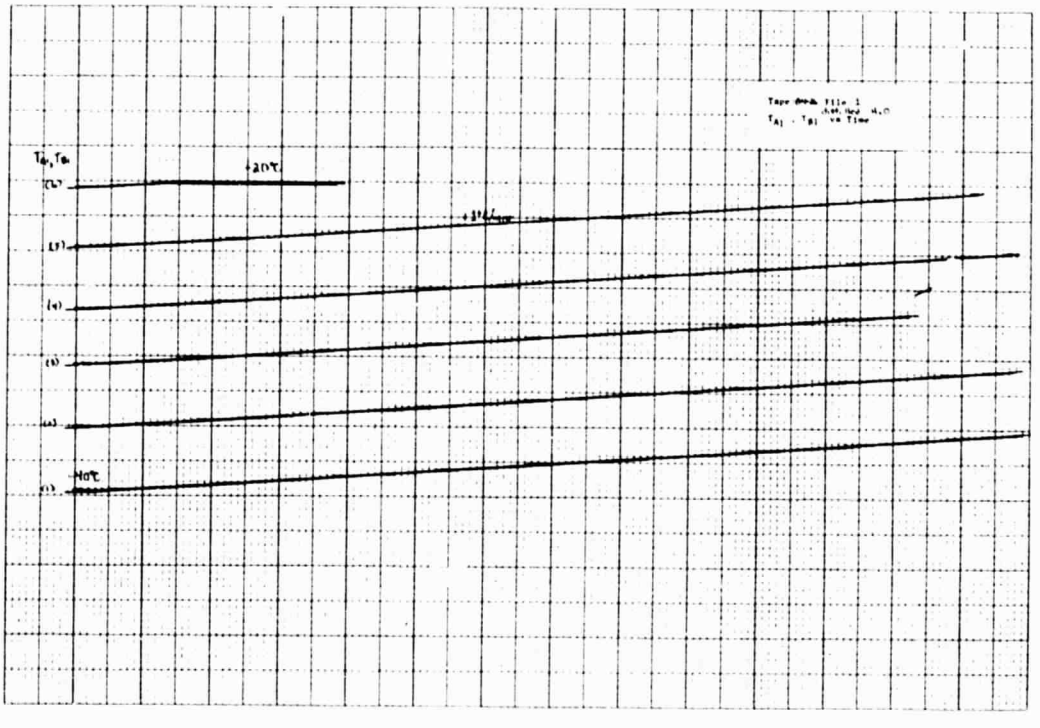

Figure D-8d

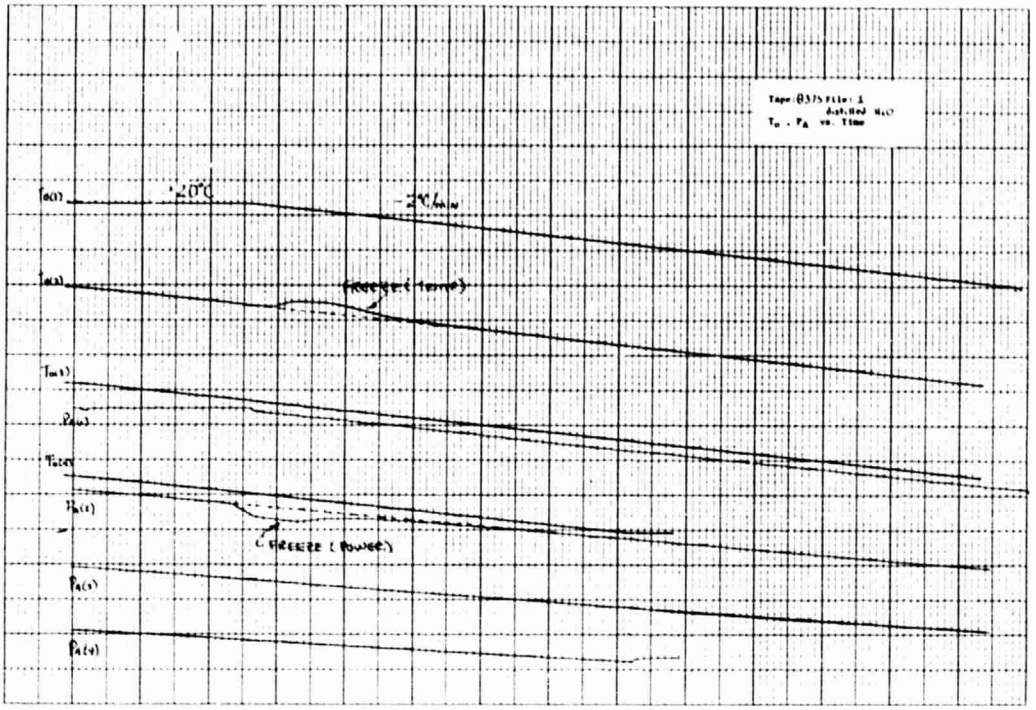

Figure D-9a

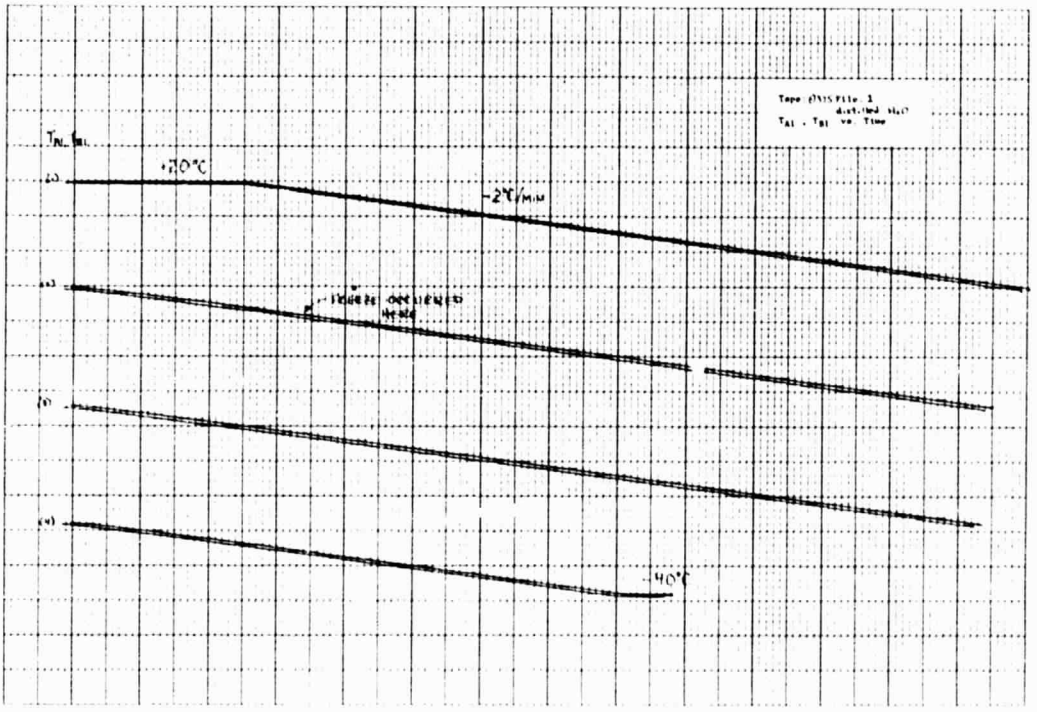

Figure D-9b

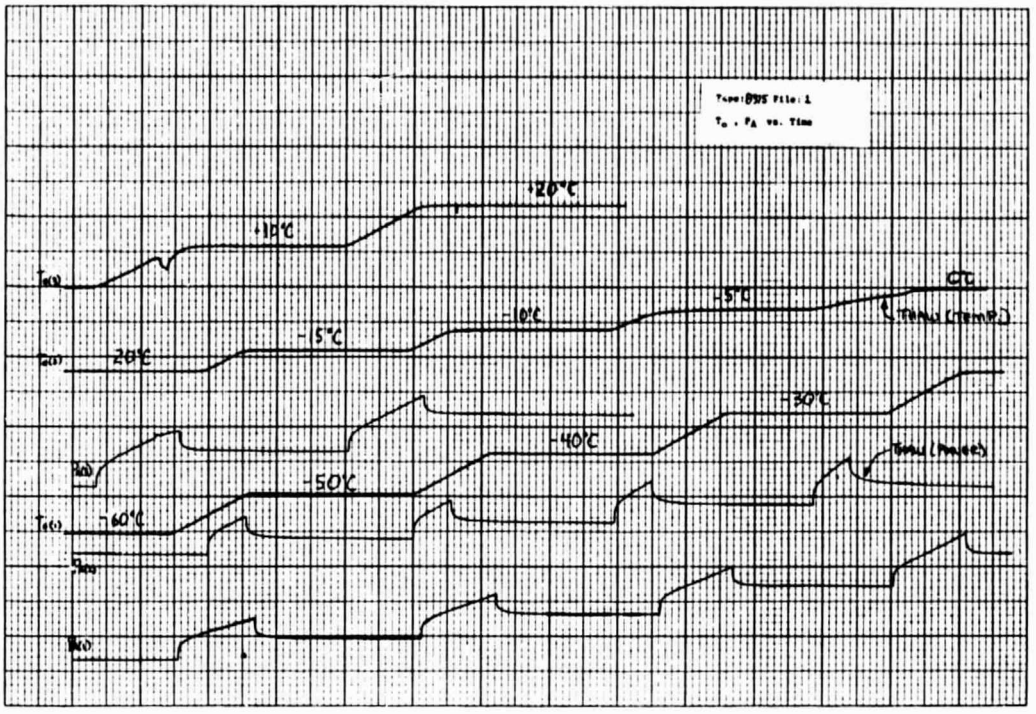

Figure D-9c

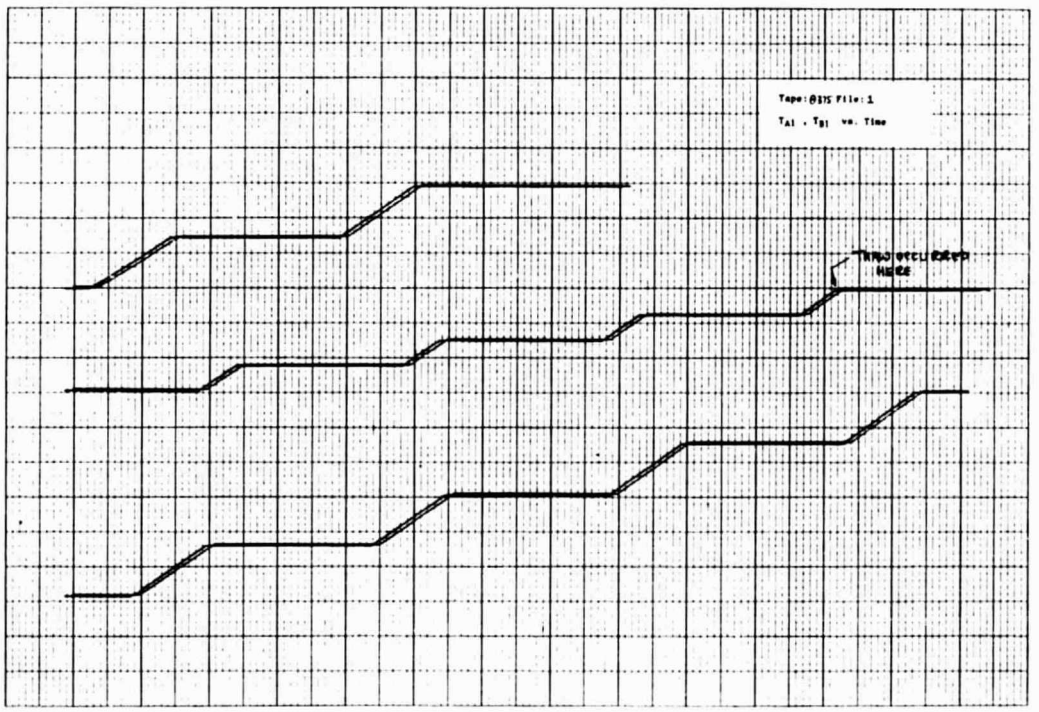

Figure D-9d

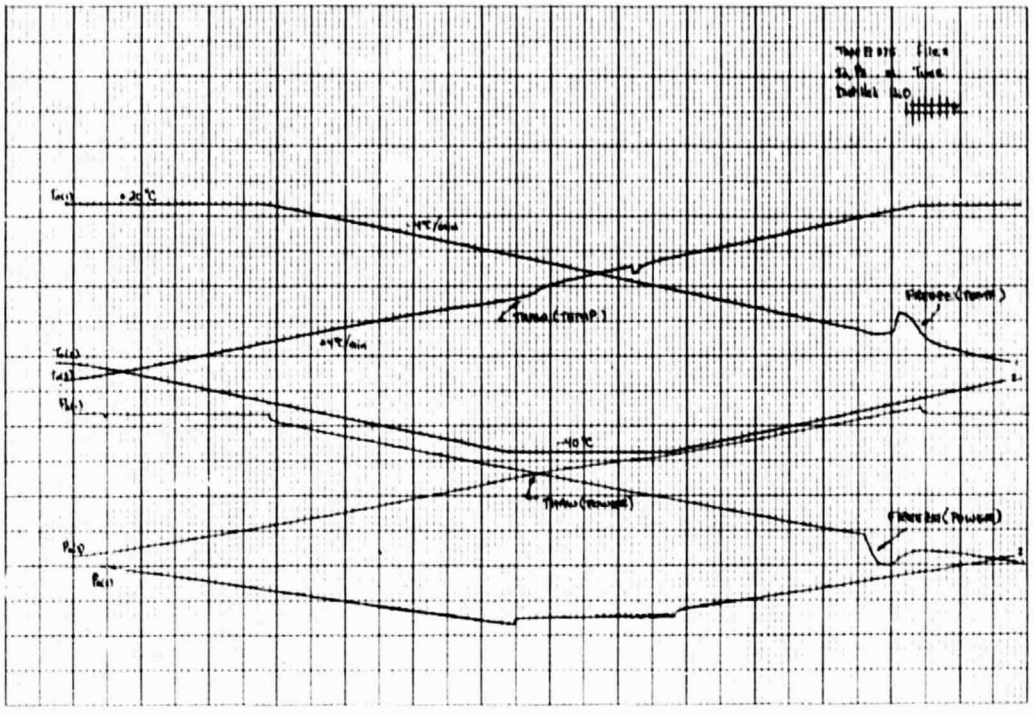

Figure D-10a

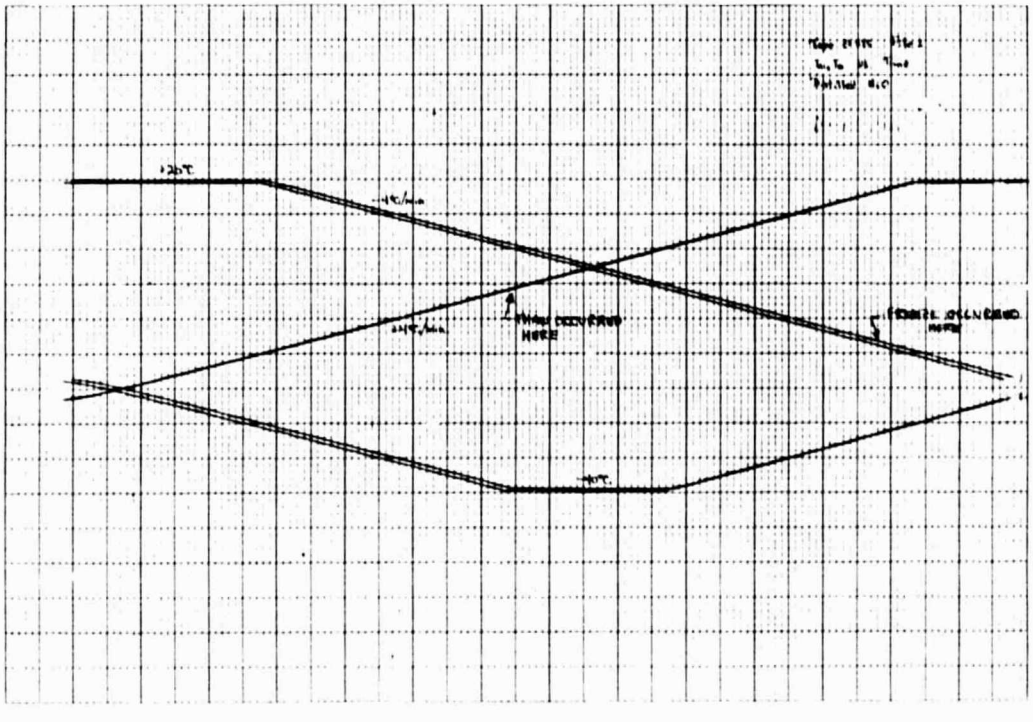

Figure D-10b

APPENDIX E

SALINE TEST DATA

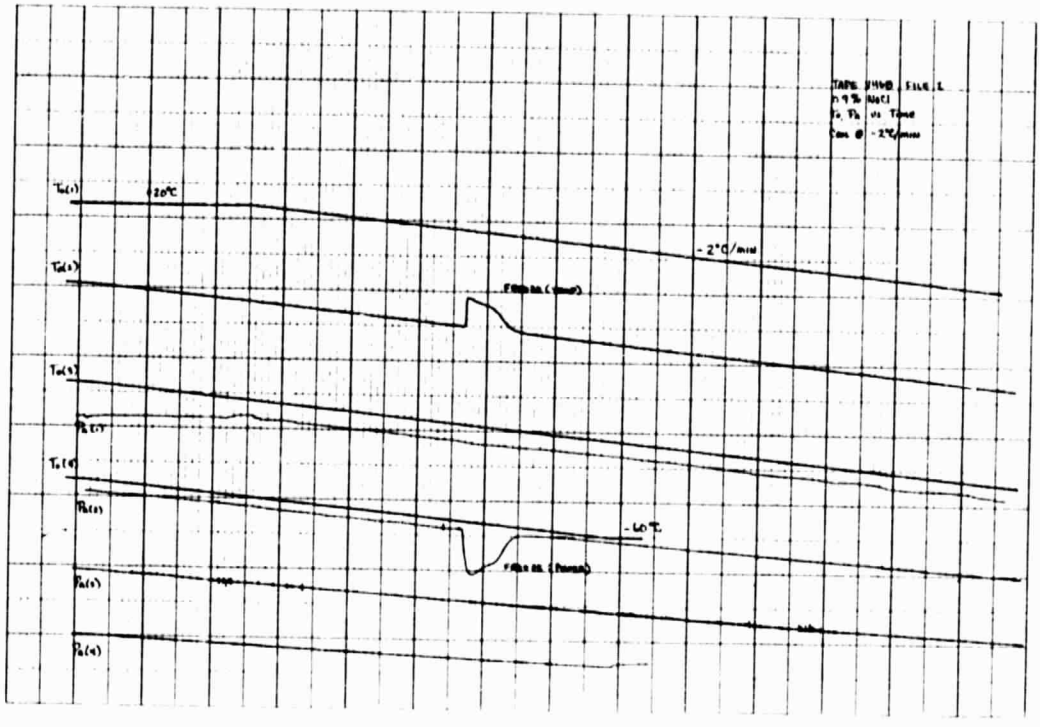

Figure E-1a

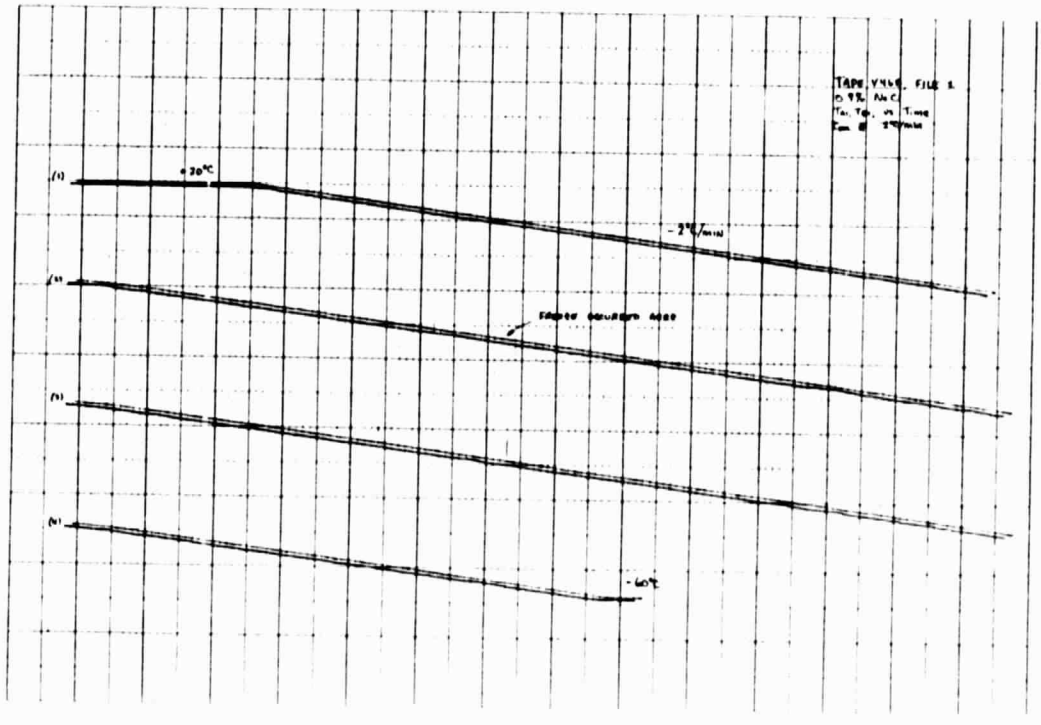

Figure E-1b

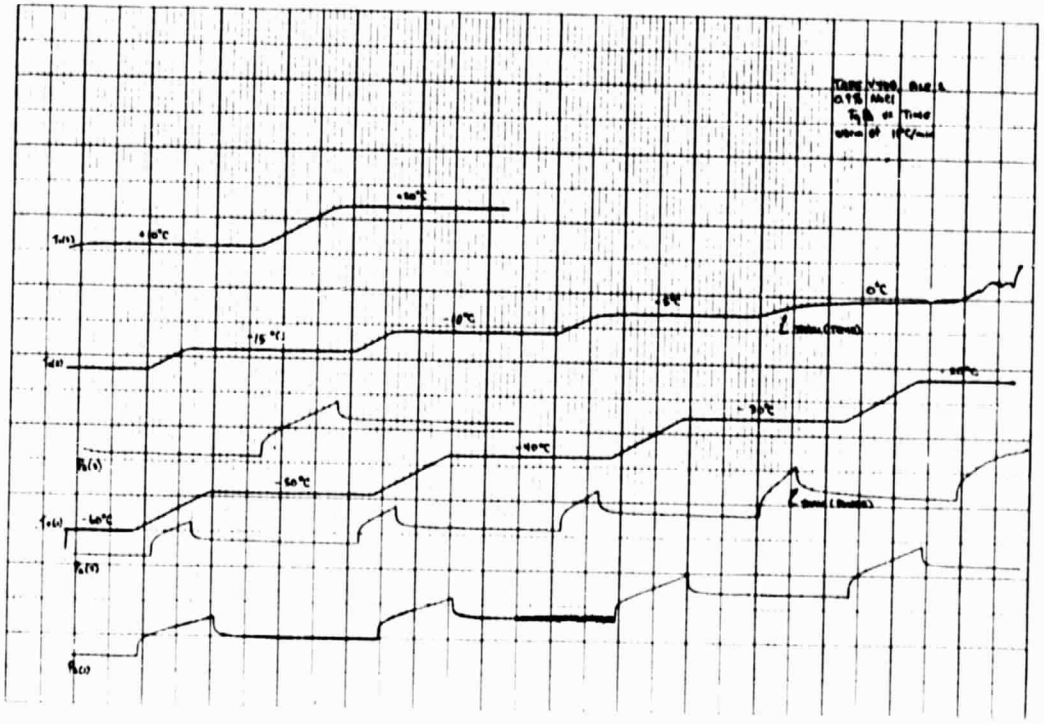

Figure E-1c

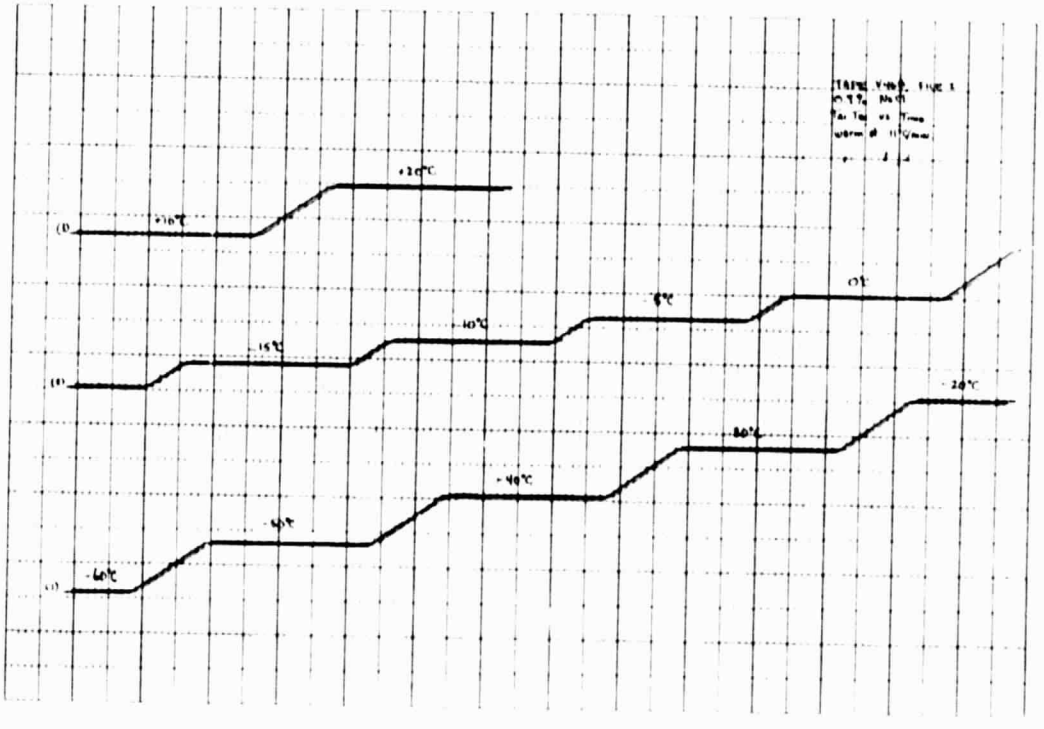

Figure E-1d

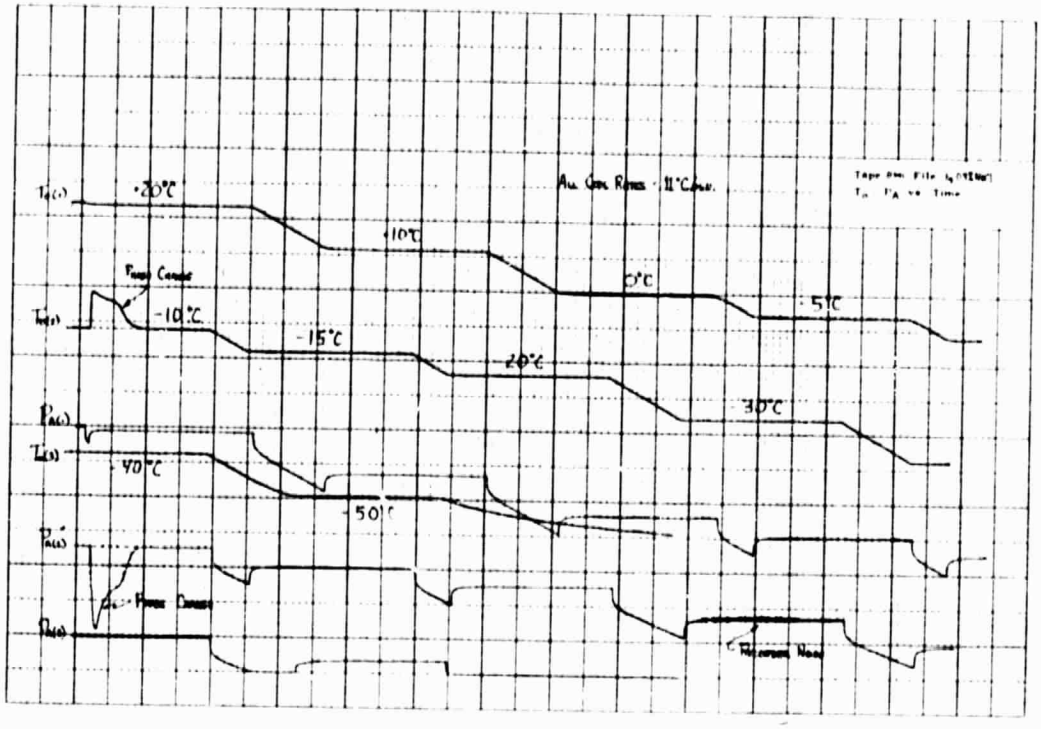

Figure E-2a

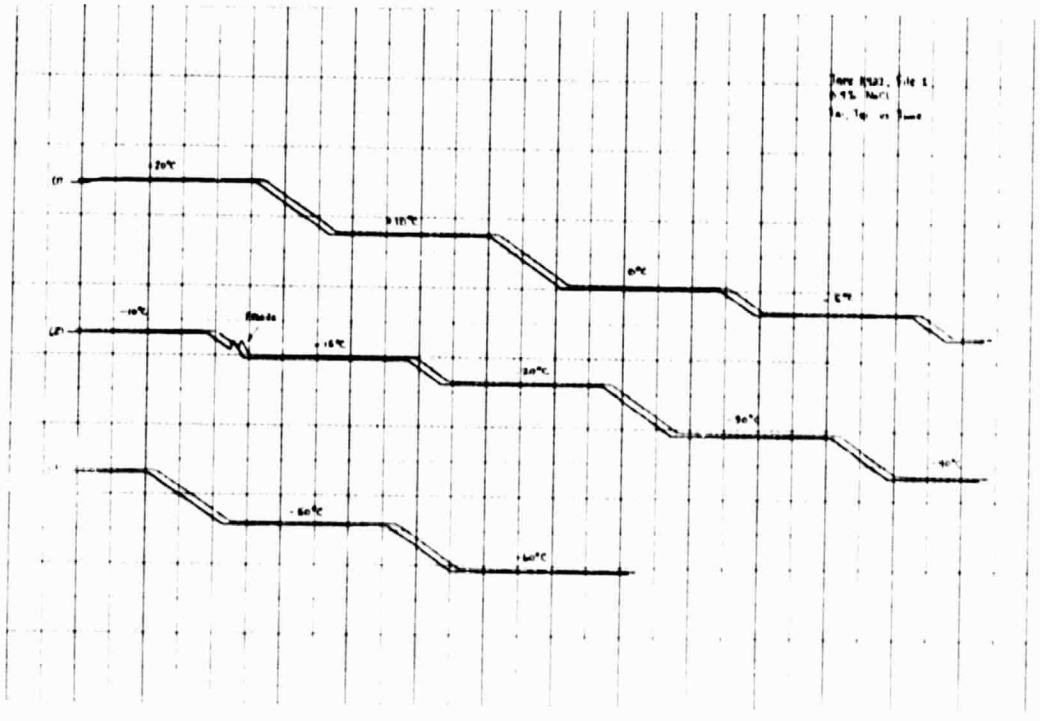

Figure E-2b

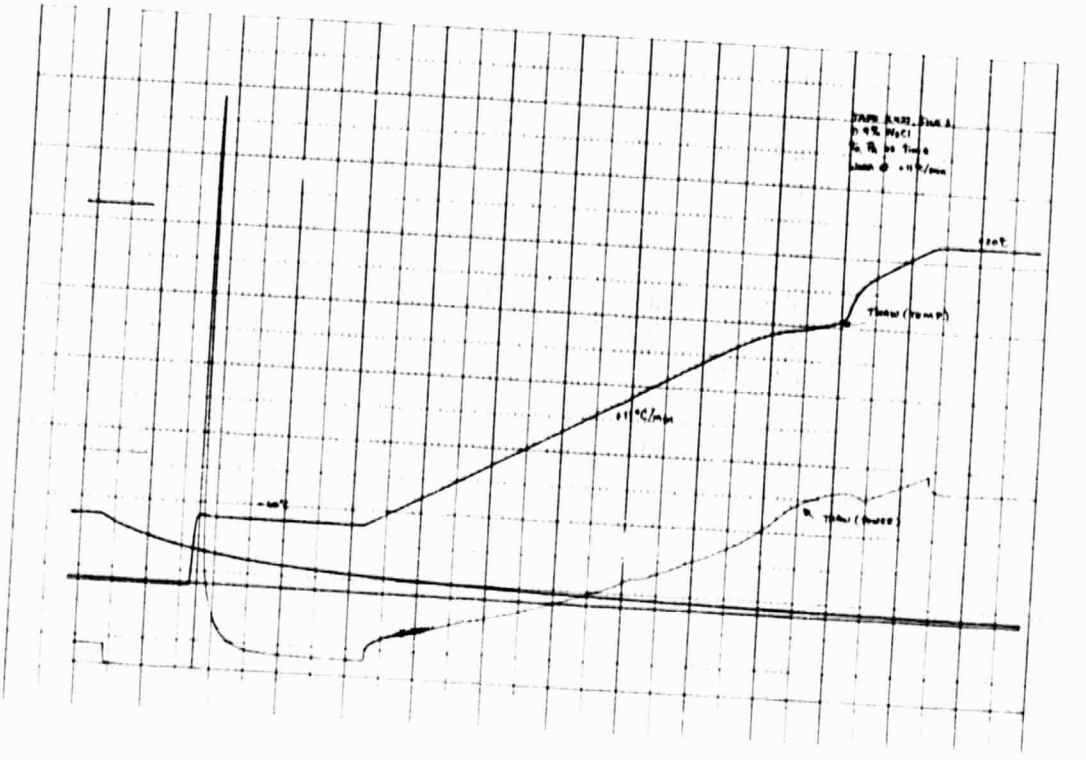

Figure E-2c

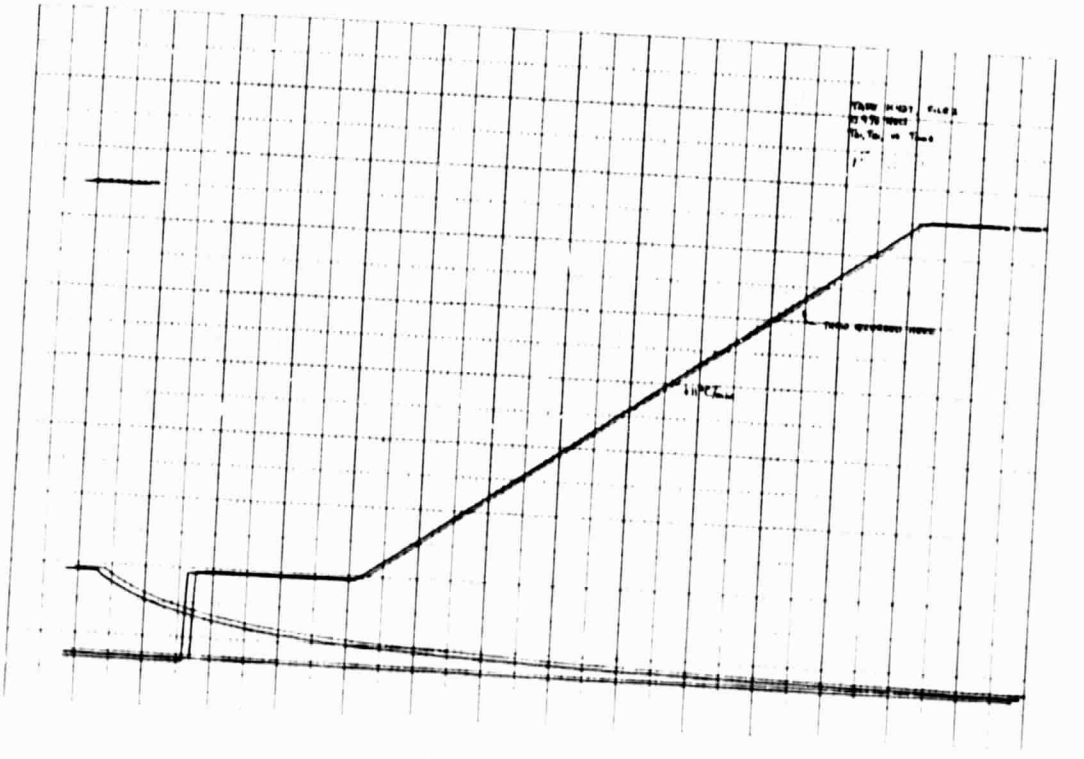

Figure E-2d

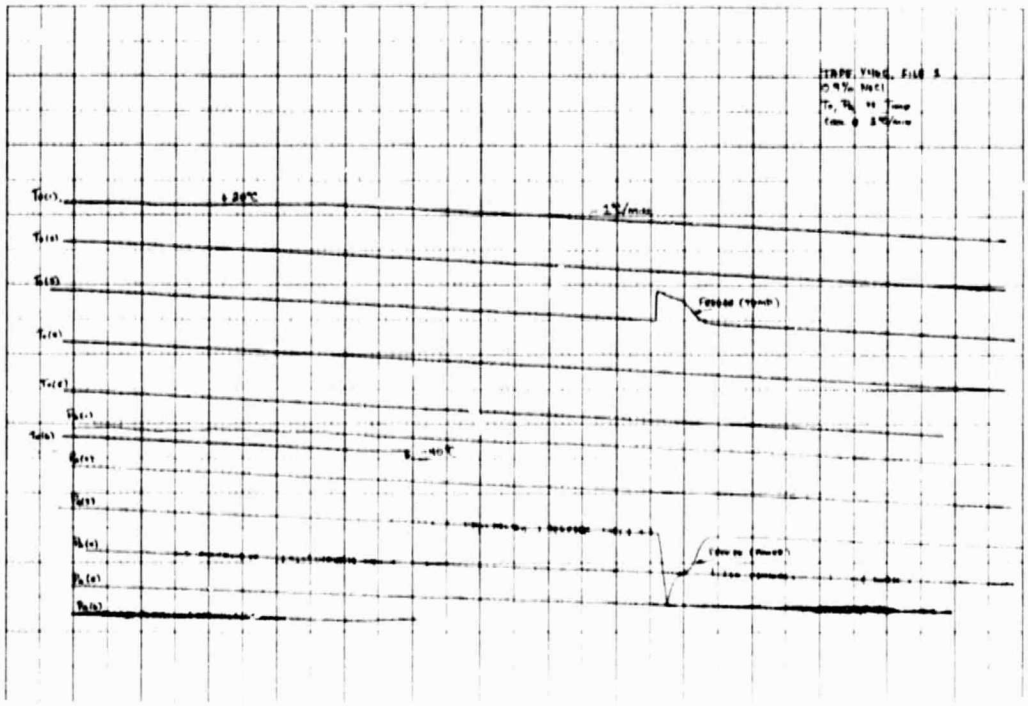

Figure E-3a

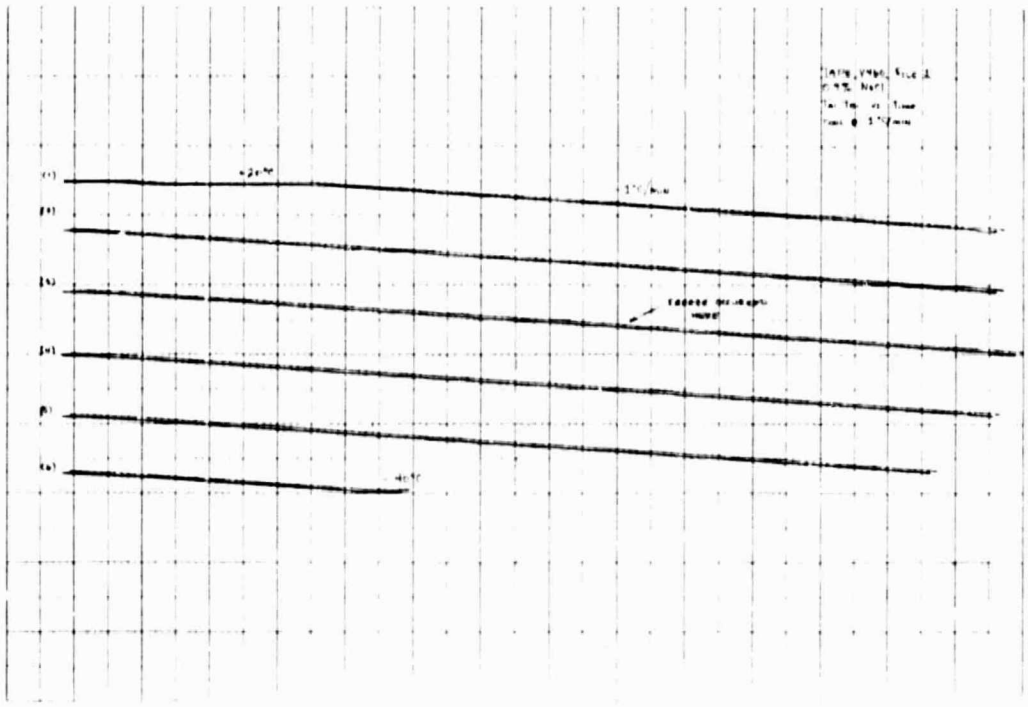

Figure E-3b

ORIGINAL PAGE IS
OF POOR QUALITY

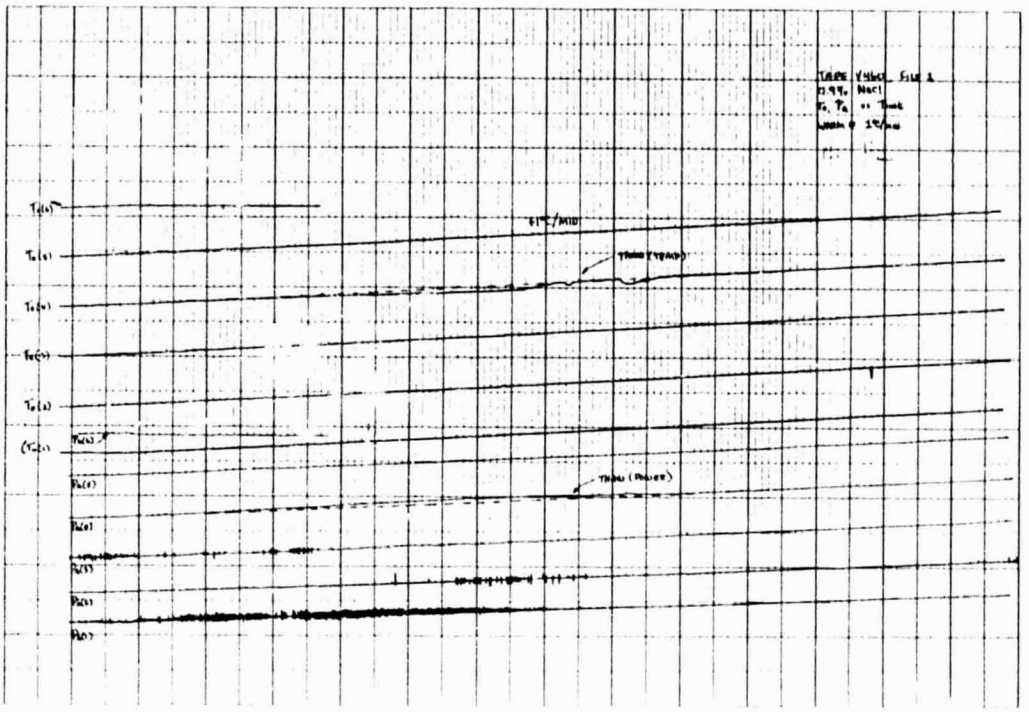

Figure E-3c

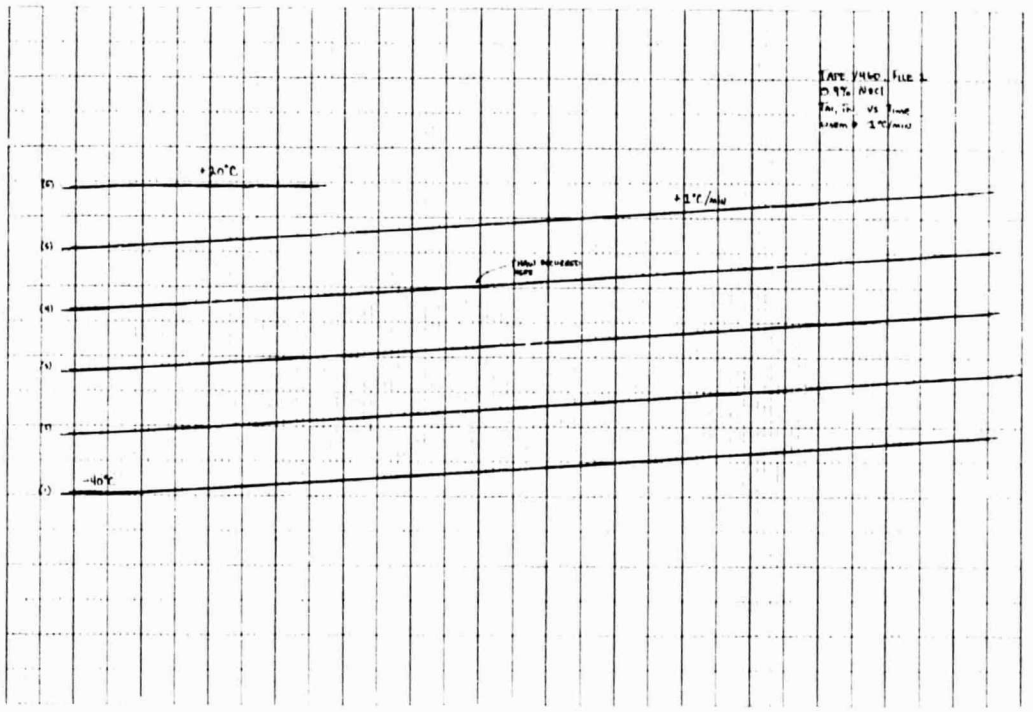

Figure E-3d

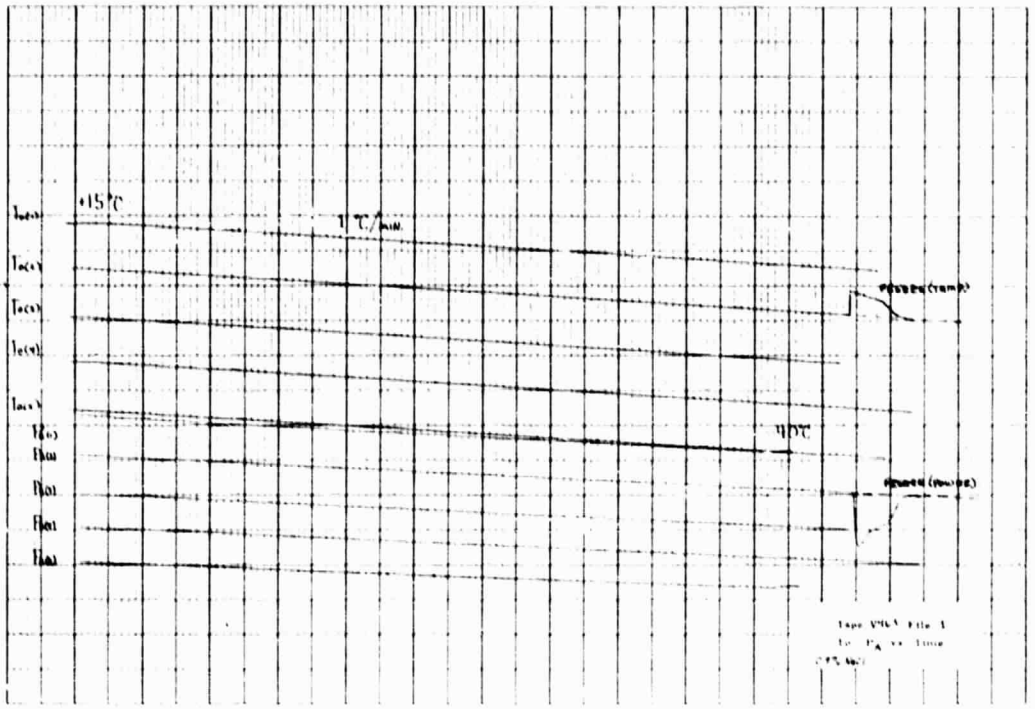

Figure E-4a

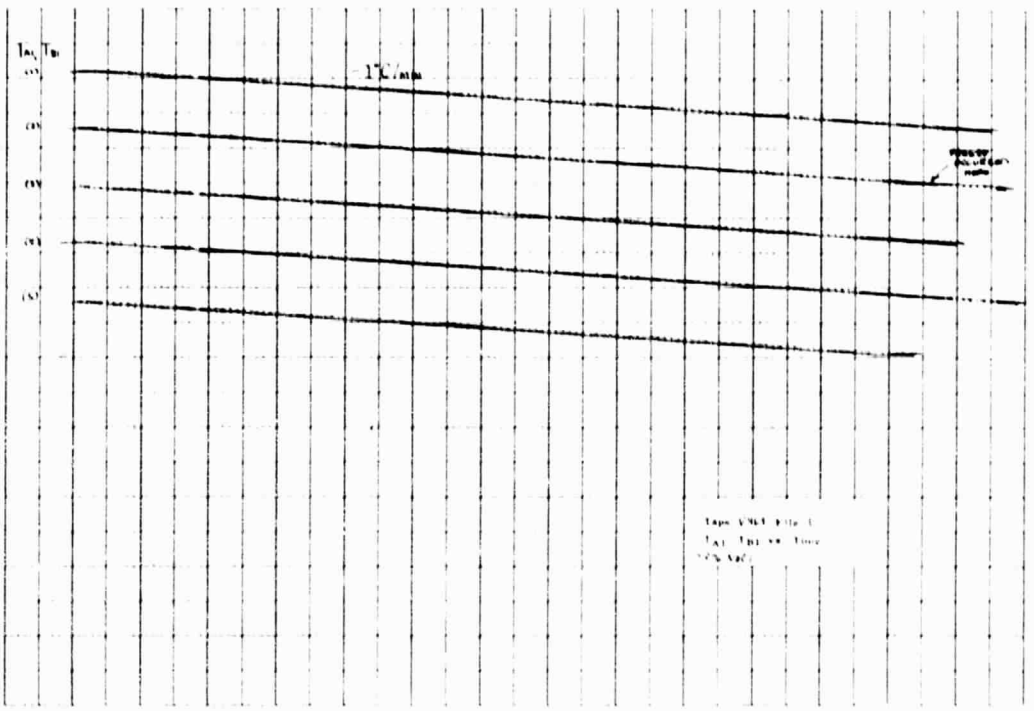

Figure E-4b

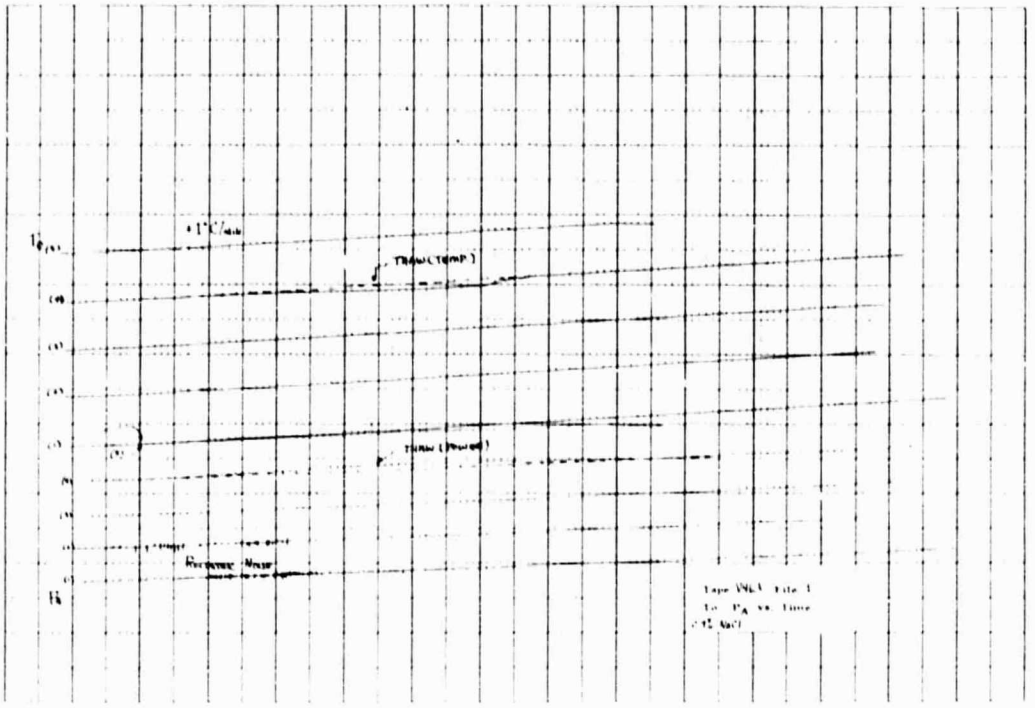

Figure E-4c

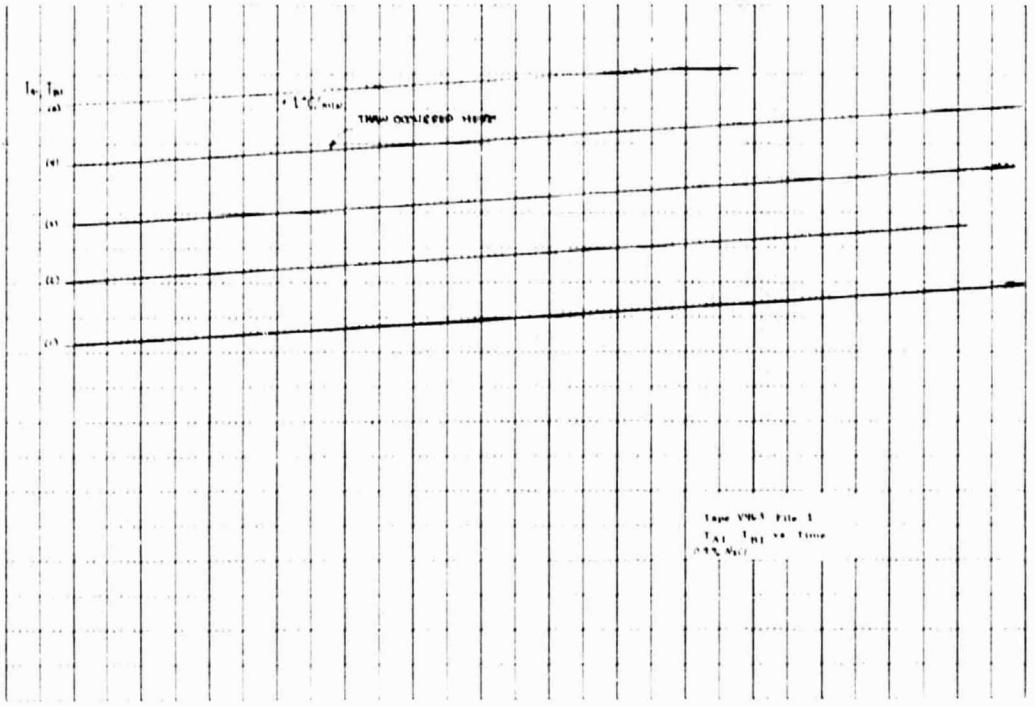

Figure E-4d

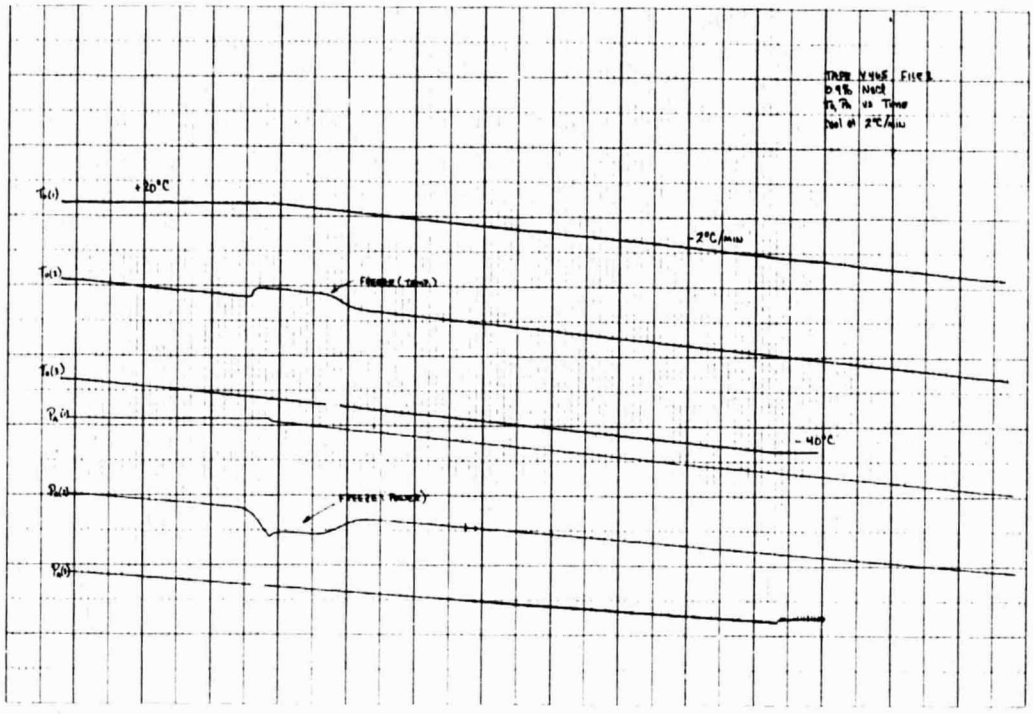

Figure E-5a

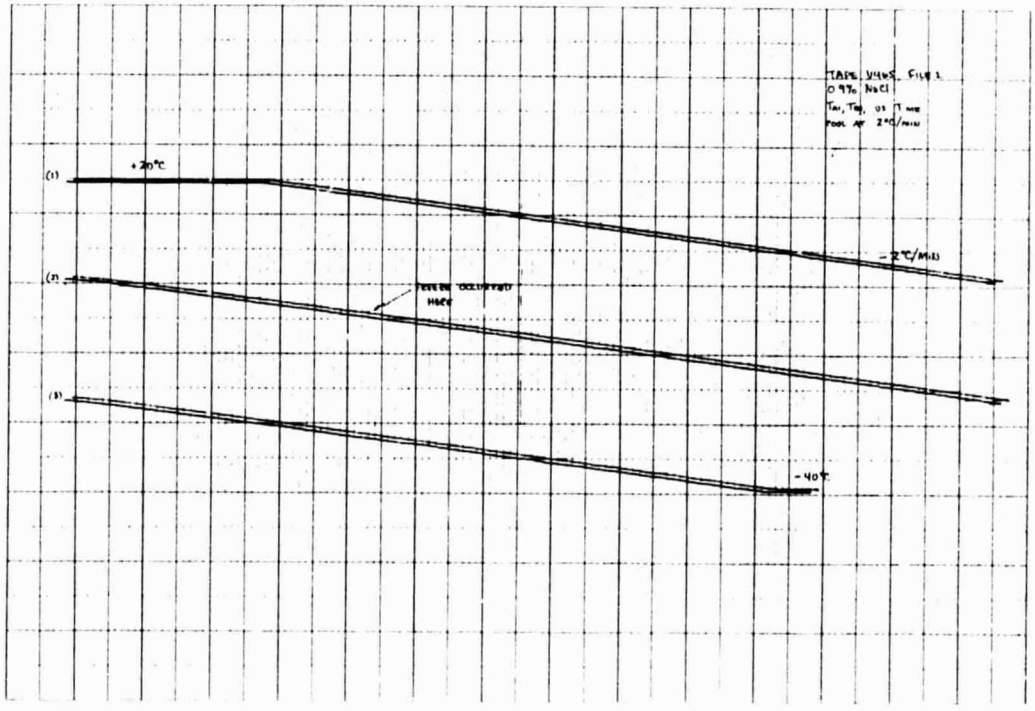

Figure E-5b

PRECEDING PAGE BLANK NOT FILMED

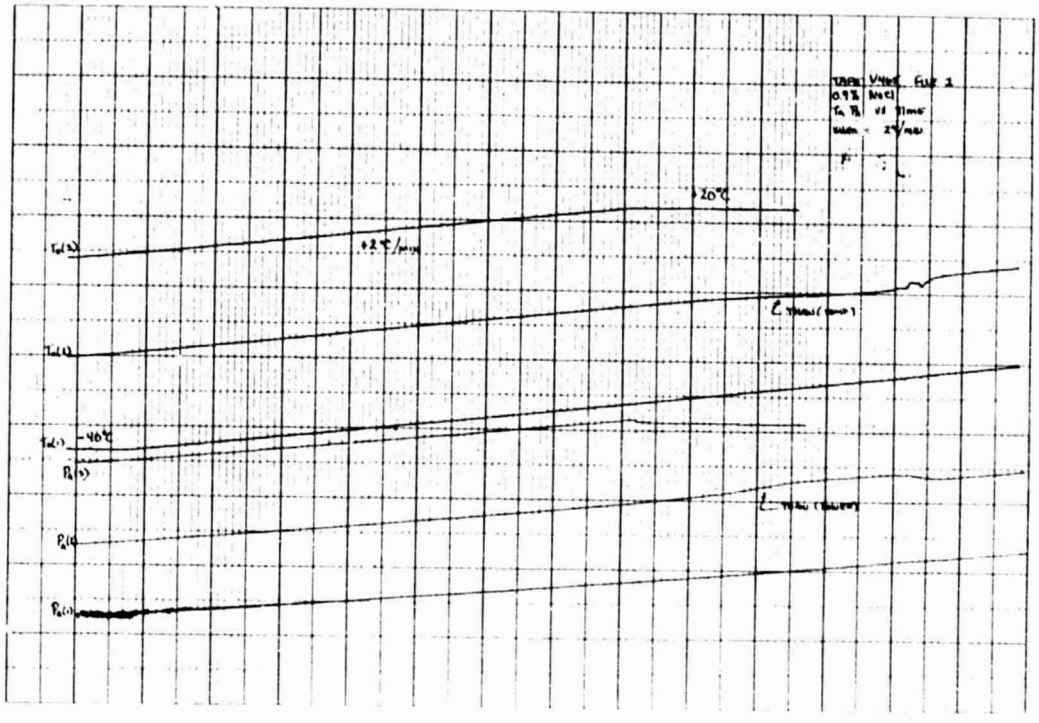

Figure E-5c

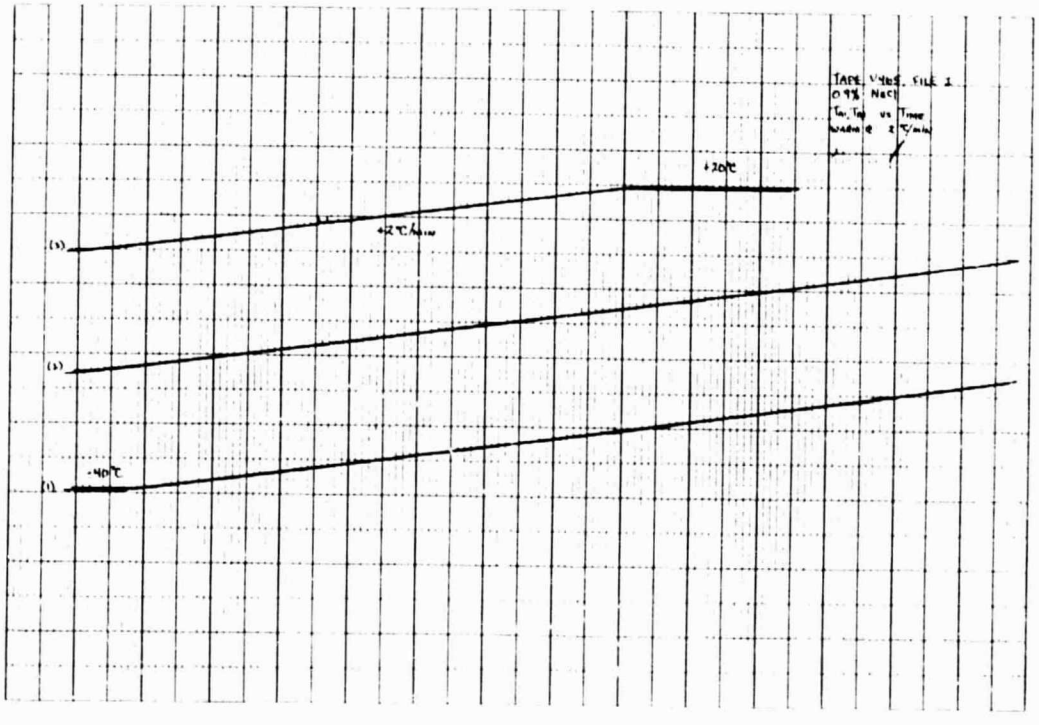

Figure E-5d

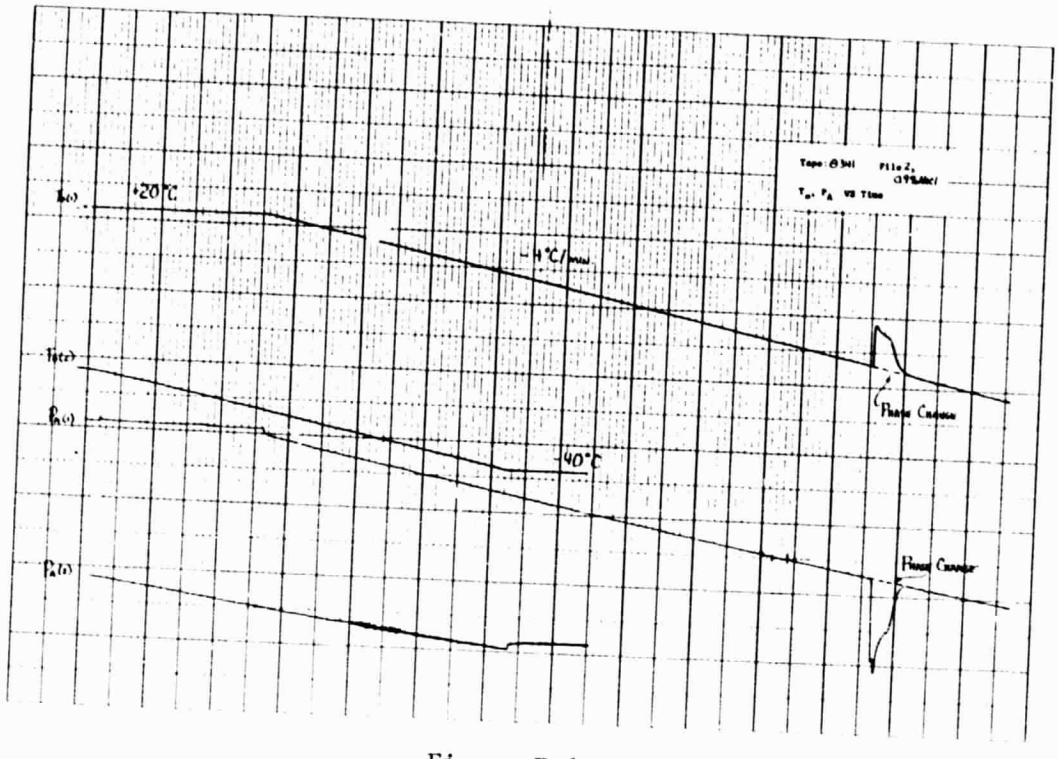

Figure E-6a

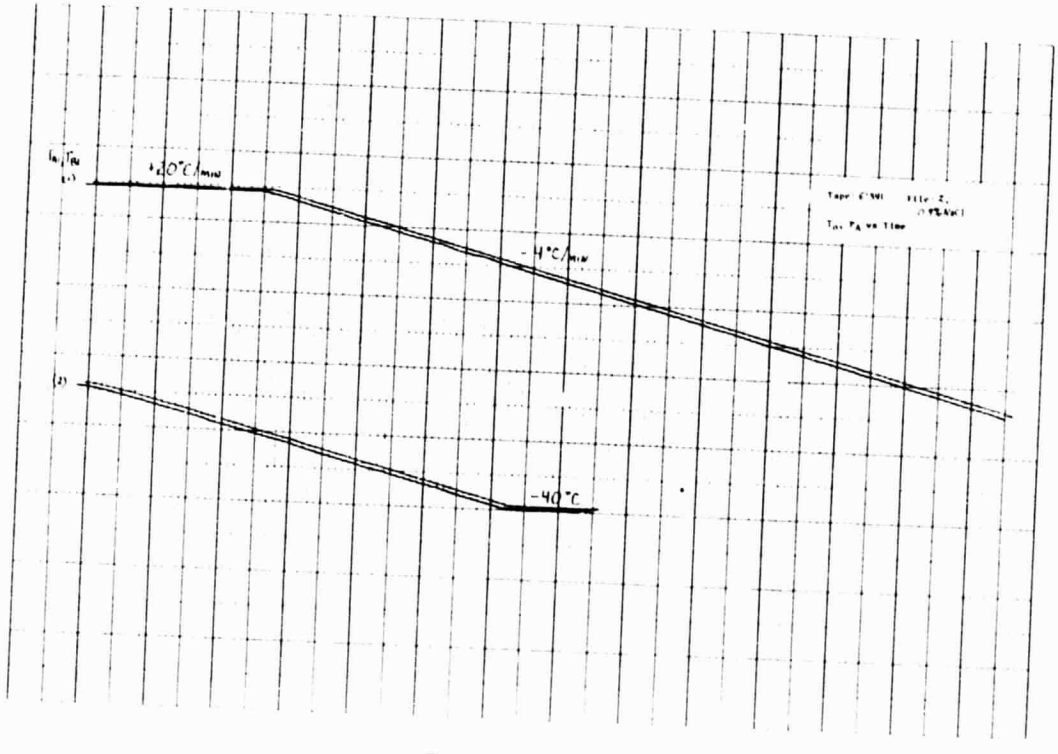

Figure E-6b

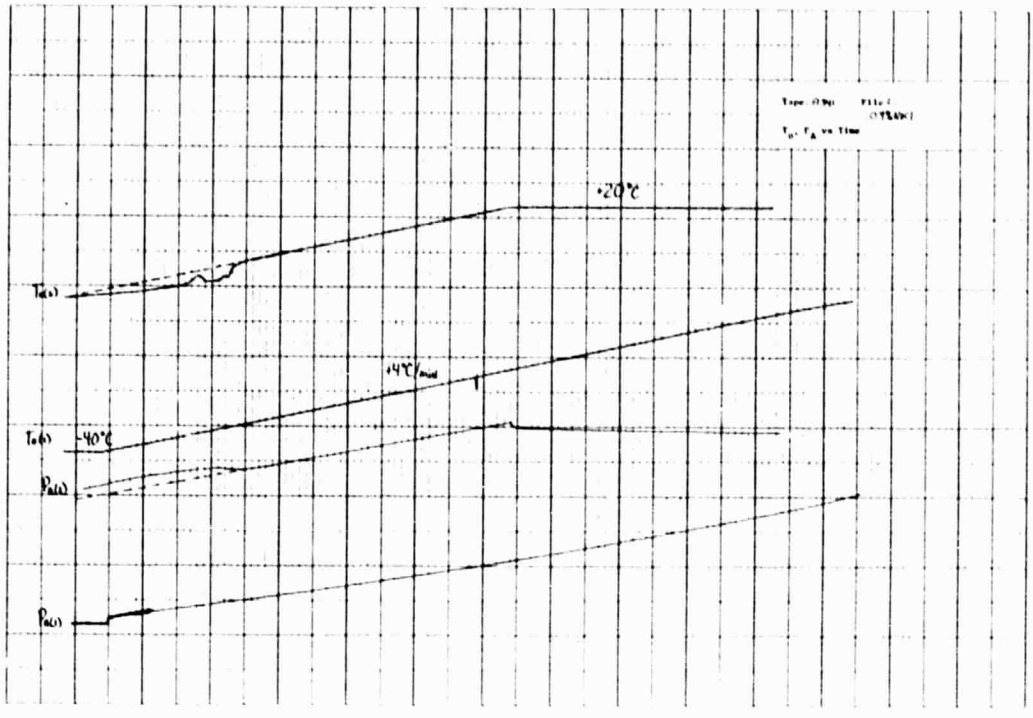

Figure E-6c

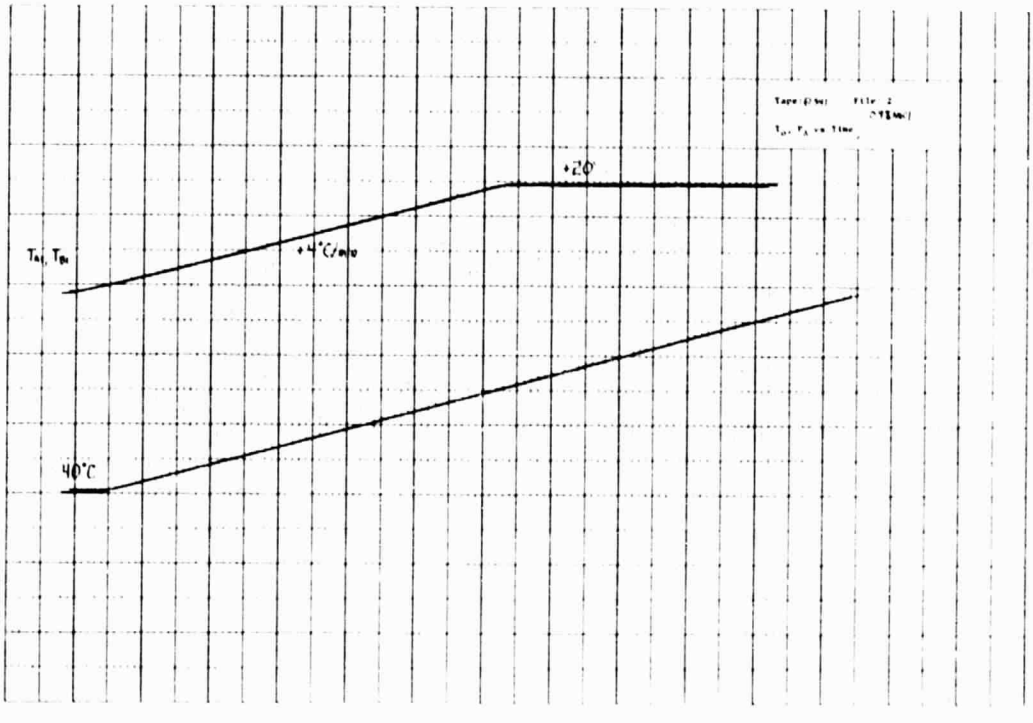

Figure E-6d

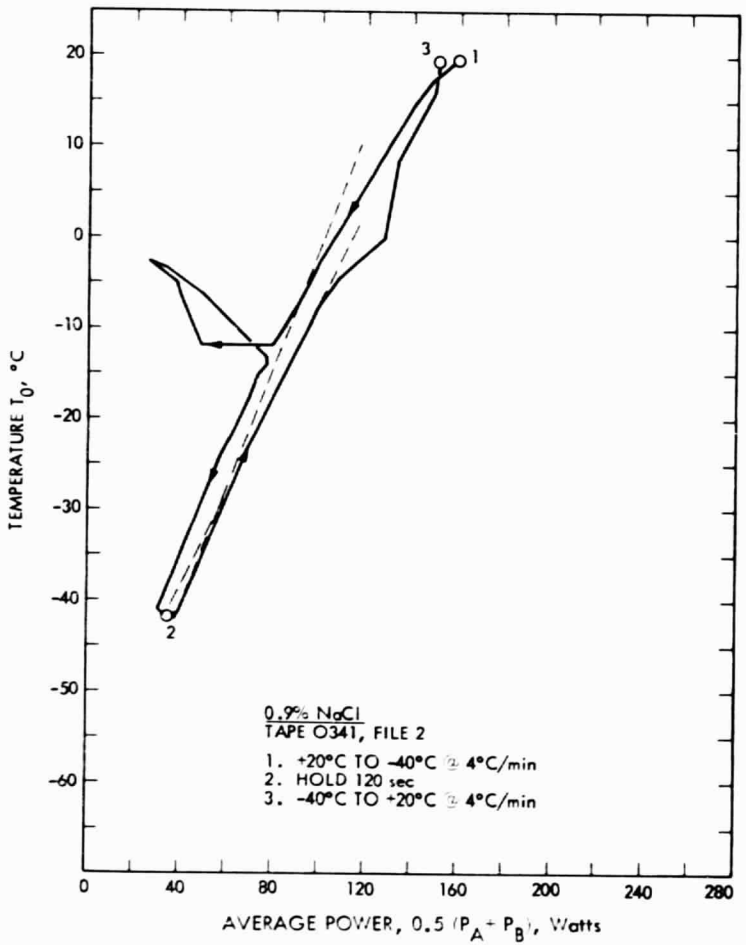

Figure E-6e

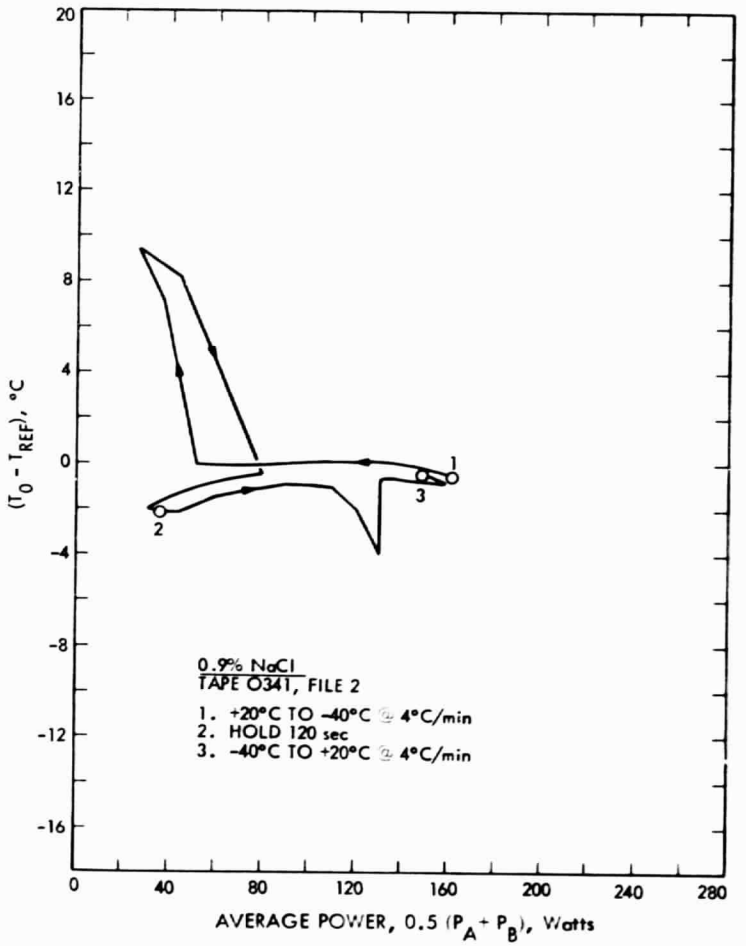

Figure E-6f

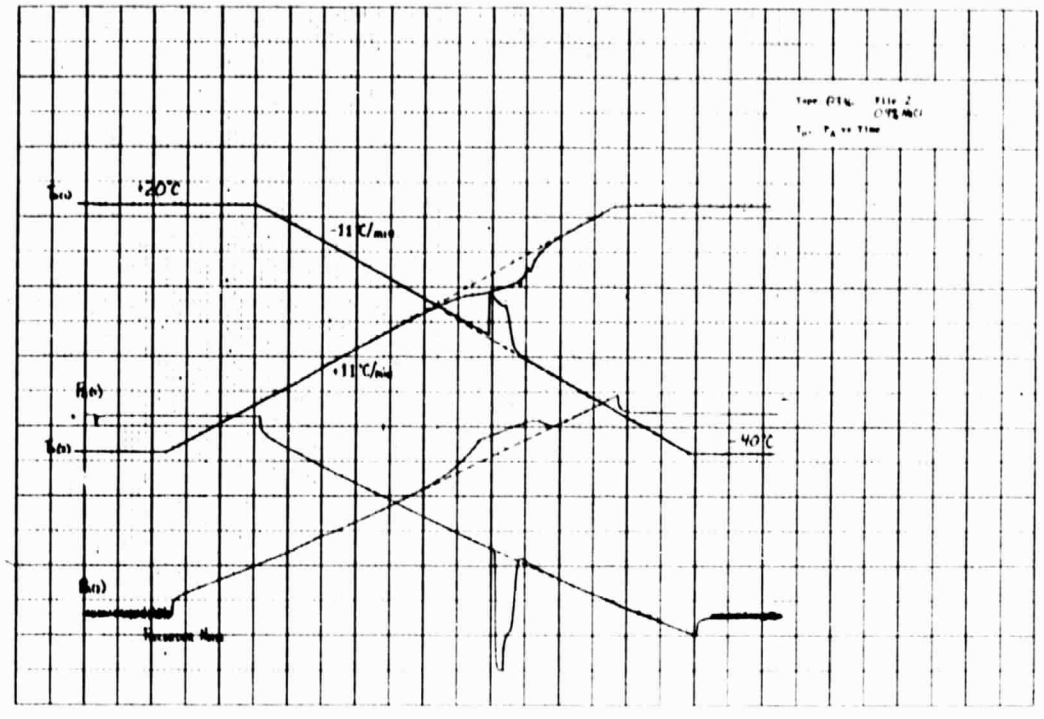

Figure E-7a

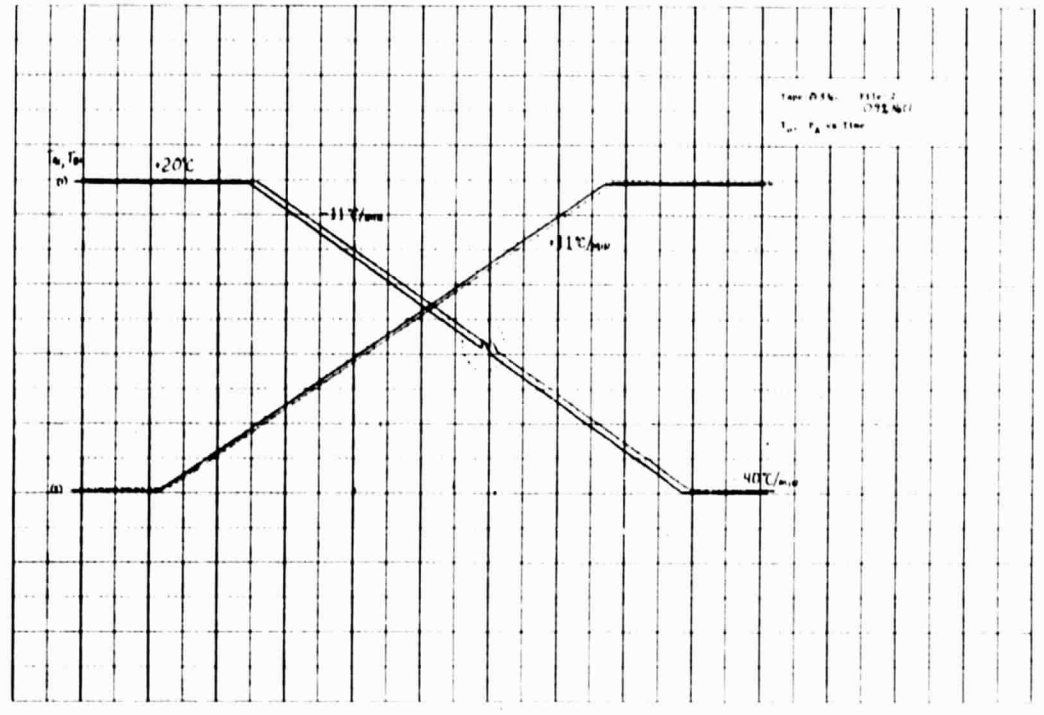

Figure E-7b

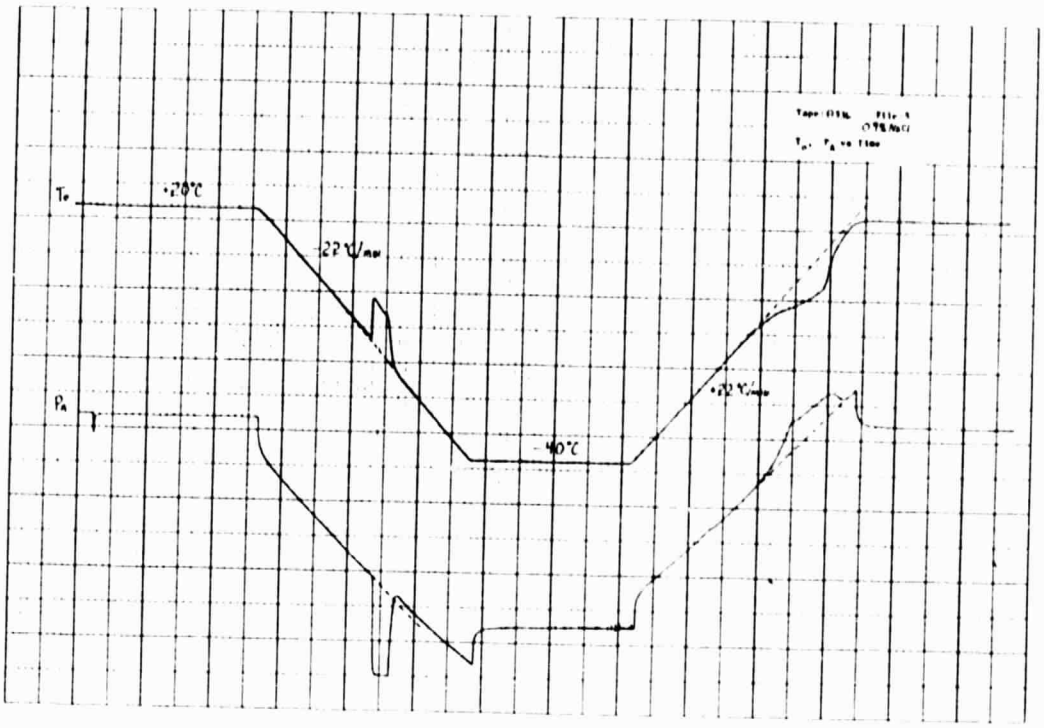

Figure E-8a

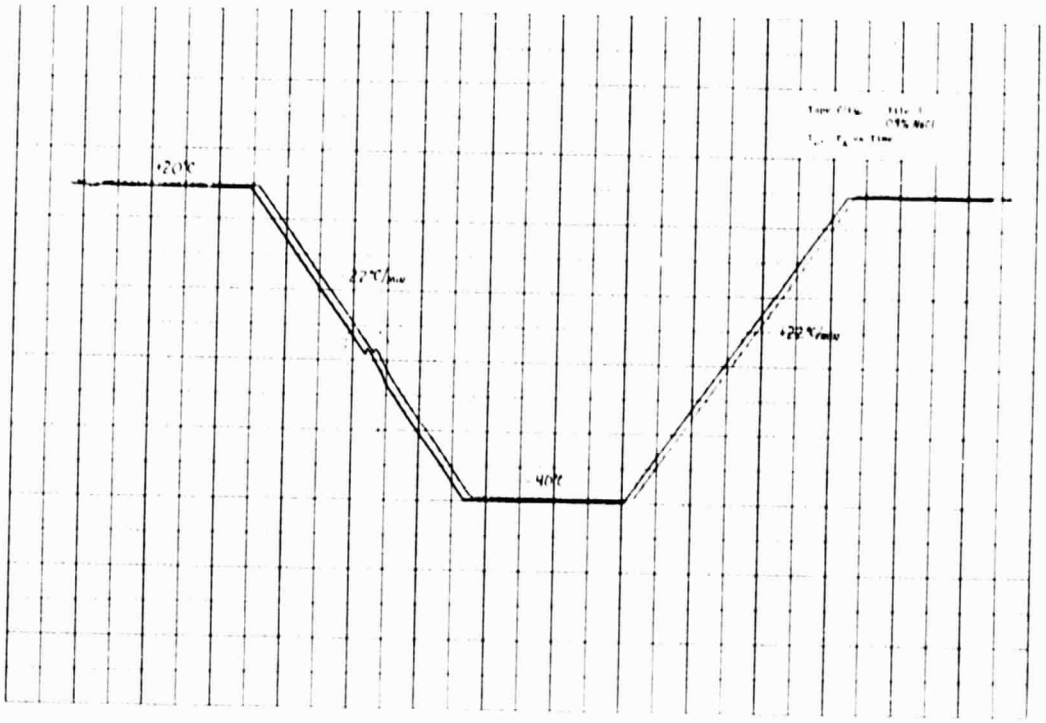

Figure E-8b

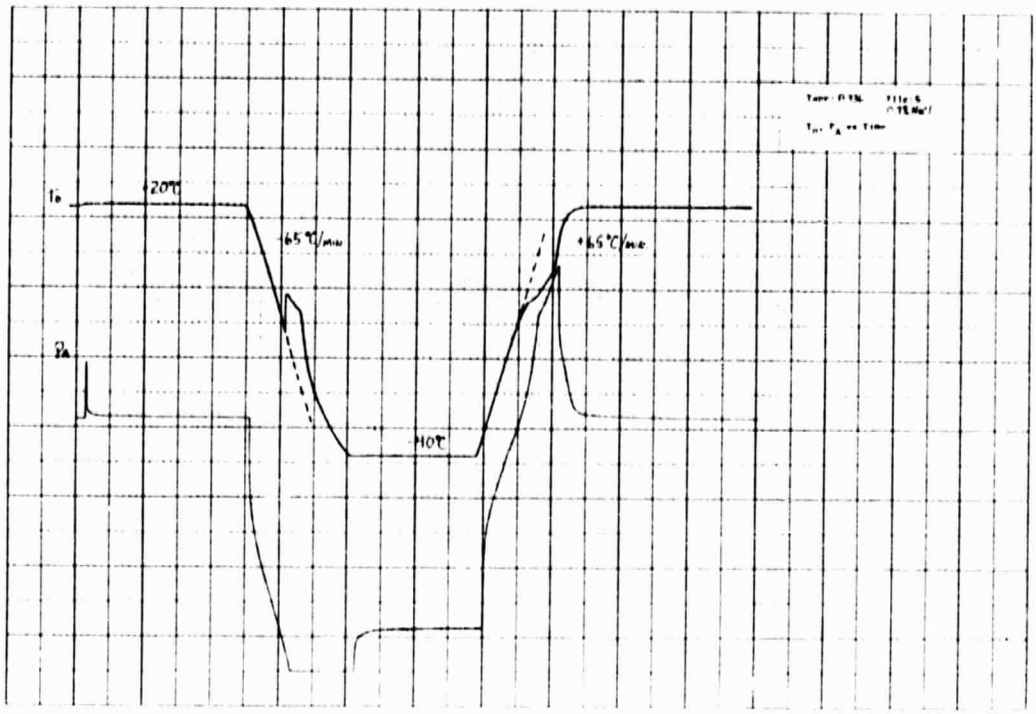

Figure E-9a

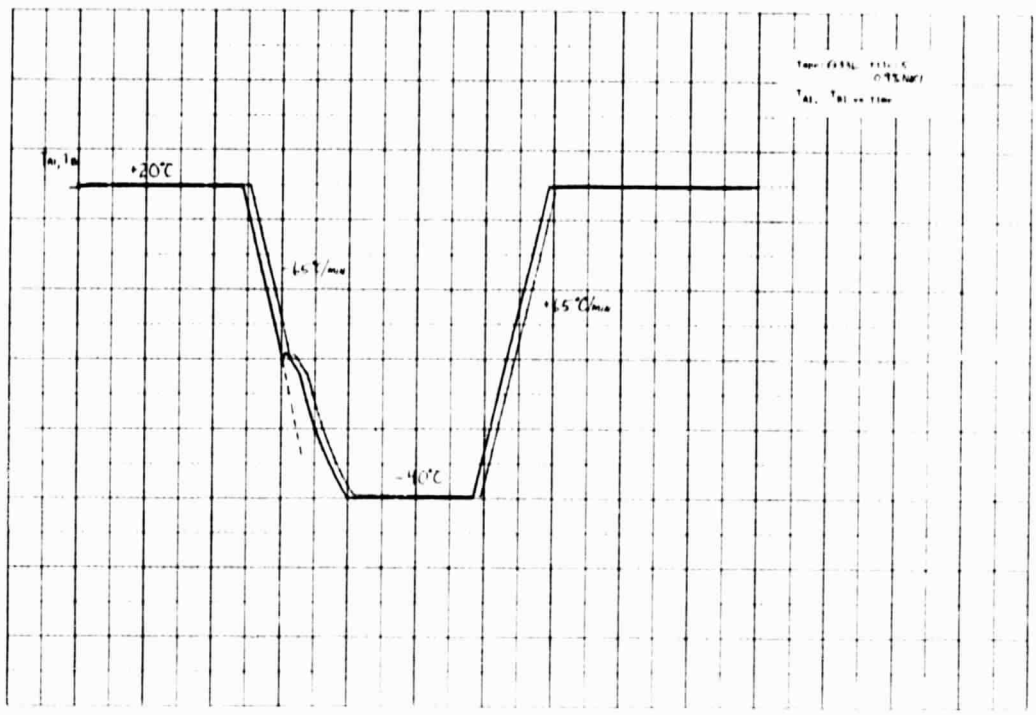

Figure E-9b

APPENDIX F

RED BLOOD CELL TEST DATA

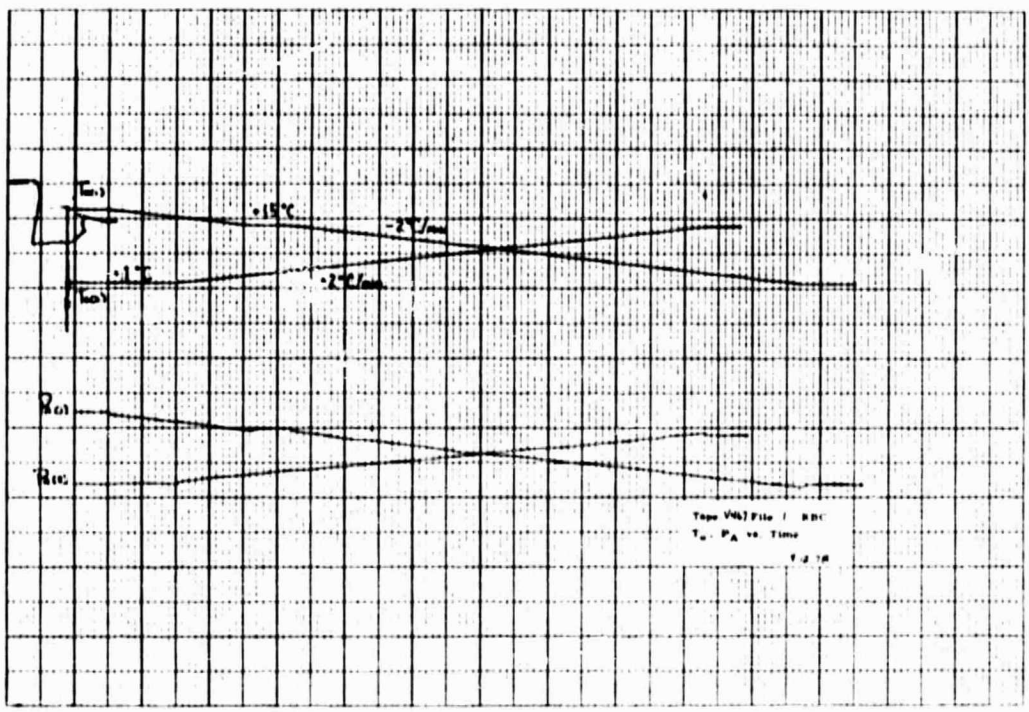

Figure F-1a

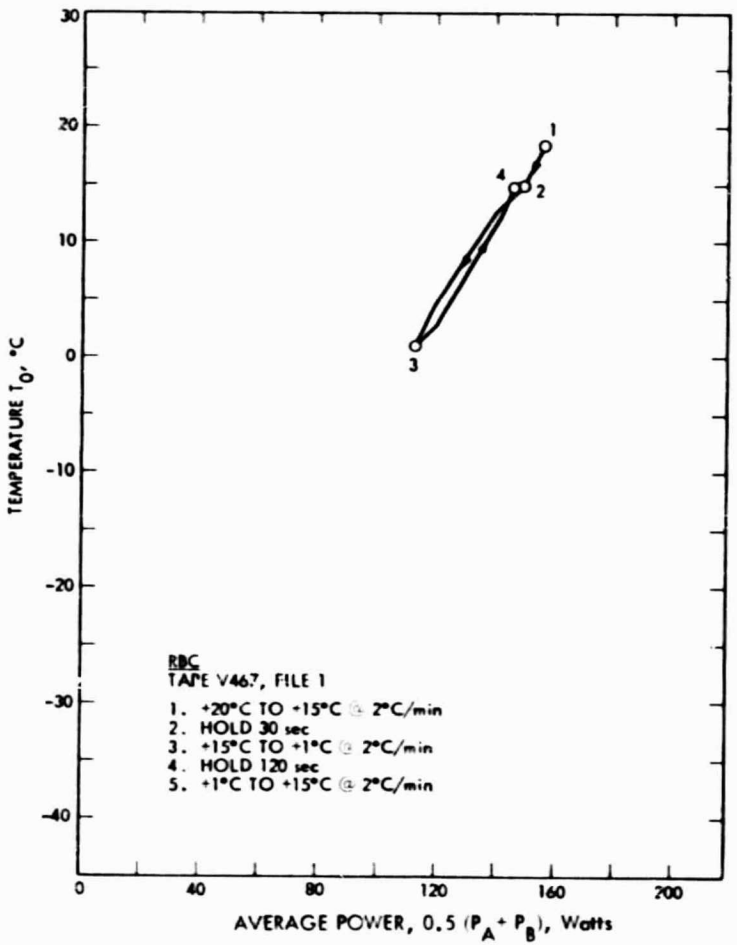

Figure F-1b

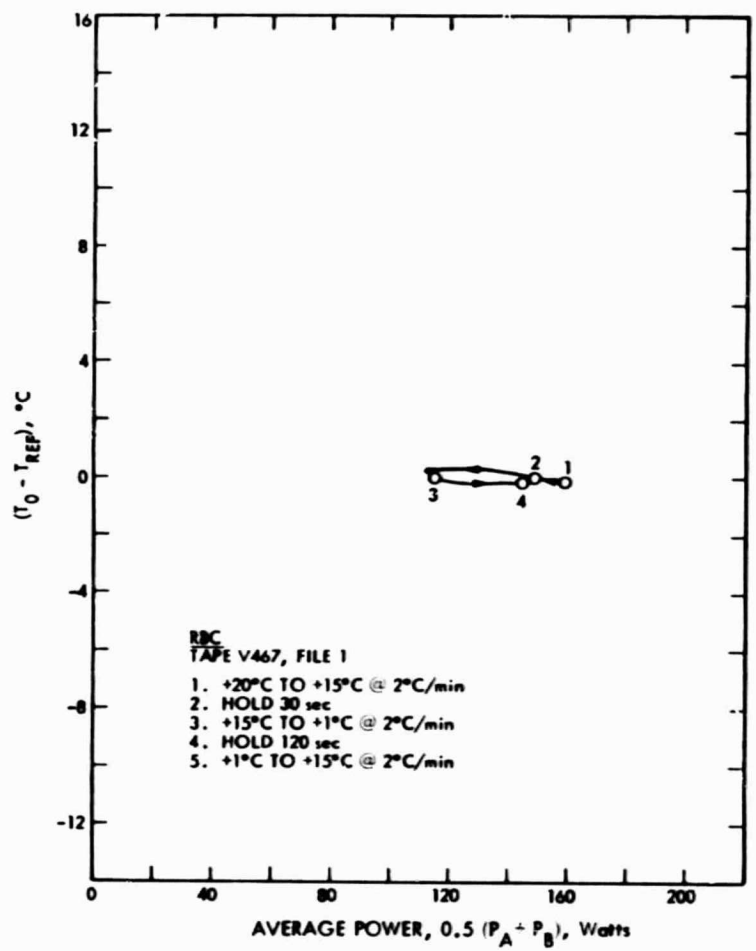

Figure F-1c

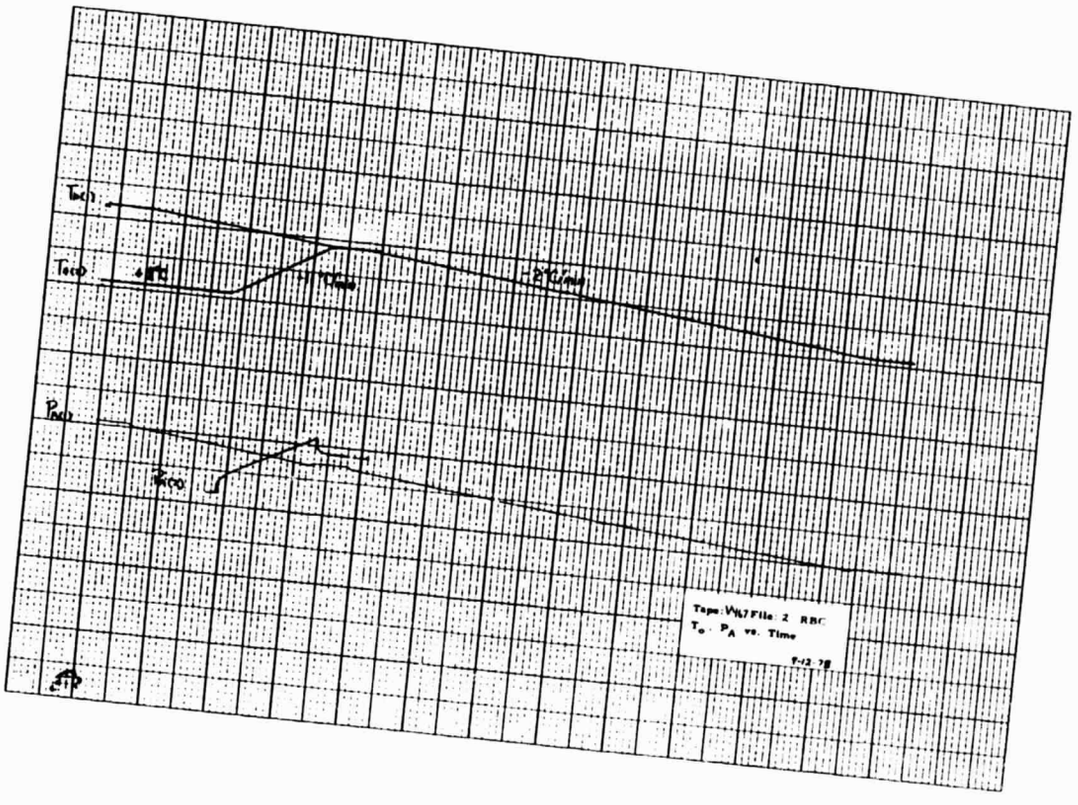

ORIGINAL PAGE IS
OF POOR QUALITY

Figure F-2a

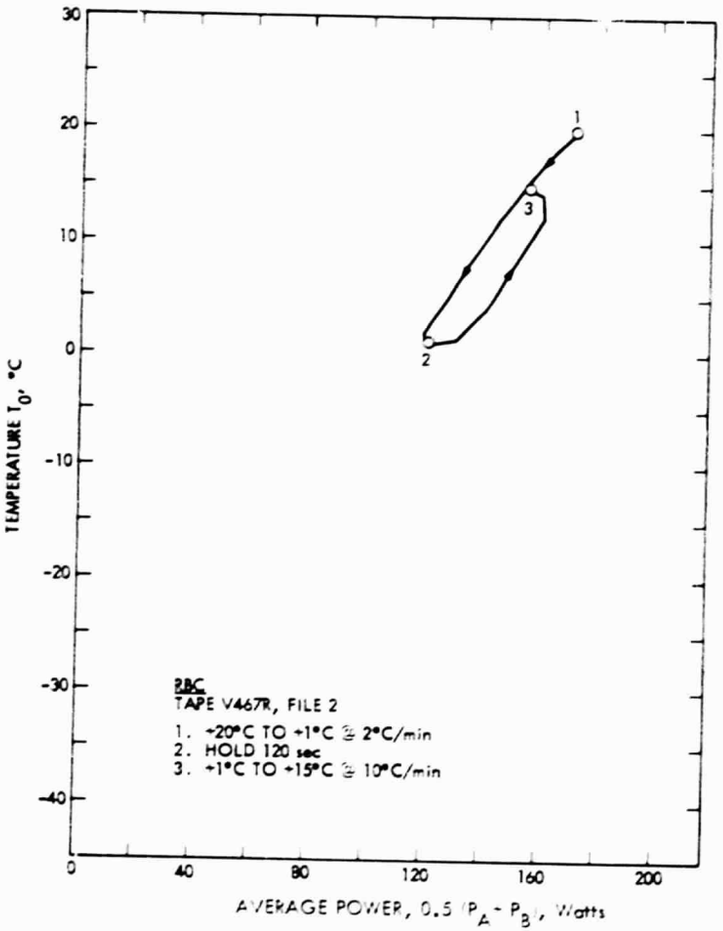

Figure F-2b

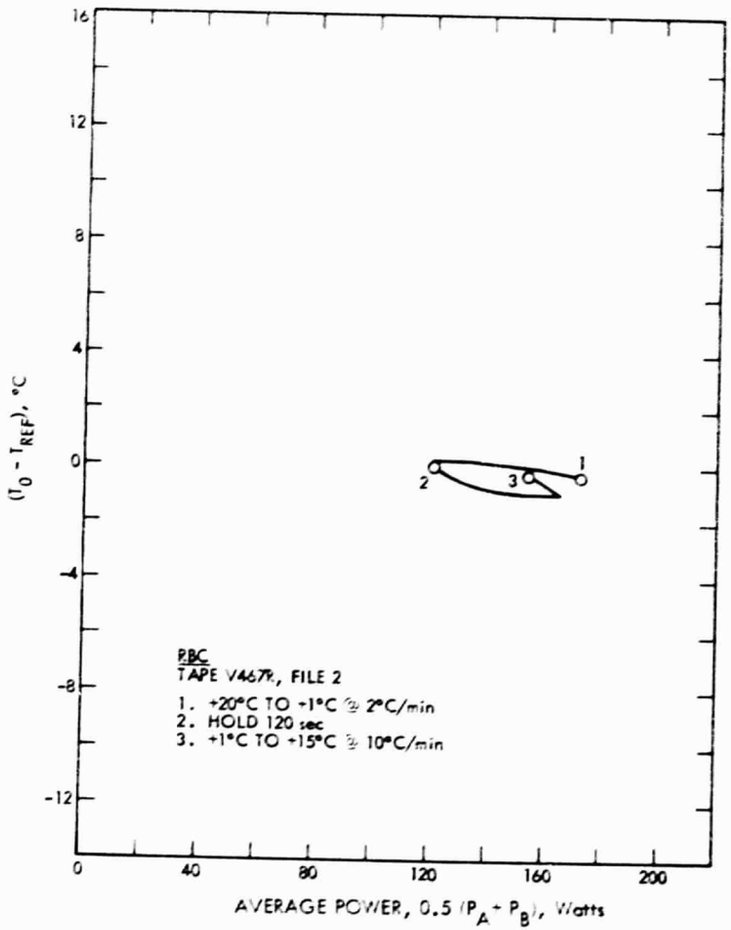

Figure F-2c

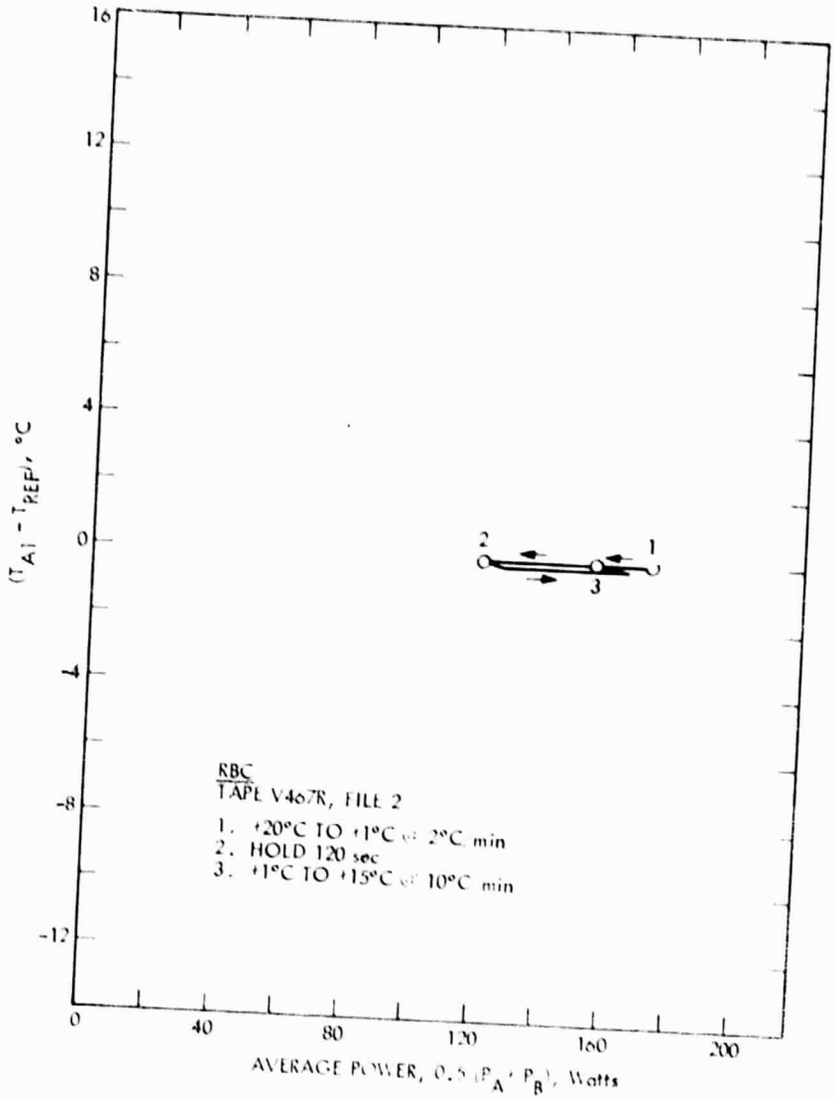
16
12
8
4
0
-4
-8
-12
$(T_{Ai} - T_{REF})$, °C
0
40
80
120
160
200
AVERAGE POWER, $0.5(P_A + P_B)$, Watts
RBC
TAPE V467R, FILE 2
1. +20°C TO +1°C @ 2°C min
2. HOLD 120 sec
3. +1°C TO +15°C @ 10°C min
1
2
3

Figure F-2d

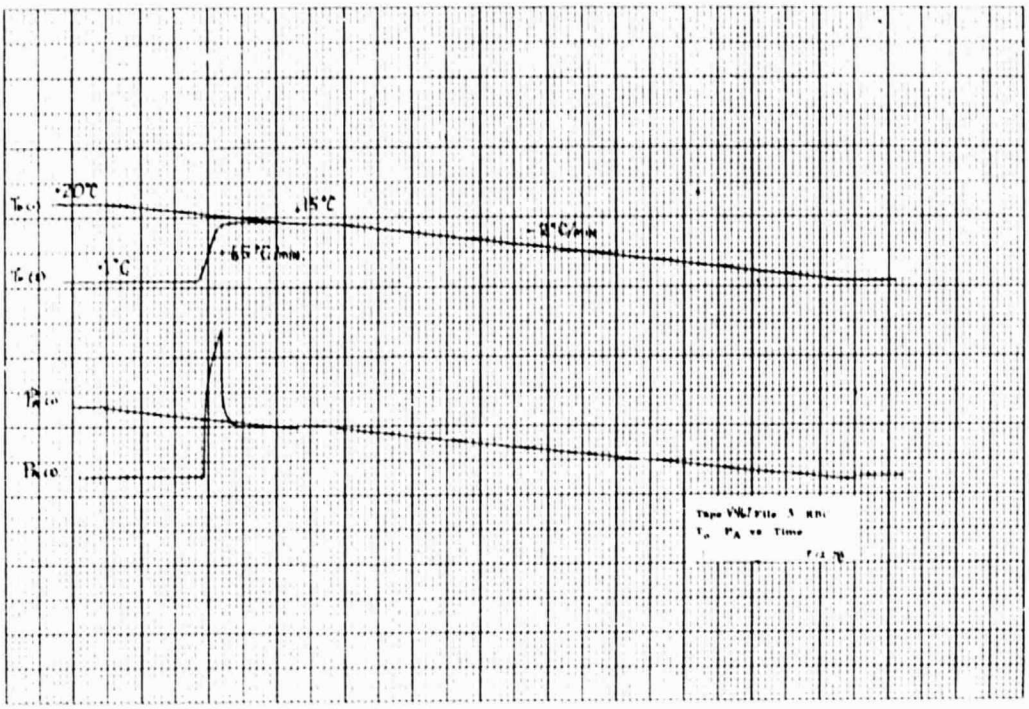

Figure F-3a

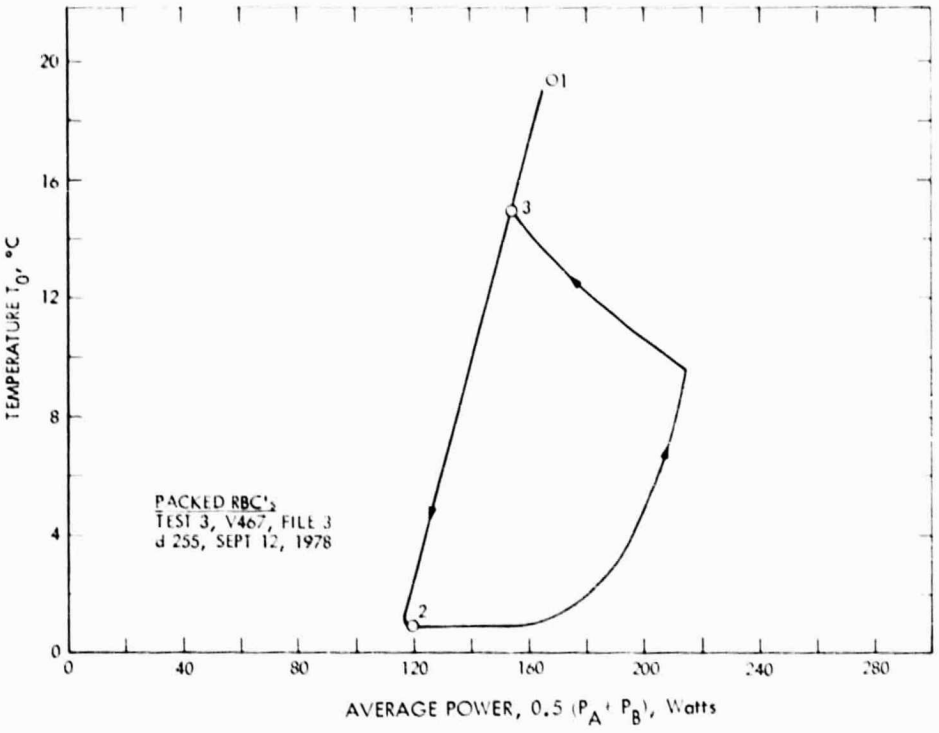

Figure F-3b

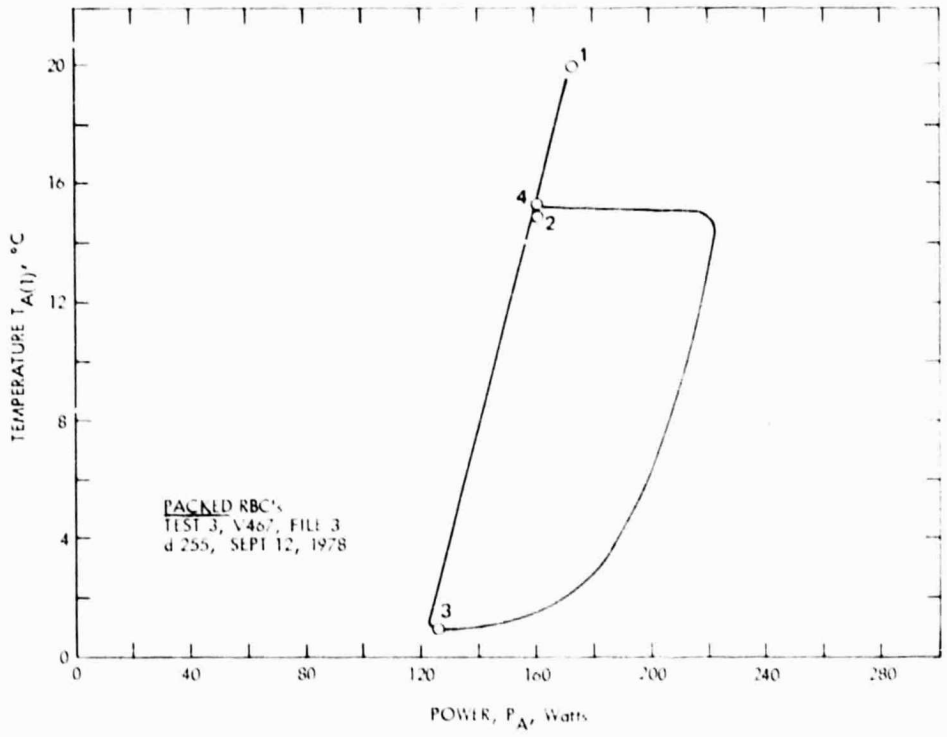

Figure F-3c

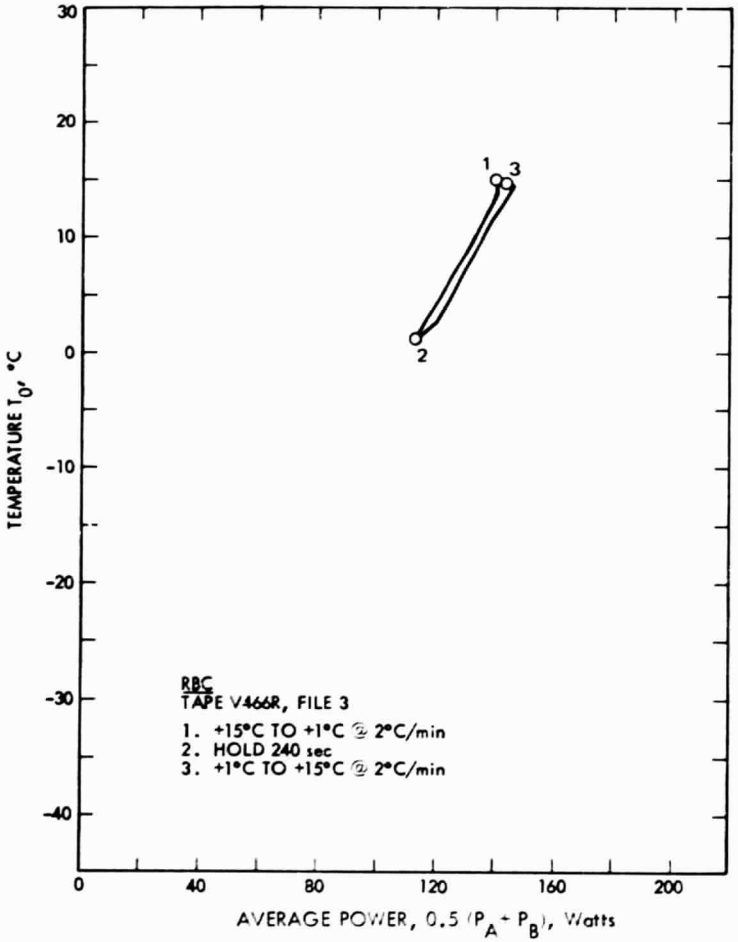

Figure F-4a

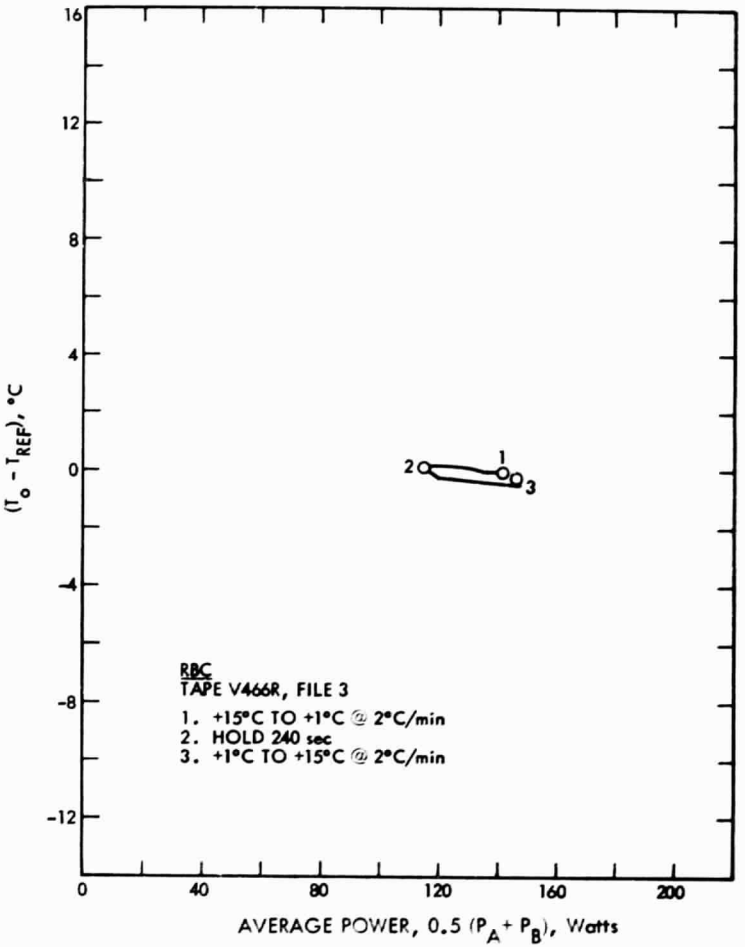

Figure F-4b

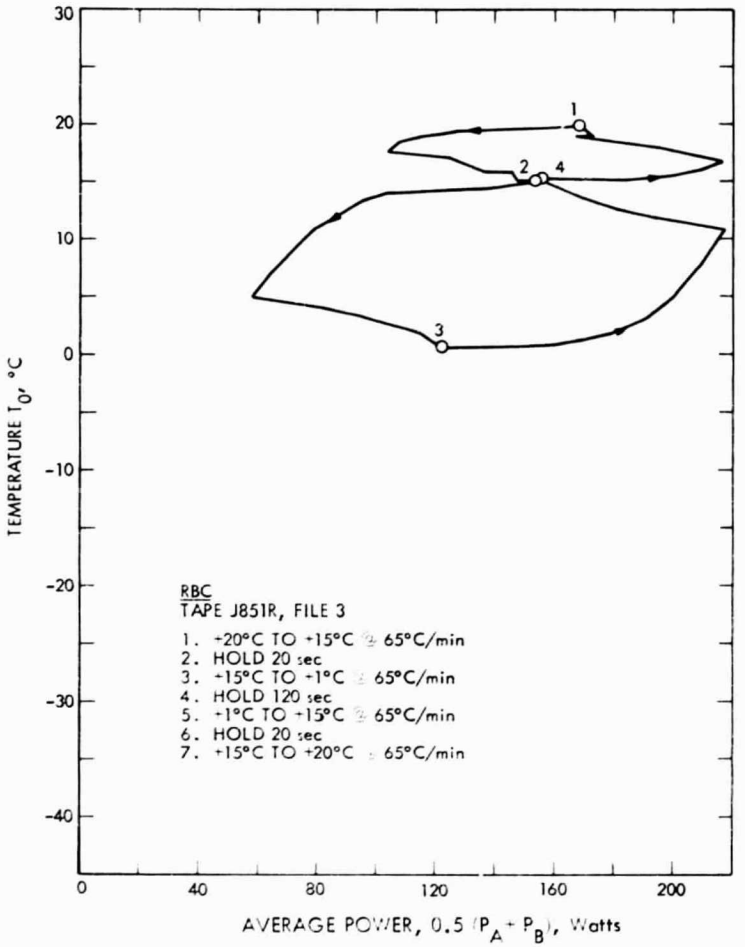

Figure F-5a

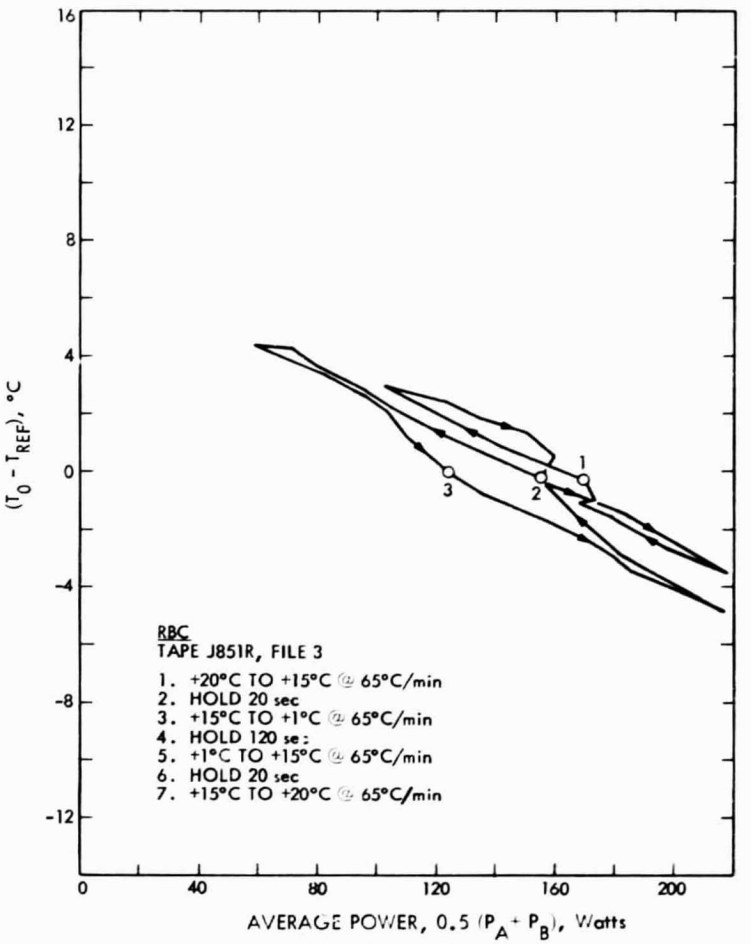

Figure F-5b

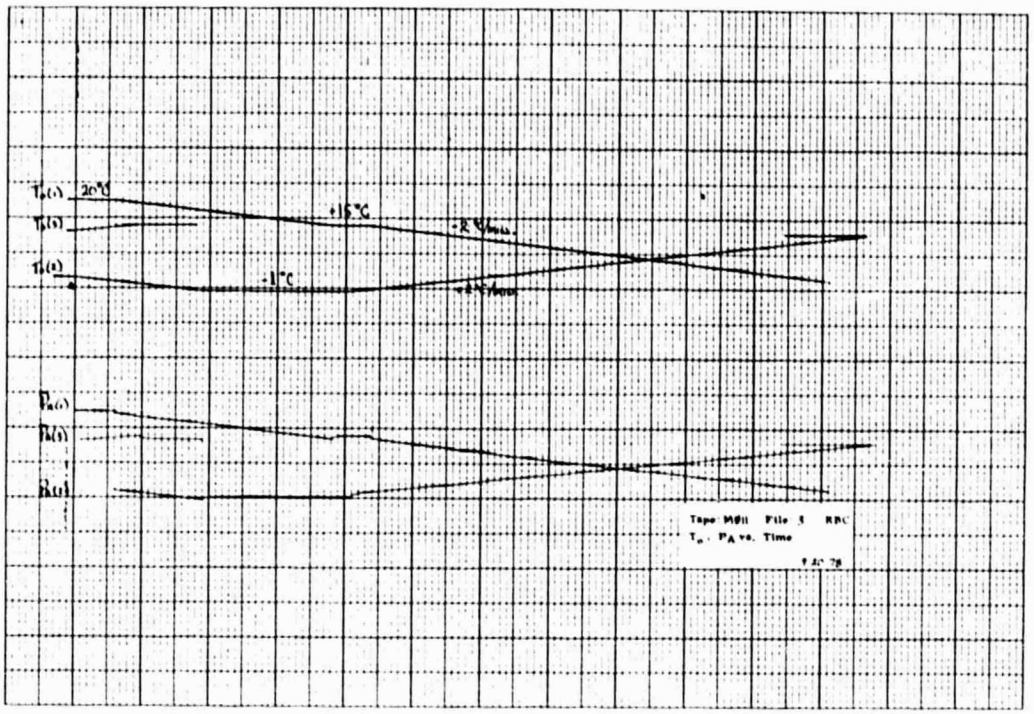

Figure F-6a

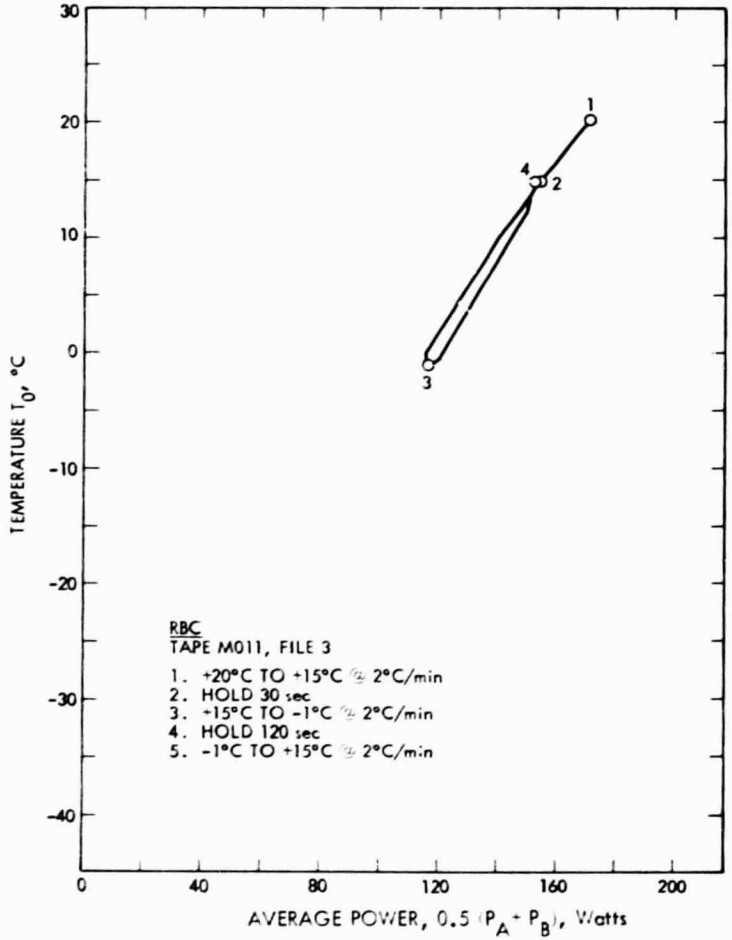

Figure F-6b

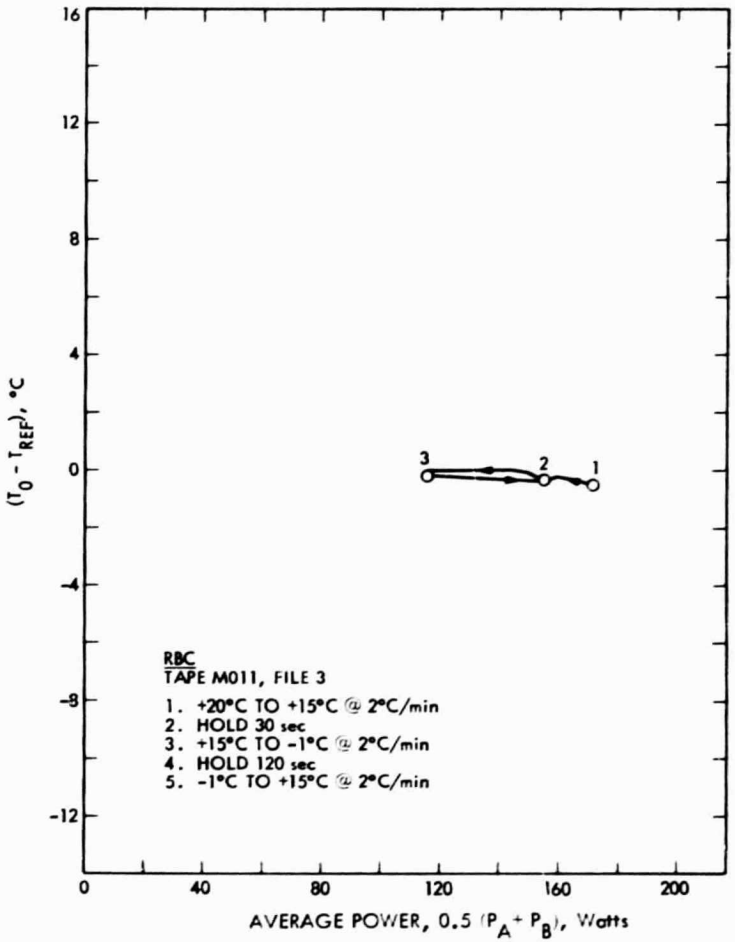

Figure F-6c

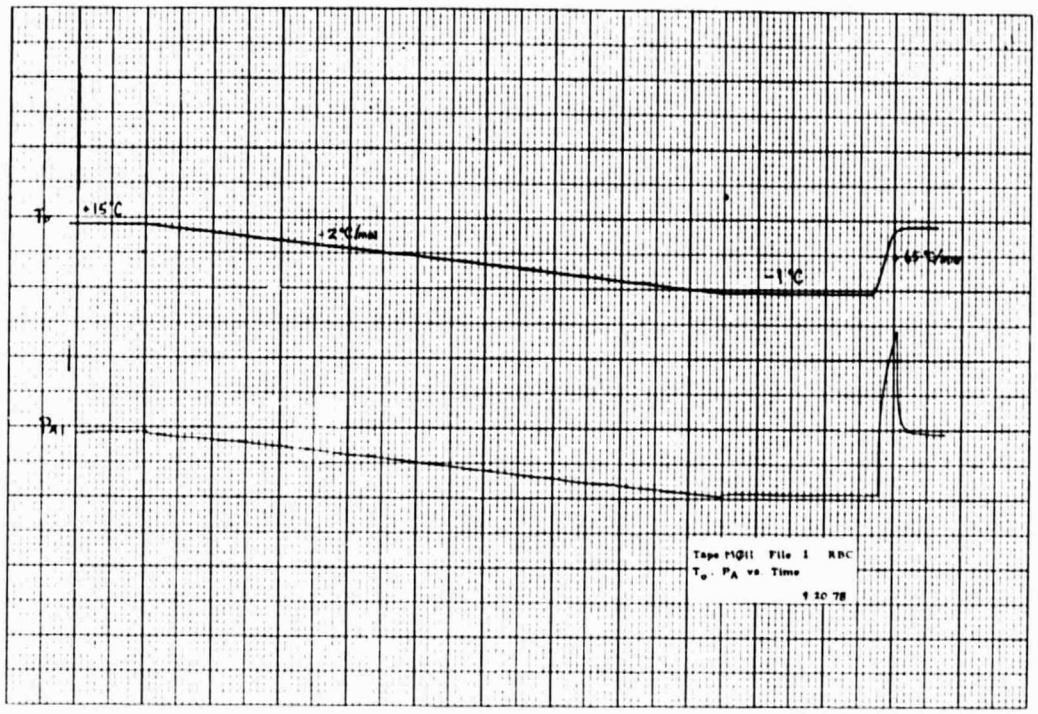

ORIGINAL PAGE IS
OF POOR QUALITY

Figure F-7a

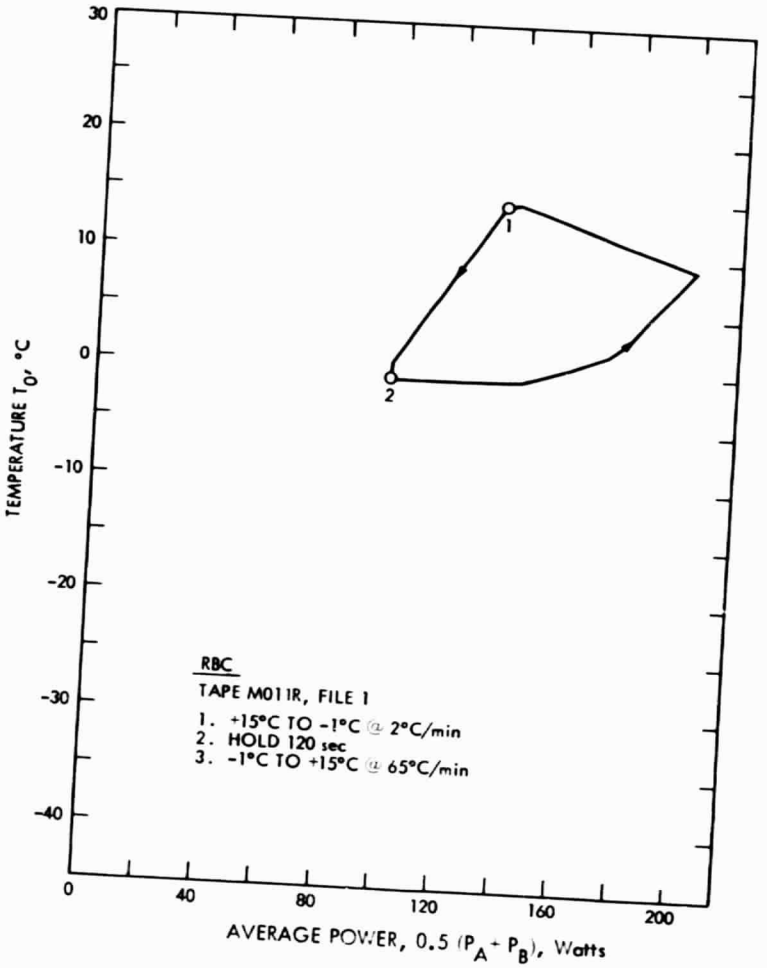

Figure F-7b

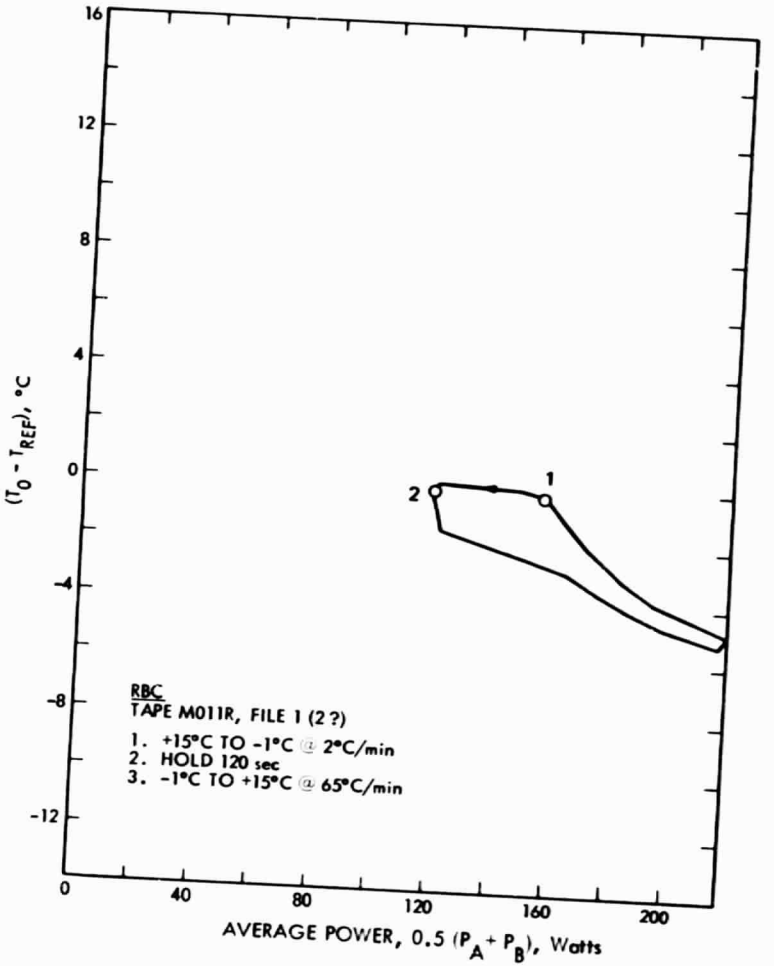

Figure F-7c

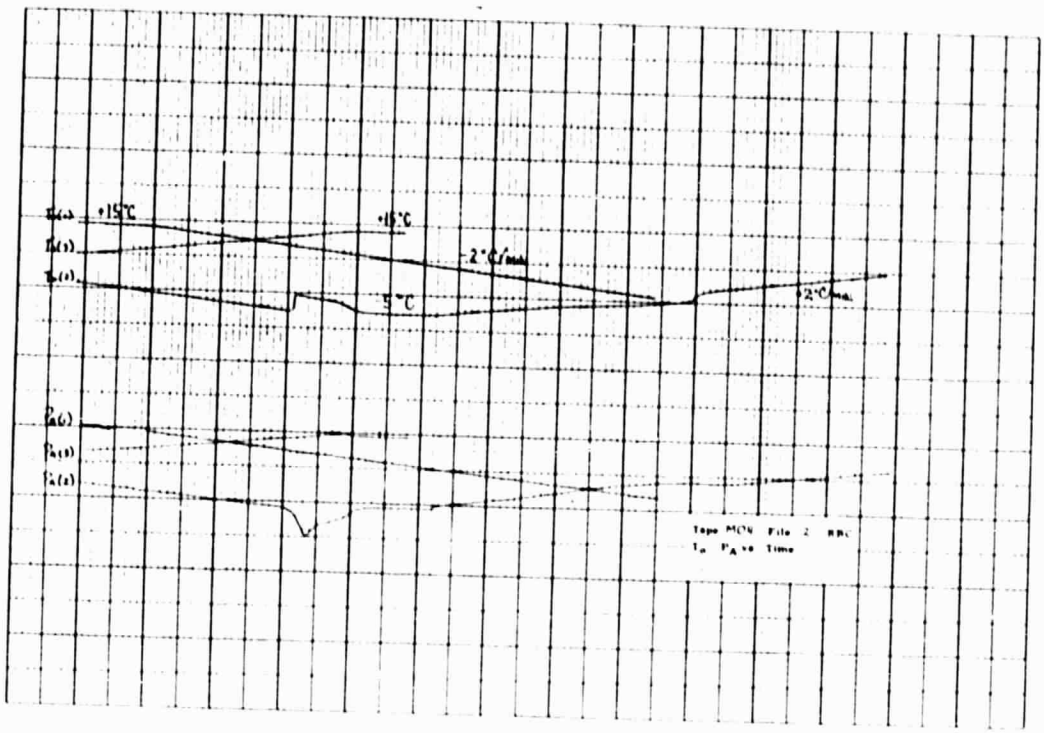

Figure F-8a

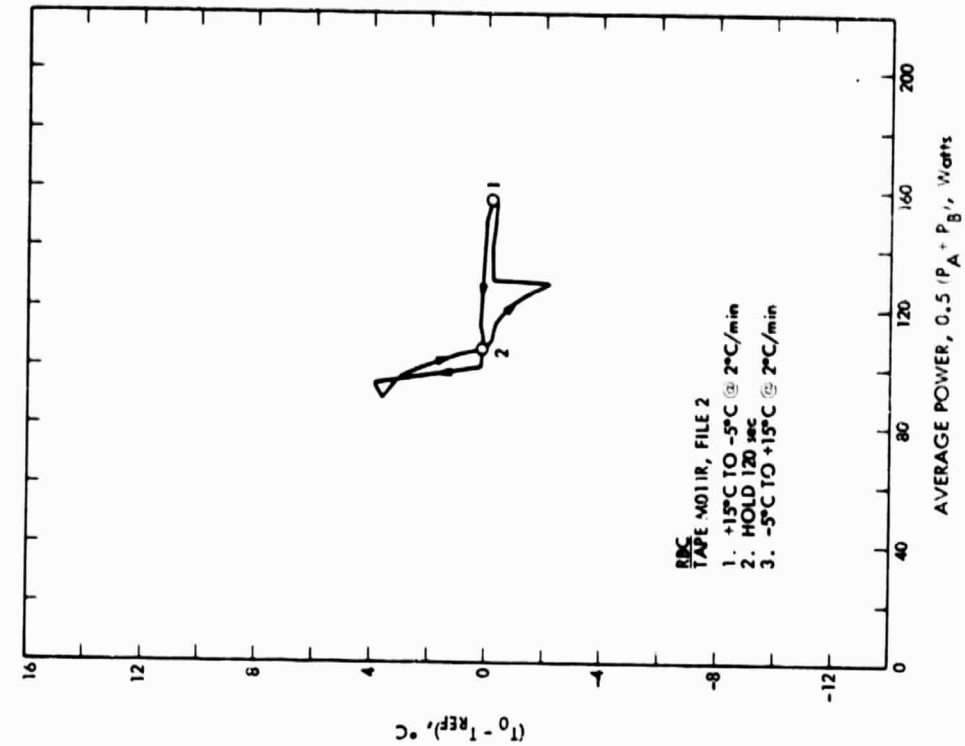

Figure F-8c

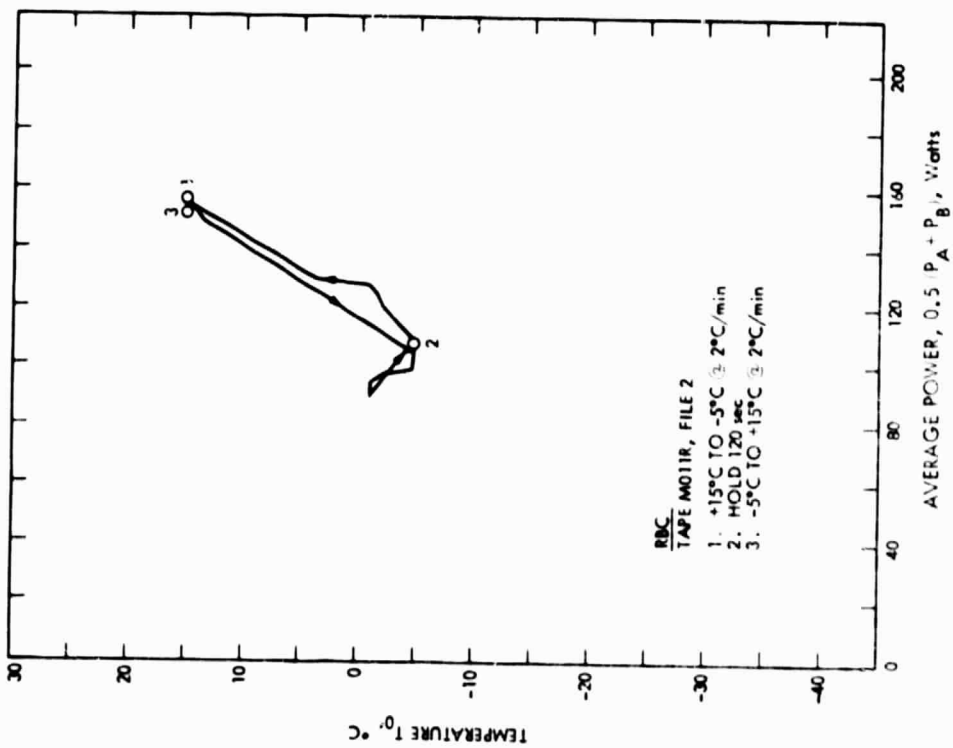

Figure F-8b

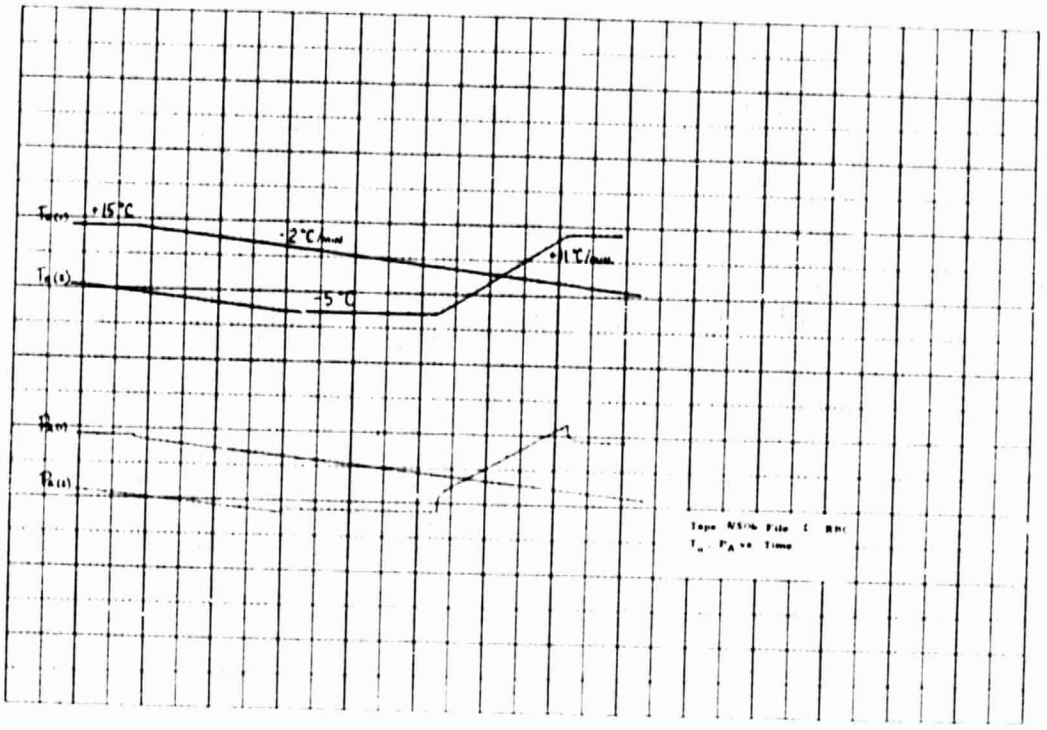

Figure F-9a

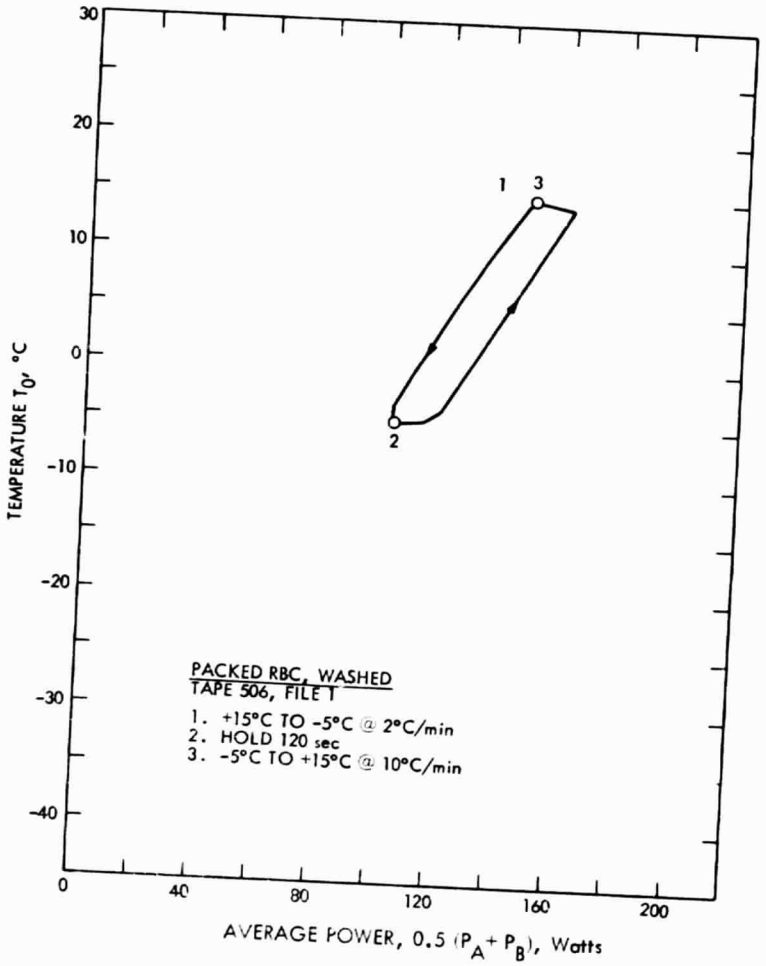

Figure F-9b

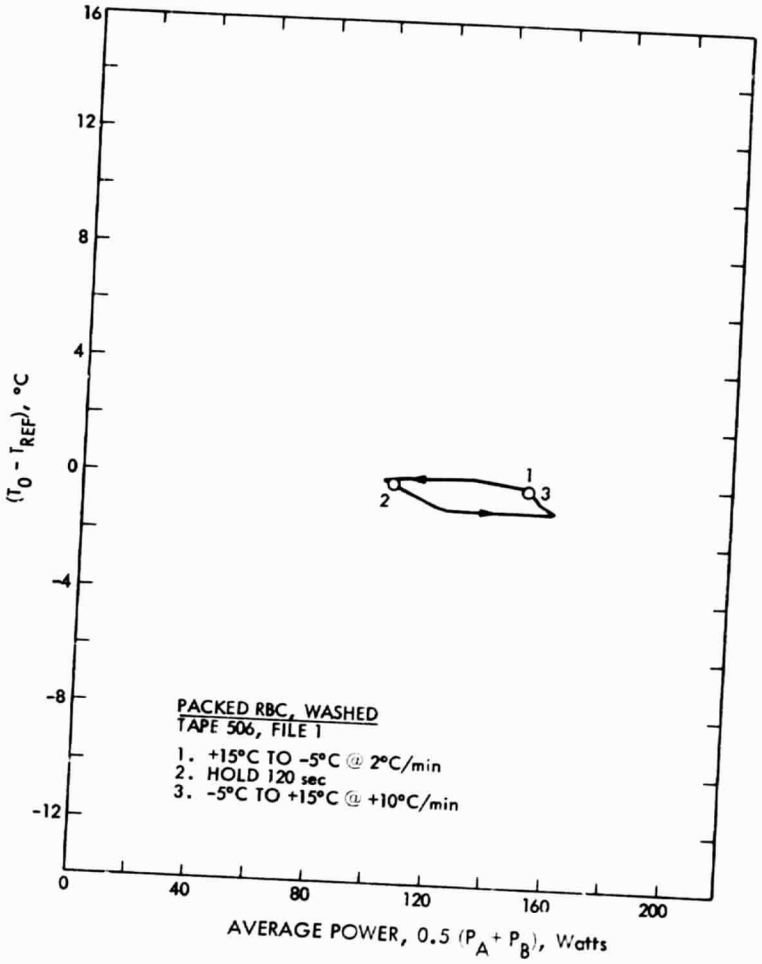

Figure F-9c

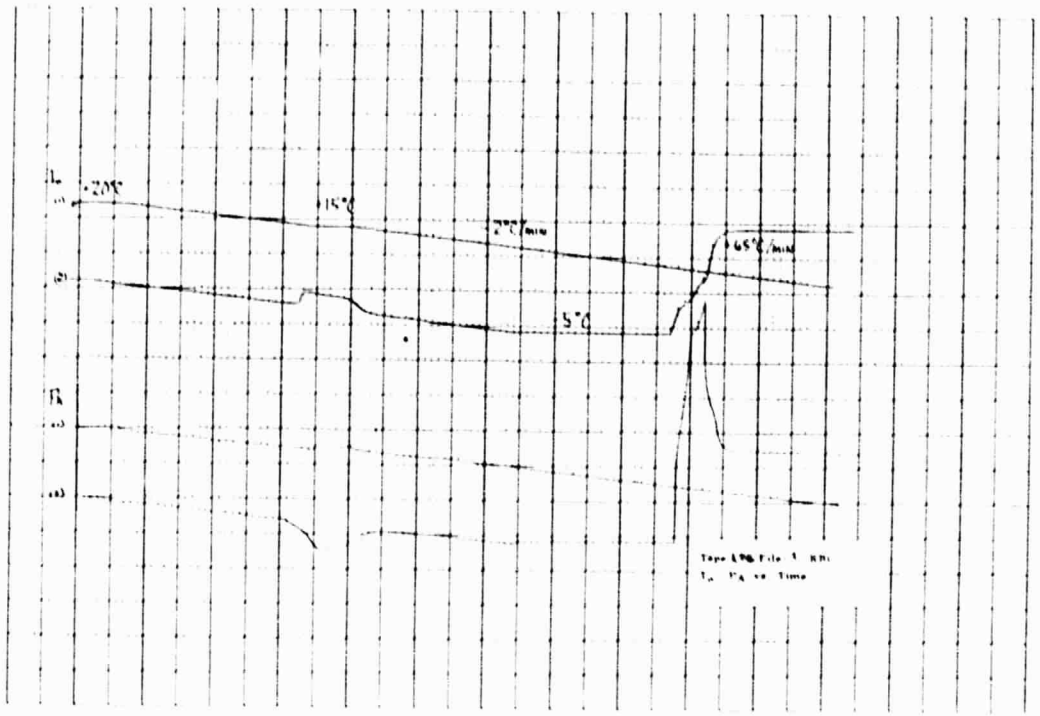

Figure F-10a

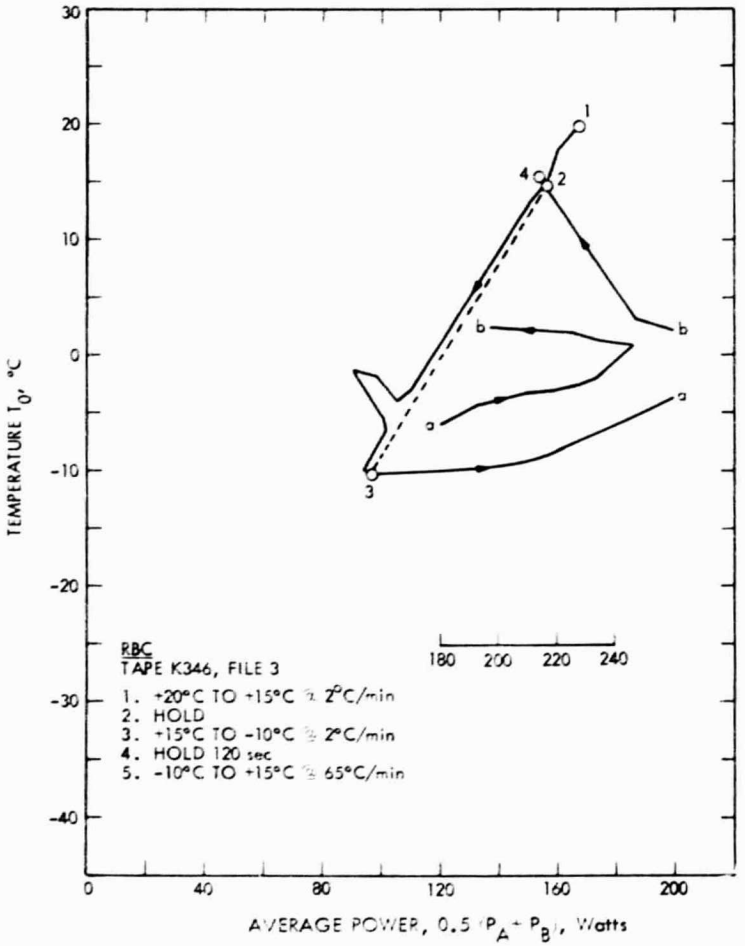

Figure F-10b

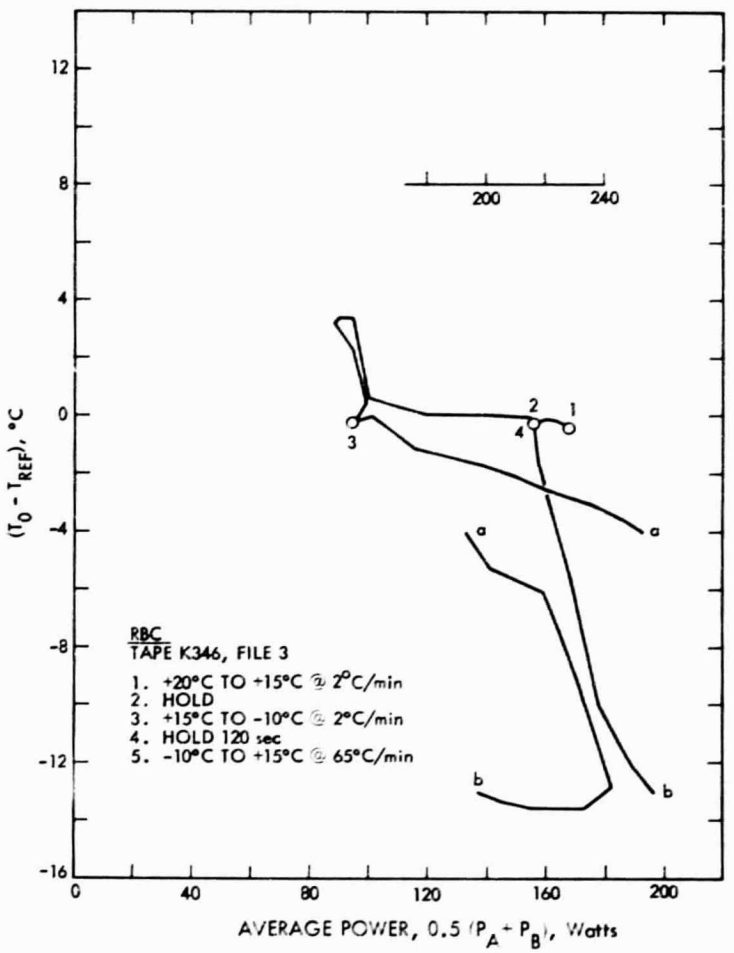

Figure F-10c

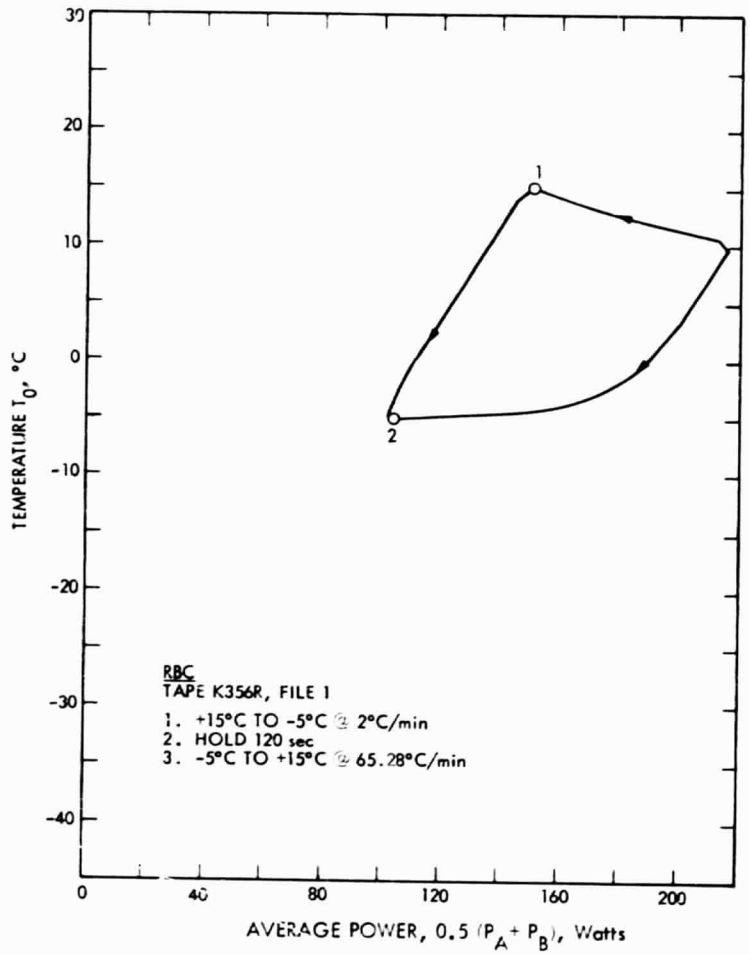

Figure F-11a

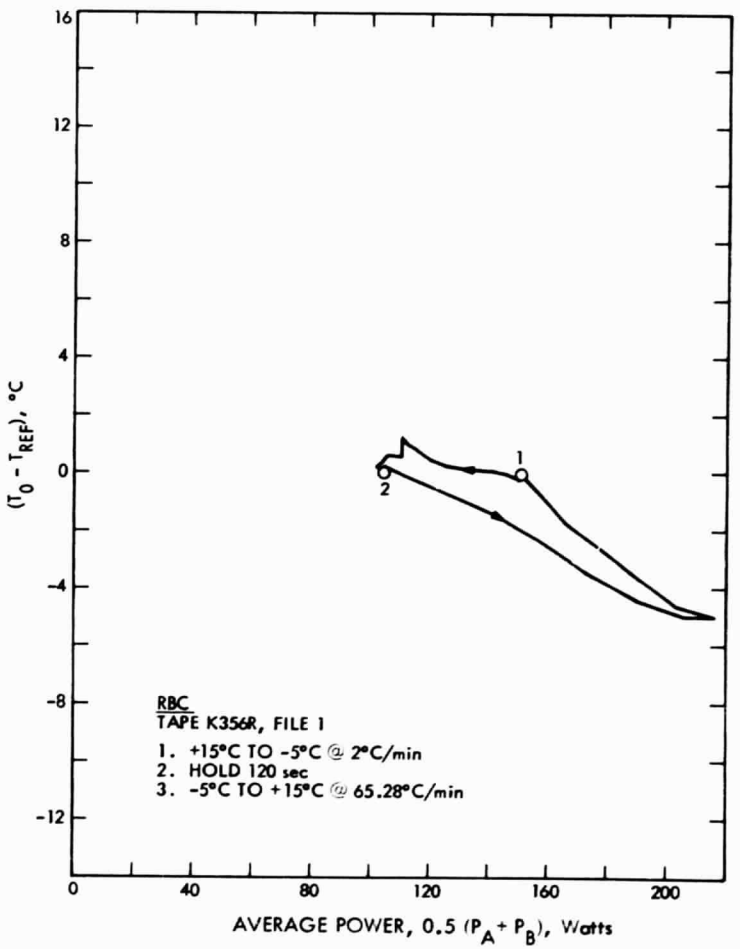

Figure F-11b

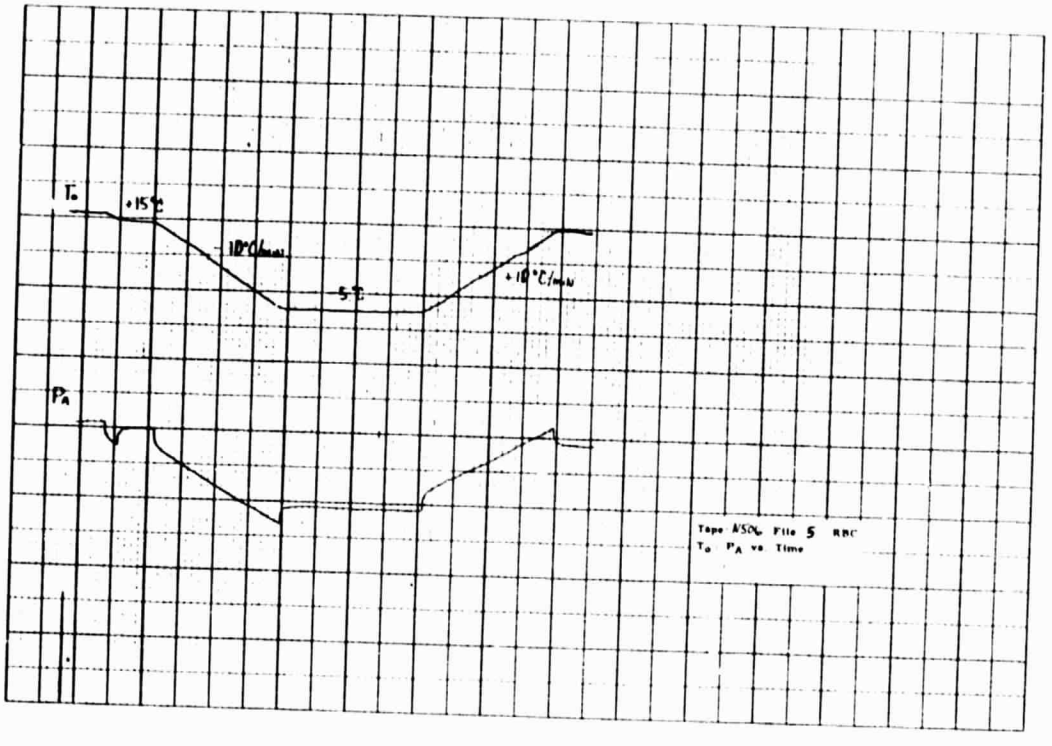

Figure F-12a

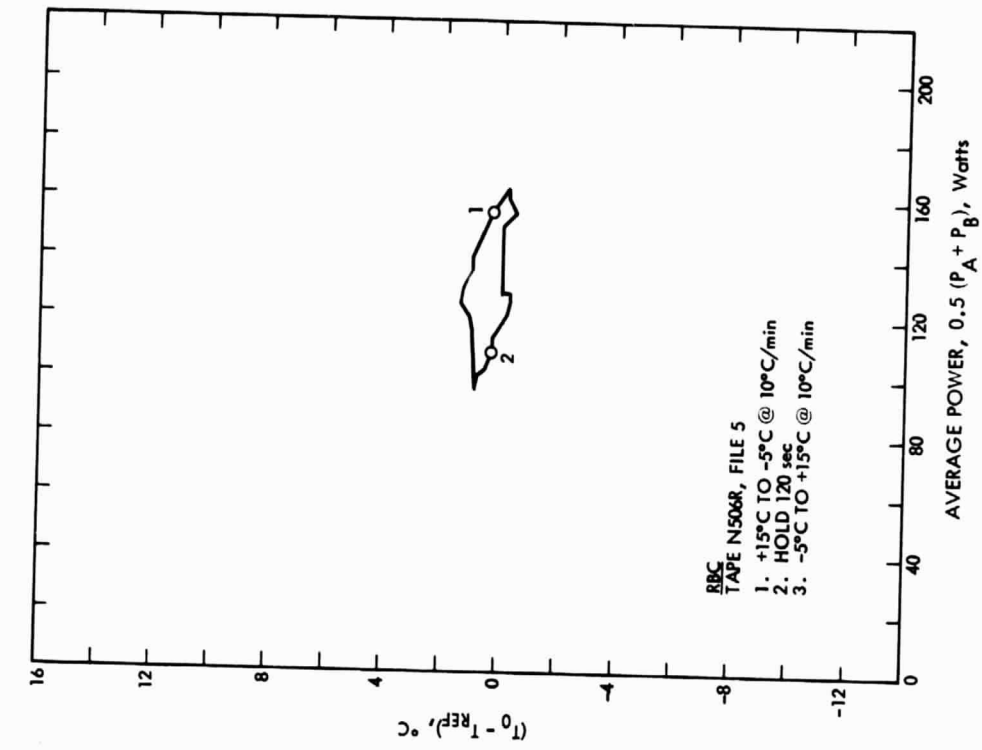

Figure F-12c

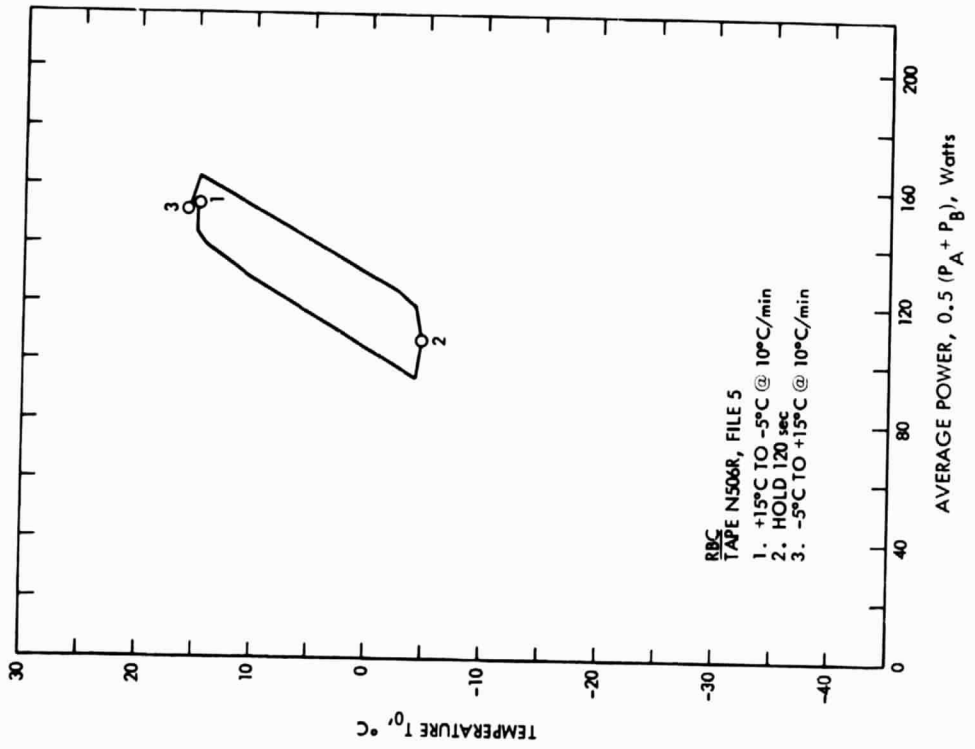

Figure F-12b

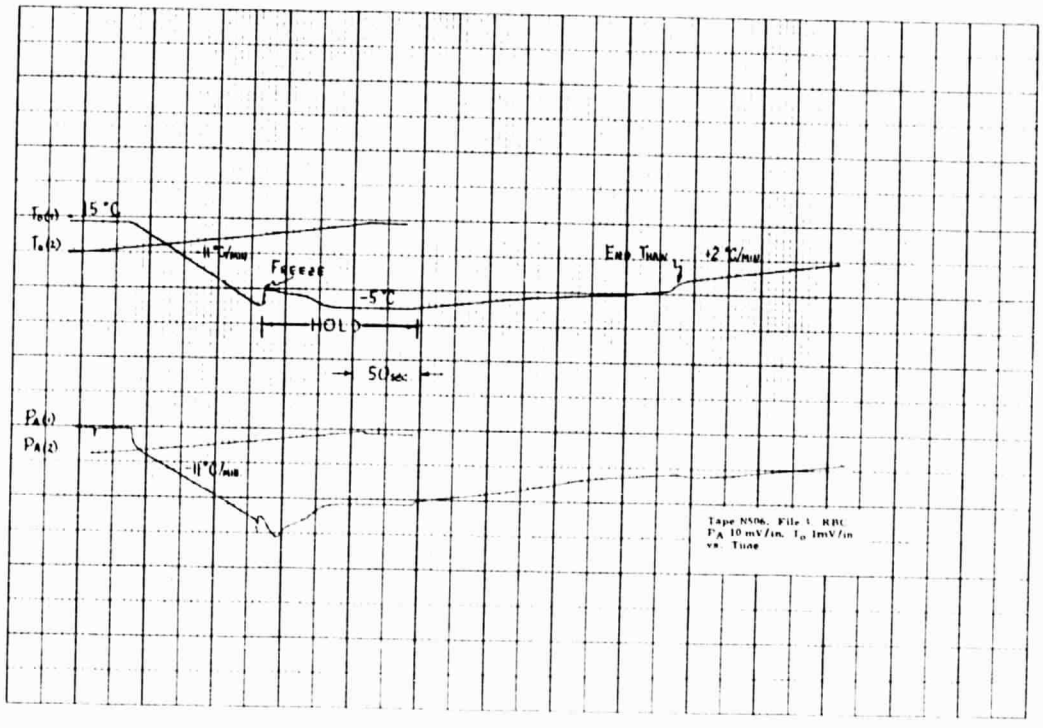
+5 °C
-11 °C/min
Freeze
-5 °C
HOLD
50 sec
END THAW
+2 °C/min
-11 °C/min
Tape NS06, File 1 RBC
PA 10 mV/in, To 1mV/in
vs. Time

Figure F-13a

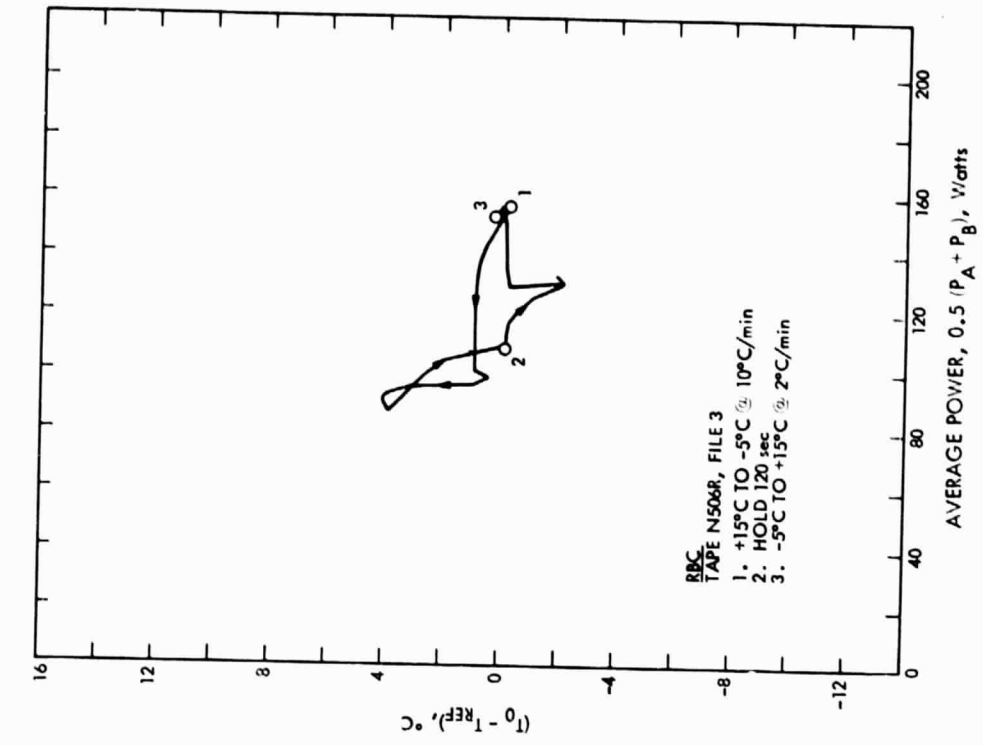

Figure F-13c

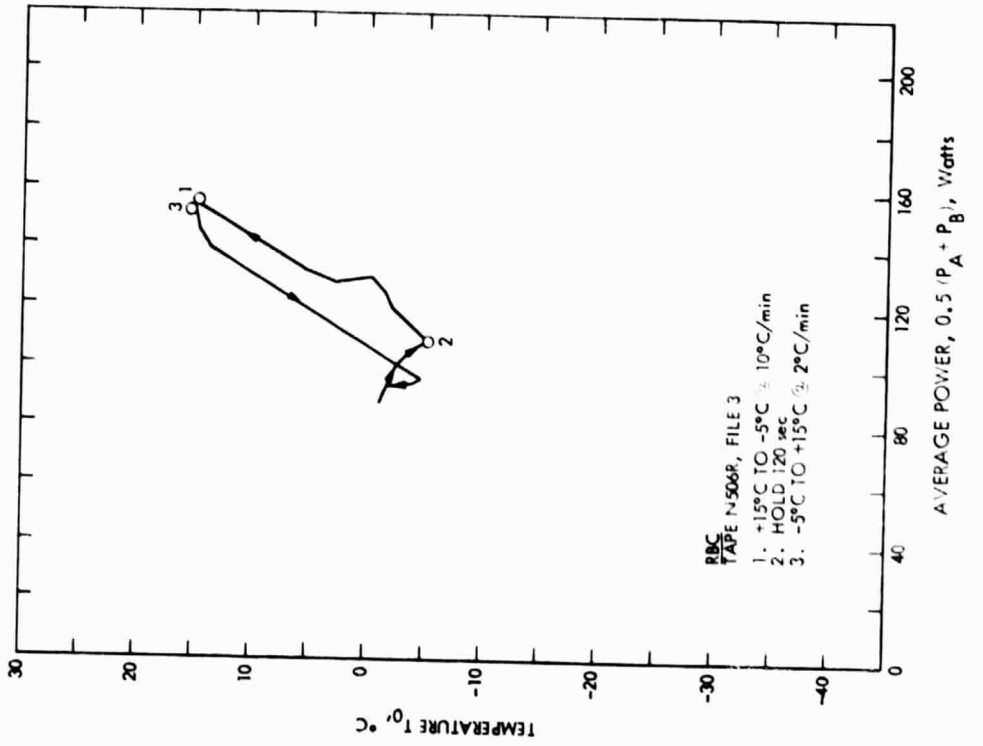

Figure F-13b

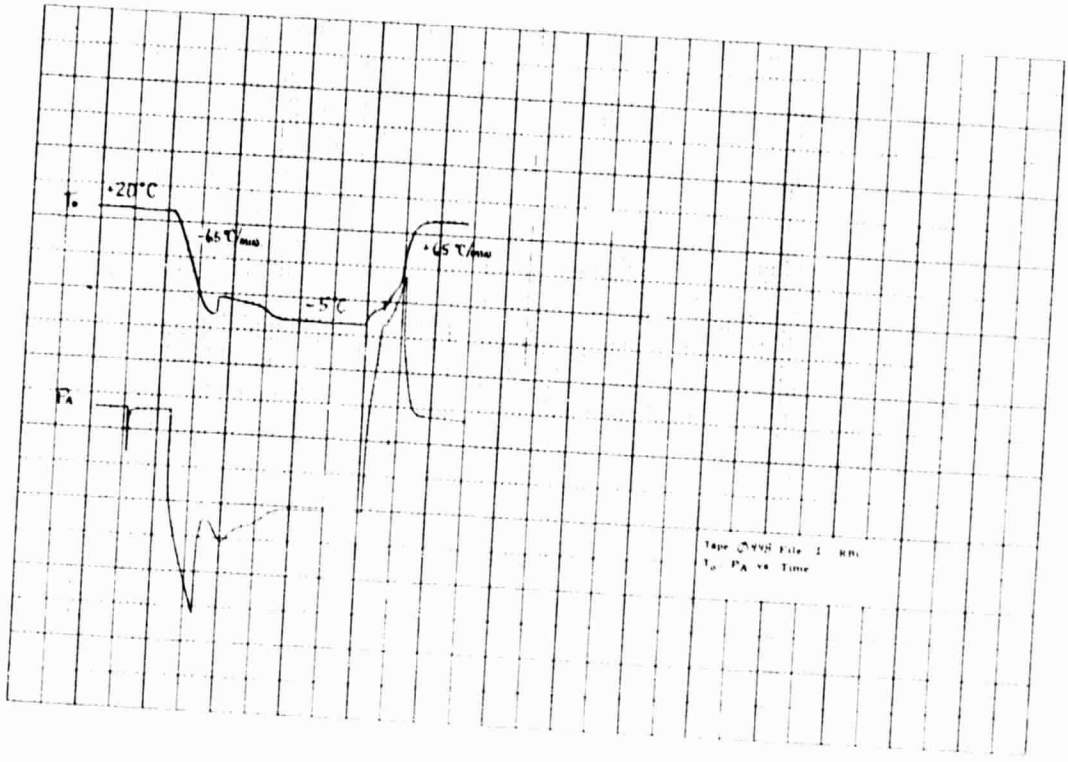

Figure F-14a

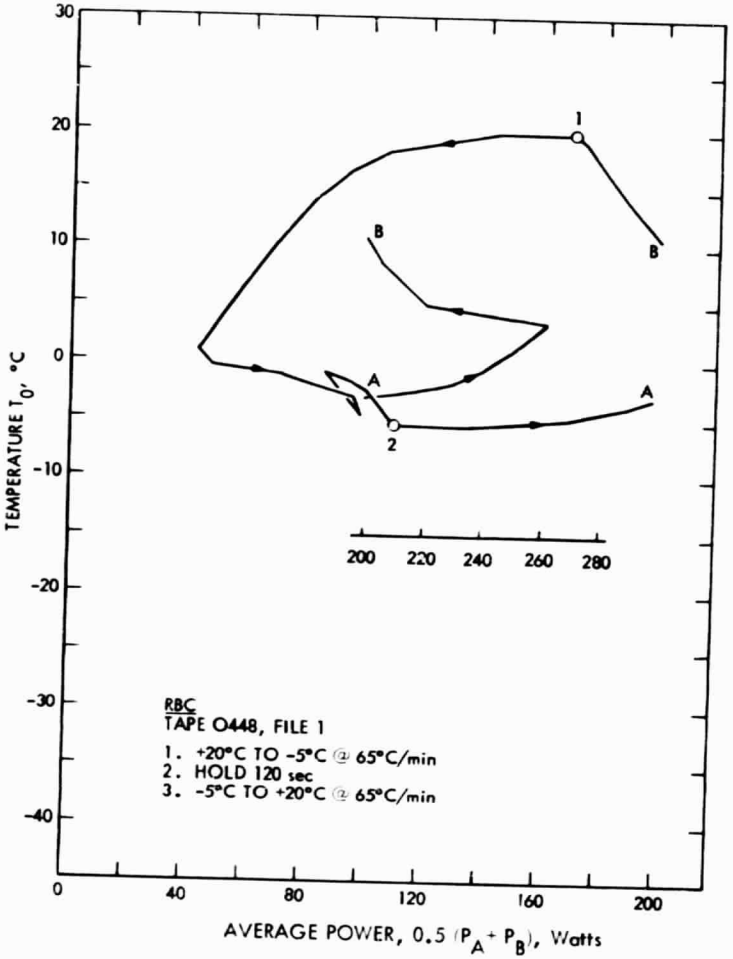

Figure F-14b

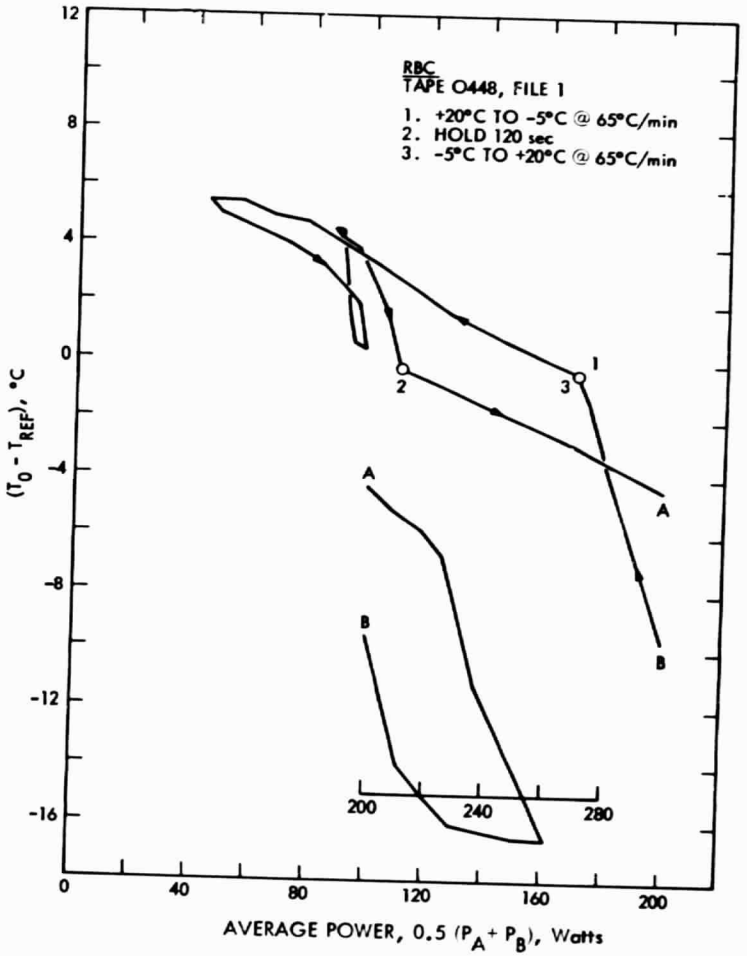

Figure F-14c

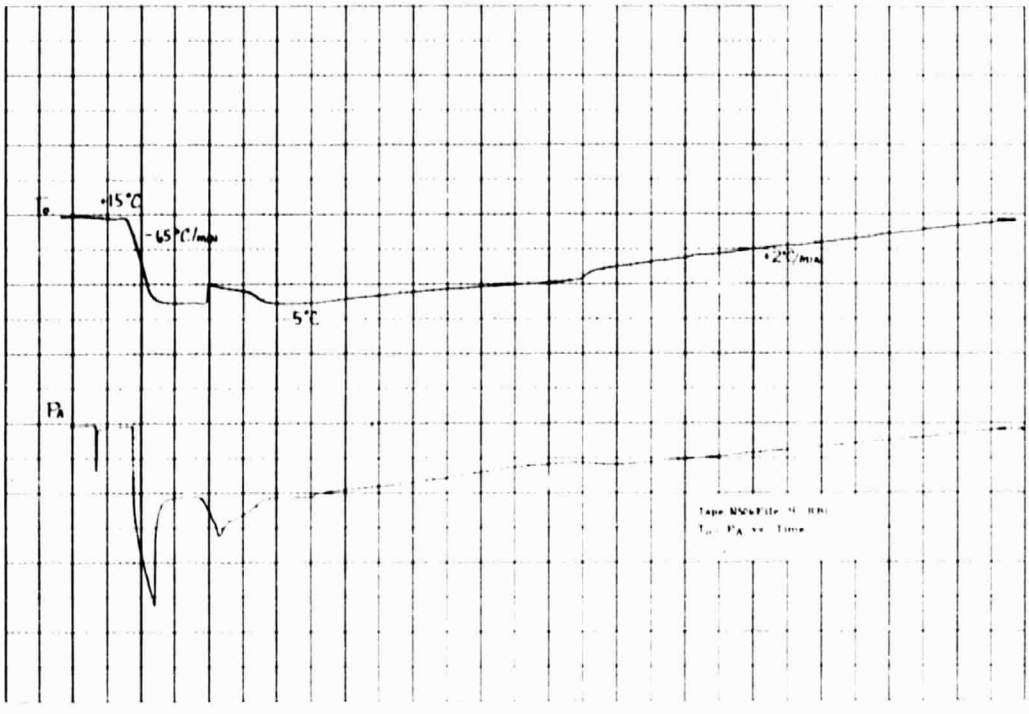

Figure F-15a

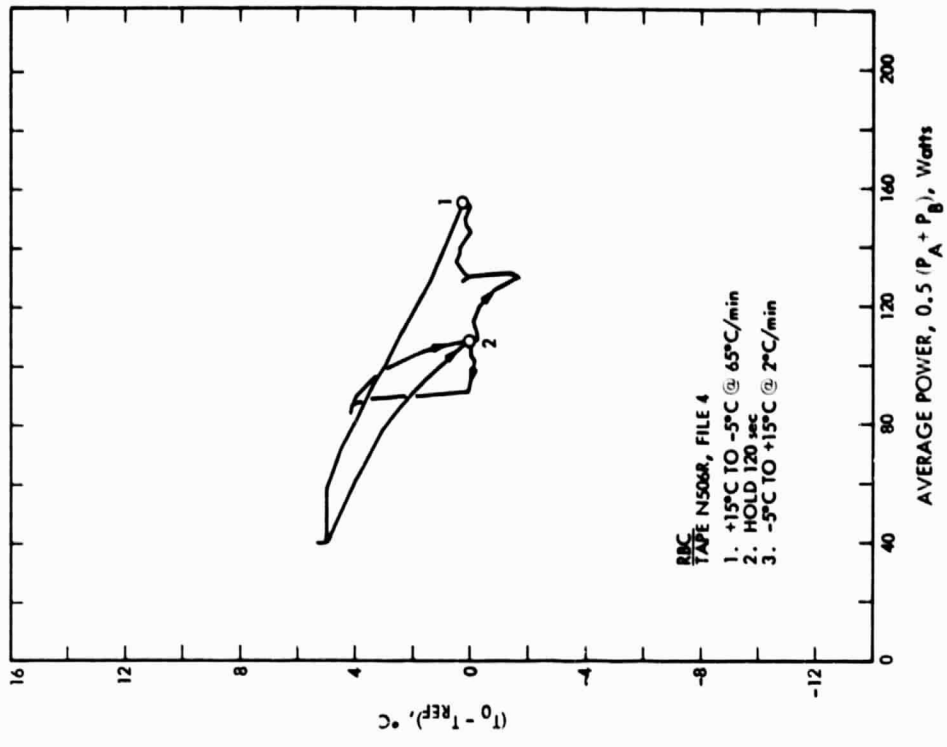

Figure F-15c

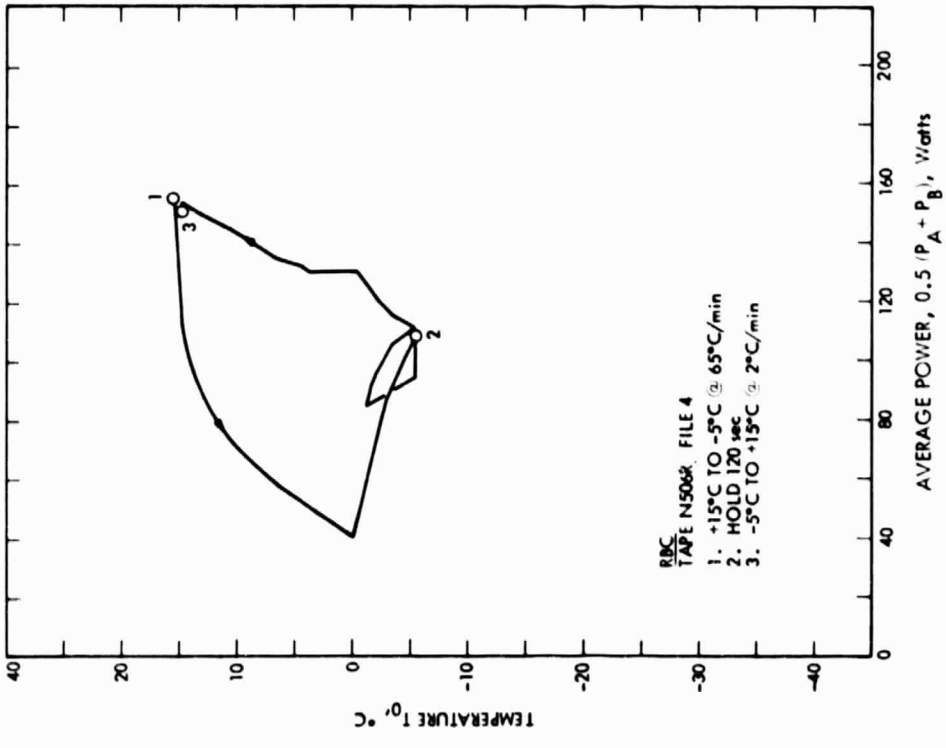

Figure F-15b

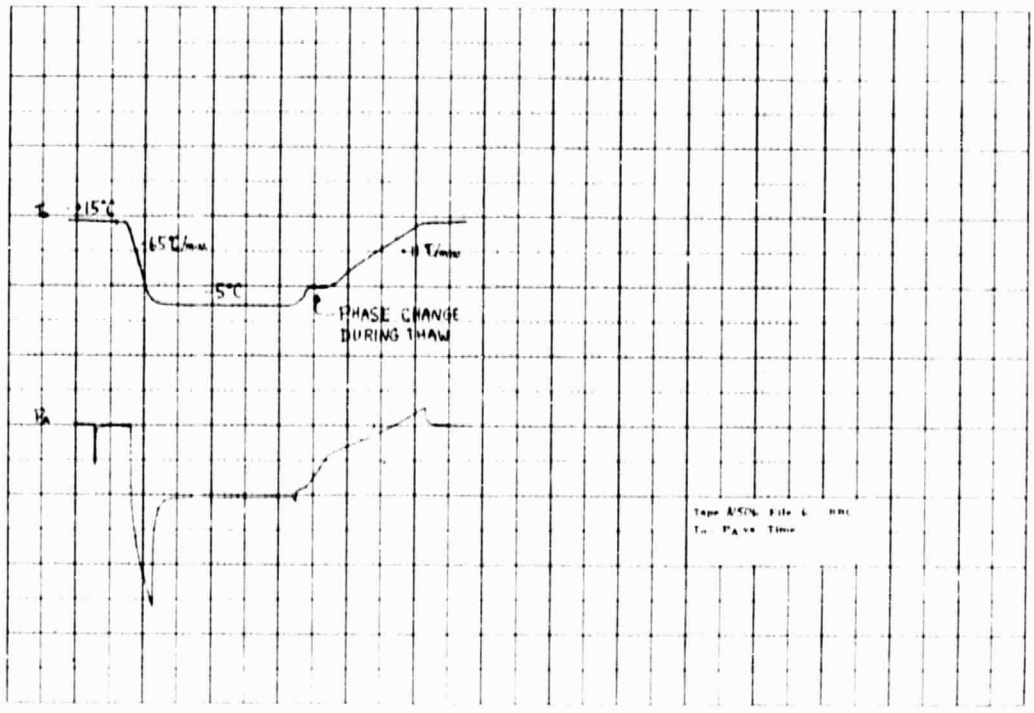

Figure F-16a

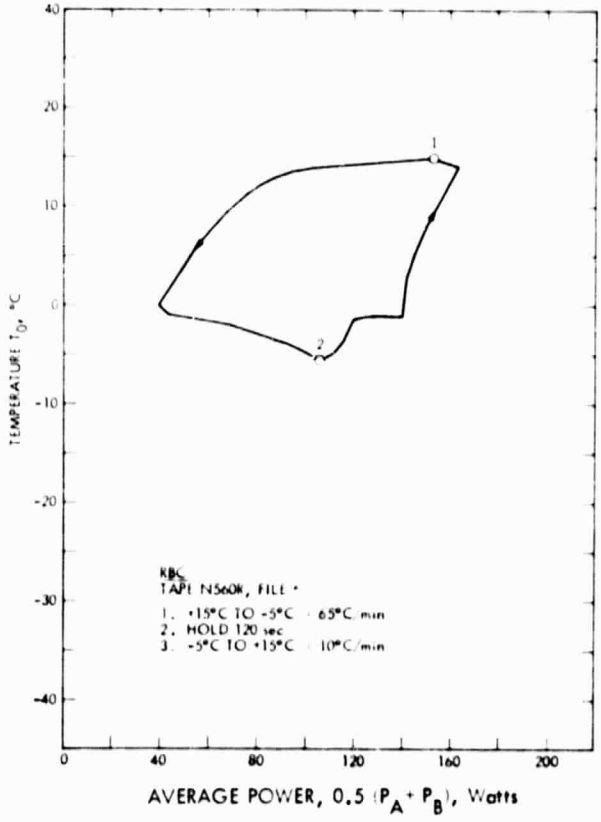

Figure F-16b

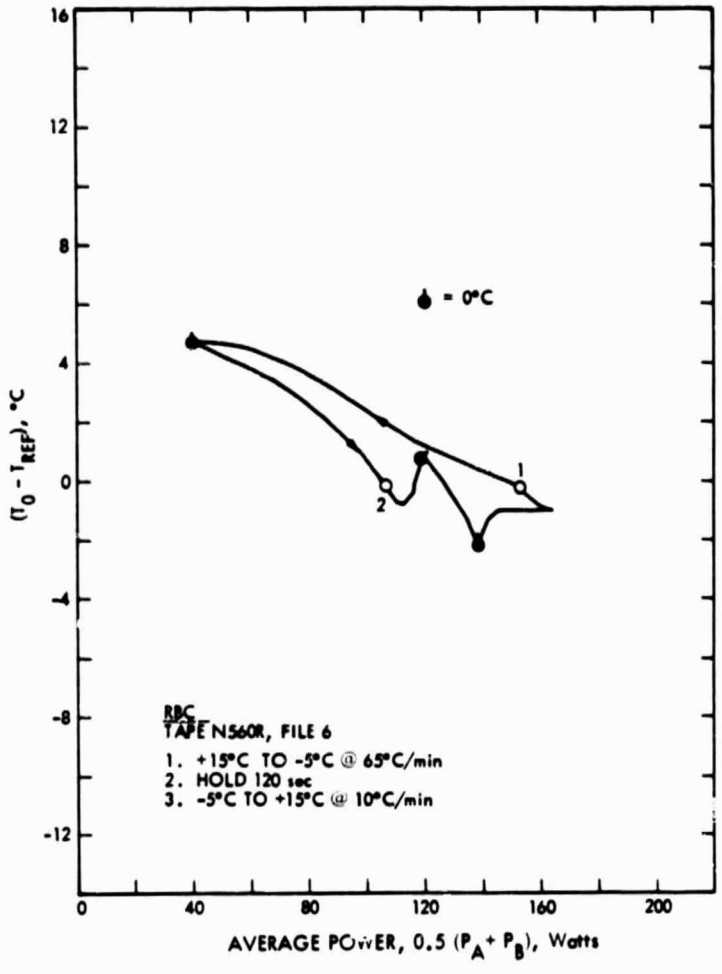
16
12
8
4
0
-4
-8
-12
0
40
80
120
160
200
$(T_0 - T_{REF})$, °C
AVERAGE POWER, 0.5 $(P_A + P_B)$, Watts
= 0°C
1
2
RBC
TAPE N560R, FILE 6
1. +15°C TO -5°C @ 65°C/min
2. HOLD 120 sec
3. -5°C TO +15°C @ 10°C/min

Figure F-16c

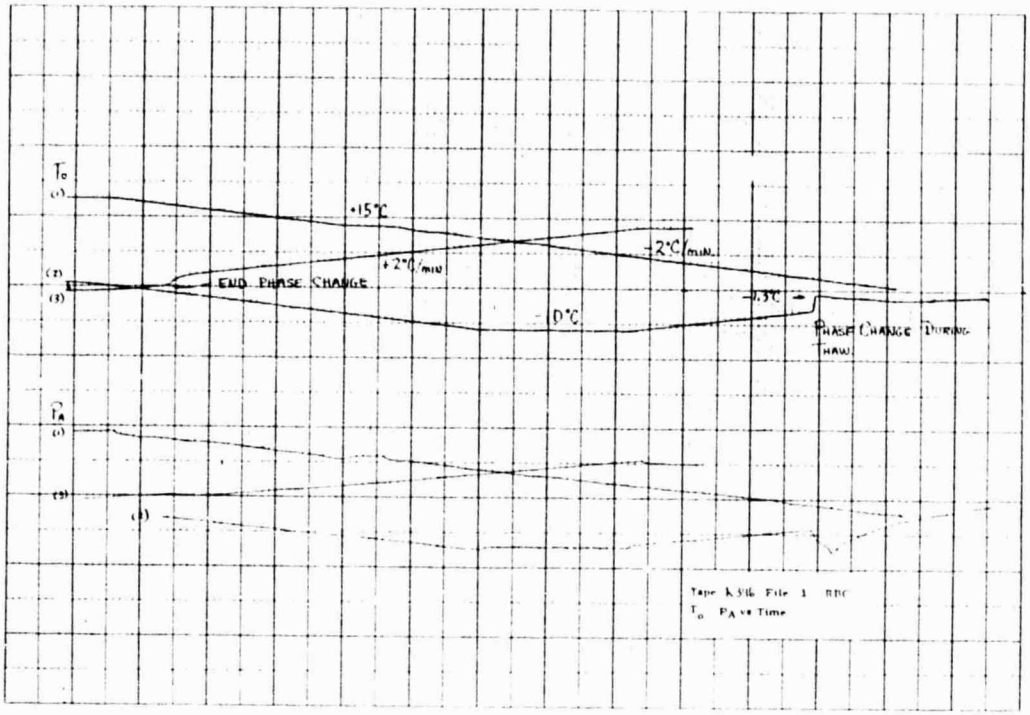

Figure F-17a

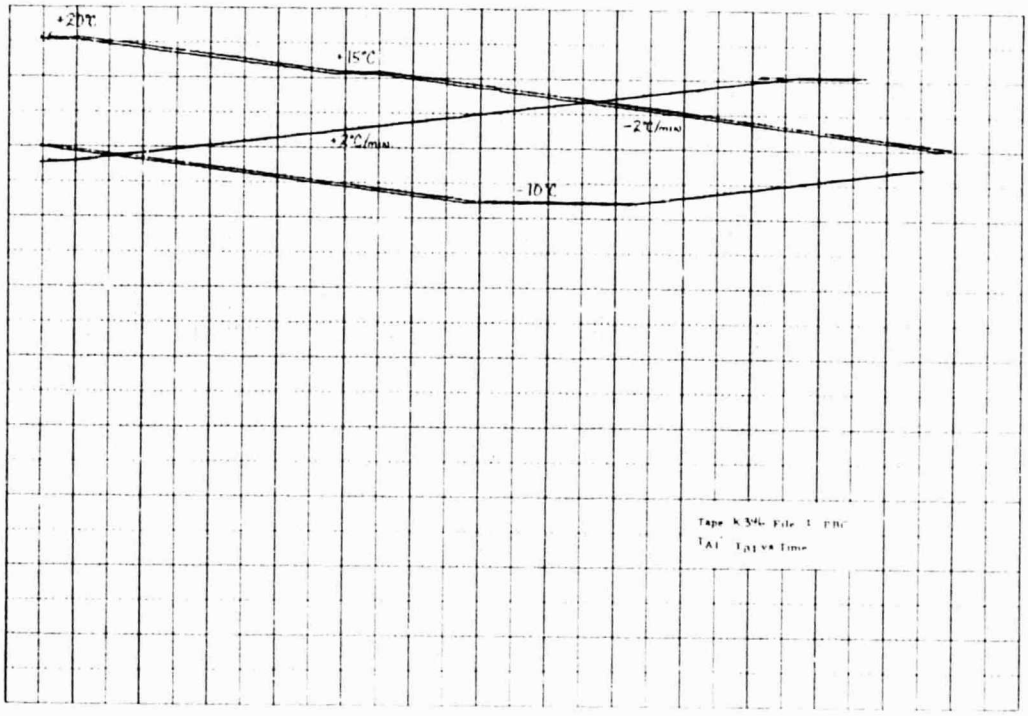

Figure F-17b

ORIGINAL PAGE IS
OF POOR QUALITY

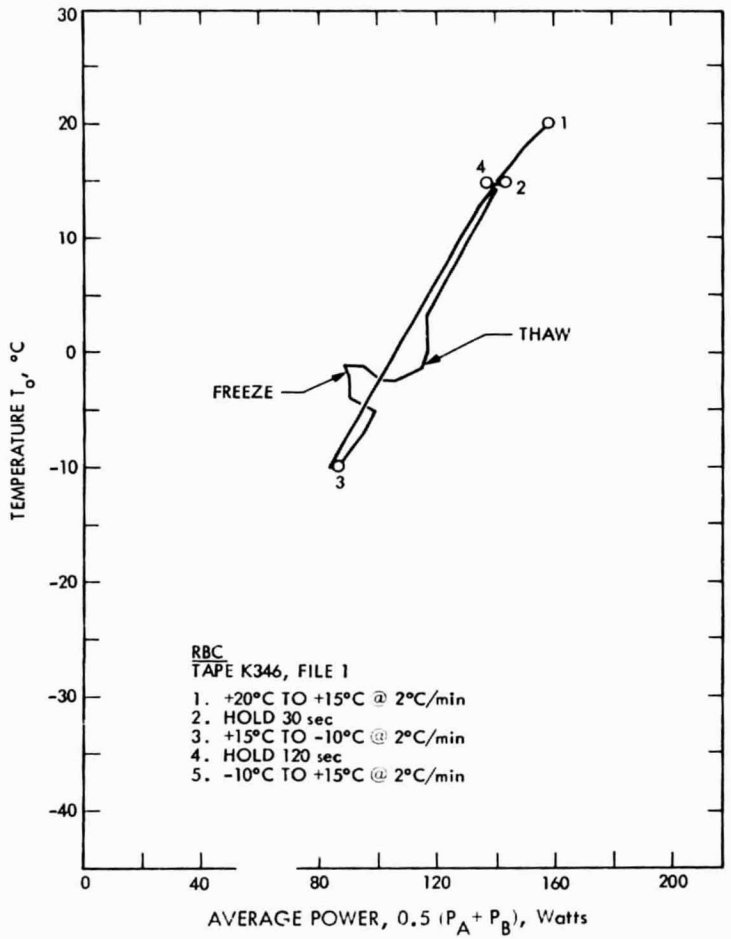

Figure F-17c

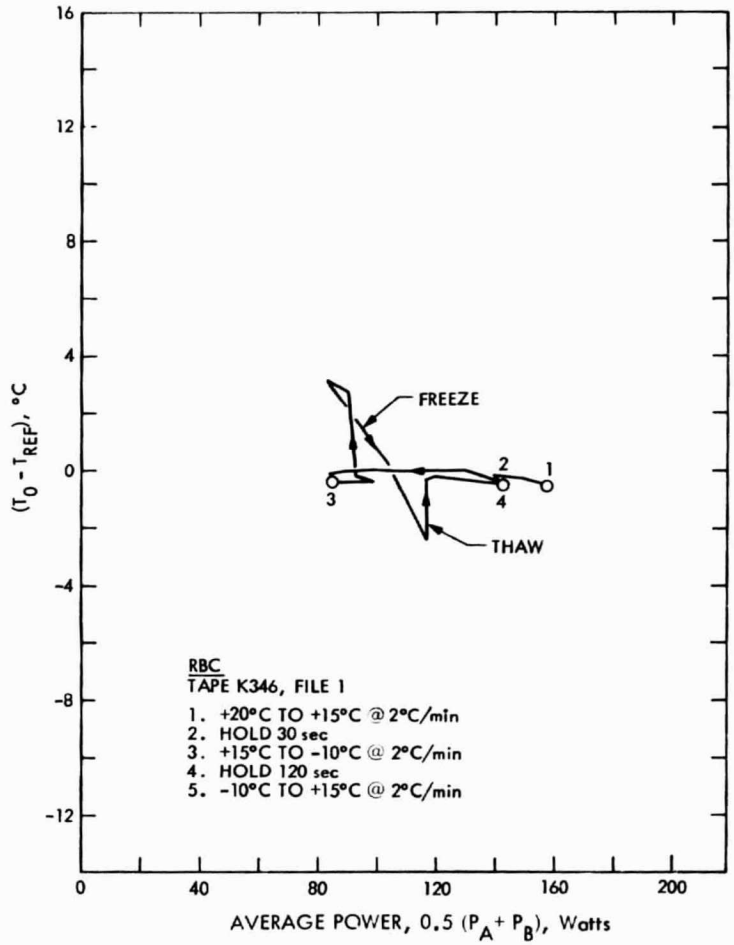

Figure F-17d